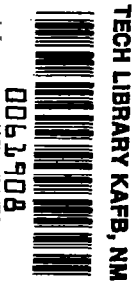

NASA Contractor Report 3118

Active Control for the Total-In-Flight Simulator (ACTIFS)

E. G. Rynaski, D. Andrisani II, and N. Weingarten

CONTRACT F33615-73-C-3051
APRIL 1979

NASA

NASA Contractor Report 3118

Active Control for the Total-In-Flight Simulator (ACTIFS)

E. G. Rynaski, D. Andrisani II, and N. Weingarten
Calspan Corporation
Buffalo, New York

Prepared for
Langley Research Center
and Air Force Systems Command
under Contract F33615-73-C-3051

National Aeronautics
and Space Administration

Scientific and Technical Information Office

1979

FOREWORD

The Active Control Technology development program described in this report was sponsored by the Langley Research Center of the National Aeronautics and Space Administration. It was conducted by the Flight and Facilities Department of the Calspan Corporation, Buffalo, New York as Task 15 of the Air Force Flight Dynamics Laboratory Contract F33615-73-C-3051. The Calspan Project Engineer for this task was Mr. Edmund G. Rynaski. The Program Manager of the Total In-Flight Simulator (TIFS) aircraft is Dr. Philip Reynolds. The NASA program director was Mr. David B. Middleton and the Air Force contract director was Mr. James Pruner.

The authors would like to express their gratitude to the NASA personnel in the ACT program office for their helpful suggestions, criticism and stimulating discussions. Particular thanks are due Mr. Lawrence W. Taylor, Mr. Ray V. Hood and Mr. David Middleton.

The analysis of the structural dynamics of the TIFS airplane and the comparison of the computed and measured structural mode frequencies and responses of Appendix C was performed by Dr. H. Daughaday. This analysis contributed greatly to the understanding of the modal coupling effects of the aircraft.

The program results presented in this report required much computation. The FLEXSTAB results were obtained only with the generous assistance of Mr. R. Schwanz and Mr. C. Stockdale of the Air Force Flight Dynamics Laboratory. The computational chores at Calspan were very ably handled by Mr. Clarence Mesiah and Mr. James Lyons. Finally, special thanks are given to Mses. F. Scribner, M. Ford, D. Kantorski and J. Cornell for their assistance in the preparation of this report.

TABLE OF CONTENTS

TABLE OF CONTENTS (CONT'D)

TABLE OF CONTENTS (CONT'D)

LIST OF TABLES

LIST OF FIGURES

Section I

INTRODUCTION

This report is about gust alleviation, structural mode and maneuver load control, three technical areas of interest that are in a continuous state of theoretical and practical development. The results outlined in this report suggest some design criteria and control system synthesis techniques for gust alleviation, structural mode and maneuver load control. No new theory was developed. It was not necessary to do so. Outstanding new theoretical developments in the area of automatic control have been amply published in the literature during the past decade. Some of this newer theory is used in this report but it also links the conventional, frequency domain oriented control system design methods to the newer, optimal control techniques based upon state space system representations.

The original objective of the research described in this report was to investigate active control techniques, develop design procedures, design a system and, finally, flight test the system: a complete cycle from applied research to practical application. However, shortly into the program it was decided by NASA not to continue this effort beyond the initial study phase because of a redirection of funds which had been budgeted. The emphasis of this program then shifted to providing guidelines and design procedures for active control technology application.

The aircraft for which the initial work was directed was the Total In-Flight Simulator (TIFS). This aircraft is ideally suited for the type of research proposed. The vehicle required only a relatively minor modification, the provision for collective aileron operation, to provide a facility that has an extraordinary range of proof-of-concept capability with little initial financial investment; a versatile and cost effective fly-before-buy vehicle for active control technology development.

The TIFS aircraft, a converted C-131H (CV-580), is fully instrumented with accelerometers, rate and attitude gyros, and a complete, fully calibrated and accurate air data system that provides inertial and gust components of air data measurements. It contains an unusually versatile control system with wide bandwidth servos driving six independent force and moment producing devices on the vehicle. Every rigid body state variable is measured and can be used for feedback to each or any of the six controllers. A large computer exists onboard for feedback control law, gain scheduling or command augmentation purposes. The techniques developed through the use of the TIFS aircraft are directly applicable to existing or proposed aircraft design. Also, the unique capability of the model-following system of TIFS provides for an in-flight simulation capability suitable to support evaluation of the flying qualities consequences of active control technology application to a wide range of existing and proposed vehicle designs. Thus, it would be a relatively simple matter to conduct flight test programs to simulate actively controlled, contemporary wide-body jets, determine their performance, and assess their acceptability potential.

Section II of this report describes the general philosophy and design concepts that were developed for active control technology use. The emphasis is on criteria, a fundamental step in any design objective that is in danger of being sidestepped in active control technology development. Optimal or modern control design principles are emphasized because explicitly stated design objectives can be directly rather than indirectly injected into the design procedure. Finally, it shows how the three functional parts of active control technology; gust alleviation, maneuver load control and structural mode control can be separated, producing physically identifiable separate parts to the system that can be operated separately or in harmony with each other without direct interference. Because the actual benefits of active control technology for commercial flight vehicles have yet to be proven cost effective and energy efficient, a separation of the active control subsystems is useful for the demonstration phase of active control technology development.

Section III addresses the modeling problem. The complete aeroelastic equations of motion were obtained for the TIFS airplane through the use of the FLEXSTAB program. The results of the analytically computed model were then compared to experimentally obtained data such as ground vibration tests, quasi-static values of the rigid body stability and control derivatives obtained using flight data and Bayesian Maximum Likelihood identification procedures, and transfer functions estimated from "frequency sweep" inputs to the direct lift flap and elevator servos. Methods were devised for gradually adjusting the analytically determined mathematical model as data becomes available from flight tests of the vehicle. An important objective of this part of the program was to determine how accurately FLEXSTAB could predict the aeroelastic equations of motion of a high aspect ratio, turboprop transport aircraft such as TIFS.

Section IV addresses the problem of the design of a gust alleviation system. For reasons of simplicity and potential effectiveness, the feedforward gust compensation technique was investigated rather than a feedback approach to the problem. It is shown that effective gust alleviation can be obtained by using a measurement of the gust and by driving the control surfaces in a way that produces forces and moments on the vehicle to counter those forces and moments produced by gusts. Independent, redundant control surfaces as proposed for active control are a functional bonus for this type of design approach.

Section V outlines design procedures to make the most effective use of available control surfaces for maneuver load control purposes. The objectives of the maneuver load control design were to minimize wing bending moments, wing torsion and control surface activity while at the same time maintaining or even enhancing the flying qualities of the vehicle itself. It is shown that maneuver load control systems can be mechanized either as feedback or command augmentation. The final configuration is shown as command augmentation, simplified for direct use on the TIFS aircraft.

Design criteria and control laws are developed in Section VI for structural mode control. A general criteria is presented for altering the

structural dynamics of the vehicle in such a way that increasingly more accurate approximations to a rigid body are specifiable in a minimum integral error squared sense. The control problem is then shown to have a relatively straightforward pole placement requirement. By a systematic extension of the phase variable form of system description used in parameter identification phase of the program, control laws are specified for both state variable and output variable form.

Section VII contains conclusions and recommendations. They are extensive because so much theoretical and application work has yet to be done, not only before active control systems can be optimized and flight proven, but even before they can be justified and properly designed from a mathematical/theoretical point of view.

Section II

GENERAL DESIGN PRINCIPLES

2.1 INTRODUCTION

There were four primary objectives for this program:

1. A comparison was made of aero-elastic equations of motion of the TIFS aircraft computed analytically with aero-elastic equations of motion obtained from in-flight test data. Validation of the analytical model and methods for updating the model from actual flight test data were developed and applied to TIFS.

2. The problems of criteria and feedback control laws for TIFS to actively control or suppress the structural dynamics of the vehicle were addressed. A mixture of modern control and conventional control techniques are shown to be most promising. Of particular interest was the development of feedback control laws not requiring complete state feedback, in order to minimize the number of sensors required for mechanization or implementation. A criterion was developed that was intuitively appealing in that it was compatible with beam theory that specifies an increase in both mode damping ratio and natural frequencies to obtain more accurate approximations to a rigid body.

3. Gust alleviation methods and techniques were studied, both from the point of view of a feedback system and an open-loop direct command system to the control surface actuators to generate forces and moments on the vehicle to counter or cancel those forces and moments produced by the turbulence.

4. Maneuver Load Control ideas were explored. The objective was to devise a procedure that would use the three control surfaces — elevator, direct lift flap and collective aileron — in such a way during piloting maneuvers as to accomplish the desired results of reducing the wing bending moments without degrading the flying qualities of the vehicle. A model-following design procedure was developed that could be used equivalently as feedback control (implicit model following) or command augmentation (explicit model following) that would not only relieve the wing bending moments but also enhance or improve the flying qualities. Suboptimal and easily mechanizable approximations to the optimal control laws were obtained.

2.2 THE MATHEMATICAL MODEL

Analytical techniques for predicting the aero-elastic characteristics of flight vehicles are under continual development from both a theoretical and computer application point of view. Several computer programs have been written to obtain the mathematical models, and the best known of these are the FLEXSTAB and the NASTRAN programs. These programs, particularly FLEXSTAB, are very comprehensive computer programs that yield complete aero-elastic equations in the conventional state space form, as well as sensor output equation coefficients and loads equations.

The FLEXSTAB program is beginning to be used widely in industry yet few, if any, attempts have been made to validate or compare the results of FLEXSTAB with mathematical models derived from actual flight test data. It was felt important to validate the analytically derived model in order to predict whether or not control laws designed for structural mode suppression purposes can use the analytically obtained model or whether flight testing is required to provide the data needed for a parameter identification of the aero-elastic vehicle.

A mathematical model derived from flight test data is likely to be more accurate than one computed analytically. However, a mathematical model may require the identification of several hundred parameters, depending upon the number of elastic degrees of freedom of motion that are to be individually retained in the model. No system identification technique can at this time be expected to handle the computational load required to simultaneously identify more than 30 or 40 parameters. Therefore, a technique was developed for a partial or sequential identification of the system dynamics. This technique and partial results are described in Section III of this report.

2.3 STRUCTURAL MODE CONTROL OR SUPPRESSION

Feedback control for the purpose of altering the elastic degrees of freedom of motion of a flight vehicle is feasible. A survey of past programs devoted to this objective indicates success (References 1, 2, 3, 4) when criteria were used that were intuitively satisfying. The general objective was to increase the damping ratio of structural modes or to suppress the motion at one or several body or wing stations on the vehicle. These designs generally minimize the elastic effects at one station on the vehicle (usually the pilot station); and this is acceptable for military aircraft. Because some of the damping ratios have been increased, the elastic effects have also been reduced at most other stations on the airplane. For commercial aircraft, however, it appears more desirable to be able to suppress the motion not only

---

1. Konar, A. F., Stone, C. R., Mahesh, J. K. and Hawk, M., "Active Control Synthesis for Flexible Vehicles, Vol. I and II KONPAC", Honeywell, Incorporated, AFFDL-TR-75-146, April 1976.

2. Burris, P. M. and Bender, M. A., "Aircraft Load Alleviation and Mode Stabilization (LAMS)", AFFDL-TR-68-163, November 1969.

3. Burris, P. M. and Bender, M. A., "Aircraft Load Alleviation and Mode Stabilization (LAMS) Flight Demonstration Test Analysis", AFFDL-TR-68-164, December 1969.

4. Stockdale, C. R. and Poyneer, R. D., "Control Configured Vehicle Ride Control System (CCV RCS)", Air Force Flight Dynamics Laboratory Report AFFDL-TR-73-83, July 1973.

at the pilot's station, but uniformly along the remainder of the fuselage and wings as well.

The theory of elastic structures indicates that the elastic mode frequencies and damping ratios should increase as the structure is made increasingly rigid. Criteria for design of a control system for structural mode control should reflect this fact. Linear optimal techniques have been used to derive a criterion,involving only the eigenvalues of the structure, that will produce a family of approximations to a more rigid vehicle in a quadratic integral error squared sense. This criterion is independent of sensors or sensor locations and independent of controllers or their location on the vehicle. This is also felt to be correct because the description or definition of an elastic structure should not be dependent upon the particular instrument used to sense the motion of that structure or the inputs used to excite or suppress the oscillations of the structure.

The criterion will define how the eigenvalues of the elastic structure should be altered to produce a better approximation to a rigid vehicle. The control problem to produce the desired changes in damping ratio and frequency is therefore one of relatively simple and straightforward pole placement. The theory of pole placement is well developed and has been reported upon extensively in the literature.

Complete pole placement requires, with few exceptions, complete state feedback using one controller or equivalent. However, it is unreasonable to expect to mechanize a control system using two sensors for each degree of freedom of elastic motion. Techniques are presented in this report that allow the designer to generate compensation networks that will serve the same purpose as individual states. The technique is a simplified version of the observer theory of Luenberger, (Reference 5), that allows for output rather than state feedback. The simplification described in this report need not

---

5. Luenberger, D. G., "Observers for Multivariable Systems", IEEE Transactions on Automatic Control, Vol. AC-11, pp. 190-197, April 1966.

involve measurements of the control input or intercouplings among the measured outputs. Section VI of this report describes these techniques.

2.4 GUST ALLEVIATION

Structural mode control is a form of gust alleviation. Feedback regulation of the elastic deformation of a vehicle to produce the effect of increased mode damping and natural frequencies will significantly alter the power spectrum of the response of the vehicle in turbulence and not as much power will appear at the mode frequencies. The increased damping of the modes will reduce the maximum deflections at the modal frequencies. An increase in modal frequencies will generally reduce the excitation to those structural modes because the power spectrum of turbulence "falls off" fairly rapidly with increased frequency.

In addition to structural mode control, this program has investigated techniques using direct gust measurements. These gust measurements are then used to command the control surfaces so as to generate forces and moments on the vehicle that counter or cancel the forces and moments produced by the turbulence. Mathematically, this can be described very simply as follows:

If the motion is described by the linearized equations

$$\dot{x} = Fx + Gu + Jv_g$$

where F represents the matrix of stability derivatives, G the matrix control derivatives, J the matrix of gust effective terms with u the control vector and v_g the gust, then the control surfaces should be commanded by the control law

$$u_c = -G^{-1}Jv_g$$

If this control law is mechanized perfectly, then $x(t) = \dot{x}(t) = 0$ after initial condition transients subside and the aircraft is unaffected by turbulence.

A study of this approach to gust alleviation is described in Section IV. An alternate approach, using feedback to have the effect of reducing L_α and desensitizing the response of the vehicle to gusts was considered and dismissed as a practical approach.

2.5 MANEUVER LOAD CONTROL

An actively controlled aircraft will have more control surfaces than is necessary to maneuver the vehicle. Therefore, more can be done than merely fly through the air. The objective in maneuver load control system design is to optimally connect or command these surfaces in such a way that the vehicle flying qualities are preserved or enhanced and at the same time the wing bending moments, torsion, maneuver drag or other detrimental effects that accompany flight in the atmosphere are minimized. A trade-off design procedure, based upon the established and accepted flying qualities criteria, MIL-F-8785(B), and incorporating the desire to minimize wing bending moments has evolved from the research of this program. The resulting control laws can be mechanized either as feedback control (implicit model following) or as command augmentation (explicit model following). Command augmentation was chosen for two reasons:

1. The system was more easily simplified from the complete optimal to a good, lower order suboptimal approximation and

2. If mechanized as feedback control it would have to be integrated with the structural mode control system. Physical disassociation with the structural mode control system allows for a more functionally simple system and complete separation of the design and analysis of the three functional components — structural mode control, gust alleviation and maneuver load control.

2.6 COMPLETE SYSTEM CONFIGURATION

Figure 1 shows the system configuration for structural mode control, gust alleviation and maneuver load control.

Each part of the system is independent in the sense that each part has a specific function and specific criteria and can be designed and analyzed separately. It appears to be a natural, systematic division. Each part of the system can be operated separately and the sum of the parts is only marginally synergistic. This approach to active control system design produces the most straightforward procedure, allowing for clear and easy assessment or evaluation of every part of the system. With this approach, it is possible to readily examine each part and determine whether or not the benefits derived from the implementation outweigh the cost and complexity of mechanization. At this point in time, there is no reason to believe that a comprehensive system designed from a synergistic point of view would be more effective or more desirable.

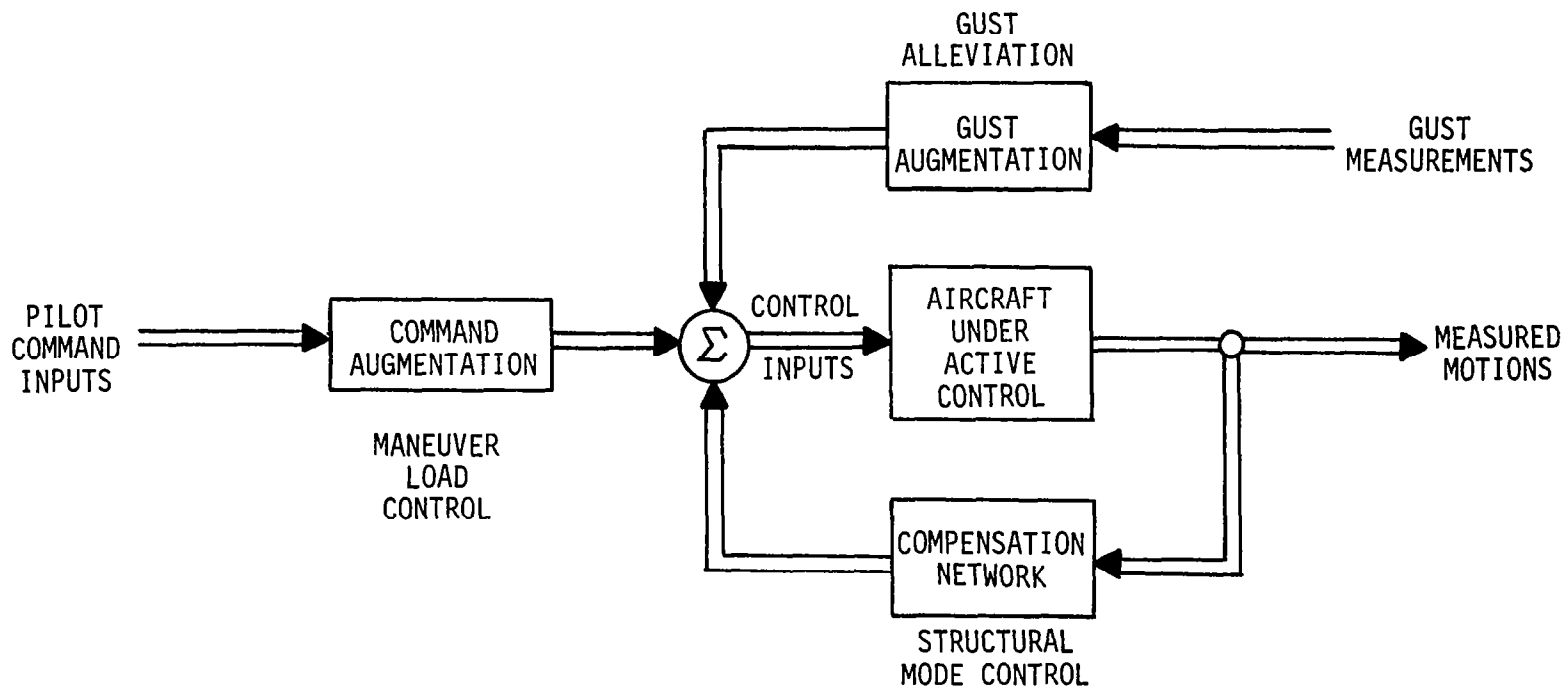

Figure 1 ACTIVE CONTROL SYSTEM CONFIGURATION

SYSTEM IDENTIFICATION AND MODELING

3.1 IDENTIFICATION OF THE ELASTIC EQUATIONS OF MOTION

A major portion of this program involved the analytic prediction of the elastic equations of motion of the TIFS airplane. A description of the FLEXSTAB computations carried out for TIFS is given in Reference 6. The flight conditions for which the computations were performed are given in Appendix B along with the results of the computations. For many of the design examples shown in this report, the analytically computed TIFS equations of motion were used. However, it was felt that accurate control law generation and computation required more accurate definitions of the aero-elastic equations than could be obtained from FLEXSTAB.

Control law development and definition for structural mode control requires data in one of two forms, 1) transfer function form if the control system design is to be done in a classical format using root locus plots or equivalent or (2) in equations of motion or state space format if optimal or state space techniques are to be used. Because this report is concerned more with the advanced or optimal control approach to control system design, it was felt necessary to evolve a procedure for system identification that would result in a complete set of equations of motion, the state space form. It was expected that control laws generated using analytically obtained data and control laws using equations of motion obtained from the in-flight tests of the TIFS vehicle could be directly compared in flight. This would have been the objective of a flight program.

---

6. Andrisani, D., Daughaday, H., Dittenhauser, J. and Rynaski, E., "The Total In-Flight Simulator (TIFS)." NASA CR-158965, 1978.

3.2 DATA SOURCES

A number of data sources were available to help in the definition of the flexible equations of motion of the TIFS vehicle, but each source is incomplete and has its own inherent degree of accuracy. Each source constitutes a valuable element of the entire picture of the flexible vehicle and each contributes to a more accurate description of the aircraft, but none by itself can be relied upon to serve as a complete mathematical model of the TIFS to develop ACT control system configurations. The problem is to be able to combine data sources in such a way that uses all the data and uses it in such a way that the resultant model can be updated sequentially and systematically as increasingly more accurate information becomes available, primarily through analysis of flight test data. The available contributory data sources are:

1. Complete equations of motion were calculated using the level 2.01 FLEXSTAB program. Mass and stiffness data supplied by Convair for the Convair 580 and modified by Calspan to conform with the TIFS configuration as well as TIFS geometry information was supplied for the FLEXSTAB program.

2. Ground vibration test data was available from the original TIFS development period.

3. Step and doublet elevator and direct lift flap inputs were applied to the TIFS aircraft during flight tests of the vehicle. These flight records were then used to obtain estimates of the quasi-static rigid body stability and control derivatives for TIFS.

4. Bode plot information was obtained from the two TIFS data flights No. 488 and 489 conducted in conjunction with this program. Discrete sinusoidal inputs varying in frequency from 1 Hz to 12 Hz were used to drive the direct lift flaps and the

elevator servos. Measurements were taken in still air of the elevator or direct lift flap surface positions, an angle of attack vane, α_v, a rate gyro mounted near the TIFS c.g., q_{cg}, and six linear accelerometers located at the simulation cockpit pilot location, n_{z_p}, the aircraft c.g., $n_{z_{cg}}$, the starboard wing tip, $n_{z_{WT}}$, the tail cone, $n_{z_{TC}}$, the starboard horizontal tail, $n_{z_{HT}}$, and forward mid-aft mid-wing stations, $n_{z_{HW_1}}$, and $n_{z_{WT_2}}$. Figure 2 is a photograph of the TIFS airplane, while the location of the angle of attack vane, the rate gyro, and the normal accelerometers are indicated in Figure 3. A compilation and description of these and all other TIFS instrumentation, gust computations and the recording system is presented in Reference 6.

As could be expected, significant differences existed between Bode plot information obtained analytically as a result of the FLEXSTAB computations and Bode plots measured directly during the flight tests of TIFS. Seven modes of elastic motion were retained from the FLEXSTAB computations, with frequencies ranging up to about 18 Hz, yet the Bode plots obtained in flight contained information only to 12 Hz, so the measured data does not contain significant higher mode information. The FLEXSTAB computations resulted in conventional time domain equations while the measured data was in frequency domain, Bode plot form.

The problem is to combine or use all the data sources available to produce as accurate a mathematical model of the flexible equations of motion of TIFS as possible. The experimental data is to be considered most accurate, although incomplete, so some FLEXSTAB results will be used to supplement the measured data, i.e. to supply that information not obtained in flight. The approach taken was to transform the FLEXSTAB results into a phase variable or transfer function form, then replace the characteristic polynomial obtained from FLEXSTAB with the characteristic polynomial obtained from the flight measured Bode plot information. In addition, the numerator

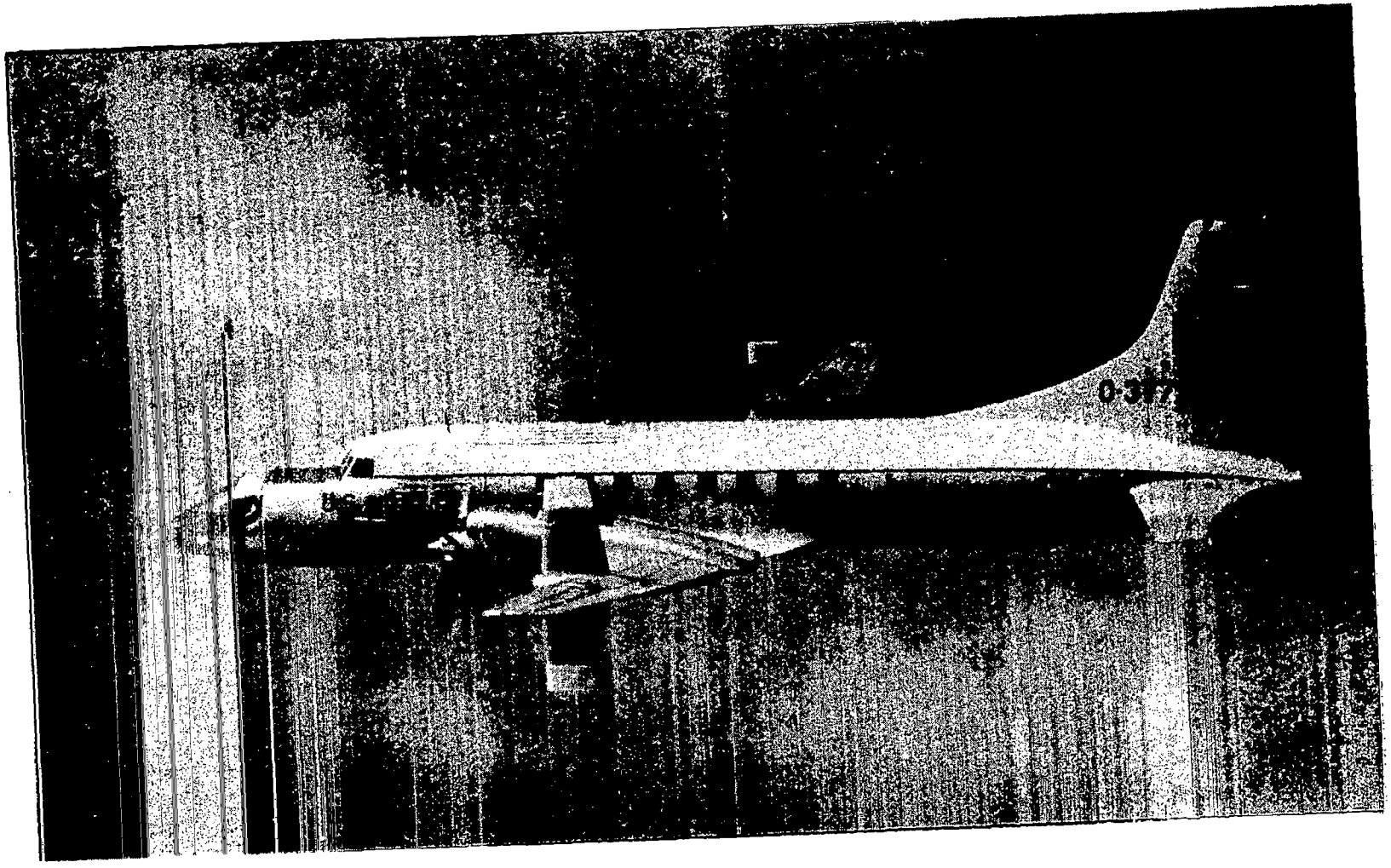

Figure 2 THE USAF TOTAL IN-FLIGHT SIMULATOR (TIFS)

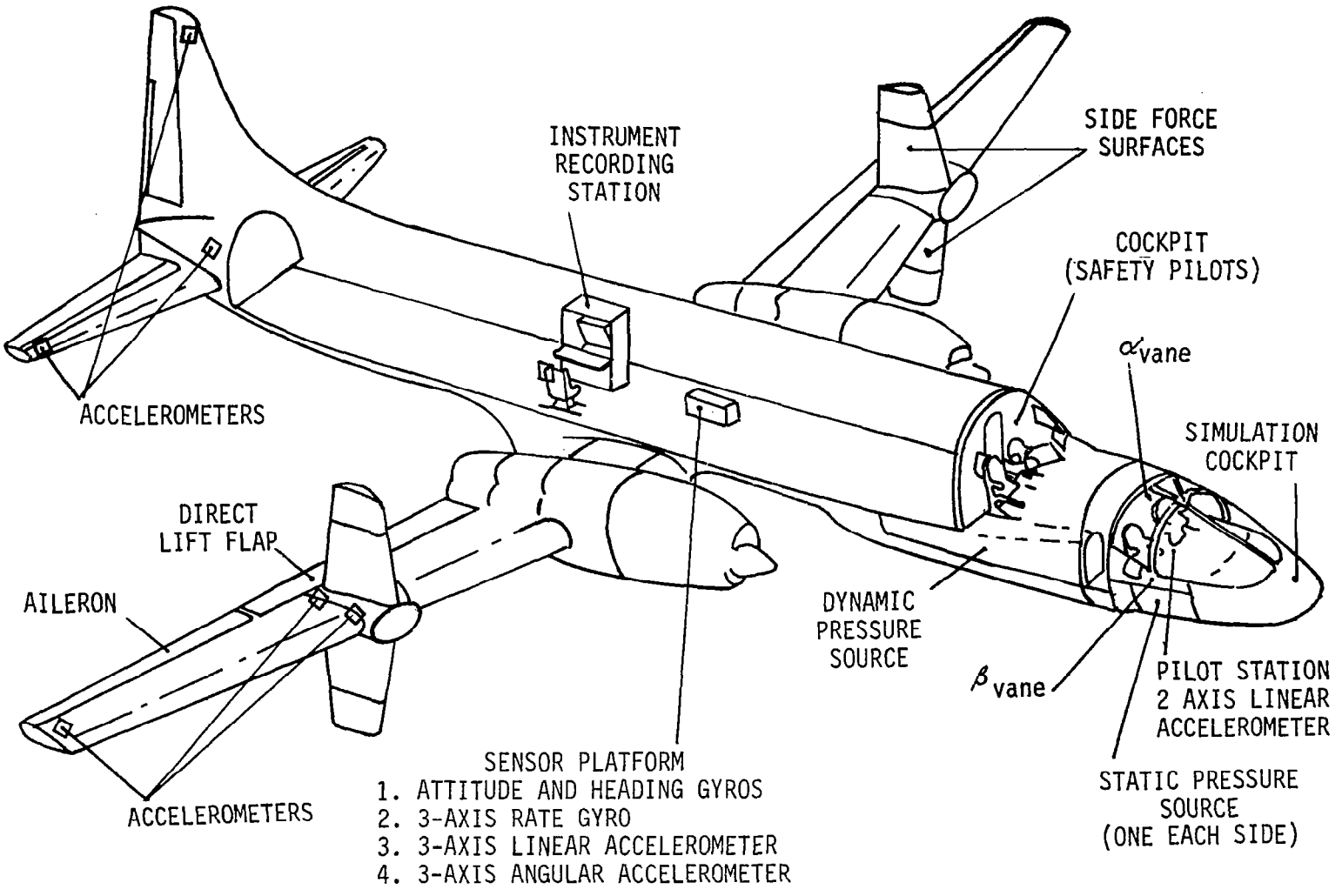

Figure 3 TIFS INSTRUMENTATION COMPLEMENT

polynomials of the in-flight estimated transfer functions were used to replace selected rows of the phase variable transformation matrix. This procedure is outlined below.

3.3 PROCEDURE FOR COMBINING DATA SOURCES

3.3.1 Manipulate FLEXSTAB Computational Results Into a State Space Format

The FLEXSTAB equations of motion were obtained in the general form

$$A\dot{x} = Bx + Cu \tag{3-1}$$

Simply by pre-multiplying Equation (3-1) by A^{-1}, the equations become

$$\dot{x} = Fx + Gu \tag{3-2}$$

where $F = A^{-1}B$ and $G = A^{-1}C$. Equation (3-2) is the conventional state space form. The state variables and control variables have been defined as

$$x^T = [\Delta V, \Delta\alpha, q, \Delta\theta, \eta_1, \eta_2, \eta_3, \eta_4, \eta_5, \eta_6, \eta_7, \dot{\eta}_1, \dot{\eta}_2, \dot{\eta}_3, \dot{\eta}_4, \dot{\eta}_5, \dot{\eta}_6, \dot{\eta}_7]$$

$$u^T = [\delta_3, \delta_e, \delta_{CA}]$$

The η_i are the normal mode variables and the $\dot{\eta}_i$ are the time derivatives. The control variables are δ_{CA}, the collective aileron deflection, δ_3, the direct lift flap deflection and δ_e, the elevator deflection.

3.3.2 Substitute In-Flight Identified Rigid Body Stability and Control Derivatives

The state space equations of motion, Equation (3-2), can be partitioned as follows:

$$\begin{bmatrix} \dot{x}_1 \\ \hline \dot{x}_2 \end{bmatrix} = \left[\begin{array}{c|c} F_{11} & F_{12} \\ \hline F_{21} & F_{22} \end{array}\right] \begin{bmatrix} x_1 \\ \hline x_2 \end{bmatrix} + \begin{bmatrix} G_1 \\ \hline G_2 \end{bmatrix} u \qquad (3\text{-}3)$$

(3-4)

where $x_1^T = [\Delta V, \Delta\alpha, q, \Delta\theta]$, the rigid body variables and x_2^T represents the remaining normal mode variables and derivatives. During steady state maneuvers, it can be assumed that the derivatives of the normal mode variables are zero, i.e. $\dot{x}_2 = 0$ and the equations can be reduced in order as follows:

$$\begin{bmatrix} \dot{x}_1 \\ \hline 0 \end{bmatrix} = \left[\begin{array}{c|c} F_{11} & F_{12} \\ \hline F_{21} & F_{22} \end{array}\right] \begin{bmatrix} x_1 \\ \hline x_2 \end{bmatrix} + \begin{bmatrix} G_1 \\ \hline G_2 \end{bmatrix} u \qquad (3\text{-}5)$$

(3-6)

Solving Equation (3-6) for x_2 yields

$$x_2 = -F_{22}^{-1} F_{21} x_1 - F_{22}^{-1} G_2 u \qquad (3\text{-}7)$$

and substituting into Equation (3-5) yields

$$\begin{aligned} \dot{x}_1 &= [F_{11} - F_{12} F_{22}^{-1} F_{21}] x_1 + [G_1 - F_{12} F_{22}^{-1} G_2] u \\ &= \hat{F} x_1 + \hat{G} u \end{aligned} \qquad (3\text{-}8)$$

The quasi-static stability and control derivatives that are obtained using time domain advanced parameter identification techniques are those of Equation (3-8) if the model form is specified as a rigid body model. Normally, the corrections to rigid body terms given by $-F_{12} F_{22}^{-1} F_{21}$ and $-F_{12} F_{22}^{-1} G_2$ are small, and to test this assumption, the complete aero-elastic equations were gradually reduced in order using Equation (3-8) to determine how the rigid body results change as fewer and fewer normal modes were included in the mathematical description of the TIFS airplane. These results are shown in Appendix A. The short period and phugoid dynamics changed negligibly between a completely rigid and a quasi-static vehicle description.

It was assumed then that the rigid body stability and control derivatives calculated by FLEXSTAB could be replaced with values obtained in flight using advanced parameter identification techniques. Multi-iterated, extended Kalman filter parameter identification methods yielded accurate estimates.

The first modification to the FLEXSTAB results was to replace the rigid body stability and control derivatives with the quasi-static values obtained by parameter identification from in-flight data. These results are shown in Table B-10 of Appendix B.

3.3.3 Modification of Mass and Stiffness Distributions

Table A-1 of Appendix A shows the in-vacuum normal mode frequencies and damping ratios computed by FLEXSTAB and the normal mode frequencies and damping ratios obtained from the original ground vibration tests of the TIFS aircraft. The agreement is reasonable, but it was decided to apply a correction to the TIFS mass and stiffness distributions in such a way that closer correspondence was obtained between the ground vibration test results and the calculated FLEXSTAB mode frequencies. The normal mode frequencies and damping ratios calculated from FLEXSTAB after the modifications are also shown in Table A-1 of Appendix A.

3.3.4 Addition of Servo Dynamics to FLEXSTAB Equations

The Bode plot data obtained from the flight records included measurements of the command input to the elevator and direct lift flap servos as well as direct lift flap and elevator surface position. Examination of the records indicated that the servos can be approximated by first order mathematical models and expressed in the usual form

$$\dot{u} = F_1 u + G_1 u_c \tag{3-9}$$

and appended to the calculated FLEXSTAB equations

$$\begin{bmatrix} \dot{x} \\ \dot{u} \end{bmatrix} = \begin{bmatrix} F & G \\ 0 & F_1 \end{bmatrix} \begin{bmatrix} x \\ u \end{bmatrix} + \begin{bmatrix} 0 \\ G_1 \end{bmatrix} u_c \tag{3-10}$$

or $$\dot{x}_A = F_A x_A + G_A u_A \tag{3-11}$$

An estimate of the servo bandwidth for a direct lift flap was also made and added in Equation (3-10) so the state and control vectors become:

$$\left[x_A^T \right] = \left[\Delta V, \Delta\theta, q, \Delta\alpha, \delta_e, \delta_z, \delta_{CA}, \eta_1 \cdots \eta_7, \dot{\eta}_1 \cdots \dot{\eta}_7 \right] \tag{3-12}$$

$$\left[u_A^T \right] = \left[\delta_{e_c}, \delta_{z_c}, \delta_{CA_c} \right] \tag{3-13}$$

Equations (3-12) and (3-13) indicate first order servo dynamics for the direct lift flap and the elevator servos. Both first and second order approximations to the control surface servo dynamics were made. These approximations are given in Appendix D. If second order servos were to be incorporated into the state space equations, then the states $\dot{\delta}_e$ and $\dot{\delta}_z$ would have had to be included in Equation (3-12).

3.3.5 Transform to a Measurable Set

There is nothing unique or even particularly desirable about the particular set of state variables of Equation (3-12). The normal mode variables (η_i) and derivatives ($\dot{\eta}_i$) cannot be measured directly in flight. Instead, functions of particular variables including the normal mode variables, are measured with accelerometers, gyros and air data vanes, and the outputs of these instruments were recorded during the TIFS flights. An output equation was calculated using the FLEXSTAB program to reflect the actual measurements used in flight. Ten direct measurements of the TIFS dynamic motions were made in flight, so the output matrix is of dimension 10 x 21. It is desirable to transform the original state vector into a new space that includes the measured outputs as variables of the new space, so an identity matrix of dimension 11 was appended to the output matrix as

$$z = Hx \tag{3-14}$$

where

$$H = \begin{bmatrix} H'_{10\times 21}\ (\text{sensor outputs}) \\ \hline 0 \;\vdots\; I_{11\times 11} \end{bmatrix} \tag{3-15}$$

and

$$z^T = \left[\Delta V, \Delta\theta, q, \Delta\alpha, \delta_e, \delta_z, \delta_{CA}, n_{zp}, n_{zcg}, n_{zWT}, n_{zTC}, n_{zHT}, n_{zWT}, \eta_4 \cdots \eta_7, \dot{\eta}_4 \cdots \dot{\eta}_7\right] \tag{3-16}$$

The matrix H is now a square, non-singular matrix and the aero-elastic equations can be transformed into a new basis or state space set in z, as

$$\dot{z} = HF_A H^{-1} z + HG_A u_c \tag{3-17}$$

This equation now yields the FLEXSTAB equations of motion with the sensor outputs actually used during the flight test program represented directly as states of the aero-elastic equations of motion of the TIFS vehicle. The sensor output equations, defining the matrix H', is given in Appendix A.

3.3.6 Reduce Dimensionality of the Elastic Equations

Two of the seven modes computed by FLEXSTAB had natural frequencies in the neighborhood of 18 Hz, well above the range of input frequencies for the experimentally obtained Bode plots and significantly higher than the bandwidth of the direct lift flap servo (approximately 9 Hz) or that of the elevator, which was planned to have a bandwidth of approximately 6 Hz. A feedback control system designed for structural mode control will have very minimal effect on those modes whose frequencies are significantly higher than the bandwidth frequency of the control surface servos, so it was decided to delete from the elastic vehicle description the two highest frequency modes of elastic motion using the residual flexibility method of dimensionality reduction given by Equation (3-8).

The resulting equations of motion will be expressed in the following form

$$\dot{z}_1 = A z_1 + B u$$

$$= A z_1 + B_1 \delta_{z_c} + B_2 \delta_{e_c} + B_3 \delta_{CA_c} \tag{3-18}$$

Matrix A of Equation (3-18) is of dimension 17 x 17 when the two highest frequency modes are deleted from Equation (3-16).

The discrete sinusoidal inputs to the TIFS airplane were injected into the direct lift flap servo and the elevator servo separately. So for any set of flight test data, only one servo was commanded and the other servo commands were zero. The mathematical model of TIFS for one command input, δ_{z_c}, for instance, can be represented by the equation

$$\dot{z}_1 = A_1 z + B_1 \delta_{z_c} \tag{3-19}$$

where matrix A is of dimension 15 x 15 and

$$z_1^T = \left[\Delta V, \Delta\theta, q, \Delta\alpha, \delta_z, n_{z_p}, n_{z_{cg}}, n_{z_{WT}}, n_{z_{TC}}, n_{z_{HT}}, n_{z_{MW}}, \eta_4, \eta_5, \dot{\eta}_4, \dot{\eta}_5 \right] \tag{3-20}$$

A separate and different mathematical model can, of course, be easily obtained for the other two command inputs, δ_{e_c} and $\delta_{c_{AC}}$, shown in Equation (3-18).

3.3.7 Transform to Phase Variable Form

The mathematical model representation of the TIFS aircraft given by Equation (3-19) can be transformed into the phase variable or transfer function form. This form defines a new basis for the equations of motion (3-19) such that each of the elements of the resulting system matrix and

transformation matrix can be directly identified as either a coefficient of the characteristic polynomial of Equation (3-19) or of the numerator coefficients of the transfer functions of the states of Equation (3-19) with respect to the command input to the direct lift flap.

The purpose for doing this is that the phase variable form yields transfer functions. The flight data yielded Bode plots for all the measurable quantities. Because Bode plots can be obtained directly from transfer functions, or vice versa, the phase variable form of a mathematical model for TIFS is directly compatible with the data taken during flight.

The phase variable form is defined as follows. A transformation T is defined that transforms the state vector of Equation (3-19) into an orthogonal set yielding a system description

$$\dot{y} = F_o y + G_o \delta_{3c} \tag{3-21}$$

by a canonical transformation

$$z_1 = T_{\delta_3} y \tag{3-22}$$

The system matrices are of the form

$$F_o = \begin{bmatrix} 0 & 1 & 0 & 0 & \cdots & 0 & 0 \\ 0 & 0 & 1 & 0 & \cdots & 0 & 0 \\ \vdots & & \ddots & \ddots & & & \vdots \\ 0 & & & & & & 0 \\ 0 & \cdots & & & & 0 & 1 \\ -d_0 & -d_1 & \cdots & & & & -d_{n-1} \end{bmatrix} \qquad G_o = \begin{bmatrix} 0 \\ \vdots \\ 0 \\ 1 \end{bmatrix} \tag{3-23}$$

The coefficients α_i of the last row of F_o are obtained from the coefficients of the characteristic polynomial of the system matrix of Equation (3-19), i.e.

$$|Is - A_1| = s^n + \alpha_{n-1} s^{n-1} + \alpha_{n-2} s^{n-2} \cdots \alpha_1 s + \alpha_0 \qquad (3\text{-}24)$$

The transformation is of the form

$$T_{\delta_{3_c}} = \begin{bmatrix} t_{11} & t_{12} & \cdots & t_{1n} \\ t_{21} & & & \vdots \\ \vdots & & & \vdots \\ \vdots & & & \vdots \\ \vdots & & & \vdots \\ \vdots & & & \vdots \\ t_{n_1} & \cdots & \cdots & t_{n_n} \end{bmatrix} \qquad (3\text{-}25)$$

The rows of the square, non-singular transformation matrix T are obtained from the coefficients of the numerators of the transfer functions of the state variables of Equation (3-19). For instance, the numerators of the transfer functions of the first two state variables ΔV and $\Delta\theta$ of Equation (3-19) with respect to the direct lift servo command input can be represented by the expression

$$N\left(\frac{\Delta V}{\delta_{3_c}}(s)\right) = t_{1n} s^{n-1} + t_{1n-1} s^{n-2} + \cdots t_{12} s + t_{11} \qquad (3\text{-}26a)$$

$$N\left(\frac{\Delta\theta}{\delta_{3_c}}(s)\right) = t_{2n} s^{n-1} + t_{2n-1} s^{n-2} + \cdots t_{21} s + t_{21} \qquad (3\text{-}26b)$$

In general, the transformation T can be found directly by using the expression

$$T_c S = |Is - A_1|[Is - A_1]^{-1} B_1 \qquad (3\text{-}27)$$

where $S^T = [1, s, s^2 \cdots s^{n-1}]$ and s is the Laplace transform variable.

This is the general expression that defines the numerator polynomials of the transfer functions of the states of Equation (3-19).

3.3.8 Obtain Estimates of Transfer Functions

To adequately and accurately describe the dynamical equation of motion of the TIFS or any other elastic vehicle, including the first five or six elastic modes of motion requires a "nearly full" system matrix such as that of Equation (3-19) of dimension 15 x 15, or approximately 200 parameters. The best time domain techniques available, such as weighted least squares, minimum variance or maximum likelihood are capable, at this point in time, of estimating only about 30-40 parameters with any degree of accuracy. Not only does the computational load become overwhelming, but the probability of designing an optimal input to render each parameter identifiable would be of a complexity completely beyond the scope of the present program and would, in fact, require information that we are trying to obtain, the values of the elements of the aeroelastic equations of motion. If such an input design were attempted, it is clear that the input should contain a spectrum that spans the frequency range of the elastic mode frequencies, similar to the frequency sweep or Bode plot data that was obtained for TIFS.

The Bode plot or "frequency sweep" data obtained during the two data flights of the TIFS airplane can be used to estimate transfer functions of the sensor output with respect to the servo command input. Direct and straightforward techniques have been developed by Levi (Reference 7) and Sanahanon and Koerner (Reference 8) to obtain estimates of the coefficients of a transfer function. These techniques have been found to work quite well if transfer functions to several Bode plots are estimated simultaneously with

---

7. Levy, E. C., "Complex Curve Fitting", IEEE Transactions on Automatic Control, Vol. AC-4, May 1949.

8. Sanahanon, C. K. and Koerner, J., "Transfer Function Synthesis as a Ratio of Two Complex Polynomials", IEEE Transactions on Automatic Control, Vol. AC-8, January 1963.

the constraint that all the transfer functions have the same denominator polynomial or characteristic equation. If this is not done, the technique will often produce estimates that indicate an unstable elastic mode.

If two transfer functions of the Bode plot data are identified simultaneously, a maximum of only 45 parameters need to be obtained at one time. Therefore, the problem associated with many of the newer identification techniques is avoided and dimensionality does not become a prohibiting consideration.

Transfer function estimates for the seven measured quantities were obtained for both the δ_{3_c} and the δ_{e_c} inputs to the TIFS aircraft, and a summary of the technique used and the results obtained are given in Appendix D. These estimates were compared with FLEXSTAB results, and the results differ considerably. The estimates obtained from the flight records are considered to be more accurate than the FLEXSTAB results. The FLEXSTAB results, however, were very important to the entire process because these computations provided important information to estimate the effects of unsteady flow and the number of elastic modes within a given frequency band, as well as good estimates of the mode frequencies. The model computations provided important information to estimate the number of elastic modes within a given frequency band, as well as good estimates of the mode frequencies. In other words, the model form but not the particular model coefficients seemed to be accurately predicted by FLEXSTAB. Model form is considered to be as important and as difficult a result to obtain as the actual values of the parameters of the model that can accurately reproduce the flight results, so FLEXSTAB results are very useful.

3.3.9 Replace FLEXSTAB Phase Variable System Matrix

Groups of transfer functions for both the direct lift flap (δ_{3c}) input and the elevator (δ_{ec}) input were estimated using the techniques described in References 7 and 8. The denominator polynomial or characteristic

equation among groups of transfer functions or between command input varied little. With the exception of the servo dynamics, average values of the coefficients were obtained weighted by engineering judgment according to the observed quality of the data recorded from each of the sensors. This data yielded a phase variable system matrix F_{o_m} of the form of Equation (3-22) but with updated, more accurate coefficients.

$$F_{o_m} = \begin{bmatrix} 0 & 1 & 0 & & 0 \\ \cdot & & \ddots & & \cdot \\ \cdot & & & \ddots & \cdot \\ \cdot & & & & \cdot \\ 0 & & & & \cdot \\ -d_0 & -d_1 & \cdot & \cdot & -d_n \end{bmatrix} \qquad (3\text{-}28)$$

3.3.10 Replace Selected Rows of Phase Variable Transformation

The identification of the transfer functions of the seven measured quantities $(q_m, n_{\zeta p_m}, n_{\zeta cg_m}, n_{\zeta WT_m}, n_{\zeta HT_m}, n_{\zeta TC_m}, n_{\zeta MW_m})$ yielded not only the common transfer function poles but the transfer function zeros of each of the transfer functions of the measured quantities. Since the coefficients of the numerators of these transfer functions are elements of the phase variable transformation, they can be expressed in the form

$$\zeta_m = T_m y \qquad (3\text{-}29)$$

where $\left[\zeta_m^T\right] = \left[q_m, n_{\zeta p_m}, n_{\zeta cg_m}, n_{\zeta WT_m}, n_{\zeta TC_m}, n_{\zeta HT_m}, n_{\zeta MW_m}\right]$

and T_m is a 7 x 15 matrix.

These seven rows of a phase variable transformation were simply substituted for the corresponding seven rows of the calculated transformation T_c to yield a square, non-singular matrix of the form

$$\begin{bmatrix} z_m \\ \hline z_{c_1} \end{bmatrix} = \begin{bmatrix} T_m \\ \hline T_{c_1} \end{bmatrix} y \tag{3-30}$$

or $$z_{mc} = T_{mc}\, y$$

where the notation T_{mc} indicates a mix of data, partly calculated by analytic methods and partly estimated from flight test data analysis. This transformation can then be used to transform back to the form of the equations of motion given by Equation (3-19). These equations, now containing mixed measured and calculated data, are given by

$$\dot{z}_{mc} = T_{mc}\, F_{o_m}\, T_{mc}^{-1}\, z_{mc} + T_{mc}\, G_o\, \delta_{z_c} \tag{3-31}$$

where $$\left[z_{mc}\right] = \left[\Delta V,\ \Delta\alpha,\ q_m,\ \Delta\theta,\ \delta_{z_m},\ n_{z_{pmc}},\ n_{z_{cg_m}},\ n_{z_{WT_m}},\ n_{z_{TC_m}},\ n_{z_{HT_m}},\ n_{z_{MW_m}},\ \eta_4,\ \eta_5,\ \dot{\eta}_4,\ \dot{\eta}_5\right]$$

Certainly if a transfer function of one of the measured variables were calculated from Equation (3-31), it would be identical to the transfer function estimated from flight.

There is no way known at this time to transform Equation (3-31) back to the original form of Equation (3-4), nor is there any known practical reason for wanting to transform back to this state space set. The in-vacuum mode variables η_i and their derivatives $\dot{\eta}_i$ are not directly measurable and cannot be used directly for control system design purposes. If they are to be obtained, they must be calculated by using the transformation of Equation (3-14), and accurate knowledge of the transformation H implies accurate knowledge of the mode shapes and slopes. If the number of direct and independent measurements of the dyanmic motions of the airplane is equal to the number of states used to define the vehicle dynamics, the equations, once identified, could then be transformed into a normal mode form similar to the form of Equation (3-10). The resulting transformation, $\hat{H}$, would then define the mode shapes and slopes.

Equation (3-31) represents a method for combining calculated and measured data, updating the analytically calculated elastic properties gradually as flight data becomes available. This procedure also negates the need for large numbers of sensors to collect data to obtain estimates of the elastic vehicle equations of motion that can be expected to be more accurate than the analytically calculated data. The data estimates can be improved even further by combining the results obtained with the elevator command input.

3.3.11 Repeat Steps 3.3.6 - 3.3.10 With Elevator Input, Then Combine Systems

Equation (3-31) expresses a mixed measured-calculated model of the aero-elastic equations of motion of the TIFS airplane. If the procedure defined by steps 3.3.6 - 3.3.10 are repeated, but this time using the flight data obtained through an elevator rather than direct lift flap input, a second measured-calculated transformation $T_{mc\delta_e}$ will be obtained and a second set of equations of motion of the same form as defined by Equation (3-31) can be obtained as

$$\dot{z}_m = T_{mc\delta_e} F_{om} T_{mc\delta_e}^{-1} z_{mc} + T_{mc\delta_e} G_o \delta_{e_c} \qquad (3\text{-}32)$$

The system expressed by Equations (3-31) and (3-32) can be combined to further improve the parameter estimates. A minor modification is required because the Equation (3-31) contains direct lift flap actuator dynamics but no elevator actuator dynamics and with Equation (3-32) the reverse is true. This minor modification involves only the definition of a system matrix that includes both servo dynamics.

When this is done, the resulting phase variable transformations T_{δ_z} and T_{δ_e} will each contain a row of zero or null elements. The row of T_{δ_e} corresponding to the numerator of the $\delta_z/\delta_{e_c}(s)$ transfer function will be zero as will the row of T_{δ_z} corresponding to the numerator of the

$\delta_e/\delta_{z_c}(s)$ transfer function. Because a row of null elements produces a singular matrix, neither of the two matrices can be used as a similarity transformation, but their sum will be non-singular. The multicontroller equations of motion can be obtained by combining as follows:

$$\dot{z}_{mc} = \left(T_{mc\delta_z} + T_{mc\delta_e}\right) F_{o_m} \left(T_{mc\delta_z} + T_{mc\delta_e}\right)^{-1} z_{mc} + T_{mc\delta_z} G_o \delta_{z_c} + T_{mc\delta_e} G_o \delta_{e_c} \quad (3\text{-}33)$$

It was possible to write the accelerometer output equations in state space form directly rather than incorporating an output equation, because the servo bandwidth was assumed to be finite, and the control deflection became state variables. Each control input can be used to continuously improve the system identification because the transformation additive process indicated by Equation (3-33) can be continued indefinitely. In general, for p control inputs to the vehicle, a general form of the equation becomes

$$\dot{z} = \left(\sum_{i=1}^{p} T_i\right) F_o \left(\sum_{i=1}^{p} T_i\right)^{-1} z + T_1 G_o u_1 + T_2 G_o u_2 + \cdots T_p G_o u_p \quad (3\text{-}34)$$

By using Equation (3-33), i.e. by combining data from several different excitation sources, the identifiability of the system is likely to be significantly improved. Often one mode is only nominally excited by a particular input, a minimal controllable situation, yet that mode is strongly excited by the second controller. So information that cannot be accurately obtained by estimating one phase variable transformation can be obtained by estimating two or more transformations and combining them according to Equation (3-34).

3.3.12 Example of the Use of Phase Variable Transformations

The rigid, three degree-of-freedom equations of motion of the TIFS are given by

$$\dot{V} = -\frac{g\theta}{57.3} - D_V \Delta V - D_\alpha \Delta\alpha - D_{\delta_e}\delta_e - D_{\delta_z}\delta_z$$

$$\dot{q} = M_q q + M_V \Delta V + M_\alpha \Delta\alpha + M_{\dot{\alpha}}\dot{\alpha} + M_{\delta_e}\delta_e + M_{\delta_z}\delta_z \qquad (3\text{-}35)$$

$$\dot{\theta} = q$$

$$\dot{\alpha} = -\frac{\alpha_t}{V_t}\dot{V} + q + Z_\theta \Delta\theta + Z_V \Delta V + Z_\alpha \Delta\alpha + Z_{\delta_e}\delta_e + Z_{\delta_z}\delta_z, \quad Z_\theta = \frac{g\theta_t}{V_t}$$

or, in matrix form, we have

$$\begin{bmatrix} 1 & 0 & 0 & 0 \\ 0 & 1 & 0 & -M_{\dot{\alpha}} \\ 0 & 0 & 1 & 0 \\ \frac{\alpha_t}{V_t} & 0 & 0 & 1 \end{bmatrix} \begin{bmatrix} \dot{V} \\ \dot{q} \\ \dot{\theta} \\ \dot{\alpha} \end{bmatrix} = \begin{bmatrix} -D_V & 0 & \frac{-g}{57.3} & -D_\alpha \\ M_V & M_q & 0 & M_\alpha \\ 0 & 1 & 0 & 0 \\ Z_V & 1 & Z_\theta & Z_\alpha \end{bmatrix} \begin{bmatrix} \Delta V \\ q \\ \Delta\theta \\ \Delta\alpha \end{bmatrix} + \begin{bmatrix} -D_{\delta_e} & -D_{\delta_z} \\ M_{\delta_e} & M_{\delta_z} \\ 0 & 0 \\ Z_{\delta_e} & Z_{\delta_z} \end{bmatrix} \begin{bmatrix} \delta_e \\ \delta_z \end{bmatrix} \qquad (3\text{-}36)$$

which is of the general form

$$A\dot{x} = Bx + Cu$$

To change to the conventional form

$$\dot{x} = Fx + Gu$$

it is necessary simply to pre-multiply by A^{-1}, as

$$\dot{x} = A^{-1}Bx + A^{-1}Cu$$

where

$$A^{-1}B = \left[\begin{array}{c|c|c|c} -D_V & 0 & -\frac{g}{57.3} & -D_\alpha \\ M_V + M_{\dot{\alpha}}\left(\frac{\alpha_t}{V_t}D_V + Z_V\right) & M_q + M_{\dot{\alpha}} & M_{\dot{\alpha}}\left(\frac{\alpha_t}{V_t}g + Z_\theta\right) & M_\alpha + M_{\dot{\alpha}}\left(\frac{\alpha_t}{V_t}D_\alpha + Z_\alpha\right) \\ 0 & 1 & 0 & 0 \\ Z_V + \frac{\alpha_t}{V_t}D_V & 1 & Z_\theta + \frac{\alpha_t}{V_t}q & Z_\alpha + \frac{\alpha_t}{V_t}D_\alpha \end{array}\right] \qquad (3\text{-}37)$$

$$A^{-1}C = \left[\begin{array}{c|c} D_{\delta_e} & -D_{\delta_z} \\ M_{\delta_e} + M_{\dot{\alpha}} Z_{\delta_e} & M_{\delta_z} + M_{\dot{\alpha}}\left(\frac{\alpha_t}{V_t} D_{\delta_z} + Z_{\delta_z}\right) \\ 0 & 0 \\ Z_{\delta_e} & Z_{\delta_z} + \frac{\alpha_t}{V_t} D_{\delta_z} \end{array}\right]\left[\begin{array}{c} \delta_e \\ \delta_z \end{array}\right] \qquad (3\text{-}38)$$

At the TIFS cruise flight condition, V_t = 146 m/sec, h = 2820 m, W = 22,680 kg, α_t = 0° and c.g. = 22.15c, the stability derivatives are

D_V	= 0.0299	$M'_V = M_V + M_{\dot{\alpha}} Z_\alpha$	= 0.0220	Z_V	= -0.0179
D_α	= -0.133	$M'_q = M_q + M_{\dot{\alpha}}$	= -1.72	Z_α	= -1.49
D_{δ_e}	= 0.0270	$M'_\alpha = M_\alpha + M_{\dot{\alpha}} Z_\alpha$	= -2.35	Z_{δ_e}	= -0.237
D_{δ_z}	= 0.0173	$M'_{\delta_e} = M_{\delta_e} + M_{\dot{\alpha}} Z_{\delta_e}$	= -7.57	Z_{δ_z}	= -0.211
		$M'_{\delta_z} = M_{\delta_z} + M_{\dot{\alpha}} Z_{\delta_z}$	= -0.594	Z_θ	$= \frac{-g\theta_t}{V_t} = 0$

Substituting into Equations (3-37) and (3-38) yields

$$\left[\begin{array}{c} \dot{V} \\ \dot{q} \\ \dot{\theta} \\ \dot{\alpha} \end{array}\right] = \left[\begin{array}{c|c|c|c} -0.0299 & 0 & -0.5614 & 0.133 \\ 0.0222 & -1.72 & 0 & -2.35 \\ 0 & 1 & 0 & 0 \\ -0.0179 & 1 & 0 & -1.49 \end{array}\right]\left[\begin{array}{c} \Delta V \\ q \\ \Delta\theta \\ \Delta\alpha \end{array}\right] + \left[\begin{array}{cc} -0.0270 & -0.0173 \\ -7.57 & -0.594 \\ 0 & 0 \\ -0.237 & -0.211 \end{array}\right]\left[\begin{array}{c} \delta_e \\ \delta_z \end{array}\right] \qquad (3\text{-}39)$$

The complete matrix of transfer functions of Equation (3-39) determine the phase variable system matrix F_o and the phase variable transformations, T_{δ_z} and T_{δ_e}, one for each control input.

The numerators of the matrix of transfer functions of Equation (3-39) are given by

$$T(s) = \left|Is - F\right|\left[Is - F\right]^{-1} G \qquad (3\text{-}40)$$

which, for the numerical example of Equation (3-39) become

$$T(s)=\left[\begin{array}{l|l} -0.0270s^3-0.11819s^2+3.05613+6.01953 & -0.0173s^3-0.0835946s^2+0.12121s+0.02185 \\ -7.57s^3-10.949s^2-0.34133s & -0.594s^3-0.407351s^2-0.0149637s \\ -7.57s^2-10.949s-0.34133 & -0.594s^2-0.407351s-0.0149637s \\ -0.237s^2-7.984s^2-0.238294s-0.0789985 & -0.211s^3-0.96292s^2-0.02846s-0.00857516 \end{array}\right] \quad (3\text{-}41)$$

and the characteristic polynomial $|Is - F|$ is

$$|I_s - F| = s^4 + 3.2399s^3 + 5.01116s^2 + 0.160412s + 0.042018 \quad (3\text{-}42)$$

From Equations (3-41) and (3-42), the matrices F_o, T_{δ_e} and T_{δ_3} are directly obtained. The matrix F_o comes from the characteristic polynomial and is given by

$$F_o = \left[\begin{array}{c|c|c|c} 0 & 1 & 0 & 0 \\ 0 & 0 & 1 & 0 \\ 0 & 0 & 0 & 1 \\ -0.042018 & -0.0160412 & -5.01116 & -3.2399 \end{array}\right] \quad (3\text{-}43)$$

The matrices T_{δ_e} and T_{δ_3} come from Equation (3-41) and are

$$T_{\delta_e}=\left[\begin{array}{c|c|c|c} 6.01953 & 3.05913 & -0.11819 & -0.0270 \\ 0 & -0.34133 & -10.949 & -7.57 \\ -0.34133 & -10.949 & -7.57 & 0 \\ -0.0789985 & -0.238294 & -7.984 & -0.237 \end{array}\right] \quad T_{\delta_3}=\left[\begin{array}{c|c|c|c} 0.02185 & 0.12121 & -0.083596 & -0.0173 \\ 0 & -0.0149637 & -0.407351 & -0.594 \\ -0.0149637 & -0.407351 & -0.594 & 0 \\ -0.008515 & -0.02846 & -0.96292 & -0.211 \end{array}\right] \quad (3\text{-}44)$$

From Equation (3-44) we combine T_{δ_e} and T_{δ_z} to obtain

$$T_{\delta_e} + T_{\delta_z} = \begin{bmatrix} 6.04138 & 3.17734 & -0.20179 & -0.0443 \\ 0 & -0.35629 & -10.9014 & -8.1640 \\ -0.35629 & -10.9014 & -8.1640 & 0 \\ -0.08757 & -0.26675 & -8.9469 & -0.4480 \end{bmatrix} \tag{3-45}$$

Transforming back to the original set of equations of motion yields

$$F = (T_{\delta_e} + T_{\delta_z})\, F_o\, (T_{\delta_e} + T_{\delta_z})^{-1}$$

$$F = \begin{bmatrix} 6.04138 & 3.17734 & -0.20179 & -0.0443 \\ 0 & -3.35629 & -10.9014 & -8.1640 \\ -0.35629 & -10.9014 & -8.164 & 0 \\ -0.08757 & -0.26675 & -8.9469 & -0.4480 \end{bmatrix} \begin{bmatrix} 0 & 1 & 0 & 0 \\ 0 & 0 & 1 & 0 \\ 0 & 0 & 0 & 1 \\ -0.042018 & -0.160412 & -5.0116 & -3.2399 \end{bmatrix} X$$

$$\begin{bmatrix} 6.04138 & 3.17734 & -0.20179 & -0.0443 \\ 0 & -3.35629 & -10.9014 & -8.1640 \\ -0.35629 & -10.9014 & -8.164 & 0 \\ -0.08757 & -0.26675 & -8.9469 & -0.4480 \end{bmatrix}^{-1}$$

which, to the 4th decimal place, becomes

$$F = \begin{bmatrix} -0.0299 & 0 & -0.5614 & 0.133 \\ 0.0222 & -1.72 & 0 & -2.35 \\ 0 & 1 & 0 & 0 \\ -0.0179 & 1 & 0 & -1.49 \end{bmatrix} \tag{3-46}$$

which is identical to the original system matrix of Equation (3-39), and thereby illustrating the use of Equation (3-40). In addition, the last of T_{δ_z} and of T_{δ_e} combine to form the G matrix of Equation (3-39).

3.4 APPLICATION OF THE TIFS AIRPLANE

Most of the results of the application of the identification procedure described above are contained in Appendices A, B, C, and D. The purpose of this section is to describe the general procedure and present some final results.

The entire reason for developing the identification procedure outlined above is to compare and assess the results obtained using the FLEXSTAB program for theoretically obtaining the aeroelastic equations of motion of an airplane. Does FLEXSTAB yield results that are sufficiently accurate to be used for control system design purposes using modern, state space design procedures? It is felt that the comparison of analytically computed FLEXSTAB results and parameter identification obtained directly from flight test data constitutes one of the very first attempts to validate an analytical model of an aeroelastic vehicle beyond the classical nominal comparisons of structural mode frequencies and perhaps damping ratios.

Every data source available was used in the process of updating and improving the mathematical model of the TIFS airplane. These sources include the original wind tunnel data for the CV-580 and the wind tunnel data taken after the TIFS modifications were made. Extensive use was made of the parameter identification results of the rigid body stability derivatives taken from flight data gathered during the present program and previous flight tests. Servo dynamics estimates were obtained from ground tests and flight tests. Ground vibration test data were used in the comparison with the FLEXSTAB results and input data to the FLEXSTAB program were altered on the basis of the ground vibration test results. The purpose was to obtain as accurate a flexible airplane representation as possible.

3.4.1 Equations of Motion Obtained From FLEXSTAB

Appendix A contains the results computed for the TIFS airplane using the FLEXSTAB program. The detailed elements of the FLEXSTAB model and a discussion of the assumptions employed in the model can be found in Reference 6 and to some extent in Appendix A. The equations of motion and sensor equations were obtained as outputs of the linear system analysis program (LSA) of FLEXSTAB. This program is described in References 9 and 10. Stability and control derivatives which were computed in the SD & SS programs of FLEXSTAB including the effects of aeroelasticity are also given in Appendix A. The loads equations were based on an experimental version of AFLOADS, January 1976, a program developed by the Air Force Flight Dynamics Laboratory for use with FLEXSTAB. The results presented should be considered preliminary because the AFLOADS program had not, at that time, been thoroughly verified. Appendix A shows comparisons of mode frequencies obtained from ground vibration tests, direct FLEXSTAB calculations, and a FLEXSTAB recalculation done to try to obtain better agreement between ground vibration tests and analytical results. A direct comparison of the quasi-static stability and control derivatives extracted from TIFS flight test data using the Calspan Bayesian Maximum Likelihood Computer program with those obtained from FLEXSTAB is given in Table A-4 of Appendix A.

This table shows fairly good agreement between analytically computed results and the results obtained from flight test data with one exception, C_{m_α}, which was identified to be consistently smaller than the FLEXSTAB calculated value. This may be due to the assumption that propeller wake effects on horizontal tail are negligible.

---

9. Boeing Commercial Airplane Company and Boeing Computer Services, Inc. "A Method for Predicting the Stability Characteristics of Control Configured Vehicles", Vol. I "FLEXSTAB 2.01.00 Theoretical Description"; Air Force Flight Dynamics Laboratory Report No. TR-74-91, Vol. I, November 1974.

10. Boeing Commercial Airplane Company and Boeing Computer Services, Inc. "A Method for Predicting the Stability Characteristics of Control Configured Vehicles", Vol. II "FLEXSTAB 2.01.00 User's Manual"; Air Force Flight Dynamics Laboratory Report No. TR-74-91, Vol. II, November 1974.

The procedure that was used for obtaining the stability and control derivatives of TIFS from flight test data and the results using two different methods is given in Appendix B. Rather simplified classical techniques are used as well as the Calspan Bayesian Maximum Likelihood Method. Fair agreement between the methods of parameter extraction was obtained and certain conclusions were drawn about the validity of using linear model forms to represent the aircraft dynamics. It was concluded that linear equations of motion, even for small perturbations, do not accurately describe the TIFS response to direct lift flap deflections.

Appendix C shows a comparison of computed and measured structural mode frequencies and responses of the TIFS airplane to "frequency sweep" command inputs to the elevator servo and to the direct lift flap servo of the TIFS airplane. The mode frequencies show fairly good agreement yet the response matches, with a few exceptions, are not very good even after the TIFS stiffness data input to FLEXSTAB was changed to obtain better agreement between FLEXSTAB and ground vibration mode frequencies. An analysis of these results is given in Appendix C. Several reasons can be proposed for these differences, but the most likely reason seems to be that the aerodynamics calculations are either insufficiently accurate or not applicable to the TIFS aircraft configuration. Specifically, inadequate modeling of the propeller and engine effects and unsteady aerodynamic effects are believed to be responsible for this lack of agreement.

Appendix D documents the results of the transfer function estimates made from the Bode plots of the "frequency sweep" command inputs to the elevator servo and to the direct lift flap servo of TIFS. The technique used is based directly upon the methods of E. C. Levy, C. K. Sanahanan and J. Koerner (References 7 and 8). The only significant Calspan changes were to identify or estimate two or more transfer functions simultaneously, forcing both to have the same denominator polynomial or characteristic equation. By this procedure, the problem of transfer function estimates that yield unstable or right half plane poles was largely avoided, and the results are thereby judged to be more accurate.

3.4.2 Substitution Into Calculated System Matrix

To demonstrate the process of substituting flight data for theoretically calculated data in the phase variable transformation matrix, the transfer function numerators were substituted for analytically calculated rows of the T matrix progressively to show the evolution or changes in the system matrix as more and more experimental data became available.

In Table 1 is listed the results of the gradual substitution of experimentally estimated data for analytically obtained results. The table shows how twelve of the 256 parameters of the system matrix changed. The state vector was

$$\zeta_T = \left[\Delta u, \Delta\theta, \dot{\eta}_1, \dot{\eta}_2, \dot{\eta}_3, n_{z_p}, n_{z_{cg}}, n_{z_{TC}}, n_{z_{WT}}, n_{z_{SFF}}, n_{z_{SFA}}, n_{z_{RT}}, q_{cg}, \alpha_v, \delta_z, \dot{\delta}_z\right] \tag{3-47}$$

where $n_{z_{SFF}}$ and $n_{z_{SFA}}$ represent forward and aft accelerometer locations on the starboard midwing station of TIFS where the side force surface is located and $n_{z_{RT}}$ represents the horizontal tail accelerometer output location of the starboard horizontal tail surface. The other states have been previously defined.

The table shows data substitutions for one control input only, the direct lift flap. If the resulting system matrix and control matrix for any group of substitutions were then used to determine transfer functions, the transfer function forms would be retained from the T matrix originally used to form the system matrix. In other words, the numerators of transfer functions of variables not substituted were as obtained analytically and the transfer function numerators estimated from flight data are also preserved intact by the transformation from phase variable form to system matrix form and back again.

The selected results listed in Table 1 indicate substantial differences between the FLEXSTAB results and the mixed FLEXSTAB/EXPERIMENTAL

TABLE 1

TREND OF CHANGES OF SYSTEM MATRIX AS FLIGHT DATA

IS SUBSTITUTED FOR ANALYTICALLY COMPUTED DATA

FLIGHT DATA SUBSTITUTED	ELEMENTS OF SYSTEM MATRIX											
	$\frac{\partial \dot{q}_{cg}}{\partial q_{cg}}$	$\frac{\partial \dot{q}_{cg}}{\partial n_{3p}}$	$\frac{\partial \dot{q}_{cg}}{\partial \dot{n}_1}$	$\frac{\partial q_{cg}}{\partial \alpha_v}$	$\frac{\partial \dot{n}_{3p}}{\partial q_{cg}}$	$\frac{\partial \dot{n}_{3p}}{\partial n_{3p}}$	$\frac{\partial \dot{n}_{3p}}{\partial \dot{n}_1}$	$\frac{\partial \dot{n}_{3p}}{\partial \alpha_v}$	$\frac{\partial \ddot{n}_1}{\partial q_{cg}}$	$\frac{\partial \ddot{n}_1}{\partial n_{3p}}$	$\frac{\partial \ddot{n}_1}{\partial \dot{n}_1}$	$\frac{\partial \ddot{n}_1}{\partial \alpha_v}$
No substitutions (FLEXSTAB results)	1.06	-18.1	-.154	8.10	-527.0	5795.0	87.0	-4659.0	.000716	219.8	-.000126	.00637
Char. Eqn. plus numerators of δ_3/δ_{3c}, $\dot{\delta}_3/\delta_{3c}$ transfer functions	.134	-27.9	-.00167	.0517	20.0	-979.8	3.04	-165.3	-6.8×10^{-6}	98.1	-1.5×10^{-5}	.00042
Above substitutions plus numerator of n_{3p}/δ_{3c} Transfer function	-1.02	5.9	-.0722	2.03	-6.19	68.4	.171	-28.0	4.05	-20.7	.248	-6.96
Above substitutions plus numerators of n_{3wr}/δ_{3c}, n_{3rc}/δ_{3c} and q_{cg}/δ_{3c} transfer functions	-4.71	59.1	-.197	1.67	3.74	79.1	-.0095	1.75	-.0138	288.4	-2.16	-102.3

Landing Flight Condition
Direct Lift Flap Inputs Only

results. Many of the elements have changed mathematical sign and have changed in value by several orders of magnitude. But this was expected because the Bode plots that compare FLEXSTAB results with flight experimental data are considerably different. In general, the numerical values of the elements of the system matrix tend to show a progressive and relatively smooth change as more and more experimental data were added to the phase variable transformation matrix. Unfortunately, the TIFS vehicle was not instrumented to the extent required to continue the data substitution process to its completion, i.e., to the point where all the rows of the phase variable transformation matrix could be replaced by experimental results. But the results indicate that the technique described above of gradual replacement of analytically calculated elements of a system matrix with experimental results is a reasonable approach.

3.4.3 Effects of Multiple Phase Variable Substitutions

As indicated by Equation (3-34), the phase variable transformations associated with many controllers of the same system can be linearly added (or subtracted) with an expected increase in the accuracy of the estimate of the elements of the system matrix. This technique was tried with the data collected from the landing approach flight condition of TIFS. Transfer functions for the seven accelerometer outputs and the pitch rate gyro were estimated for both the direct lift flap input and the elevator input. The identification procedure was modified to require the same characteristic polynomial or denominator with the exception that the servo actuators were different for the direct lift flap and the elevator servos.

The result was two phase variable transformations, one for the direct lift flap servo input (T_{δ_z}) and the other for the elevator servo input (T_{δ_e}). These two transformations were combined linearly to obtain an estimate of the system matrix, as

$$\dot{z} = (T_{\delta_z} + T_{\delta_e})\, F_o\, (T_{\delta_z} + T_{\delta_e})^{-1} z + T_{\delta_z} G_o \delta_z + T_{\delta_e} G_o \delta_e$$

$$= F z + G u \qquad (3\text{-}48)$$

The transfer functions were then obtained from the resulting equations of motion as

$$H(s) = (Is - F)^{-1}G \tag{3-49}$$

and a comparison was made of the roots of the numerator polynomials that were estimated from the flight data and those that were calculated from Equation (3-49) after the data was manipulated according to Equation (3-48). It was not expected that the results would be exact. At least two major sources of error exist. First, the phase variable transformations were of a hybrid form, partially estimated from flight data and partially computed from FLEXSTAB. Secondly, the process of obtaining transfer functions from the flight data is not free of error.

Table 2 gives a sampling of the results of first combining data according to Equation (3-48), then calculating transfer functions using Equation (3-49). In this table the zero locations, the values of the roots of the numerator polynomials for the n_{z_p}/δ_z and u/δ_z transfer functions are listed. The two transfer functions show typical sample results of the effect of errors introduced by combining analytical and identified flight data and errors accrued in the identification process itself. Not too many conclusions can be reached concerning the accuracy or validity of the results. The comparison between the directly identified and the transformed u/δ_z numerator results appear reasonably good. Several additional steps beyond those investigated in this program would be required to verify and refine the process of identification described in this section. These steps are:

1. A complete state vector set of independent measurements of the vehicle dynamics would be required to estimate a complete phase variable transformation matrix from flight test data. Without this data, it is not possible to separate errors introduced by mixing analytical and experimental data with errors inherent in the identification process itself.

2. Data for δ_z and δ_e inputs, if taken separately, cannot be done for exactly the same flight condition. It is not known how much error is introduced by this limitation. If

TABLE 2

NUMERATOR POLYNOMIAL ROOTS (ZEROS) FOR PARTIALLY IDENTIFIED SYSTEM MATRIX $\left[T_{\delta_e} + T_{\delta_z}\right] F_o \left[T_{\delta_e} + T_{\delta_z}\right]^{-1}$

Transfer Function	Numerators Estimated From Flight Data			Numerators Calculated From Partially Identified System Matrix		
	ζ	ω rad/sec	τ sec	ζ	ω rad/sec	τ sec
n_{z_p}/δ_z (Numerator of n_z response at pilot location to direct lift flap input)	.0468	76.2	-.050 -22.2	-.0599	54.3	-.0577 10.8
	.0158	47.1	-.0517 31.1	.539	42.9	-.0395 -.005
	.0975	36.5	.361	.0374	36.4	-.647
	-.0527	30.7	-.937	.924	14.3	-6.04
u/δ_z (Numerator of change in airspeed response to direct lift flap input)	.0418	61.2	-.741	.0513	63.3	.0103
	.145	45.3		.0131	43.6	-.0813
	.056	43.9		-.143	39.4	
	.076	31.7		.071	35.2	
	.455	23.1		.918	25.4	
	.0225	1.57		.365	.972	

+ Characteristic Equations Are Identical For Estimated and Calculated Results

+ Data For TIFS Landing Flight Condition

+ n_{z_p}/δ_z Transfer Function Estimated From Flight Data

  u/δ_z Transfer Function Not Estimated From Flight Data

frequency sweep inputs were injected into the direct lift flaps and the elevator servos simultaneously and in phase, estimates to the transformation $\left[T_{\delta_e} + T_{\delta_\gamma}\right]$ could be made directly, and a comparison can be obtained between individual T matrix identification and simultaneous identification.

3. The calculation of transfer functions from state space equations of high dimension is in itself subject to error. A useful result would be to compare time histories of command inputs between identified aircraft transfer functions and those calculated from partially identified data. Time histories are normally less sensitive to such errors.

The process for the identification of large-scale systems outlined above was developed during the course of the investigation. At this time not very much can be definitively concluded from the limited data taken from the flight tests of the TIFS airplane. The technique does show promise as the only known way of trying to verify from flight test the high order, extended dimension aeroelastic equations of motion computed from analytical sources such as FLEXSTAB. More importantly, the technique provides the promise of a method for the systematic update or replacement of the analytical data as flight test data becomes available. The simplicity of the actual estimation technique is attractive as is the fact that this technique uses the standard frequency sweep data that has been used for many years to obtain structural mode and flutter data for an airplane.

Section IV

GUST ALLEVIATION

4.1 INTRODUCTION

Gust alleviation design techniques fall into two general categories. The most often used technique is feedback control, or regulation to alter the closed loop static and dynamic behavior of the airplane in a way to be affected less (in some sense) to the forces and moments generated on the aircraft by the gusts. Regulation implies an increase in the speed of response of the vehicle and the normal decrease in static sensitivity associated with the increased natural frequencies that speed up the response. However, feedback can also be used to have the effect of a decreased L_α, thereby decreasing the responsiveness of the aircraft to turbulence. Unfortunately, this kind of a design also generally reduces the maneuver capability of the airplane, so it was decided to avoid this approach and concentrate on another technique described below.

A second technique involves a direct measurement of the gusts or atmospheric turbulence itself. The gust measurement is used to drive the control surfaces of the airplane in such a way to attempt to generate forces and moments on the airframe that counter or cancel those forces and moments produced by the turbulence. Exact or nearly exact cancellation requires an independent force or moment generating surface or device for each degree of freedom of motion of the airframe. For a rigid airframe, three controllers can very effectively gust alleviate the three longitudinal-vertical degrees of freedom of motion. A flexible aircraft, however, involves many degrees of freedom and therefore gust alleviation of an aircraft having fewer independent controllers than degrees of freedom of motion is less effective. This report addresses the problem of how to use the existing controllers to get the "best" feedforward gust alleviation system. An "open loop" or feedforward matrix of gains is devised to drive the controllers. This matrix of gains is derived using the theory of generalized matrix inverses.

4.2 CRITERIA FOR GUST ALLEVIATION

The possibilities are nearly endless for gust alleviation criteria, those that can mathematically specify an objective or model for gust alleviation. The general statement that the controllers should move in such a way to minimize the motions of the vehicle, both rigid and elastic, is not really good enough. General criteria associated with design techniques need to be developed so that they can be used as systematic design tools and as standards upon which a design can be evaluated relative to other designs. A few of the possible criteria and design techniques are developed and discussed below.

4.2.1 Ideal Open Loop Solution

The most simple and direct open loop or direct drive solution involves a design to move the vehicle control surfaces in such a way to counteract the forces and moments generated on the aircraft by the gusts.

The linearized, small motion perturbation equations of motion are given by:

$$\dot{x} = Fx + Gu + Jv_g \tag{4-1}$$

where x^T is the state vector, u the control vector and v_g the gust input. The matrix F is the matrix of the stability derivatives of the vehicle equations of motion, G the matrix of control derivatives and J is a matrix of gust effectiveness terms.

To eliminate the effects of turbulence, it is a relatively simple matter to solve for the control input that counters the effects of the gusts, i.e.

$$Gu + Jv_g = 0 \tag{4-2}$$

or

$$u = -G^{-1}Jv_g \tag{4-3}$$

The three degrees of freedom of longitudinal-vertical motion of an airplane require three controllers driven by wide bandwidth actuators whose bandwidth spans the frequency range of interest of the phugoid and short period motions of the vehicle. For the situation of longitudinal-vertical rigid body motions and fast acting servo actuators, the exact solution to Equation (4-3) is given by

$$u = -(G^T G)^{-1} G^T J v_g \tag{4-4}$$

to completely alleviate three components of the turbulence.

4.2.2 Appreciable Actuator Dynamics

Compensation can be made for the effects of actuators in several ways.

a. By using a lead network for compensation
   To the original equations of motion

$$\dot{x} = Fx + Gu + Jv_c$$

the actuator dynamics are appended

$$\dot{u} = Au + Bu_c \tag{4-5}$$

By using Laplace transform methods and the criterion defined by Equation (4-2), we have the requirement that

$$Gu(s) + Jv(s) = 0 \tag{4-6}$$

from Equation (4-5),

$$u(s) = (Is - A)^{-1} B u_c(s) \tag{4-7}$$

Substitution of Equation (4-7) into Equation (4-6) yields

$$u_c(s) = -B^{-1}(Is - A)\,G^{-1}J v(s) \tag{4-8}$$

or

$$u_c(s) = -(B\ B)^{-1}B^T(Is - A)(G^TG)^{-1}J v(s) \tag{4-9}$$

which defines a general lead network.

Direct compensation for first order actuator dynamics by using measurements of v_g and $\dot{v}_g$ is also obtained simply and directly from Equation (4-9).

$$u_c(t) = (B^TB)^{-1}B^TA\,(G^TG)^{-1}G^TJ v(t) - (B^TB)^{-1}B^T(G^TG)^{-1}G^TJ\dot{v}(t) \tag{4-10}$$

4.2.3 Output Gust Alleviation

An output equation to represent the acceleration motions of the vehicle is added to Equation (4-1) as

$$y = Cx + D\dot{x}$$

then the criterion becomes

$$y = 0 = Cx + D\dot{x} = Cx + D\,(Fx + Gu + Jv_g) \tag{4-11}$$

from which can be obtained

$$u = -(G^TG)^{-1}G^TJv - (G^TG)^{-1}G^T(D^TD)^{-1}D^T(C + DF)x \tag{4-12}$$

The gust alleviation solution given by Equation (4-12) requires invertibility of both matrices G and D. The fact that the control input is now a function of the state means that the solution is a feedback control law, and stability is not guaranteed.

4.2.4 Least Squares Solution

A least squares approximation to the solution shown by Equation (4-12) is easily obtainable in the following manner. Given, as before, the state space and output equations

$$\dot{x} = Fx + Gu + Jv_g$$

$$y = Cx + D\dot{x}$$

a quadratic expression is formed. This is a scalar function of the output y and the control effort u. The outputs y and the control motions u are weighted relative to each other by the positive definite symmetrical matrices Q and R. The resultant scalar expression takes the form

$$L = (y^T Q y + u^T R u) \tag{4-13}$$

$$= (Cx + D\dot{x})^T Q (Cx + D\dot{x}) + u^T R u \tag{4-14}$$

and substitution for $\dot{x}$ in Equation (4-14) yields

$$L = \left[(C+DF)x + DGu + DJv_g\right]^T Q \left[(C+DF)x + DGu + DJv_g\right] + u^T R u \tag{4-15}$$

To minimize the function L with respect to the control activity, simply obtain ∇u and set to zero. The result is

$$0 = G^T D^T Q (C+DF)x + G^T D^T Q D J v_g + (G^T D^T Q D G + R)u \tag{4-16}$$

or

$$u = -(G^T D^T Q D G + R)^{-1} G^T D^T Q \left[(C+DF)x + DJu_g\right] \tag{4-17}$$

The weighted least squares solution to the gust alleviation problem expressed by Equation (4-17) is dimensionally compatible with the number of control surfaces available for this activity, so the solution can be directly implemented. However, like the solution of Equation (4-12), it is a

feedback solution that does not guarantee stability, nor does it suggest in any way that the solution will be practically implementable.

Nevertheless, the solution to Equation (4-17) that does not restrain the control activity, i.e. $R = 0$ does serve as a criterion or ideal model that will define the best feedback solution possible if stability does not turn out to be a limiting consideration.

The stability problem can be addressed by using linear optimal control theory.

4.2.5 Linear Optimal Control Solution

The problem is to minimize a weighted function of the output and the control. A guaranteed stable solution is desired. A quadratic performance index is specified of the form

$$2V = \min_{u} \int_{o}^{\infty} (y'Qy + u'Ru)\,dt \tag{4-18}$$

Subject to the constraint of the linear differential equations of motion of Equation (4-1); $\dot{x} = Fx + Gu + Jv$, $y = Cx + D\dot{x}$. Substituting for y and in Equation (4-18) yields the equivalent performance index.

$$2V = \min_{u} \int_{o}^{\infty} \left\{ \left[(C+DF)x + DGu + DJv_g \right]^T Q \left[(C+DF)x + DGu + DJv_g \right] + u^T R u \right\} dt \tag{4-19}$$

The solution is straightforward and well-known. A Lagrangian is formed as

$$\mathcal{L} = \frac{1}{2} \left[(C+DF)x + DGu + DJv_g \right]^T Q \left[(C+DF)x + DGu + DJv_g \right] + \frac{1}{2} u^T R u + \lambda^T \left(-\dot{x} + Fx + Gu + Jv \right) \tag{4-20}$$

The stable solution to the Euler-Lagrange equations defines the optimal solution. The Euler-Lagrange equations are

$$\frac{\partial \mathcal{L}}{\partial x} - \frac{d}{dt}\left(\frac{\partial \mathcal{L}}{\partial \dot{x}}\right) = 0 \qquad \text{(a)}$$

$$\frac{\partial \mathcal{L}}{\partial u} - \frac{d}{dt}\left(\frac{\partial \mathcal{L}}{\partial \dot{u}}\right) = 0 \qquad \text{(b)} \qquad (4\text{-}21)$$

Performing the indicated operations yields

$$\frac{\partial \mathcal{L}}{\partial u} - \frac{d}{dt}\left(\frac{\partial \mathcal{L}}{\partial \dot{u}}\right) = G^T D^T G(C+DF)x + (G^T D^T Q D G + R)u + G^T D^T Q D J v + G^T \lambda = 0 \qquad (4\text{-}22)$$

$$\frac{d\mathcal{L}}{\partial x} - \frac{d}{dt}\left(\frac{\partial \mathcal{L}}{\partial \dot{x}}\right) = (C+DF)^T Q(C+DF)x + (C+DF)^T Q D G u + (C+DF)^T Q D J v + F^T \lambda + \lambda^T = 0 \qquad (4\text{-}23)$$

The optimal feedback control law is obtained from Equation (4-22).

$$u = -(G^T D^T Q D G + R)^{-1} G^T \left[D^T Q (C+DF)x + \lambda + D^T Q D J v\right] \qquad (4\text{-}24)$$

A comparison between Equations (4-17) and (4-24) shows that the only difference between the weighted least squares and the linear optimal control solution is λ, the term that guarantees a stable linear optimal control solution.

The feedback term λ is part of the regulator or feedback solution that is independent of the gust excitation v. To obtain λ as a function of the state x is the linear optimal regulator problem. Substituting Equation (4-24) into Equations (4-22) and (4-1) yields

$$0 = \dot{\lambda} + (F^T - A^T Q D G \hat{R}^{-1} G^T)\lambda + (A^T Q A - A^T Q D G \hat{R}^{-1} G^T D^T Q A)x \qquad (4\text{-}25)$$

$$0 = -\dot{x} + (F - G\hat{R}^{-1} G^T D^T Q A)x - G\hat{R}^{-1} G^T A \lambda \qquad (4\text{-}26)$$

where $A = C + DF$ and $\hat{R} = R + G^T D^T Q D G$.

Assuming the feedback is linear, i.e., $\lambda = P\mathcal{x}$, $\dot{\lambda} = P\dot{\mathcal{x}}$, the Riccati equation is obtained after Equation (4-25) and (4-26) have been combined

$$0 = \hat{F}^T P + P\hat{F} - PG\hat{R}^{-1}G^T P + \hat{Q} \qquad (4\text{-}27)$$

where

$$\hat{F} = F - G\hat{R}^{-1}G^T QA$$

$$\hat{Q} = A^T QA - A^T QDG\hat{R}^{-1}G^T D^T QA$$

The solution of Equation (4-27) for P produces the feedback control matrix term $\lambda = P\mathcal{x}$ that guarantees a stable solution for the control problem represented by the performance index of Equation (4-18).

So gust alleviation can be accomplished in many ways and a thorough examination of the efficacy of the methods should be investigated to determine which way is best in terms of design complexity, stability requirements and level of gust alleviation attainable.

The investigation documented in this report concentrates on the fundamental open loop or feedforward solution represented by Equation (4-3) and its variations. Linear optimal feedback is addressed in Section VI, structural mode control, for it is felt that if feedback control can have the effect of stiffening the vehicle, then feedforward gust alleviation can alleviate the rigid body vehicle motions and perhaps one or more of the lower frequency modes without excessive excitation of the remainder of the regulated structural modes.

4.3 GUST ALLEVIATION - ILLUSTRATION OF PRINCIPLES

The traditional approach to gust alleviation has been to feed back n_z signals to the pitching moment generating surface or the direct lift producing surface or to both surfaces. The intended purpose is to create a tightly regulated aircraft to gust inputs such that the response of the vehicle is minimized. The command input gain is then increased to enable the pilot to adequately maneuver the airplane.

It is concluded that the approach to gust alleviation described above is not necessarily the best approach for aircraft that have been designed for active control technology. There are several reasons for this:

1. An aircraft having an aft c.g. is excited much less by gust inputs than is a normally statically stable aircraft, particularly in pitching motions. One of the important gust excitation terms, $M_\alpha \alpha_g$, may be small or even zero for relaxed static stability aircraft.

2. Tightly regulated aircraft are generally less sensitive to lower frequency turbulence inputs but no less sensitive and often more sensitive to higher frequency inputs. By decreasing the amplitude of the normal acceleration, the bandwidth of the response to turbulence inputs is increased. Also, the pitching motions of the aircraft relative to the heaving motions may be increased.

3. By emphasizing higher frequency motions relative to the lower frequency motions, the bandpass of frequencies most likely to be objectionable to the pilot in turbulence (1-3 Hz) are accentuated.

To illustrate the effects or principles stated above, consider the following discussion of the application of gust alleviation to the simplified two degrees-of-freedom motions of a rigid aircraft. If it is assumed that the aircraft static stability, i.e. M_α is zero and the change in lift produced by an elevator deflection is zero, equations can be written as follows:

$$\begin{bmatrix} \dot{q} \\ \dot{\alpha} \end{bmatrix} = \begin{bmatrix} M_q + M_{\dot{\alpha}} & -M_{\dot{\alpha}} L_\alpha \\ 1 & -L_\alpha \end{bmatrix} \begin{bmatrix} q \\ \alpha \end{bmatrix} + \begin{bmatrix} M_{\delta_e} \\ 0 \end{bmatrix} \delta_e \qquad (4\text{-}28)$$

If measured with a vane, the angle of attack signal can be considered to be made up of two components, an inertial component α_I and a gust component α_g. The equations may then be written as

$$\begin{bmatrix} \dot{q} \\ \dot{\alpha} \end{bmatrix} = \begin{bmatrix} M_q + M_{\dot{\alpha}} & -M_{\dot{\alpha}} L_\alpha \\ 1 & -L_\alpha \end{bmatrix} \begin{bmatrix} q \\ \alpha_I \end{bmatrix} + \begin{bmatrix} M_{\delta_e} \\ 0 \end{bmatrix} \delta_e + \begin{bmatrix} -M_{\dot{\alpha}} L_\alpha \\ -L_\alpha \end{bmatrix} \alpha_g \qquad (4\text{-}29)$$

which represents the gust as a separate disturbance input.

Now assume feedback from a vane that senses $\alpha_I + \alpha_g$ to the elevator and a command input has been implemented, i.e. $\delta_e = \delta_{e_c} - K(\alpha_I + \alpha_g)$. Substituting this control law into the equations of motion (4-29) yields

$$\begin{bmatrix} \dot{q} \\ \dot{\alpha} \end{bmatrix} = \begin{bmatrix} M_q + M_{\dot{\alpha}} & -M_{\dot{\alpha}} L_\alpha + K_1 M_{\delta_e} \\ 1 & -L_\alpha \end{bmatrix} \begin{bmatrix} q \\ \alpha_I \end{bmatrix} + \begin{bmatrix} M_{\delta_e} \\ 0 \end{bmatrix} \delta_{e_c} + \begin{bmatrix} -M_{\dot{\alpha}} L_\alpha - K_1 M_{\delta_e} \\ L_\alpha \end{bmatrix} \alpha_g \qquad (4\text{-}30)$$

From Equation (4-30), the transfer functions that describe the response in angle of attack to separate elevator command and α_g inputs can be obtained

$$\frac{\alpha}{\delta_{e_c}}(s) = \frac{M_{\delta_e}}{s^2 + s(L_\alpha - M_q - M_{\dot{\alpha}}) - L_\alpha M_q + K_1 M_{\delta_e}} \qquad (4\text{-}31)$$

$$\frac{\alpha}{\alpha_g}(s) = \frac{L_\alpha s - L_\alpha M_q + K_1 M_{\delta_e}}{s^2 + s(L_\alpha - M_q - M_{\dot{\alpha}}) - L_\alpha M_q + K_1 M_{\delta_e}} \qquad (4\text{-}32)$$

The responses in α and q to a step command and a "step" gust are sketched below for $K_1 = 0$ and for K_1 = negative value.

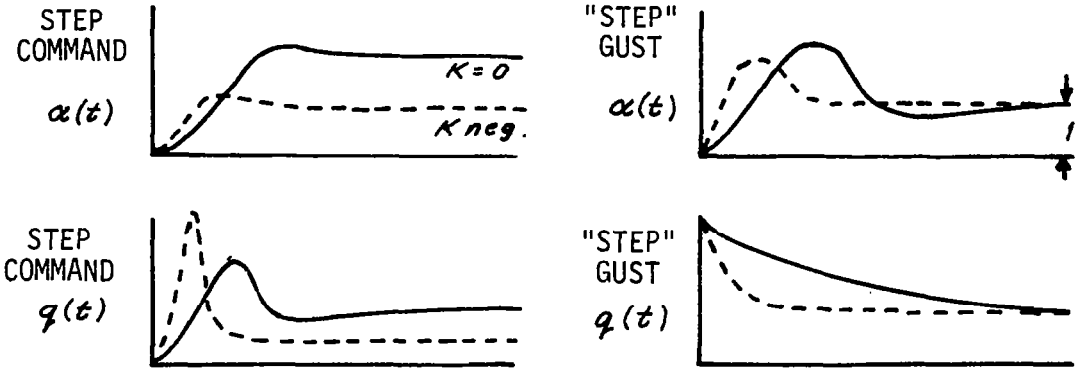

These sketches show that feedback from a vane will do nothing for the gust sensitivity except speed up the response. The c.g. acceleration response of the vehicle will be approximately the same as the α response, since $n_z(t) \approx \frac{V}{g} L_\alpha \alpha(t)$.

If the inertial part of the angle of attack vane signal is separated from the gust part of the signal and fed back to the elevator, i.e. $\delta_e = \delta_{e_c} - K_1 \alpha_I$, the equations become

$$\begin{bmatrix} \dot{q} \\ \dot{\alpha} \end{bmatrix} = \begin{bmatrix} M_q + M_{\dot{\alpha}} & -M_{\dot{\alpha}} L_\alpha - K_1 M_{\delta_e} \\ 1 & -L_\alpha \end{bmatrix} \begin{bmatrix} q \\ \alpha_I \end{bmatrix} + \begin{bmatrix} M_{\delta_e} \\ 0 \end{bmatrix} \delta_e + \begin{bmatrix} -M_{\dot{\alpha}} L_\alpha \\ -L_\alpha \end{bmatrix} \alpha_g \qquad (4\text{-}33)$$

The $\alpha/\delta_{e_c}(s)$ transfer function remains the same as given by Equation (4-31) but the transfer function to a gust input becomes

$$\frac{\alpha}{\alpha_g}(s) = \frac{L_\alpha (s - M_q)}{s^2 + s(L_\alpha - M_q - M_{\dot{\alpha}}) - M_q L_\alpha + K_1 M_{\delta_e}} \qquad (4\text{-}34)$$

and the responses to a step gust become as sketched below.

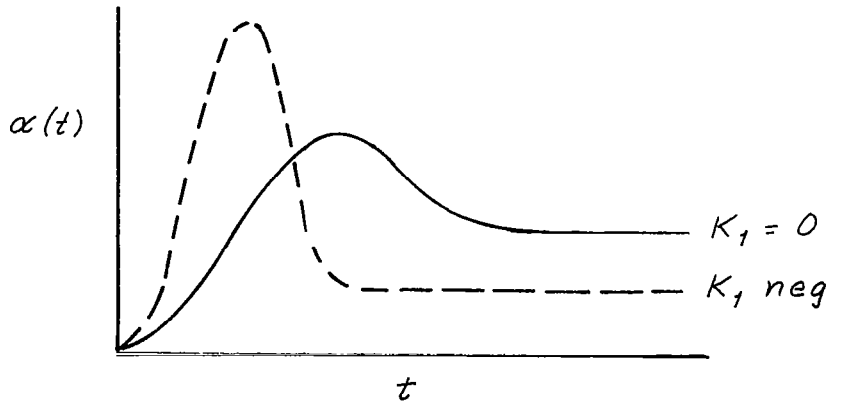

This sketch shows that the response in angle of attack to a gust input is decreased in sensitivity and amplitude at the low frequency end of the gust spectrum, but amplified at the higher frequency, pilot sensitive region of the spectrum. If command augmentation to improve flying qualities

were now used in addition to feedback, the responses to command and gusts could be as sketched below.

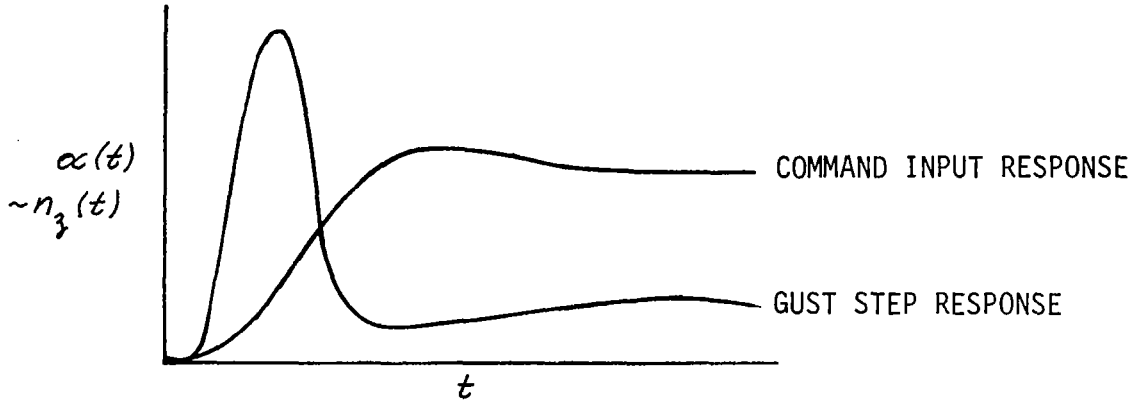

Therefore, although the vehicle can be given good flying qualities with α (or n_z) and, of course, pitch rate damping feedback and command augmentation, little can be done with feedback to eliminate the high frequency sensitivity of the airplane to turbulence.

If we directly sense the turbulence and drive both the elevator and a direct lift flap with the sensed α_g signal, the vehicle can be made insensitive to turbulence. Assume a control law $\delta_e = \delta_{e_c} - K_1\alpha_I + K_2\alpha_g$, $\delta_f = K_3\alpha_g$ where δ_f is a direct lift flap, assumed for simplicity and no loss in generality to act through the aircraft c.g. The equations of motion now become

$$\begin{bmatrix}\dot{q}\\ \dot{\alpha}\end{bmatrix} = \begin{bmatrix}M_q + M_{\dot{\alpha}} & -M_{\dot{\alpha}}L_\alpha & -K_1M_{\delta_e}\\ 1 & -L_\alpha & \end{bmatrix}\begin{bmatrix}q\\ \alpha_I\end{bmatrix} + \begin{bmatrix}M_{\delta_e}\\ 0\end{bmatrix}\delta_{e_c} + \begin{bmatrix}-M_{\dot{\alpha}}L_\alpha + K_2M_{\delta_e}\\ -L_\alpha + K_3L_{\delta_f}\end{bmatrix}\alpha_g \quad (4\text{-}35)$$

If the gains K_2 and K_3 are chosen such that $K_2 = \frac{M_{\dot{\alpha}}L_\alpha}{M_{\delta_e}}$ and $K_3 = \frac{L_\alpha}{L_{\delta_f}} = \frac{C_{L_\alpha}}{C_{L_{\delta_f}}}$, then the gust excitation term of Equation (4-35)

vanishes, yielding a control system configuration that does not allow the vehicle to be excited by turbulence.

The gust alleviation system described by Equation (4-35) is simplified and only approximate. These equations assume that the elevator has no lift and the direct lift surfaces produce no pitching moment, but these realisms can be incorporated into a design without difficulty. The equations do assume that the control surface servos are fast, high performance servos that can drive the surfaces at the turbulence spectrum frequencies. It is also assumed that the stability and control derivatives of the vehicle are known to a fair degree of accuracy. For future aircraft designed for the application of active control technology, the requirements for high performance servos and accurately known stability and control derivatives do not appear to be overly demanding.

4.4 DESIGN OF TIFS GUST ALLEVIATION SYSTEM

A gust alleviation system that senses the turbulence and drives the surfaces can be very effective. Therefore, the gust alleviation system that was chosen for TIFS involves only open loop compensation. This section describes the investigation of feedforward compensation that minimizes the response of the TIFS airplane to atmospheric turbulence using direct gust measurements to drive the control surfaces. Such a design would be extremely simple to mechanize and presents almost no possibility for stability problems. With the addition of feedback for structural mode control or sensitivity minimization the gust alleviation is expected to be even more effective.

The mathematical model is formally defined as follows:

System equations	$\dot{x} = Fx + Gu + Jv$	
Output or measurement equations	$y = Ax + Bu + Cv$	(4-36)
Feedforward control law	$u = Kv$	

where

x = $N \times 1$ state vector

u = $M \times 1$ control vector

v = gust input, a scaler for this study

y = output vector

The matrices F, G, J, A, B, C for the TIFS aircraft are described in Appendix A where the TIFS is modeled with various numbers of structural bending modes included in the state equations.

The feedforward gains are to be selected to minimize (in some sense) the inputs to the system, $Gu + Jv$, the excitation to the system defined by the equations of motion of the airframe.

The standard solution to this problem, called the Generalized Inverse solution (Reference 11), is given by

$$u = Kx$$

where

$$K = -G^{+}J$$

and G^{+} = Generalized inverse of G

$$G^{+} = \left[G^{T} G\right]^{-1} G^{T} \tag{4-37}$$

The need for the inverse of $G^{T}G$ requires that G be of maximum rank, a condition that is almost always obtained for an aircraft with multiple control surfaces.

Note that if G is invertible directly, i.e. G^{-1} exists, then $G^{+} = G^{-1}$ and perfect gust alleviation is attained. That is

$$Gu + Jv = -GG^{-1}Jv + Jv = 0$$

---

11. Lewis, T. O. and Odell, P. L., Estimation in Linear Models, Prentice-Hall, Inc., Chapter 1, 1971.

However, if G^{-1} does not exist, only an approximate solution exists. This approximation is such that if

$$u^* = -G^+ J v \tag{4-38}$$

then

$$\| Gu^* + Jv \| \leq \| Gu + Jv \| \tag{4-39}$$

where

$\| x \|$ is the norm of vector x defined as $\|x\| \equiv \sqrt{x^T x}$,

and u is any other solution for the feedforward control.

If the equality is true in the above equation, the following additional property holds:

$$\| Gu^* \| \leq \| Gu \|$$

In this study up to five symmetric modes of motion of the TIFS at the landing flight condition were considered. The equations of motion as predicted by FLEXSTAB are documented in Appendix A. The symmetric modes of motion included in this model and their natural frequencies (as predicted by FLEXSTAB) at landing condition are given below:

	ω_n, rad/sec
Phugoid (Ph)	.047
Short Period (SP)	2.25
First Wing Bending (1WB)	23.1
First Wing Torsion (1WT)	32.9
First Fuselage Bending (1FB)	41.5
First Horizontal Tail Bending (1HTB)	52.2
Second Wing Bending Mode (2WB)	61.7

The three controllers studied were collective aileron, (δ_{cA}), direct lift flap, (δ_{ℓ}), and elevator, δ_e.

One would suspect that the closer G is to being invertible, the better the solution will be. However, for the case of the seven modes of motion given above, G is of dimension 14 x 3 and a good generalized inverse solution is not likely. A multitude of solutions are possible.

One approach involves partitioning the G and J matrices as follows:

$$\begin{bmatrix} G_1 \\ \hline G_2 \end{bmatrix} u + \begin{bmatrix} J_1 \\ \hline J_2 \end{bmatrix} v \tag{4-40}$$

where G_1 is 3 x 3 and therefore invertible directly. We define the control law as

$$u = -G_1^{-1} J_1 v \tag{4-41}$$

and the resulting substitution leads to the following equations of motion:

$$\dot{x} = Fx + \begin{bmatrix} 0 \\ \hline J_2 - G_2 G_1^{-1} J_1 \end{bmatrix} v \tag{4-42}$$

Note that while the gust input into three rows of the equations of motion can be made equal to zero, one might expect that the gust input into the other equations might increase. Since the equations of motion are coupled it is not apparent at this point what level of gust alleviation will be attained.

A modification to this approach involves making the upper part of the partitioned G matrix, G_1, other than exactly invertible but still more invertible than G. The resulting control law would then be

$$u = -G_1^{*} J v \tag{4-43}$$

Either of the two approaches mentioned above, Equations (4-41) or (4-43) can be used on lower order mathematical models by first performing a quasistatic deletion of one or more modes thus reducing the order, N, of the system equations. For instance,if alleviation of only short period and phugoid responses is desired, then a quasistatic rigid body model of order N = 4 is first obtained. In this case, when the resulting control law is then simulated on the more accurate 14th order model, the property shown in Equation (4-42) will not be true.

Considerable simplification of the gust alleviation problem results because both G and J have zero elements in the same rows. If the state vector for the rigid body motion is written as

$$x = [w \; q \; u \; \theta]$$

then the J matrix and each column of the G vector will have the following form:

$$[D_1 \quad D_2 \quad D_3 \quad 0]^T$$

One can now observe that under these conditions, partitioning the G and J matrices as in equation (5) will yield perfect gust alleviation ($Gu + Jv = 0$) since $G_2 = [0, 0, 0]$ and $J_2 = 0$. Similarly if a structural mode is added to the equations of motion, two differential equations are added but only one nonzero row of G and J. As a result, it is possible with feedforward to three controls to make the gust input terms zero in the short period mode equations (w, q) and any one other mode [phugoid ($u, \dot{\theta}$) or structural bending mode] .

4.4.1 Feedforward Design Evaluation

In the final evaluation of the effectiveness of the gust alleviation systems in this study, the most accurate model of the flexible TIFS was used regardless of the order model used in the feedforward gain computation. This model, as described previously, was 14th order containing two rigid body and

five structural modes. Many designs were obtained with considerably different results. Tables 3 and 4 summarize these results. Figure 4 shows power spectral plots of several of these cases.

The second column of Table 3 indicates the dynamic order of the equations of motion from which the J and G matrices were obtained. When the order N is less than 14, it indicates a quasistatic reduction which was first performed prior to gain computations. The third column indicates which rows of equations of motion (4-36) were included in the Matrix G_1 of Equation (4-40) in order to calculate the feedforward control law $u = -G_1^+ J v$. However, recall that each pair of rows,which may loosely be said to contribute the predominate characteristics of one second order mode,are actually coupled to every other mode.

The last three columns of Table 3 are the feedforward gains, K_i , for the three controllers.

$$\begin{bmatrix} \delta_{CA} \\ \delta_3 \\ \delta_e \end{bmatrix} = \begin{bmatrix} K_1 \\ K_2 \\ K_3 \end{bmatrix} v = -G_1^+ J_1 v$$

Table 4 summarizes the performance of the various designs in two ways. Columns 2, 3, 4 and 5 contain root mean square (RMS) accelerations for four vehicle stations, pilot's station, c.g., tail, and wing tip. The final two columns contain the norm of the closed loop gust effectiveness matrix

$$-G G_1^+ J_1 + J \tag{4-44}$$

and the norm of closed loop output equation gust effectiveness matrix (for the same four accelerometers)

$$-B G_1^+ J_1 + C$$

TABLE 3

FEEDFORWARD DESIGNS

DESIGN	DYNAMIC ORDER OF THE STATE EQUATIONS USED TO COMPUTE GAINS	MODES INCLUDED IN G_1 AND J_1 OF $u = -G_1^+ J_1 v$	COMMENTS	FEEDFORWARD GAINS		
				δ_{CA}	δ_3	δ_e
0	14	None	Unaugmented	0	0	0
1	14	All	$u = -G^+ J v$	- 1.74	- 1.36	- 1.03
2	14	PH + SP	$u = -G_1^+ J_1 v$	- 9.78	5.43	.755
3	4	PH + SP	"	- 9.93	3.33	.262
4	14	SP + 1WB	"	-137.0	189.0	12.5
5	6	SP + 1WB	"	751.0	-1026.0	15.0
6	14	All	Norm includes 4 accelerometers, K = 1000	- 1.84	- .899	- .725
7	14	All	Norm includes 4 accelerometers, K = 10,000	- 2.27	2.17	- .377
8	14	All	Uses Modified Jordan form	- 1.87	.236	- .351
9	14	1HT + 2WB	Uses Modified Jordan form	- 1.39	- .643	- .998
10	14	PH + SP	Uses Modified Jordan form	- 9.81	3.23	.261
11	14	PH + SP + 1WB	Uses Modified Jordan form	- 2.44	- .709	- .0586
12	14	SP + 1WB	Uses Modified Jordan form	+ 1.12	- 5.45	- .196

TABLE 4

PERFORMANCE OF FEEDFORWARD DESIGNS

DESIGN	RMS ACCELERATIONS				$\|-GG_1^+J_1+J\|$	$\|-BG^+J_1+C\|$
	$\sigma_{n_{z_P}}$	$\sigma_{n_{z_{c.g.}}}$	$\sigma_{n_{z_T}}$	$\sigma_{n_{z_{WT}}}$		
0	.135	.0948	.155	.772	199	1.84
1	.153	.141	.145	.183	30	.069
2	.335	.274	.455	---	540	---
3	.361	.240	.443	---	564	---
4	5.95	5.99	9.37	---	10,575	---
5	33.4	31.7	52.8	---	61,735	---
6	.111	.0998	.101	.173	38	.049
7	.106	.0850	.123	.773	160	.014
8	.0730	.0627	.0739	.358	81	.130
9	.141	.128	.132	---	64	---
10	.356	.235	.436	3.05	556	6.87
11	.0526	.0491	.0672	.296	81.5	.531
12	.139	.147	.232	1.30	281	2.18

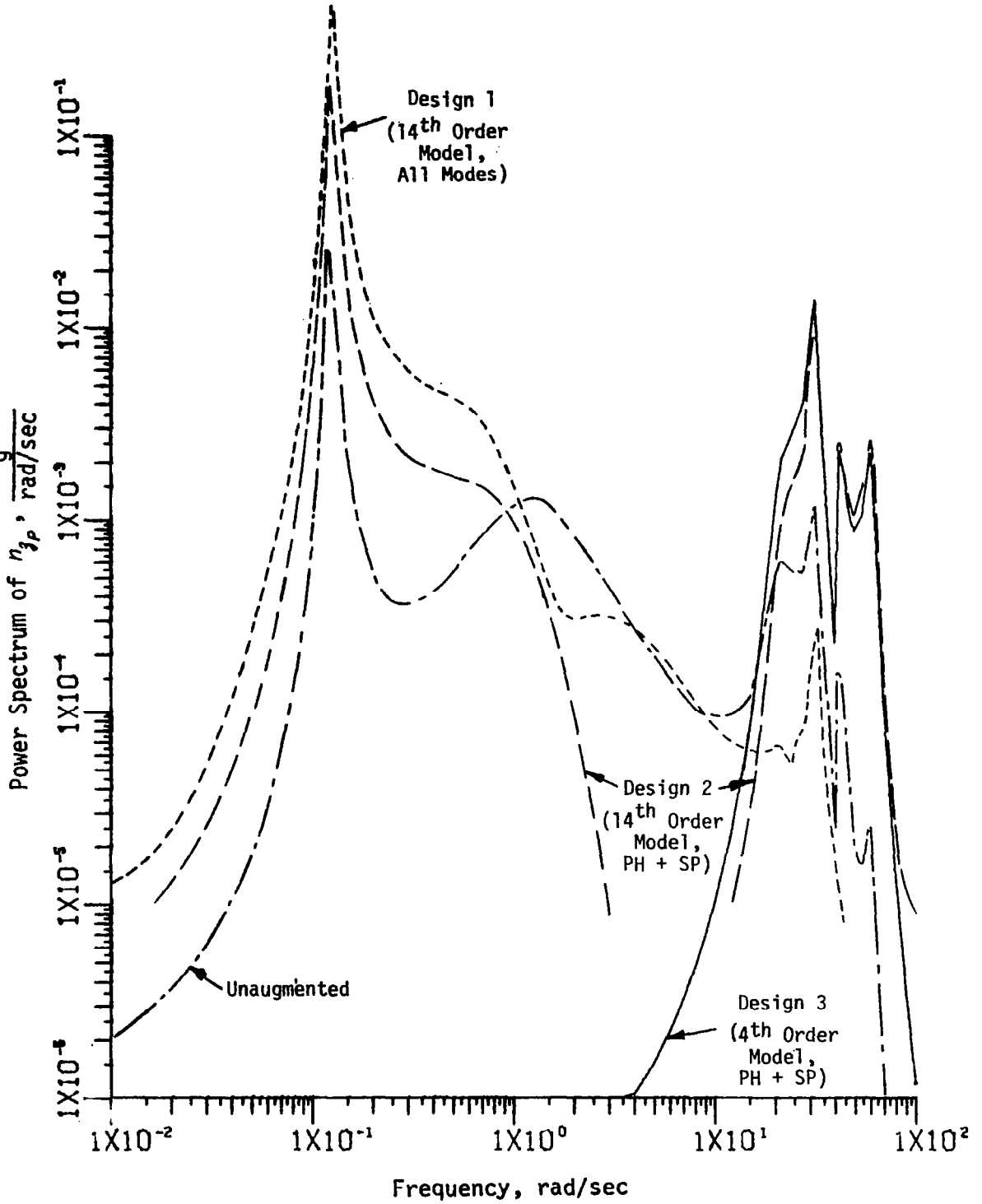

Figure 4 POWER SPECTRUM OF PILOT STATION ACCELEROMETER FOR VARIOUS FEEDFORWARD DESIGNS

The various types of feedforward designs are discussed below.

- Design 1

This formulation involved finding the minimum norm gust effectiveness matrix for the entire 14th order system. When compared to the unaugmented case (first row of Table 4) the norm of the gust effectiveness matrix was reduced from 199 to 30, a sizable improvement. However, the rms accelerations were increased at the pilot's station and the c.g., decreased slightly at the tail, and decreased considerably at the wing tip.

It would seem from this result that if ride quality was the principal goal (minimize accelerations along the fuselage) then this design is not very desirable. If, however, the primary goal is alleviation of wing loads, then this design may be quite useful.

In this design process there is no clear cut way of weighting one mode or modes (wing modes) more or less than other modes (fuselage modes). Simple weighting of the rows of the gust effectiveness matrix in minimizing the norm may be useful. However, this ignores the coupling known to exist between all these modes. This suggests the need for first decoupling the modes of motion using one of several decoupling transformations. This is discussed further in a subsequent section.

- Designs 2 and 3

These designs are based on the assumption that limited actuator bandwidth and limited ability to measure the gust may preclude the alleviation of all modes using feedforward as in Design 1. Designs 2 and 3 attempt to alleviate only the rigid body modes, phugoid and short period. For Design 2 the G and J matrix was from a 14th order model and the first three rows of $-GG_1^{-1}J_1 + J$ were made identically equal to zero (as in Equation (4-42). In Design 3 a quasi-static reduction was first performed so as to eliminate all structural modes. The remaining 4th order model was then used to compute the feedforward gains,

$u = -G_1^+ J_1 v$. The system was, of course, tested on the 14th order system, yielding the gust effectiveness matrix, $-GG_1^+ J_1 + J$. Although no rows of this will be identically zero, however, the quasistatic effects of the structural modes will be included in the gains.

Table 4 shows that overall these systems are not effective. Both the norm of the gust effectiveness matrix and the rms accelerations have increased. What has been accomplished is shown more clearly in Figure 4. Design 3 has all but eliminated the response of the vehicle below a frequency of 4 rad/sec as desired. Considerable amplification of the PSD at higher frequencies has caused the rms to be larger than the unaugmented case. However, in practice sharp filters could be placed at 4 rad/sec and the unaugmented response might be approached in the higher frequency range.

The noticeable lack of success of Design 2 results because of the static effects of the structural modes coupling into the rigid body equations of motion. The rather startling differences between Designs 2 and 3 testify to the importance of quasistatic corrections.

Once again these designs have shown the influence of coupling between the various equations of motion.

- Designs 4 and 5

Designs 4 and 5 are based on the desire to alleviate only the short period and first wing bending mode response of the vehicle. Like the previous two designs, Design 4 used the 14th order model while the Design 5 used a 6th order quasistatic model (PH, SP, 1WB).

Tables 3 and 4 indicate that these designs are totally unacceptable because 1) the feedforward gains are unrealistically high (Table 3),

2) the PSD of n_{z_p} has increased more than 10-fold in the frequency range below 1 rad/sec and 3) because of substantial amplification of structural mode responses at higher frequencies ($\omega > 20$ rad/sec).

4.4.2 Output Equation Gust Alleviation

Thus far in this section of the report concern has been for a feed-forward system designed to minimize the closed loop gust effectiveness matrix for the system equation. We have then evaluated the performance of our system in terms of accelerometers. In this we have ignored the fact that the accelerometers are influenced by the gust velocity in three ways, i.e.

$$y = Ax + Bu + Cv$$

When a control law $u = -G_1^+ J_1 v$ is applied the output equations become

$$y = Ax + \left[-BG_1^+ J_1 + C\right] v$$

Minimization of the norm of closed loop system gust effectiveness ($-GG_1^+ J_1 + J$) is not necessarily consistent with minimization of the closed loop output gust effectiveness matrix

$$\left[-BG_1^+ J_1 + C\right] \tag{4-45}$$

In order to determine the tradeoffs between these two minimizations the following norm was minimized using the generalized inverse solution to obtain the control u*.

$$\left\| \begin{array}{c} Gu^* + Jv \\ \hline k \mid Bu^* + Cv \end{array} \right\| \tag{4-46}$$

The scalar k was used to weight the output equations in the norm more than the system equations. As the parameter k is increased, the term $\|B\dot{u}^* + Cv\|$ tends toward zero.

- Designs 6 and 7

Designs 6 and 7 of Tables 3 and 4 are cases where four accelerometers (pilot station, c.g., tail and wing tip) are weighted into Equation (4-46) with k = 1000 and 10,000 respectively.

Comparing the two gust norms (Table 4) show clearly that minimizing one is not consistent with minimizing the other. Design number 6 represents a substantial improvement over Design 1 and represents the best overall alleviation yet discussed.

We have seen in this section how our criterion of "best" has been expanded from minimizing $\|G\dot{u}^* + Jv\|$ to minizing Equation (4-46) and that improved gust alleviation of the acceleration results.

4.4.3 Feedforward Gust Alleviation Using Modified Jordan Form

The earlier designs indicated the need to compensate in some way for the coupling between modes and for some technique for weighting one mode relative to another. One solution is to first apply a decoupling transformation to the original system of Equations (4-36). In this way the transformed state equation separates or decouples the effects of one mode from the other. Feedforward alleviation can then proceed as before.

For this end we define the transformation $x = RZ$ to the system of Equations (4-36) yielding

$$\dot{z} = R^{-1}FRz + R^{-1}Gu + R^{-1}Jv$$
$$y = ARz + Bu + Cv \qquad (4\text{-}47)$$

For the case considered here with distinct complex eigenvectors, the transformed system matrix has the following form

$$R^{-1}FR = \begin{bmatrix} \sigma_1 & \omega_1 & & & & \\ -\omega_1 & \sigma_1 & & 0 & & \\ & & \sigma_2 & \omega_2 & & \\ & 0 & -\omega_1 & \sigma_1 & & \\ & & & & \ddots & \\ & & & & & \sigma_k \quad \omega_k \\ & 0 & & & & -\omega_k \quad \sigma_k \end{bmatrix} \tag{4-48}$$

The quantities σ_i and ω_i are the coefficients of real and imaginary parts of the ith eigenvalue. The transformation R is derived from the eigenvectors of system (1). The first column of R is the real part of the first eigenvector, the second column of R is the coefficient of the imaginary part of the first eigenvector. Subsequent columns are derived from subsequent eigenvectors in the same manner. As a result R is a matrix of real numbers and the differential Equation (4-47) contains all real numbers. Had we used the matrix of eigenvectors, M, rather than R Equations (4-47) would have contained complex numbers, an undesirable consequence.

The relationship between R and M is given below.

$$R = MK$$

where

$$K = \begin{bmatrix} \frac{1}{2} & -\frac{j}{2} & & & \\ \frac{1}{2} & \frac{j}{2} & & & \\ & & \frac{1}{2} & -\frac{j}{2} & \\ & & \frac{1}{2} & \frac{j}{2} & \\ & & & & \ddots \end{bmatrix} \tag{4-49}$$

Since neither matrix K or matrix M (except for when $F = F^T$) are orthogonal ($M^T = M^{-1}$) matrix R is not orthogonal.

Several comments are pertinent at this point. Equation (4-47) shows that alleviation of the output equation gust effectiveness $Bu + Cv$ is not altered by the decoupling transformation and therefore can be treated exactly as treated earlier. Equations (4-48) show the essential decoupled nature of the new system equation. Each pair of differential equations describes one complex mode which is uncoupled from every other complex mode. It was noted earlier that G and J have several rows of zeroes. This is not the case in general of $R^{-1}G$ and $R^{-1}J$.

The columns of R are determined only to within an arbitrary constant since the eigenvectors of any system are only determined to within an arbitrary constant. To indicate this explicitly, we will define a family of transformations, $\tilde{R}$, computed by multiplying each pair of columns of R by arbitrary constants, i.e.

$$\tilde{R} = RD \tag{4-50}$$

where

$$D = \begin{bmatrix} d_1 & & & & \\ & d_1 & & & \\ & & d_2 & & \\ & & & d_2 & \\ & & & & \ddots \end{bmatrix}$$

Using the generalized inverse solution of the form (4-38) to the system of Equations (4-47) yields the control law

$$u_2^* = -\left[G^T \; R^{-T} \; D^{-T} \; D^{-1} R^{-1} G\right]^{-1} G^T R^{-T} D^{-T} D^{-1} R^{-1} J v(t) \tag{4-51}$$

$$u_2^* = -\left[G^T \tilde{R}^{-T} \tilde{R}^{-1} G\right]^{-1} G^T \tilde{R}^{-T} \tilde{R}^{-1} J v(t)$$

where R^{-T} is the transpose of the inverse of R.

Note that if G is invertible, the control law simplifies to $u = -G^{-1}Jv$ as expected.

The appropriate norm minimized in the generalized inverse solution (4-45) is

$$\left\| D^{-1}R^{-1}G u_2^* + D^{-1}R^{-1}J v \right\| \leq \left\| D^{-1}R^{-1}G u + D^{-1}R^{-1}J v \right\|$$

The square of the left hand side of the above equation is

$$\left[-D^{-1}R^{-1}G u_2^* + D^{-1}R^{-1}J v\right]^T \left[D^{-1}R^{-1}G u_2^* + D^{-1}R^{-1}J v\right]$$

$$= \left[G u_2^* + J v\right] R^{-T}D^{-T}D^{-1}R^{-1} \left[G u_2^* + J v\right] \qquad (4\text{-}52)$$

Minimizing this expression, a weighted norm, is clearly a different problem than the problem addressed earlier, i.e. minimizing (4.1). It is therefore expected that a different control law would be forthcoming. In fact, every new D matrix would produce a new control law. Equations (4-36) and (4-52) will be the same only if

$$R^{-T}D^{-T}D^{-1}R^{-1} = I$$

but neither D nor R are, in general, orthogonal ($D^{-1} = D^T$) so this, in general, is not true.

Control laws derived in accordance with Equation (4-51) is shown in Tables 3 and 4, (Designs 8-12). All seven modes are included in the computations, D = I and the normalization of R is as computed by the eigenvector routine (EISPAC) employed at Calspan.

Once again a multitude of designs are possible. All or part of the rows of $D^{-1}R^{-1}G$ and $D^{-1}R^{-1}J$ can be included in the generalized inverse solution as described earlier, Equations (4-40) - (4-42).

Designs 8 - 12

These designs use the Modified Jordan form equations but include different modes in the generalized inverse solution. The modes included in each design are indicated in Table 3. Power spectra for several of these designs are included in Figure 5.

Design 8,which includes all modes in the generalized inverse solution, has substantially reduced rms accelerations at the four stations compared to the unaugmented case. Design 8 also represents a substantial reduction in fuselage accelerations compared to design 6. However, the wing tip acceleration is reduced in the Design 6. Note that these excellent results were obtained with arbitrary normalization of eigenvectors and without the need to incorporate output gust alleviation, Equation (4-46).

Modified Jordan form designs which attempt to alleviate the responses of only selected modes (Designs 9-12) appear to be superior to earlier designs (Designs 2-5) in that the feedforward gains are in general substantially smaller and performance in terms of rms accelerations considerably improved. The Modified Jordan form design which attempts to suppress the input into only the rigid body modes (Design 10) is remarkably similar in gains and performance to the quasistatic rigid body design (Design 3). This indicates a similarity exists between the four rows of the modified Jordan equations of motion which correspond to the rigid body motion and the fourth order quasistatic rigid body model derived in a different way from the original 14th order system.

Design 11, which includes the two rigid body modes and the first wing bending mode shows reduced rms accelerations compared to Design 8 at all four stations. Design 11 is therefore the design with the lowest fuselage acceleration and should be compared with Design 6 which has lower wing tip accelerations. Which of these designs is best is a matter of priorities to the designer

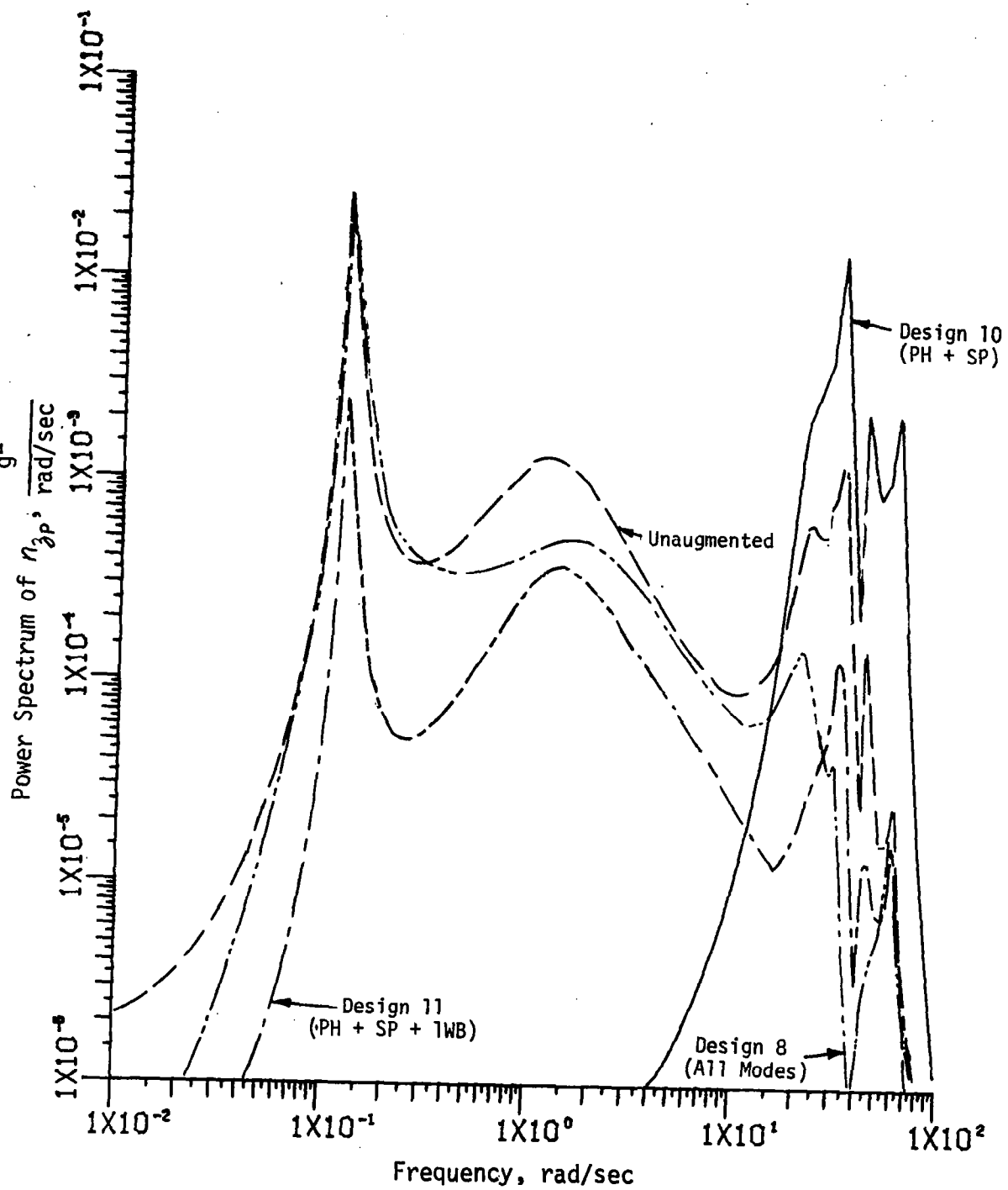

Figure 5 POWER SPECTRUM OF PILOT STATION ACCELERATION FOR THREE MODIFIED JORDAN FORM GUST ALLEVIATION DESIGNS

None of the twelve designs shown in Tables 3 and 4 included actuator dynamics, which were expected to reduce the effectiveness of the designs somewhat. Figure 6 is a plot of the power spectrum of n_{z_p} for gust alleviation Design 11, which includes the phugoid, short period and 1st wing bending mode in the design, but evaluated using the entire set of equations of motion. It was assumed that the actuator dynamics could be approximated by first order, with a bandwidth of 35.1 rad/sec for the collective aileron and direct lift flap and 30 rad/sec for the elevator servo. The results are not as good with the actuator dynamics included, but significant gust alleviation is still demonstrated for frequencies up to about 40 rad/sec. Above that frequency, some slight amplification can be seen. Although not tried, the servo dynamics can be included in the design process, but Figure 6 shows that this would not, in general, be necessary.

The modified Jordan form appears to offer considerable advantages over earlier methods, but several unanswered questions remain in the use of the Jordan form for feedforward gust alleviation design. The first involves whether or not inclusion of output equation gust alleviation would improve the results obtained to date. The second more interesting one concerns how to select the D matrix in order to get "best" results. A first approximation might be to examine the bode plots of Z(s) to determine approximate amplitudes of each Z in the frequency range of interest. (This procedure,of course, ignores the phase angle). Comparison of these amplitudes with the matrix AR from Equation (4-47) may establish the relative imporance of the modes in the frequency range. This relative importance can then be translated into new weighting and the control law then recomputed. Several iterations may be required.

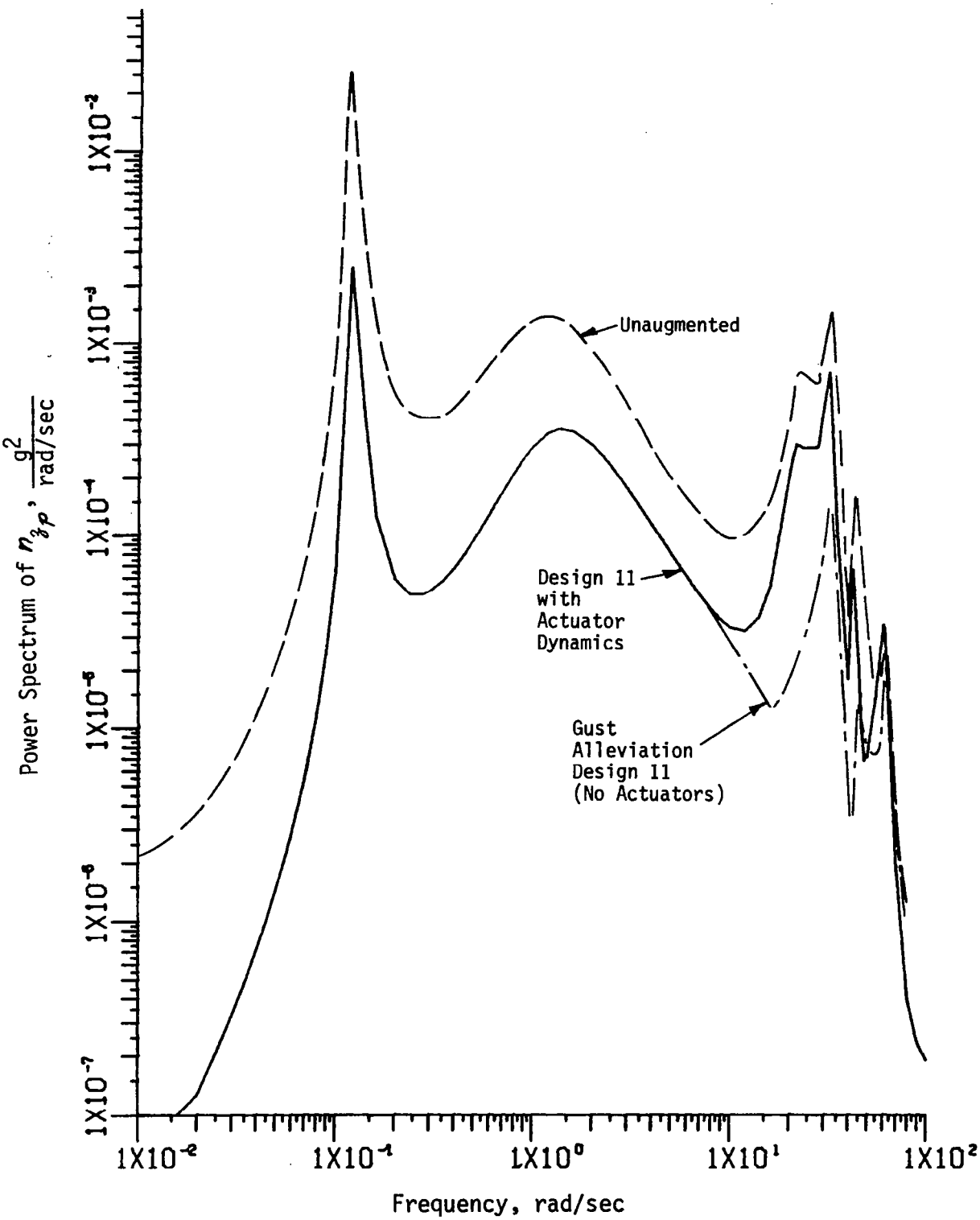

Figure 6 POWER SPECTRUM OF PILOT STATION ACCELERATION FOR GUST ALLEVIATION DESIGN NO. 11, WITHOUT AND WITH ACTUATORS

Section V

MANEUVER LOAD CONTROL

5.1 INTRODUCTION

This section describes a maneuver load control design procedure that has been developed for aircraft under active control. A step-by-step technique is described that is applicable to any aircraft. It is a computer aided rather than a completely automated procedure. Options are provided at every step of the way to allow and incorporate intuition or engineering judgment into the design.

Maneuver load control will involve methods for intercoupling the control surfaces of the vehicle. Many of these surfaces are unorthodox or new in the sense that in the past they have not been used for purposes of maneuvering. It is important then to consider flying qualities requirements very carefully. The maneuver load control system design procedure explicitly incorporates flying qualities requirements as specified by MIL-F-8785B (Reference 12) to guarantee that the interconnections among the various control surfaces will have minimum effect on the flying qualities of the vehicle as specified by the flying qualities criteria.

Control activity or deflection is also an important design consideration. Assuming that the placement and sizing of the control surfaces have been properly done, the control system design should then use all the surfaces adequately and equally to accomplish a load-minimizing maneuver. For instance, a maneuver to increase altitude can be accomplished by using the elevator to rotate the aircraft or by using a direct lift flap to have the effect of an increased L_α. Either method for an actively controlled aircraft would not be taking advantage of the full control capability of the

12. Anon: Military Specification "Flying Qualities of Piloted Airplanes", MIL-F-8785B(ASG), 7 August 1969.

aircraft. Additional control surfaces should enhance the controllability or maneuverability of an air vehicle.

So the design is a tradeoff, and the following procedure allows for complete interaction by the engineer to use his inherent human intelligence to alter the design in a way that incorporates the constraints, criteria and desirable features known intuitively by the experienced engineer, but cannot be adequately put into mathematical form.

The final design is a command augmentation or explicit model following system, although feedback control techniques are used during the course of the design process. Essentially the process can be described as using linear optimal control techniques to define an optimally responding model, the recasting the solution into model-following form. Finally, the system is simplified.

Therefore, feedback control is not an end result, and the maneuver load control system poses no potential stability problems. In fact, the command augmentation model is formulated in such a way that a step command input by the pilot, a fairly abrupt command, will minimally excite the elastic modes of motion of the vehicle. This is a desirable design objective, for if the structural mode control system is either turned off or has become inoperative, command inputs can still be properly filtered to avoid structural oscillations exited by pilot commands.

One of the primary objectives of Maneuver Load Control (MLC) in transport aircraft is to redistribute the wing lift generated in maneuvers to reduce wing bending moments, primarily the wing root bending moment. This was accomplished in the TIFS design in addition to meeting the secondary objectives of minimizing wing root torsion, improved flying qualities and minimum control activity. The resulting system could be mechanized on any transport aircraft and still be completely compatible with other active control concepts. After simplification, the resulting system consisted only of three second order filters inserted between the pilot command inputs and the three control surface actuators.

5.2 SUMMARY OF DESIGN PROCEDURE

The basic design procedure for maneuver load control can be summarized in the steps given below. These steps are enumerated before the actual design is presented so that the procedure does not become lost in the detail of actually carrying out the design example for the TIFS airplane.

1. Define or identify a mathematical model for the vehicle to be controlled.

2. Based upon this analytical description and knowledge of the vehicle, select a mathematical model of an airplane from MIL-F-8785(B) that would produce excellent flying qualities for a transport aircraft of the type under consideration.

3. Solve the implicit model or "model-in-the-performance index" linear optimal control problem. The performance index contains not only the errors between the equations of motion of the actual aircraft and flying qualities model, but also a measure of wing bending moment, torsion and control activity.

4. Using the resulting controlled vehicle, calculate feedforward command gains that yield desirable steady state responses and control deflections during a maneuver, in this case a pull-up maneuver.

5. Transform the solution into the model following configuration. (See Appendix E).

6. Transform the model with its feedforward matrix of gains into transfer function form.

7. Simplify and reduce the order of the resulting transfer function for ease in mechanization. The resulting system

is three second order filters, located between the pilot stick and each of the three control surfaces to be used for maneuvering.

5.3 APPLICATION TO THE TIFS AIRCRAFT

5.3.1 Step One, the TIFS Mathematical Model

The analytical model for the basic TIFS aircraft shown in Table 5 was taken from the FLEXSTAB estimates that are fully described in Appendix A. A quasistatic reduction was performed on the complete equations to reduce them to sixth order. Only the first three complex modes were retained: phugoid, short period, and 1st wing bending. The equations for the sensors, wing root bending moment, torsion, and shear were also obtained from these FLEXSTAB estimates. The TIFS was assumed to have the following three controllers available for MLC:

δ_{CA} - outboard collectively acting ailerons
δ_z - direct lift flaps
δ_e - elevator

For some of the calculations the actuator dynamics were needed. Second order estimates of these were obtained from flight data for δ_z and δ_e (Appendix D). The δ_{CA} actuator was assumed to be the same as that for δ_z. The cruise flight condition was chosen as a design example because this is where the largest maneuver loads for pullups would be encountered.

The equations are presented in the following form:

$$\dot{x} = Fx + Gu \qquad \text{state equations} \qquad (5\text{-}1)$$

$$y = Ax + Bu \qquad \text{sensor equations} \qquad (5\text{-}2)$$

TABLE 5

COEFFICIENTS OF THE MATRICES OF THE TIFS EQUATIONS OF MOTION

CRUISE CONDITION

MATRIX F

-1.65245E-02	-5.10653E-05	1.48578E+00	-9.80567E+00	-5.79269E-05	-4.09037E-04
-1.43273E-01	-1.70442E+00	1.50866E+02	9.74633E-02	3.62694E-01	2.80316E-02
-4.27360E-04	-1.45166E-02	-1.61463E+00	-2.35165E-04	-4.61323E-03	-2.67665E-04
0.0	0.0	1.00000E+00	0.0	0.0	0.0
0.0	0.0	0.0	0.0	0.0	1.00000E+00
2.87526E+01	3.18270E+02	-1.13045E+03	-7.72187E-01	-5.12806E+02	-1.17597E+01

MATRIX G

-1.14242E-02	7.62336E-04	-1.32623E-02
-5.32292E-01	-6.55420E-01	-5.92636E-01
-1.69244E-02	-9.59832E-03	-1.37267E-01
0.0	0.0	0.0
0.0	0.0	0.0
2.16602E+02	1.56207E+02	-3.96892E+01

MATRIX A

9.49719E-03	1.03683E-01	9.33359E-01	-3.02472E-04	-3.79519E-01	-6.51838E-03
-5.87587E-03	-7.67488E-02	-1.73186E-01	-1.48274E-04	-1.18170E-01	-6.94909E-04
9.57288E-03	8.20338E-02	-2.81840E+00	-8.71249E-04	-4.08983E-01	-7.56602E-03
-2.03880E-01	-2.26975E+00	7.40380E+00	5.13795E-03	3.41169E+00	8.02311E-02
-7.32216E-02	-8.22465E-01	2.43304E+00	1.65409E-03	1.08264E+00	2.68378E-02
-7.61618E-02	-8.55919E-01	2.39736E+00	1.71019E-03	1.13394E+00	2.79993E-02
2.36946E-02	2.38142E-01	-3.40853E+00	-1.25578E-03	-6.61107E-01	-1.33512E-02
4.34353E-04	4.88840E-03	5.72079E+01	2.88694E-04	-6.57159E-03	-7.34742E-03
8.29826E-05	3.83341E-01	-3.90529E+00	9.88909E-05	-1.14016E-03	2.91664E-03
-9.42940E+02	-3.09600E+03	-2.62120E+03	3.29500E+00	1.52725E+04	2.11843E+02
-7.14202E+03	-5.30917E+03	2.72893E+04	1.32045E+01	1.09504E+05	5.69811E+02
1.68233E+02	3.09937E+03	-2.49615E+04	-1.30144E+01	-2.78838E+03	-3.69365E+01

MATRIX B

1.42175E-01	7.20293E-02	5.60957E-02
1.19916E-02	-1.91205E-02	-6.72606E-02
1.11253E-01	5.57201E-02	-2.60783E-01
-1.48138E+00	-1.09576E+00	1.88498E-01
-4.95693E-01	-3.85180E-01	2.21894E-02
-5.19114E-01	-4.01829E-01	1.34646E-02
2.17343E-01	1.32285E-01	-2.83226E-01
3.02156E-03	2.31215E-03	1.72205E-04
5.51026E-04	4.36197E-04	9.58817E-05
-4.22551E+03	3.75863E+01	1.89571E+03
-7.15948E+03	2.80967E+02	1.25943E+04
-1.26557E+03	-4.60523E+03	-1.81411E+02

where: x =

u,	m/sec
w,	m/sec
q,	rad/sec
θ,	rad
η_1,	normalized 1st wing
$\dot{\eta}_1$,	bending mode

y =

$n_{z\,PILOT}$	accelerometers, g's
$n_{z\,CG}$	
$n_{z\,TAIL}$	
$n_{z\,WING\,TIP}$	
$n_{z\,FWD\,SFS}$	
$n_{z\,AFT\,SFS}$	
$n_{z\,HORIZ.\,TAIL\,TIP}$	
q_{CG},	deg/sec
α_{VANE},	deg
wing root shear,	Newton's
wing root torsion,	N-m
wing root bending moment,	N-m

u =

δ_{CA},	deg
δ_z,	deg
δ_e	deg

actuator dynamics:

$$\frac{\delta_{CA}}{\delta_{CA_{COMMAND}}} \equiv \frac{\delta_z}{\delta_{z_{COMMAND}}} \equiv \frac{2524}{s^2 + 100.5s + 2524} \qquad (5\text{-}3)$$

$$\frac{\delta_e}{\delta_{e_{COMMAND}}} \equiv \frac{840}{s^2 + 42s + 900} \qquad (5\text{-}4)$$

5.3.2 Flying Qualities Model

The TIFS aircraft has fairly good longitudinal flying qualities according to the specifications of MIL-F-8785B. At the cruise flight condition of:

$$V = 150 \text{ m/sec}$$
$$h = 3050 \text{ meters}$$
$$wt = 24700 \text{ Kg}$$

its characteristics are:

short period $\zeta = .694$
$\omega = 2.25$ rad/sec

phugoid $\zeta = .147$
$\omega = .047$ rad/sec

first wing bending mode $\zeta = .266$
$\omega = 22.5$ rad/sec

$n_z/\alpha = 22.57$ g/rad

This puts the TIFS in the level 1 region of flying qualities but near the lower boundary of the frequency requirements. In order to improve upon these characteristics it was decided to increase the ω_{sp} so that $\omega^2/(n_z/\alpha) \equiv 1$, and increase the ζ_{sp} to .7. The fourth order description of the TIFS from FLEXSTAB was used as a start for the good flying qualities model. This would yield a model without the first wing bending mode of the TIFS and would hopefully force the final TIFS configuration with its MLC system operating to respond with little motion from this mode. The only derivatives of the base fourth order TIFS model that had to be changed were M_w and M_q. These were obtained from the short period approximations of:

$$\omega_{SP} = \sqrt{M_q Z_\alpha - V M_w} \tag{5-5}$$

$$\zeta_{SP} = \frac{-Z_\alpha + M_q + V M_{\dot{w}}}{2\omega_{SP}} \tag{5-6}$$

The flying qualities model obtained from this procedure yielded the following characteristics:

short period	ζ	= .699
	ω	= 4.76
phugoid	ζ	= .104
	ω	= .070

5.3.3 Linear Optimal Control Solution

The object of obtaining an optimal control solution is to synthesize an analytical MLC model which the TIFS can simulate with its standard model following system. The model should exhibit good flying qualities and produce a minimum maneuver wing root bending moment and torsion with a minimum of control activity. The feedback gains from this solution along with the command gains obtained in the next step of the design procedure will completely define the new MLC model.

To satisfy the requirements of this MLC model, a performance index was formulated that included quadratic measures of the error in dynamic response between the actual aircraft and the flying qualities model, maneuver wing root bending moment and torsion, and control surface motions. The quadratic performance index is an indirect, rather than direct, measure of the design objectives but it does provide a stable solution and a way to obtain systematic trade-offs among the different requirements. The modeling error, wing root bending moment and torsion are minimized relative to each other in a way that

produces a most useful kind of solution to the problem. The control motions are relatively smooth and well behaved and the control effort and maximum deflections are managed by the judicious choice of weighting parameters in the performance index. The resulting control law is linear for a linearized description of the airplane dynamics. The performance index, originally investigated in Reference 13, is of the general form:

$$2J = \min_{u} \int_{0}^{\infty} \left[\| \dot{x} - \mathcal{L} x \|^2_{Q_1} + \| WRBM \|^2_{Q_2} + \| TORSION \|^2_{Q_3} + \| u \|^2_{R} \right] dt \tag{5-7}$$

which is solved for the feedback gains, K, of the control law

$$u = -Kx \tag{5-8}$$

subject to the constraint of the equations of motion of the base TIFS:

$$\dot{x} = Fx + Gu$$

In the performance index of Equation (5-7),

where:

$\mathcal{L}$ = matrix of coefficients of good flying qualities model

u = control deflections $\left[\delta_{CA}, \delta_{\zeta}, \delta_{e}\right]^T$

x = state vector $\left[u, \omega, q, \theta, \eta_1, \dot{\eta}_1\right]^T$

Q_1, Q_2, Q_3, R = weighting matrices

$\| x \|^2_Q = x^T Q x$

The problem of minimizing a quadratic performance index is a well established method of flight control system synthesis and literally hundreds of papers and reports have been written on the subject since the technique

13. Rynaski, E. G. and Weingarten, N. C., "Flight Control Principles for Control Configured Vehicles", Calspan Corporation Report No. TB-3052-F-1, also AFFDL-TR-71-154, January 1972.

was formalized and popularized by R. E. Kalman (Reference 14) and S. S. Chang (Reference 15). Later reports, like Reference 16, established the relationships that exist between the performance index form of solution (called linear optimal control) and the more conventional control system synthesis techniques, like root locus methods.

Many cases were run with varying values for the weighting matrices. The final solution which was selected for further analysis was chosen on the basis of matching the good flying qualities model short period characteristics with a first wing bending mode having a high frequency and damping ratio. The wing root bending moment and torsion were not affected much by the different weighting matrices, but were mostly a function of the steady state values of the states chosen in the following step. The characteristics obtained are summarized below.

		Good Flying Qualities Model	Basic TIFS	Optimal Control MLC Model	
Phugoid	ζ	.104	.147	.131	Phugoid basically unchanged
	ω	.070	.047	.090	
Short Period	ζ	.699	.694	.702	Short period frequency increased
	ω	4.76	2.25	4.73	
First Wing Bending	ζ	---	.266	.904	1st wing bending frequency and damping increased
	ω	---	22.5	43.8	

14. Kalman, R. E., Englar T. and Bucy, R., "Fundamental Study of Adaptive Control Systems", Vol. I and II, ASD-TR-61-27, March 1961 and March 1962.

15. Chang, S. S. L., "Synthesis of Optimum Control System", McGraw-Hill Book Company, Inc., 1961.

16. Rynaski, E. G. and Whitbeck, R. F.: "The Theory and Application of Linear Optimal Control", Calspan Corporation Report No. IH-1943-F-1, AFFDL-TR-65-28, October 1965.

The feedback matrix K of u = -Kx was:

(deg)	u (m/s)	w (m/s)	q (rad/s)	θ (rad)	η_1	$\dot{\eta}_1$
δ_{sn} /	4.68241E-02	8.50169E-01	-6.19373E+00	-7.80913E-01	-9.24156E-01	1.15226E-01
δ_s /	-9.79215E-01	2.31855E+00	4.37801E+01	2.79169E+00	1.37443E+01	3.32422E-01
δ_c /	-5.18436E-01	9.68570E-03	-2.33896E+00	-5.05465E-01	7.86013E+00	1.03279E-01

(5-9)

This type of feedback control law cannot be mechanized in a real airplane since the normalized mode deflection (η_1) and rate ($\dot{\eta}_1$) can not directly be measured. However, since this control law is just being used to analytically define a new MLC model for the model following system, it can be used in this analysis.

For an idea of the size of these gains, however, an approximate (infinitely fast actuators) transformation was performed on them to describe them in terms of the following sensors:

$$y = \begin{bmatrix} \Delta u & (m/sec) \\ \Delta \alpha_{VANE} & (deg) \\ q_{CG} & (deg/sec) \\ \Delta\theta & (deg) \\ \Delta n_{z_{CG}} & (g's) \\ \Delta n_{z_{WING\ TIP}} & (g's) \end{bmatrix}$$

if $u_c = -Kx$

or $u_c = [-KO]\begin{bmatrix} x \\ u \end{bmatrix}$

and $y = Ax + Bu$

or $\begin{bmatrix} y \\ u \end{bmatrix} = \begin{bmatrix} A & B \\ O & I \end{bmatrix}\begin{bmatrix} x \\ u \end{bmatrix}$

then $\begin{bmatrix} x \\ u \end{bmatrix} = \begin{bmatrix} A & B \\ O & I \end{bmatrix}^{-1}\begin{bmatrix} y \\ u \end{bmatrix} = [S]^{-1}\begin{bmatrix} y \\ u \end{bmatrix}$

$\therefore$ $u_c = [-K \vdots O][S]^{-1}\begin{bmatrix} y \\ u \end{bmatrix}$

or

$$u_c = [P : Q]\begin{bmatrix} y \\ u \end{bmatrix}$$

let

$$u_c = u$$

then

$$[I - Q]u_c = [P]y$$

$$u_c = [I - Q]^{-1}[P]y \qquad (5\text{-}10)$$

This above control law is:

$$\delta_{CA} = .0423\ \Delta u + .122\ \Delta\alpha_V - .157 q_{CG} - .0186\Delta\theta + 2.75\Delta n_{z_{CG}} - .180\Delta n_{z_{WT}}$$

$$\delta_z = -.0115\ \Delta u - 1.17\ \Delta\alpha_V - .689 q_{CG} + .0105\Delta\theta - 5.15\Delta n_{z_{CG}} - 1.03\Delta n_{z_{WT}}$$

$$\delta_e = -.1227\ \Delta u - 1.57\Delta\alpha_V - .259 q_{CG} + .0111\Delta\theta - 9.19\Delta n_{z_{CG}} + .067\Delta n_{z_{WT}} \qquad (5\text{-}11)$$

Units

δ_i	(deg)	q_{CG}	(deg/sec)
Δu	(m/sec)	$\Delta\theta$	(deg)
$\Delta\alpha_V$	(deg)	Δn_{z_i}	(g's)

None of the gains are particularly large. However, if this type of control system was chosen for MLC, it could be in conflict with other active control concepts such as gust alleviation or relaxed static stability due to the feedback of α_{VANE} and measured accelerations. So the control system was reformulated as a model following system.

5.3.4 Command Gains and Complete MLC Model Development

The linear optimal control solution described in the above step describes only the feedback or regulator part of the solutions to the MLC problem. The input or command gains must also be defined. It was decided to separately compute the feedforward command gains to yield a good quasi-

steady state match of the model at some time into a given maneuver, while the feedback gains would give a good dynamic match.

The maneuver chosen for the MLC system was pilot command input for a one-g pullup and the quasi-steady state final time was t = 3 seconds. At this time the short period had responded but there would be no significant speed change. Since there are only three control surfaces to control the four degrees of freedom of motion of the TIFS (including η_1) the problem cannot be exactly solved. However, the command gains do yield values for the states close to those desired.

The command input gains are obtained by solving for the values of the control vector u_c in the following equation:

$$\dot{x}_m(t_f) = \left[F - GK\right] x_m(t_f) + G u_c$$

$$u_c = (G^T G)^{-1} G^T \left\{ \dot{x}_m(t_f) - \left[F - GK\right] x_m(t_f) \right\} \qquad (5\text{-}12)$$

where t_f = 3 sec

F, G = the 6th order base TIFS model

K = feedback gains from the optimal control solution

$x_m(t_f)$ & $\dot{x}_m(t_f)$ are the values for the states of the good flying qualities model at t = 3 sec for u, w, q, θ. The values for η_1 and $\dot{\eta}_1$ were originally fixed at 0 to force little motion in the first wing bending mode at t = 3 sec.

This guarantees that the states of the MLC model have nearly the same values as the good flying qualities model 3 seconds after the command input. The trajectory of the response between t = 0 and t = 3 seconds will be different and this difference will be a function of how closely the re-

quirement of minimum dynamic error between the model and actual response compared to the other minimization requirements of the performance index.

To determine how well the optimal control solution was working compared to the unaugmented TIFS, a one-g δ_e pullup was generated. Using δ_z and δ_e together without feedback was also investigated. It turned out that the center of lift due to δ_z was outboard of the center of lift due to α. Therefore, gearing δ_z and δ_e increased wing root bending moment and only decreased $\Delta\alpha$ as δ_z was used to generate the one-g pullup. Gearing δ_{CA}, δ_z, and δ_e without feedback would produce the same steady state values as the optimal control solution with command gains, but of course would not have the improved flying qualities of the MLC model.

The optimal control solution with command gains chosen to match all states of the good flying qualities model at t = 3 sec yielded an 85% reduction in maneuver wing root bending moment (64,000 N-m vs. 450,000 N-m) but increased the torsion by 600% (60,000 N-m vs. 9,000 N-m) over the base TIFS δ_e pullup. This increase in torsion is not as large as it may appear since δ_{CA} and δ_z will torque the wing while α alone has little effect on torsion. However, it was felt that the torsion should be held to a minimum. If more positive δ_z was used (by reducing the α at t = 3 seconds) to balance out the negative δ_{CA}, reduced wing root torsion would result. This, of course, would increase the bending moment, but as it turned out, not by much. When $\Delta\alpha$ at t = 3 seconds was reduced from the exact match of 4 degrees to 3 degrees a minimum plus/minus excursion in torsion resulted ($\pm$16,000 N-m) while bending moment only increased slightly (98,000 N-m). However, the magnitude of δ_{CA} needed for the one-g pullup increased to -16.2 degrees. This was judged to be excessive. Also the 78% reduction in bending moment was not felt to be necessary. Therefore the goal of a 50% reduction in maneuver wing root bending moment with minimum torsion was set. To obtain the increased bending moment, the value of η_1 at t = 3 seconds was allowed to increase from its original value of zero. The 50% reduction in bending moment was attained while torsion was held to $\pm$18,000 N-m with only -10 degrees of δ_{CA}

necessary. This is a 100% increase in torsion over a δ_e only pullup but is equivalent to the torsion produced by a 5.5 degree aileron input.

The command gains obtained for a one-g pullup were:

$$\delta_{CA}/\delta_{CMD} = -5.33$$
$$\delta_z/\delta_{CMD} = 51.7$$
$$\delta_e/\delta_{CMD} = 13.7$$

The control deflections required are not as large as the above gains imply due to the feedback gains that are also used.

A summary of the above procedure is shown in Table 6. All values shown are the quasi-steady state values at t = 3 seconds. Figure 7 shows the comparison of the augmented TIFS and MLC model one-g pullup responses.

5.3.5 Model Following System for TIFS

In cases of global controllability, the model following and the feedback solutions to the problem of forcing one vehicle to respond exactly as programmed are exact equivalents or duals of one another. Appendix E discusses this duality and shows the general relationships and restrictions for implicit and explicit model following.

A standard model following system for TIFS was obtained next. Using just the unaugmented fourth order equations for TIFS, feedforward gains were calculated that would force this description of TIFS to exactly follow u, w, q, and θ of the sixth order MLC model. It was felt that if the states were matched, then η_1, wing root bending moment and torsion would also closely match the MLC model's response.

The model following gains were calculated from the following equations:

TABLE 6

ONE-G PULL-UP MLC RESULTS

	Unaugmented TIFS δ_e only	Unaugmented TIFS δ_z and δ_e Pull-up	Opt. Cont. Sol. Match all states at t = 3 sec	Opt. Cont. Sol. Vary $\Delta\alpha$ (t=3) for Min. Tors.	Opt. Cont. Sol. Vary η_1 (t=3) for Smaller $\delta_{i_{s.s.}}$
Maximum Wing Root Bending Moment, N-m	450,000	564,000	64,000	98,000	226,000
Maximum Wing Root Torsion, N-m	9,000	-51,000	60,000	±16,000	±18,000
$\Delta\alpha$, deg	2.6	1.3	4.0	3.0	2.9
$\eta_{1_{s.s.}}$	4.5	5.4	0.	0.	1.7
$\delta_{e_{s.s.}}$, deg	-1.67	-2.05	0.	0.	-.6
$\delta_{z_{s.s.}}$, deg	--	10.0	-2.3	6.4	3.4
$\delta_{CA_{s.s.}}$, deg	--	--	-13.8	-16.2	-10.
Remarks	Yields high wing root bending moment, low torsion	No Improvement, just trades $\Delta\alpha$ with δ_z with increasing WRBM & Torsion	Very low WRBM, high torsion (but same level as that due to unaugmented TIFS δ_z pull-up)	By reducing $\Delta\alpha$ in pull-up, more δ_z & δ_{CA} are required but torsion was minimized at equal ± excursion	By letting WRBM and η_1 increase to about half of unaugmented TIFS maneuver values, lower control motions are required, torsion is equivalent to that due to a 5.5 deg δ_{CA} input

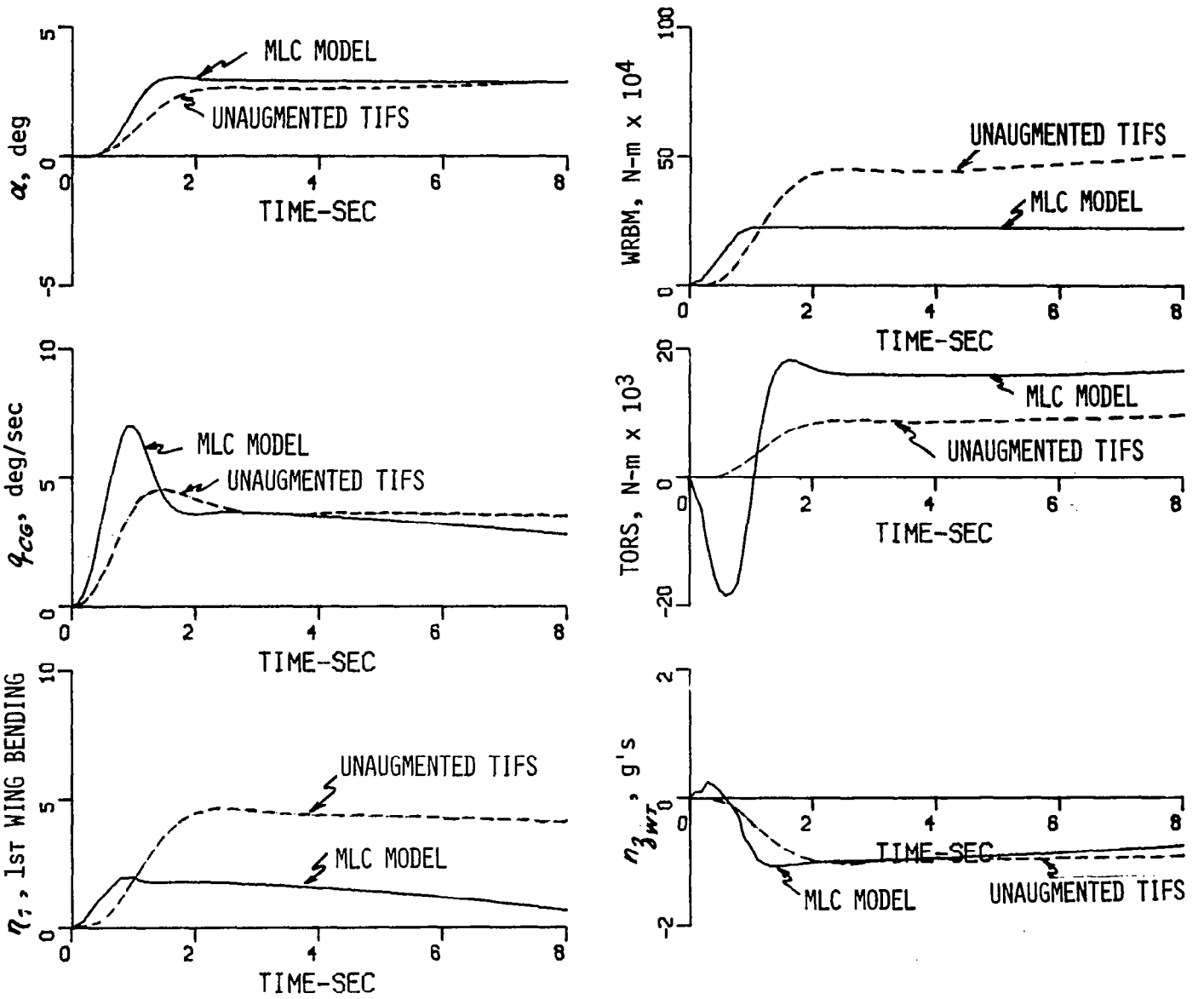

Figure 7 RESPONSE OF UNAUGMENTED TIFS AND MLC MODEL TO ONE-G PULL-UP COMMAND

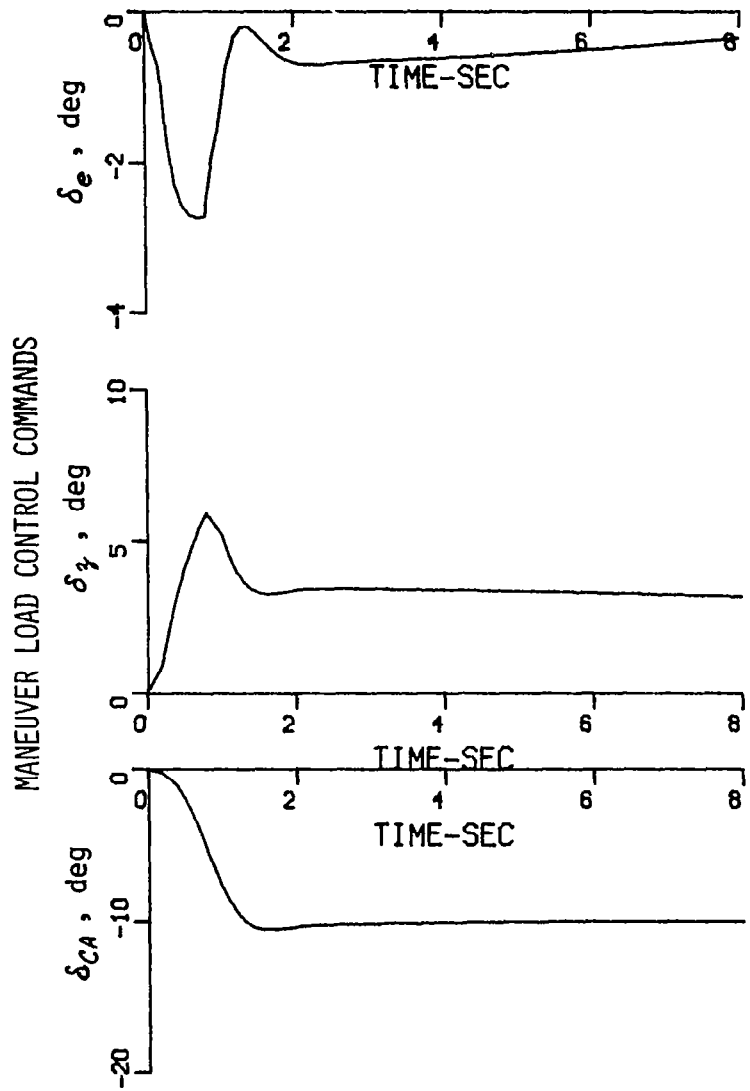

Figure 7 (Cont'd) RESPONSE OF UNAUGMENTED TIFS AND MLC MODEL TO ONE-G PULL-UP COMMAND

$$\dot{x}_{TIFS} = F_{TIFS} x_{TIFS} + G_{TIFS} u$$

if $$u = -K_1 x_{MLC} - K_2 \dot{x}_{MLC}$$

where $$[x]^T = [u, w, q, \theta]$$

then $$\dot{x}_{TIFS} = F_{TIFS} x_{TIFS} - G_{TIFS} K_1 x_{MLC} - G_{TIFS} K_2 \dot{x}_{MLC}$$

if $$x_{TIFS} = x_{MLC} \quad \text{and} \quad \dot{x}_{TIFS} = \dot{x}_{MLC}$$

then $$K_1 = \left[G^T G\right]^{-1} G_{TIFS}^T F_{TIFS} \tag{5-13}$$

$$K_2 = -\left[G^T G\right]^{-1} G_{TIFS}^T \tag{5-14}$$

To check the results of this model following setup, the complete system was mechanized on a digital computer. The above model following gains were used with the sixth order TIFS equations and controllers modeled with second order actuators. This complete system is shown in Figure 8. Almost exact model following was achieved as is shown in Figure 9. The slight mismatches were primarily due to actuator lags.

5.3.6 Transfer Function Form

The complete MLC model and model following system could be mechanized on the TIFS. However, a system as complex as this would not be practical to be implemented on a production transport aircraft. Therefore, a simplification to this system was sought.

It was decided to transform the entire MLC model mechanization and model following system into a command augmentation system. This could be done since no feedback was required to obtain the proper responses. The complete MLC system of Figure 8 can then be written as:

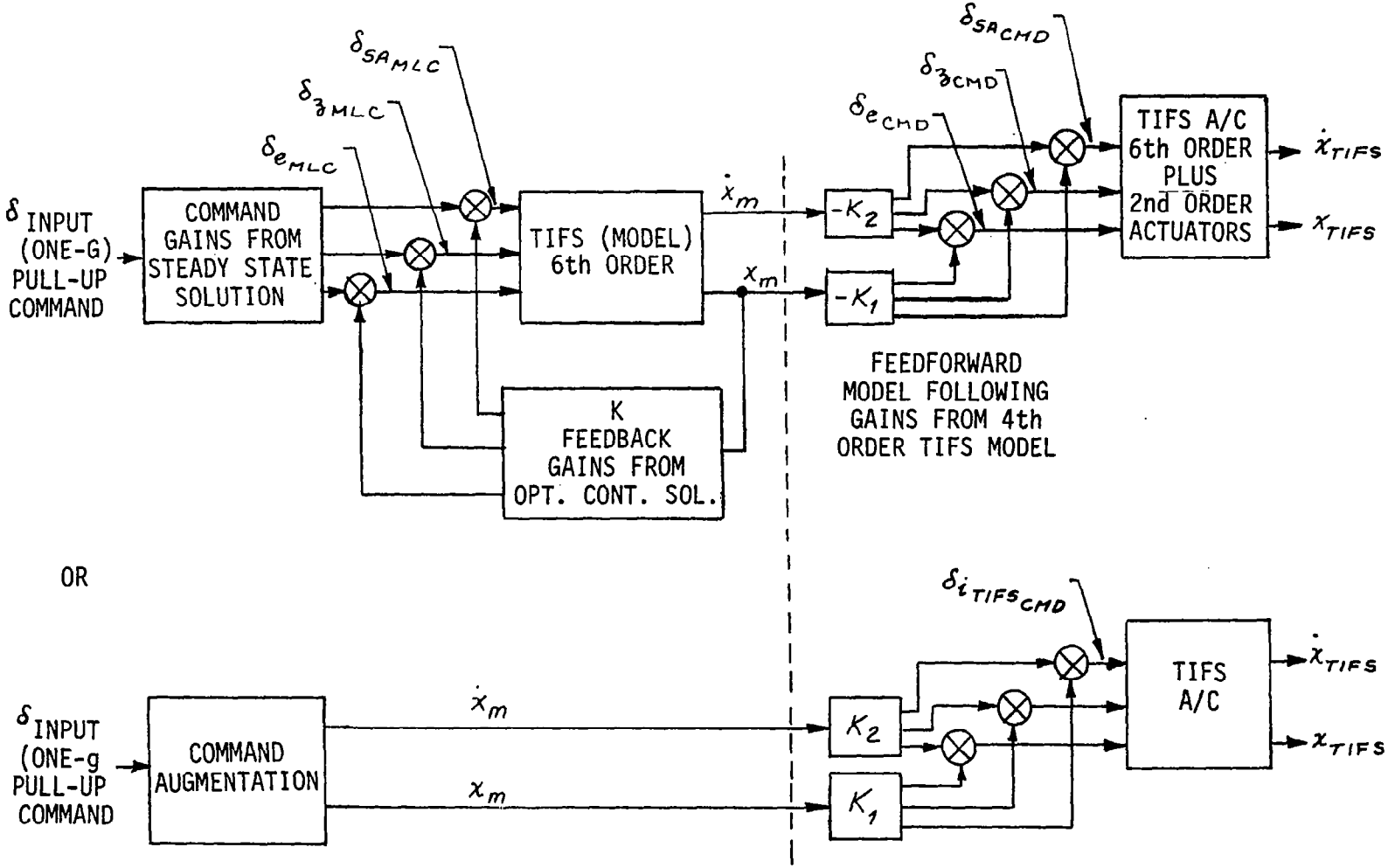

Figure 8 MLC MODEL AND TIFS MODEL FOLLOWING SYSTEM

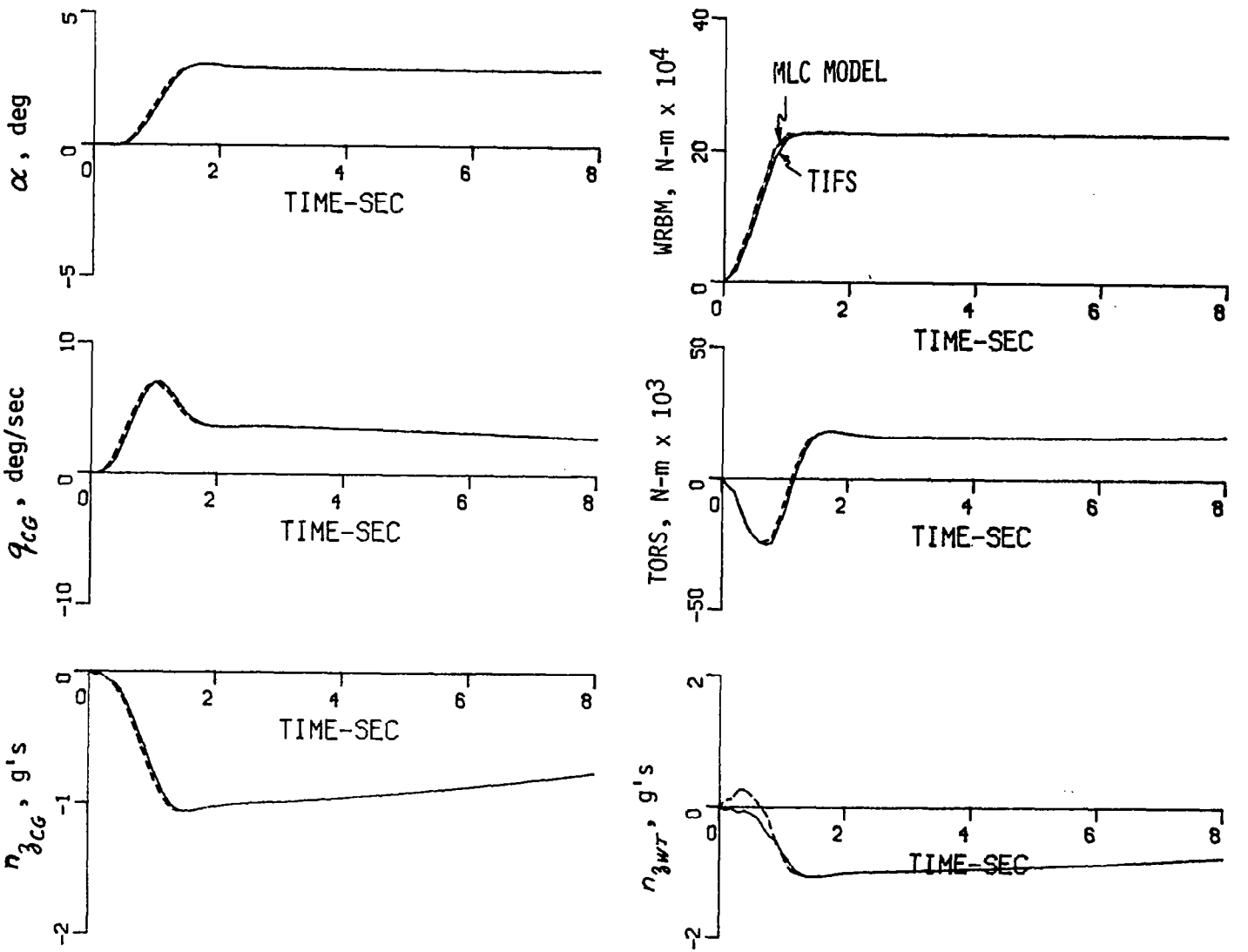

Figure 9 RESPONSE OF MLC MODEL AND TIFS WITH MODEL FOLLOWING

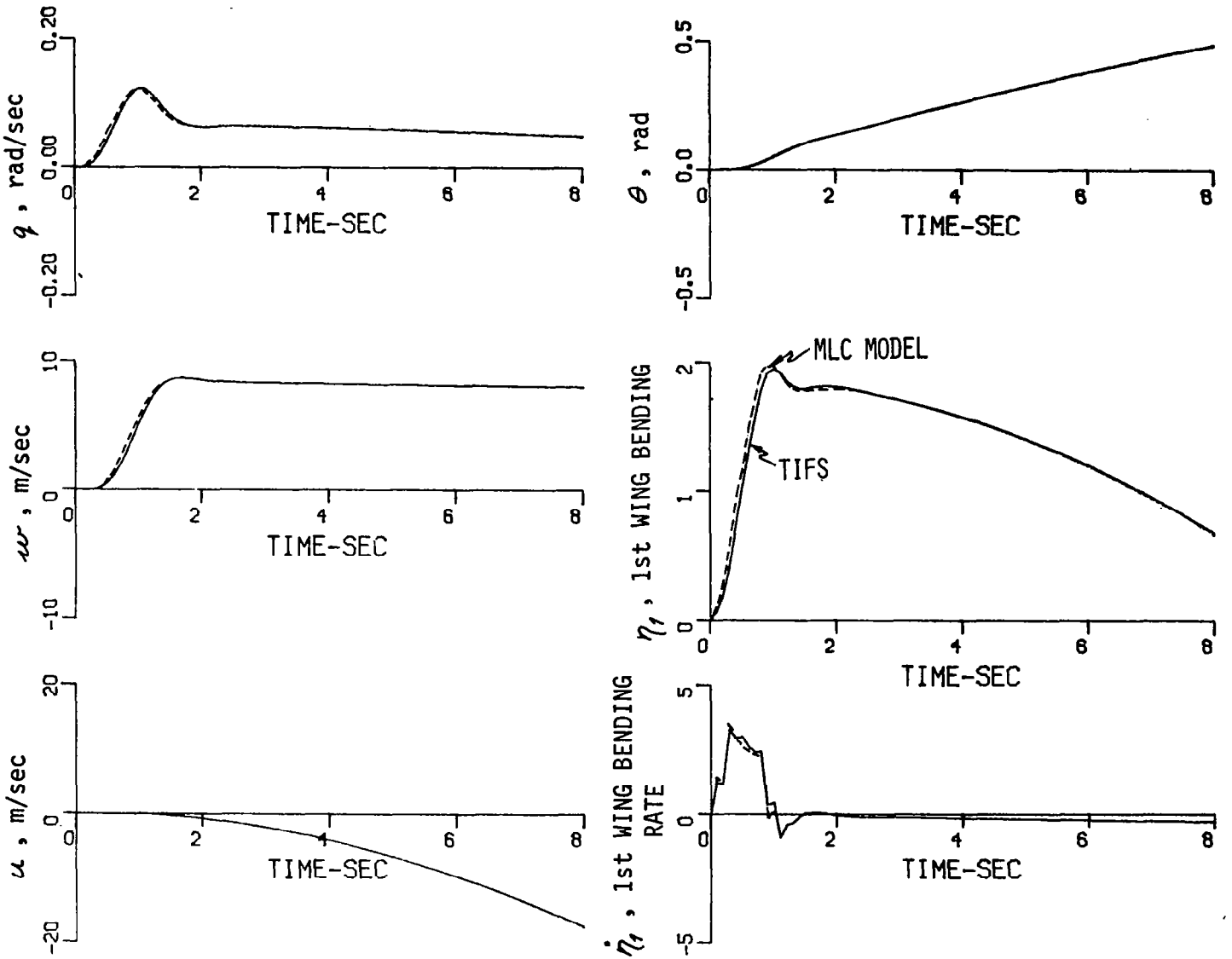

Figure 9 (Cont'd) RESPONSE OF MLC MODEL AND TIFS WITH MODEL FOLLOWING

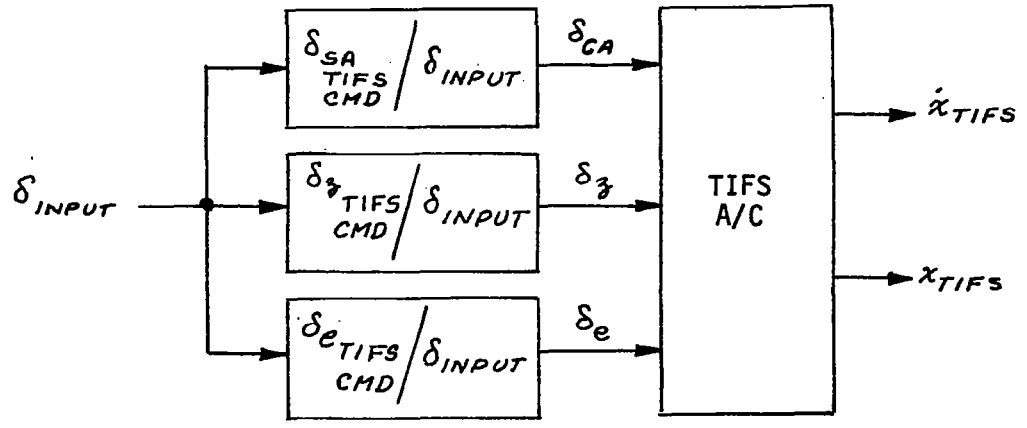

where each of the three ($\delta_{i_{TIFS\ CMD}} / \delta_{INPUT}$) blocks are simply transfer functions or filters that the input is processed through to obtain the TIFS commands. These transfer functions were obtained by multiplying the MLC model transfer functions by the feedforward model following gains

$$\frac{\delta_{i_{TIFS\ CMD}}}{\delta_{INPUT}}(s) = \left[-K_1\right]\left[\frac{x_m}{\delta_{INPUT}}(s)\right] + \left[-K_2\right]\left[\frac{\dot{x}_m}{\delta_{INPUT}}(s)\right] \qquad (5\text{-}15)$$

The resulting transfer functions were sixth order numerators over sixth order denominators. These filters would produce the same response as the complete MLC model and model following mechanization.

The characteristics of these transfer functions or filters are summarized below:

	NUMERATORS		DENOMINATOR		
$\frac{\delta_{CA}}{\delta_{INPUT}}$	ζ_1 =	.057	ζ_1 =	.131	phugoid
	ω_1 =	.0981	ω_1 =	.0895	
	ζ_2 =	- .101	ζ_2 =	.702	short period
	ω_2 =	6.53	ω_2 =	4.725	
	τ_1 =	.090	ζ_3 =	.905	first wing bending
	τ_2 =	.0035	ω_3 =	43.83	
	gain =	-12.47			

$\frac{\delta_z}{\delta_{INPUT}}$

$\zeta_1 = .215$

$\omega_1 = .068$

$\zeta_2 = .778$

$\omega_2 = 17.65$

$\tau_1 = .987$

$\tau_2 = .128$

gain = 1.98

$\frac{\delta_e}{\delta_{INPUT}}$

$\tau_1 = -12.78$

$\tau_2 = 7.91$

$\tau_3 = 1.67$

$\tau_4 = .437$

$\tau_5 = -.0383$

$\tau_6 = .0153$

gain = .834

5.3.7 Simplification of Transfer Functions

Even though the transfer functions defined above may be more practical to implement than the original MLC system, they still are somewhat complex. Therefore, it was decided to simplify or approximate these transfer functions with lower order filters which would be much easier to mechanize.

The method used was to fit the Bode diagrams with lower order transfer functions by a least squares method. This is the same method which was used to model the flexible characteristics of the TIFS from flight data (References 7 and 8). The simplest approximation that was attempted was to fit the Bode diagrams with second order numerators over second order denominators. The denominator characteristics were held fixed at the desired short period characteristics of the full transfer functions and the steady state gains were also fixed. Second order numerators were then identified. It was felt that this would yield command augmentation filters which would

produce control motions for response matches in the frequency range of interest. The characteristics of these transfer function approximations are shown below:

	NUMERATORS	DENOMINATOR
$\frac{\delta_A}{\delta_{INPUT}}$	ζ = .063	ζ = .702
	ω = 6.67	ω = 4.725
	gain = -10.15	
$\frac{\delta_z}{\delta_{INPUT}}$	τ_1 = .683	
	τ_2 = .261	
	gain = 3.45	
$\frac{\delta_e}{\delta_{INPUT}}$	τ_1 = 3.33	
	τ_2 = 1.64	
	gain = - .48	

The transfer function Bode diagram matches are shown in Figures 10, 11 and 12. Small gain adjustments had to be made to account for the quasi-steady state effect of the phugoid mode in the lower order transfer function. Time histories for a one-g pullup command input were run on the digital computer with these simplified transfer functions acting as command augmentation filters. These time histories are shown in Figure 13. The responses match the MLC model fairly well. There is some overshoot in wing root bending moment but the maximum value still remains less than 60% of the base TIFS values for the one-g pullup.

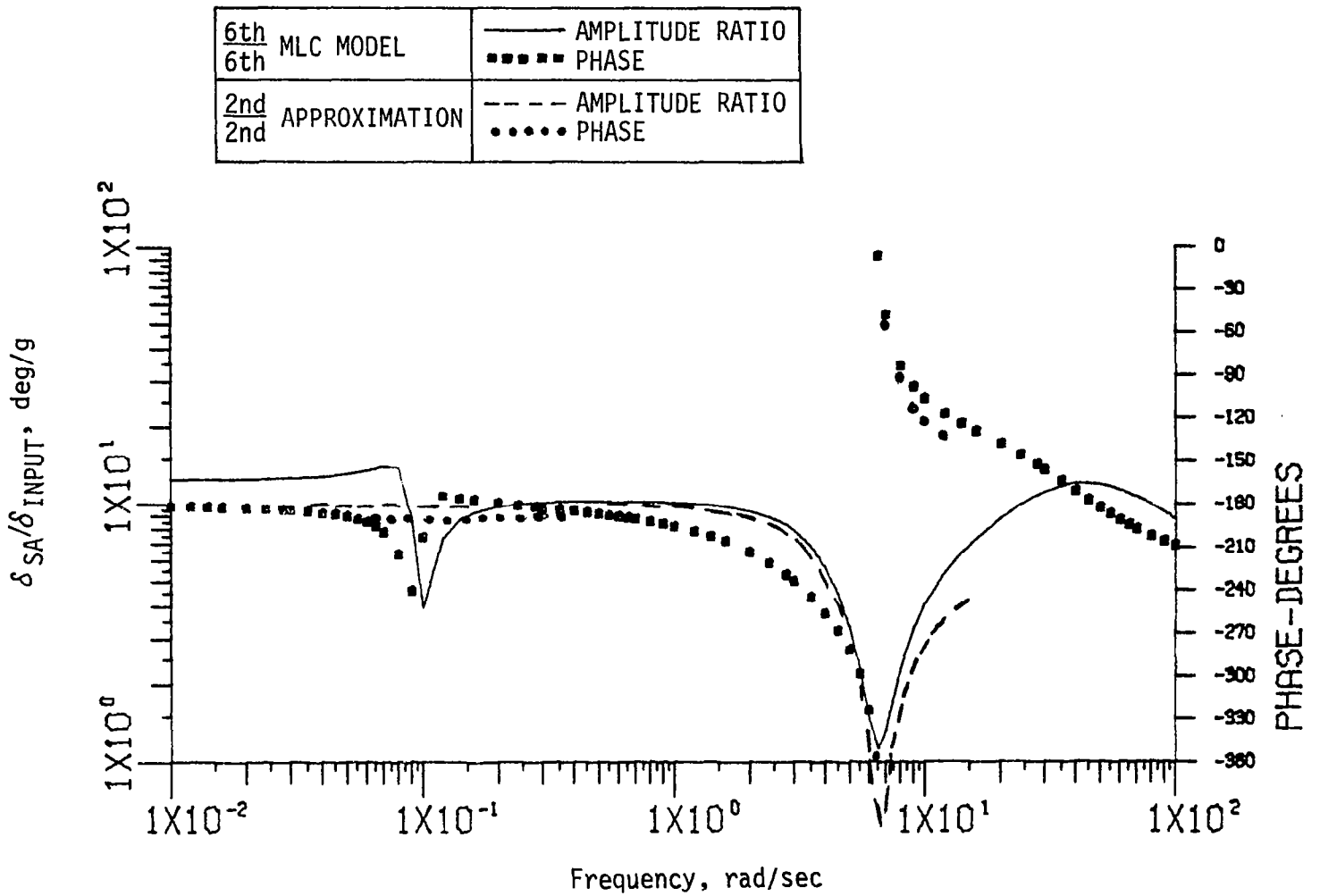

Figure 10 $\frac{\delta_{SA}}{\delta_{INPUT}}(s)$ TRANSFER FUNCTION APPROXIMATION

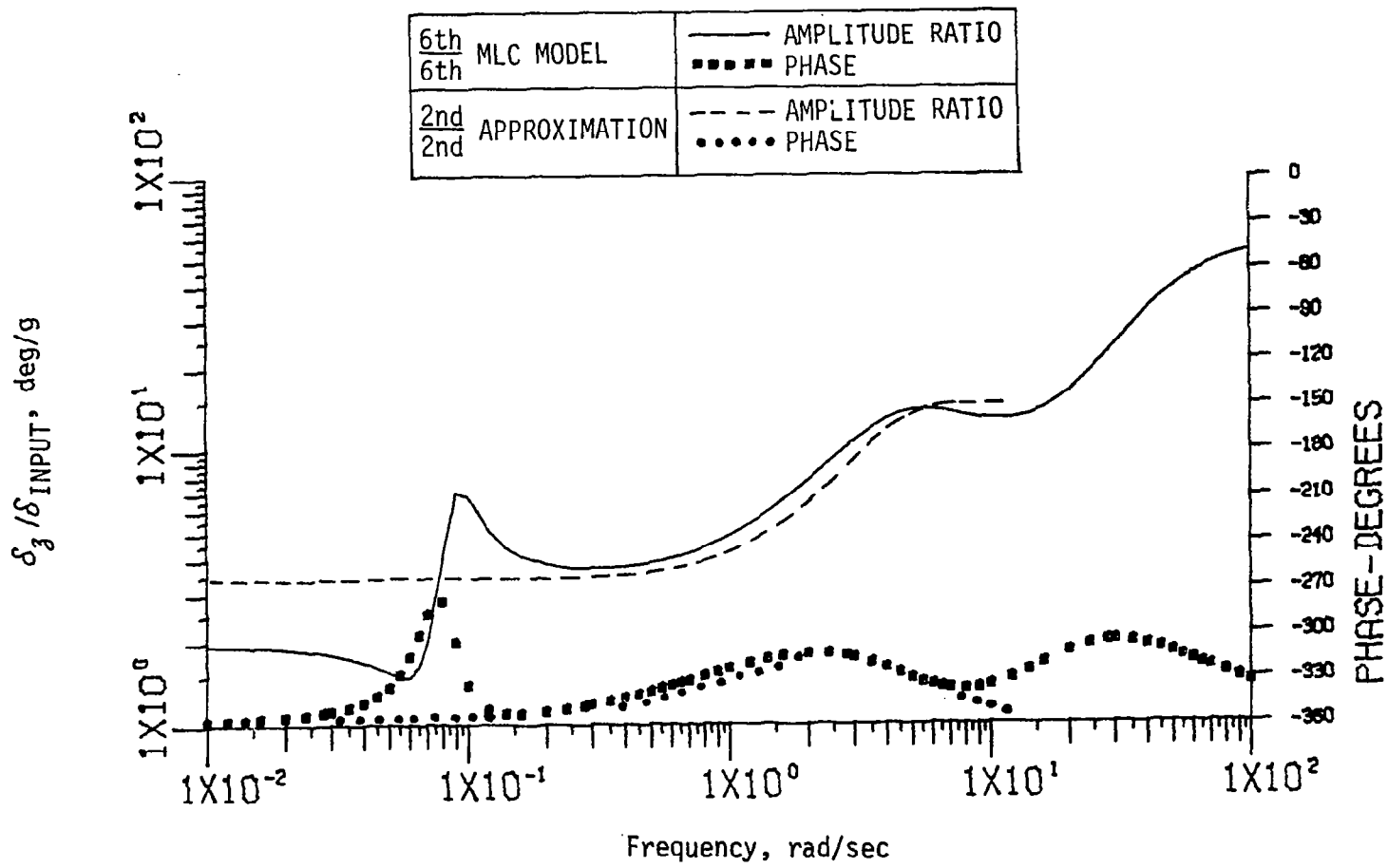

Figure 11 $\frac{\delta_{\ddot{y}}}{\delta_{INPUT}}(s)$ TRANSFER FUNCTION APPROXIMATION

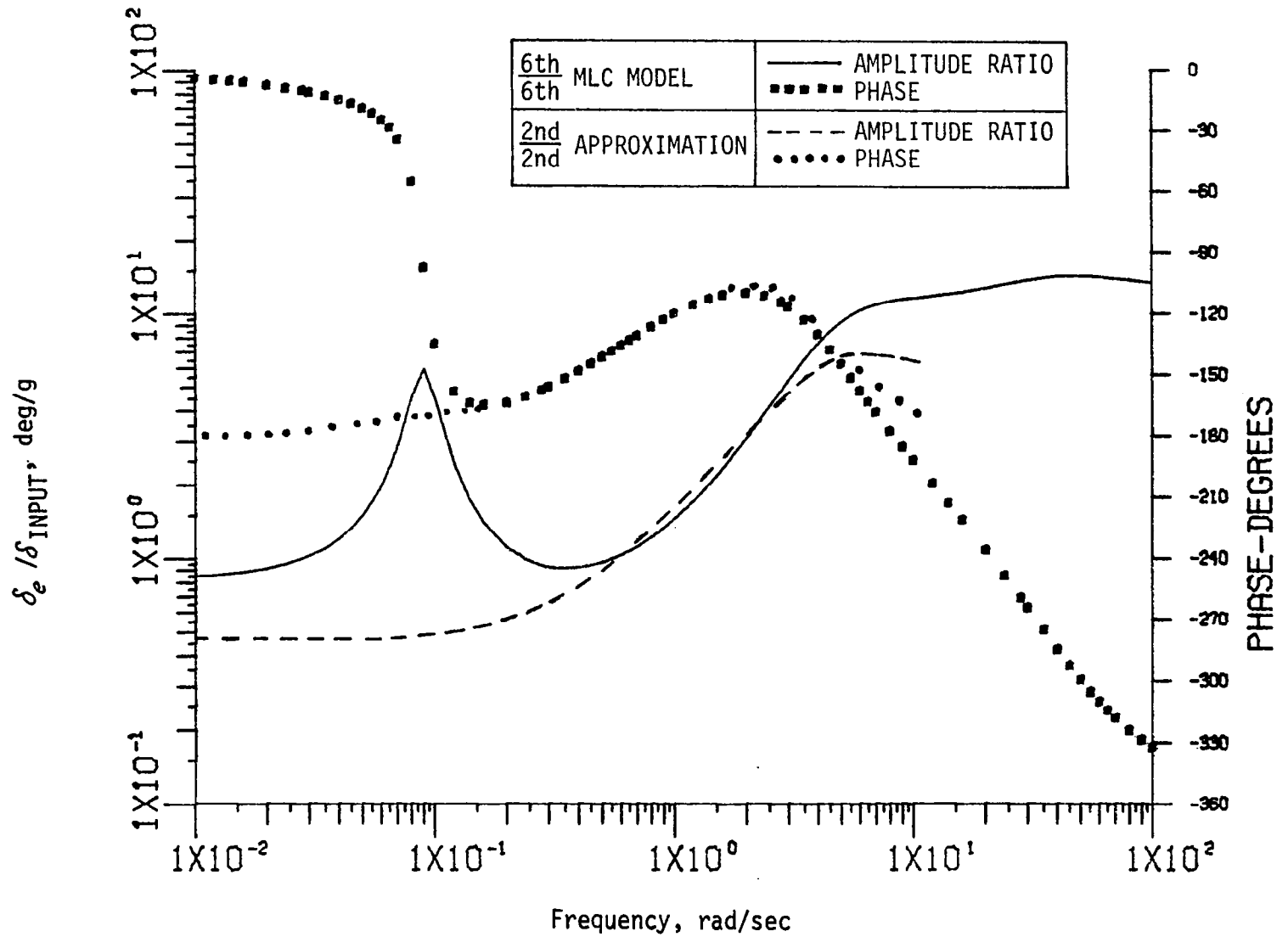

Figure 12 $\frac{\delta_e}{\delta_{INPUT}}$(s) TRANSFER FUNCTION APPROXIMATION

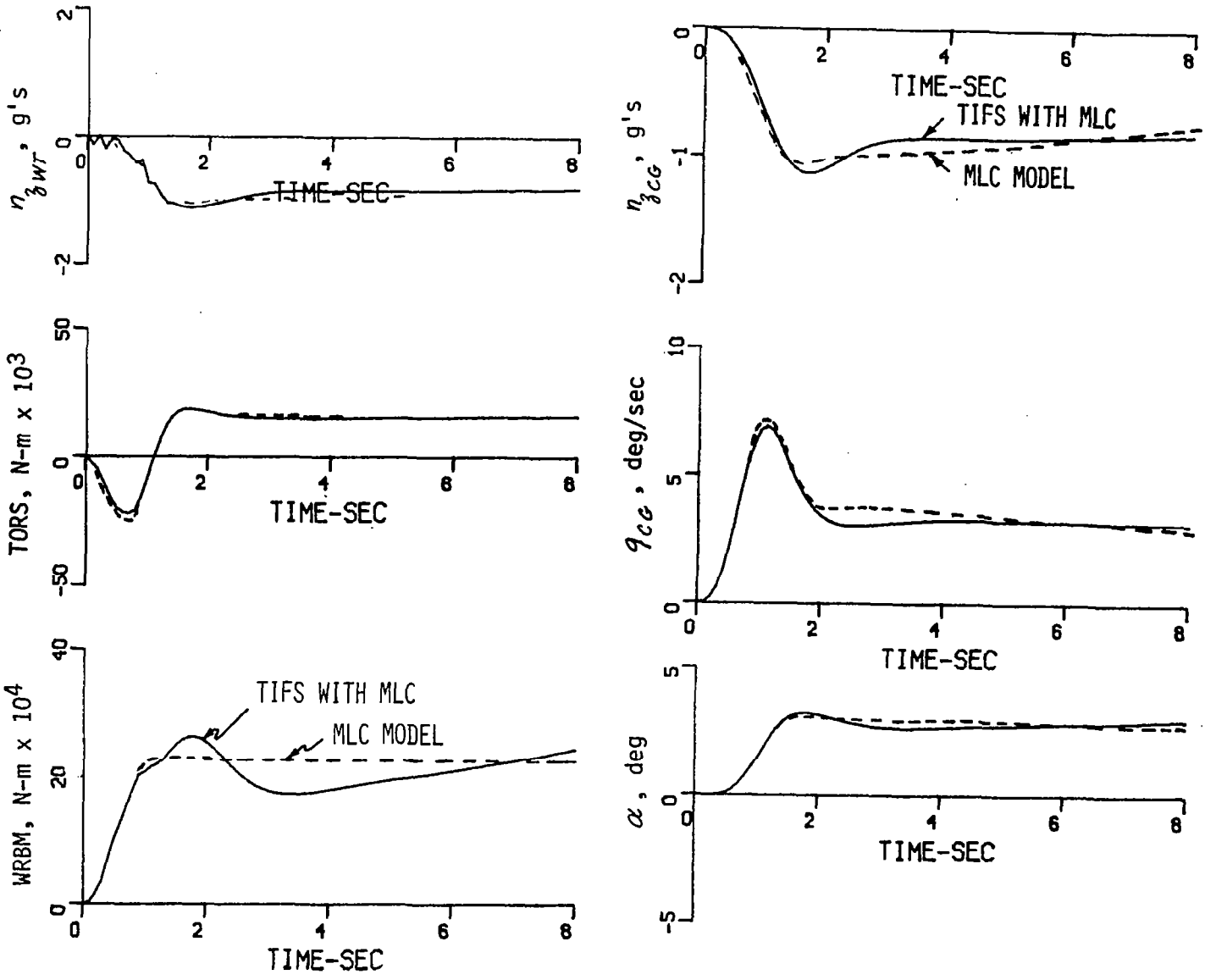

Figure 13 RESPONSE OF TIFS WITH COMMAND AUGMENTATION MLC SYSTEM

Section VI

STRUCTURAL MODE CONTROL

6.1 CRITERIA DEVELOPMENT

Criteria development for structural mode control was given primary emphasis in the structural mode suppression effort of this program. Without at first considering the elements of the feedback control system for mode suppression, it seemed appropriate to consider what should be done to the elastic vehicle if complete freedom was allowed in choice of sensors and the control surfaces used to produce forces and moments that would have the effect of altering the damping ratios and natural frequencies of the structural modes. Ideally the feedback control system should act to rigidize the vehicle, or rather, to force the vehicle to respond as a rigid vehicle would respond. It can be weakly argued that the structure should deform during maneuvering to relieve wing or body loads, but from a fatigue point of view, where fatigue failure is caused by strain, the structure should not be in dynamic elastic deformation.

If an ideal feedback control system is to have the effect of rigidizing an elastic vehicle, then the feedback should increase the natural frequencies and damping ratios of the structural modes. A perfectly rigid vehicle theoretically has all its elastic modes at infinite frequency. It is unrealistic to expect a control system to be able to do this, but it is relatively simple, within the stated objective, to formulate a performance index that yields successively more accurate approximations in an quadratic sense. The general conceptual form for this performance index becomes:

$$V = \min_{u} \int_0^\infty \left\{ \left\| x_{FLEX} - x_{RIGID} \right\|_Q^2 + \left\| u \right\|_R^2 \right\} dt \qquad (6\text{-}1)$$

where x_{RIGID} is the state vector of a rigid vehicle model and x_{FLEX} represents the state vector of the flexible aircraft model. The performance index of Equation (6-1) represents an explicit model following or servo problem.

The implicit or response feedback equivalent to Equation (6-1) is given by the performance index

$$V = \int_0^\infty \left\{ \left\| \dot{x}_{FLEX} - L x_{FLEX} \right\|_Q^2 + \left\| u \right\|_R^2 \right\} dt \qquad (6\text{-}2)$$

where L represents the system matrix of a mathematical model of a rigid vehicle, represented by the equation

$$\dot{\xi} = L\xi \qquad (6\text{-}3)$$

and ξ is the model state vector, a 4 x 1 vector to represent the longitudinal degress of freedom of motion of a rigid vehicle.

The performance index of Equation (6-2), although closer to the desired criteria, still will not necessarily yield a control system design that forces the flexible vehicle to tend to behave as a rigid vehicle. To show this, consider the Hamiltonian equations associated with the performance index of Equation (6-2). For the system equations or constraint of the performance index

$$\dot{x} = Fx + Gu \qquad (6\text{-}4)$$

the Hamilton equations become

$$\dot{x} = Fx - GR^{-1}G^T\lambda \qquad (6\text{-}5a)$$

$$-\dot{\lambda} = F^T\lambda - Q\ddot{x} + QL\dot{x} - L^TQ\dot{x} + L^TQLx \qquad (6\text{-}5b)$$

where $\lambda = Px$, with P the Riccati equation variable.

The characteristic polynomial of the Hamiltonian equations are given by the root square locus expression

$$\left| I + R^{-1}G^T(-Is - F^T)^{-1}(-Is - L^T)Q(Is - L)(Is - F)^{-1}G \right| = 0 \qquad (6\text{-}6)$$

Equation (6-6) is a general equation for the closed loop eigenvalues of the optimal and adjoint system resulting from the performance index of Equation (6-2). This equation shows that closed loop eigenvalues or poles of the flexible vehicle will originate as expected with the open loop poles. However, they will not terminate at the eigenvalues of the model or at infinity, but at a location intermediate between the open loop values and infinity. This intermediate terminus is defined by the adjugate of $[-Is - F^T]$ and of $[Is - F]$ as well as from $(-Is - L^T)$ and $(Is - L)$. . This means that implicit model following for structural mode suppression as formulated by Equation (6-2) is still very heavily dependent upon specific control variables, sensors and sensor locations, a dependency that should be avoided.

Because it is only the eigenvalues that may be specifiable for a flexible vehicle control criteria, and the eigenvectors or zeros are sensor and control surface dependent, the flexible vehicle and the rigid mathematical model could well be defined in the phase variable form, as outlined in Section III. In the phase variable space with state vector y , the system description is invariant for any controller and is independent of the outputs, which are defined by the transformation matrices T_i . In this form the performance index becomes

$$V = \min_{n} \int_0^\infty \left\{ \left\| \dot{y}_{FLEX} - F_{O_R} y_{FLEX} \right\|_Q^2 + ru^2 \right\} dt \qquad (6\text{-}7)$$

where $Q = \begin{bmatrix} qI_{4x4} & 0 \\ 0 & 0 \end{bmatrix}$ and r is a scalar that can represent a weighting on a general, but unspecified control input. F_{O_R} is the system matrix of the rigid airframe in phase variable form. It can be shown (Reference 16) that the root square locus expression for the performance index of Equation (6-7) is given by

$$1 + \frac{q}{r} \frac{|-I_s - F_{O_R}^T||Is - F_{O_R}|}{|-Is - F_O^T||Is - F_O|} = 0 \qquad (6\text{-}8)$$

or

$$|-Is - F_O^T||Is - F_O| + \frac{q}{r}|-Is - F_{O_R}^T||Is - F_{O_R}| = 0 \qquad (6\text{-}9)$$

The root locus expression of Equation (6-9), associated with the performance index of Equation (6-7), shows that the closed loop poles of the flexible aircraft will originate at the open loop poles and terminate either at the poles or eigenvalues of the model and at infinity. It is believed that the performance index of Equation (6-7) and the associated root square locus expression of Equation (6-9) properly defines a logical design criterion for structural mode suppression. As was desired, this criterion will define the eigenvalue locations of a particular flexible aircraft for systematically better approximations, in a quadratic sense, to a completely rigid vehicle. The eigenvalues of the flexible aircraft associated with the short period motions will terminate at the model eigenvalues. The remaining eigenvalues, those associated with the vehicle flexibility, will tend towards infinity. This is the result that was sought.

The advantage of the performance index of Equation (6-7) and the resultant root square locus expression of Equation (6-9) is that they are independent of the control surfaces and the instrumentation to be used. It defines only how to state the objectives of a structural mode control system design in terms of what we should attempt to do with damping ratios and natural frequencies of the structural modes. The mechanization of the feedback control law is independent of the specification for the location of the closed loop roots of the system. The mechanization of the control law, as developed in Section 6.3 below, is independent of the criteria or performance index. This is a desirable result.

6.2 CRITERIA APPLICATION TO TIFS

The equations of motion used to generate the root square locus plot were taken from the 14th order FLEXSTAB analytic representation of the TIFS aircraft for the cruise condition. This included the phugoid and short period poles, and the five lowest frequency modes attributable to the aeroelasticity of the vehicle. The complete equations of motion for this flight condition are given in Appendix A and the modal frequencies and damping ratios are given below.

The model that was chosen was the 4th order approximation to the TIFS aircraft, which includes only the phugoid and short period poles of the vehicle.

For this model, the poles are:

ω_1 = 2.25 rad/sec	ζ_1 = 0.678	short period
ω_2 = 0.047 rad/sec	ζ_2 = 0.146	phugoid

For the flexible vehicle, the poles are:

ω_1 = 2.25 rad/sec	ζ_1 = 0.678	short period
ω_2 = 0.047 rad/sec	ζ_2 = 0.146	phugoid
ω_3 = 23.1 rad/sec	ζ_3 = 0.255	1st wing bending
ω_4 = 32.9 rad/sec	ζ_4 = 0.092	1st wing torsion
ω_5 = 41.55 rad/sec	ζ_5 = 0.042	1st fuselage & hor. tail bending
ω_6 = 52.2 rad/sec	ζ_6 = 0.218	2nd fuselage & hor. tail bending
ω_7 = 61.7 rad/sec	ζ_7 = 0.079	2nd wing bending

Combining these roots into polynomial expressions, the results that are to be included into Equation (6-8) are as follows:

Model:

$$|Is - F_{OR}| = s^4 + 3.100s^3 + 5.034s^2 + .07594s + 1.1033$$

$$|-Is - F_{OR}^T| = s^4 - 3.100s^3 + 5.034s^2 - .07594s + 1.1033$$

Elastic Airplane:

$$\begin{aligned}|Is - F| = {} & s^{14} + 5.694\times10^{1}s^{13} + 1.1095\times10^{4}s^{12} + 4.570\times10^{5}s^{11} \\ & + 4.2868\times10^{7}s^{10} + 1.2448\times10^{9}s^{9} + 7.1495\times10^{10}s^{8} + 1.3928\times10^{12}s^{7} \\ & + 5.0725\times10^{13}s^{6} + 5.685\times10^{14}s^{5} + 1.1823\times10^{16}s^{4} + 3.3763\times10^{16}s^{3} \\ & + 5.278\times10^{16}s^{2} + 7.946\times10^{14}s + 1.564\times10^{14}\end{aligned}$$

$|-Is-F^T|$ is the same as $|Is-F|$ with changed signs for all the odd powers of s.

Figure 14 shows the resultant root square locus plot, i.e., a plot of the roots of Equation (6-9) using the polynomials given above. The parameter of the locus is q/r , and the values for q/r shown in the plot indicate the exponent, i.e., q/r = 34 in the figure should be read $q/r = 10^{34}$. Only one quadrant of the entire root square locus plot is shown in the figure, the entire plot is symmetrical about both the x-axis and the y-axis. It is not surprising that a ratio of weighting on the error to the control effort should reach such very high values before significant changes to the closed loop poles are obtained. The s^0 coefficient of the product $|Is-F||-Is-F'|$ is on the order of 10^{28}, while the s^0 coefficient of $|Is-L||-Is-L'|$ is on the order of 1. Therefore the ratio q/r has to be on the order of 10^{28} before the dynamic characteristics of the optimal system are significantly different from the open loop. The closed loop roots of the optimal, closed loop system will be those in the left half plane of the root square locus plot.

Using the root square locus plot as an aid to optimal system design, the selection of the matrix of weight factors Q and R have been reduced to the selection of a scalar weighting factor q/r. In turn, the selection of the scalar weighting factor q/r is reduced to the selection from among a family or grid of closed loop roots or poles. Every set of closed loop poles from the root square locus plot is an optimal solution, an approximation in a least error square sense to an increasing more rigid vehicle. The actual selection of the closed loop poles to be obtained by feedback control has more to do with the capability or control power of the controllers to produce forces and moments on the vehicle that would alter the poles, i.e., the controllability of the system.

The root square locus plot of Figure 14 is drawn for the TIFS airplane at the cruise condition. The actual plot for other aircraft would differ from the one shown only in detail in the sense that the open loop dynamics or eigenvalues would differ from those of the TIFS airplane. The migration of the roots as defined by Equation (6-8) would be approximately the same.

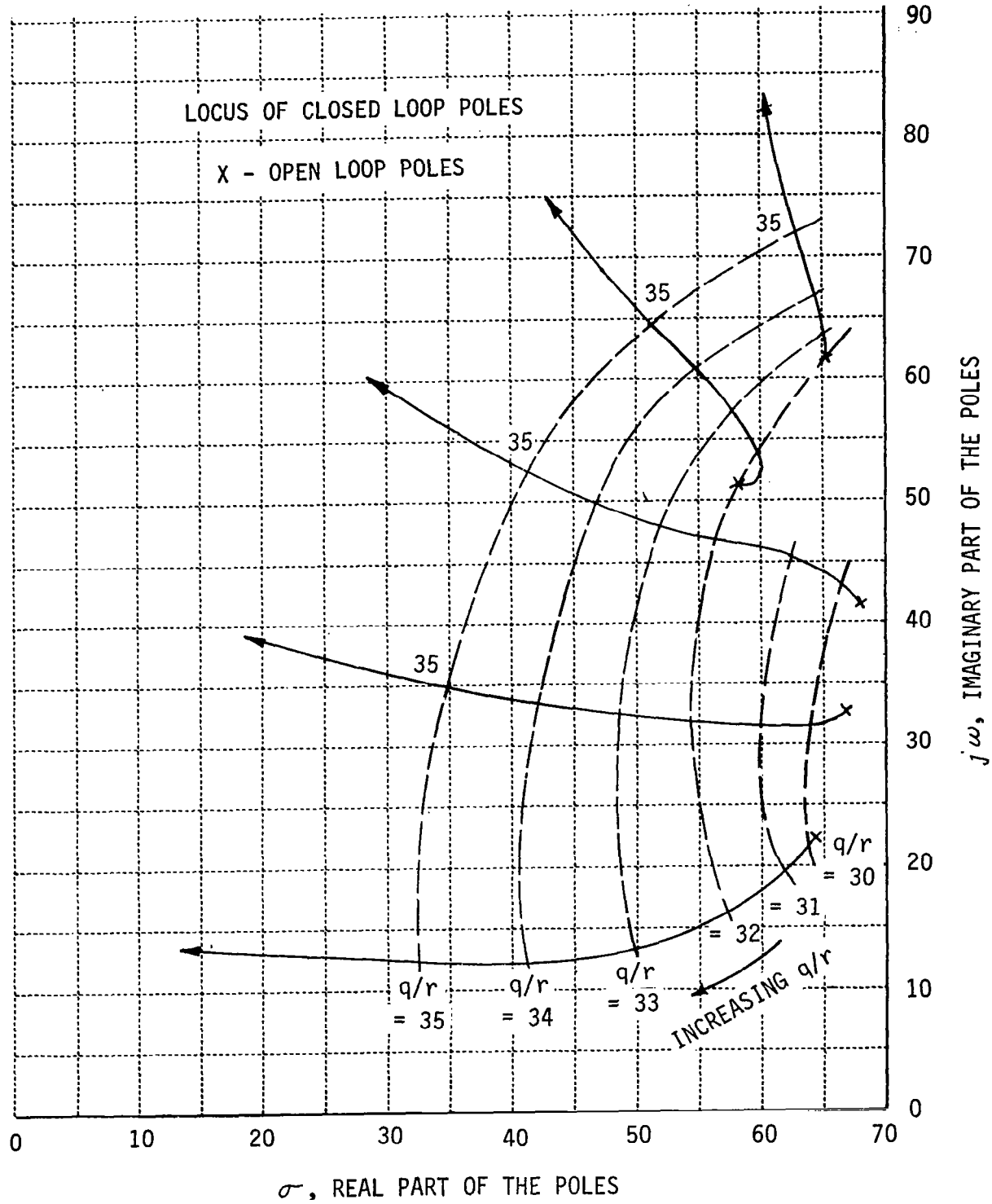

Figure 14 INTEGRAL ERROR SQUARED APPROXIMATIONS TO A RIGID TIFS AIRCRAFT

The root square locus plot of Figure 14 shows that, in general, the first objective of structural mode control should be to increase the damping ratios of the lower frequency structural modes that are included in the dynamic description of the system. In this, the criterion is in agreement with past practice. The next effort, in general, should be to increase the natural frequency of the lowest frequency roots of the elastic vehicle. For this particular case of the TIFS aircraft, the increase in damping ratios of the three lowest modes would constitute a good first approximation to a more rigid vehicle. The actual values of closed loop roots chosen for mechanization include an increase in damping and slight decrease in frequency of the first wing bending mode, an increase in damping ratio with little or no change in frequency of the wing torsion mode and an increase in both damping ratio and frequency of the first fuselage-tail bending mode.

6.3 CONTROL LAW SYNTHESIS

Linear optimal control is a synthesis technique for the design of regulators. The integrand of the performance index defines the states or outputs to be regulated by the control variables that appear in the performance index. Structural mode control, as defined in this report, is the proper use of control surfaces that will attempt to have the effect of forcing the vehicle to behave as a more rigid structure in the minimum integral error squared sense.

The theory of elastic structures indicates that the eigenvalues of an elastic structure should become both higher in frequency and, in general, have a higher damping ratio as a more rigid structure is approximated. The performance index or the resultant root square locus expression of Equation (6-9) directly reflects the elastic structure theory. The root square locus expression shows higher frequency eigenvalues with higher damping ratios.

This criterion is independent of the outputs or measurements on the elastic structure and independent of the control surfaces that will be used to produce the effect of rigidizing the structure. Therefore, the root square

locus plot of Figure 14 contains only poles, no zeros as would be expected. Zeros of any input-output transfer function are a direct function of the controllers used and the measurements or outputs of the system.

The control law mechanization problem then reduces to the problem of pole placement. Complete pole placement is theoretically possible using a single controller or several controllers linearly connected in a way that improves the controllability of the system. In practical control system design terms, this means that lower feedback gains will be required to move the poles of a closed loop system to new values from their original, open loop values.

The control law problem therefore reduces to a single controller problem or a series of single control problems. Adams (Reference 17) appears to have come to the same conclusion. The use of the phase variable canonical transformation is again very useful in obtaining control laws for pole placement purposes. Starting with the original linearized system

$$\dot{x} = Fx + Gu \tag{6-10}$$

A canonical transformation can be found

$$x = Ty \tag{6-11}$$

to transform the system into the phase variable form

$$\dot{y} = F_o y + G_o u \tag{6-12}$$

The system matrix F_o of the phase variable form has the structure

$$F_o = \begin{bmatrix} 0 & 1 & 0 & 0 & \cdots & 0 & 0 \\ 0 & 0 & 1 & 0 & \cdots & 0 & 0 \\ \vdots & & & & & & \vdots \\ 0 & \cdots & \cdots & \cdots & \cdots & 0 & 1 \\ -d_0 & -d_1 & \cdots & \cdots & \cdots & \cdots & d_{n-1} \end{bmatrix} \qquad G_o = \begin{bmatrix} 0 \\ 1 \\ \vdots \\ 0 \\ 1 \end{bmatrix} \tag{6-13}$$

17. Adams, R. M., "A Design of a Modal Controller for the B-52 Control Configured Vehicle (CCV)", Thesis, Air Force Institute of Technology, December 1975.

The elements d_i of F_o are obtained from the characteristic polynomial of the original equations,

$$D(s) = |Is - F| = s^n + d_{n-1}s^{n-1} + \cdots + d_1 s + d_0 \qquad (6\text{-}14)$$

$$= \prod_{i=1}^{n} (s + a_i)$$

where the a_i are the poles of the system of Equation (6-10).

The transformation T from the original system matrix to the phase variable form is obtained from the equation

$$TS = |Is - F|\left[Is - F\right]^{-1} G \qquad (6\text{-}15)$$

where S is a vector, $S^T = \left[1 \quad s \quad s^2 \quad \cdots \quad s^{n-1}\right]$

The matrix TS is a polynomial matrix made up of the numerators of the transfer functions of the states X of the system of Equation (6-10) with respect to the control vector.

The canonical transformation T is a matrix made up of the elements of any column of the polynomial matrix TS. There is then a different phase canonical transformation for every controller of the original system. Each phase variable transformation is of the form

$$T = \begin{bmatrix} t_{11} & t_{12} & \cdots & t_{1n} \\ \vdots & & & \\ t_{n1} & \cdots & & t_{nn} \end{bmatrix} \qquad (6\text{-}16)$$

and is, of course, a square, non-singular matrix for a completely controllable system.

6.3.1 Calculation of Feedback Gains

Let $\Delta(s)$ represent a polynomial constructed from the root square

locus plot of Figure 14. If α_i represents the desirable root or pole locations for an approximation to a more rigid structure, then for every value of q/r from that plot a desirable closed loop characteristic polynomial can be obtained

$$\Delta(s) = \prod_{i=1}^{n} (s + \alpha_i) = s^n + \delta_{n-1} s^{n-1} + \delta_{n-2} s^{n-2} + \cdots \delta_1 s + \delta_0 \quad (6\text{-}17)$$

A feedback control law that will force the open loop poles a_i to have the closed loop poles α_i is simply given by

$$u = -\left[\delta_0 - d_0, \delta_1 - d_1, \cdots \delta_{n-1} - d_{n-1}\right] y \quad (6\text{-}18)$$

Since from Equation (6-) we have that $y = T^{-1} x$, the control law becomes

$$u = -\left[\Delta - D\right] T^{-1} x \quad (6\text{-}19)$$

and a separate control law can be obtained for each of the controllers of the system. Δ and D are row matrices constructed from the polynomials $\Delta(s)$ of Equation (6-17) and $D(s)$ of Equation (6-14), i.e.

$$\Delta = \left[\delta_0 \quad \delta_1 \quad \delta_2 \cdots \delta_{n-1}\right]$$

$$D = \left[d_0 \quad d_1 \quad d_2 \cdots d_{n-1}\right]$$

Equation (6-19) is a very simple expression that will yield a complete state feedback control law for the performance index of Equation (6-2) or, for that matter, any pole placement problem. A more detailed development of this control law is discussed in many papers and reports. Reference 18 shows several examples of the application of this technique.

---

18. Rynaski, E. G.; Whitbeck, R. F. and Wierwille, W. W., "Optimal Control of a Flexible Launch Vehicle", Calspan Corporation Report No. IH-2089-F-1, NASA CR-80772, July 1966.

6.3.2 Control Law Synthesis - Output Feedback

Each column of the matrix TS is an $n \times 1$ polynomial matrix of the form

$$TS = \begin{bmatrix} t_{11} + t_{12}s + t_{13}s^2 + \cdots + t_{1,n-1}s^{n-1} \\ t_{21} + t_{22}s + t_{23}s^2 + \cdots + t_{2,n-1}s^{n-1} \\ t_{31} + t_{32}s + \cdots + t_{3,n-1}s^{n-1} \\ \vdots \\ t_{n1} + t_{n2}s + \cdots + t_{n,n-1}s^{n-1} \end{bmatrix} \tag{6-20}$$

Each row of T represents the numerator polynomial of a transfer function of one of the states to a control input. For instance, the transfer function $x_1/u_1(s)$, in general, given by

$$\frac{x_1}{u_1}(s) = \frac{t_{11} + t_{12}s + t_{13}s^2 + \cdots + t_{1,n-1}s^{n-1}}{D(s)} \tag{6-21}$$

Assuming that x_1 represents a measurable output of the original system, additional independent measurements or states of the system can be reconstructed by passing that measured output through a filter with one or more poles having a value to that of zeros of the associated transfer function.

If x_1 is a measured output of the system, with transfer function

$$\frac{x_1}{u_1}(s) = \frac{t_{1,n-1}}{D(s)} \prod_{i=1}^{n-1} (s + z_i) \tag{6-22}$$

then another independent measurement is given by

$$\frac{x_1'}{u_1}(s) = \frac{t_{1,n-1}}{D(s)} \prod_{i=1}^{n-2} (s + z_i) \tag{6-23}$$

$$= \frac{1}{D(s)}\left[t_{1,n-1}s^{n-2} + C_{n-2}s^{n-3} + \cdots + C_2 s + C_1\right]$$

This reconstructed output is generated by passing the original output x_1 through a simple low pass filter.

Schematically, the generation of $x_1'(s)$ is shown below.

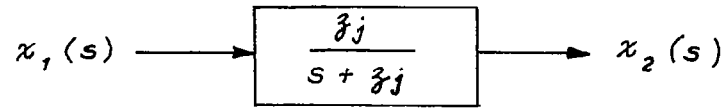

where $S = -z_j$ is the zero of the transfer function removed from Equation (6-22) to form Equation (6-23).

The polynomial of Equation (6-23) can then be used to replace any of the rows of $T S$. With the replacement indicated above, Equation (6-20) becomes

$$T_1 S = \begin{bmatrix} t_{11} + t_{12} s + t_{13} s^2 + \cdots t_{1,n-2} s^{n-2} + t_{1,n-1} s^{n-1} \\ C_1 + C_2 s + C_3 s^2 + \cdots t_{1,n-1} s^{n-2} \quad 0 \\ t_{13} + t_{32} s + \cdots t_{3,n-2} s^{n-1} + t_{3,n-1} s^{n-1} \\ \vdots \\ t_{n1} + t_{n2} + \cdots + t_{n,n-1} s^{n-1} \end{bmatrix}$$

and a new control law using a filter or compensation network to reconstruct an independent system measurement can be again computed from Equation (6-19), as

$$u = -\left[\Delta - D\right] T_1^{-1} \qquad (6\text{-}24)$$

This method of compensation network or simplified observer construction can be continued indefinitely. It becomes possible then, to obtain a very large, near infinite number of control laws using one minimum phase measurement and n^{-1} compensation networks or any number of measurements plus networks such that the number of measurements plus poles of the networks is equal to n, the number of states of the system.

In general, the structure of the feedback system becomes as shown in Figure 15 given below:

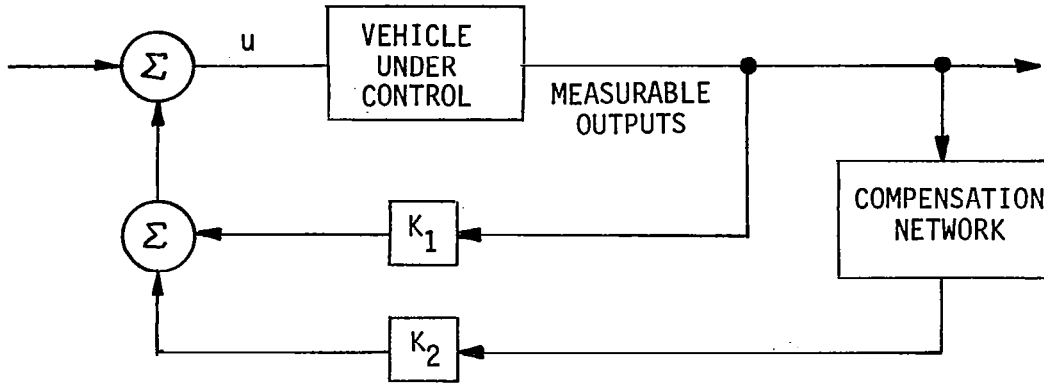

Figure 15 GENERAL STRUCTURE OF COMPENSATION SYSTEM

6.3.3 Restrictions to Compensation Design

In order to keep the compensation or observer system complexity within reason, a number of restrictions to compensation network design should be observed. These are listed below:

1. The transformation matrix T must be non-singular. Therefore, at least one measurement or output must have a transfer function with a numerator polynomial of order $n-1$, one less than the denominator polynomial. This can be guaranteed if a measurement of the control input is used.

2. Stability demands that none of the compensation networks have right half plane poles. Therefore, if only one measurement or output of the system is to be made, this measurement must be a minimum phase measurement.

These restrictions can be removed at the expense of additional system complexity if the sensors or outputs can be expressed in the form

$$\begin{aligned} z &= Cx + D\dot{x} \\ &= Ex + Fu \end{aligned} \tag{6-25}$$

where C and D or E and F are completely variable, i.e., at the disposal of the designer.

The technique of compensation network construction outlined above is considered to be a simplification or special case of the general observer theory of Luenberger (Reference 5). As described above, the observer poles are limited to the values of the zeros of the output transfer functions. If complete freedom is allowed in the interconnection of measured outputs and control inputs, the compensation networks may have any eigenvalues.

6.4 APPLICATION TO TIFS

The compensation network or simplified and practical observer theory described above was used to define a structural mode control system for TIFS. The fourteenth order cruise condition analytical model from the FLEXSTAB calculations (Appendix A) was used as the mathematical model of the aircraft. The characteristics of the modes of this aircraft and the desired "more rigid" aircraft obtained from one of the family of solutions to the optimal control problem is presented in Table 7.

The state vector for this model of the TIFS was:

$$x^T = \left[u, w, q, \theta, \eta_1, \dot{\eta}_1, \eta_2, \dot{\eta}_2, \eta_3, \dot{\eta}_3, \eta_4, \dot{\eta}_4, \eta_5, \dot{\eta}_5\right] \qquad (6\text{-}26)$$

where the η_i and $\dot{\eta}_i$ are the normalized structural modes. Nine of these higher order states were replaced by the accelerometers, pitch rate, and angle-of-attack sensors that were installed on the TIFS to transform the state vector into:

$$z = \left[u, \theta, \dot{\eta}_1, \dot{\eta}_2, \dot{\eta}_3, n_{z_{pilot}}, n_{z_{eq}}, n_{z_{TC}}, n_{z_{WT}}, n_{z_{SFSF}}, n_{z_{SFSA}}, n_{z_{AT}}, q_c, \alpha_v\right] \qquad (6\text{-}27)$$

This yielded a system in which more measurable states could be used for feedback.

TABLE 7

CHARACTERISTICS OF THE UNAUGMENTED TIFS AIRPLANE AND OPTIMALLY "RIGID" TIFS

MODE		UNAUGMENTED TIFS	OPTIMAL SYSTEM $q/r = 10^{31}$
Phugoid	ζ	.146	.146
	ω	.047	.047
Short Period	ζ	.678	.679
	ω	2.25	2.25
1st Wing Bending	ζ	.255	.379
	ω	23.1	20.9
1st Wing Torsion	ζ	.092	.309
	ω	32.9	33.5
1st Fuselage + Horizontal Tail Bending	ζ	.042	.162
	ω	41.55	46.0
2nd Fuselage + Horizontal Tail Bending	ζ	.218	.210
	ω	52.2	52.1
2nd Wing Bending	ζ	.079	.079
	ω	61.7	61.8

Using a wide band actuator model for the elevator: $\delta_e/\delta_{e_c} = \frac{200}{s + 200}$ the feedback gains needed to produce the desired closed loop poles from the root square locus plot were calculated. The wide band actuator was initially used in the following calculations for purposes of simplification. The results using more realistic actuator dynamics are shown later. This method used the phase variable canonical form of the equations in which the numerators of the transfer function of each sensor plus the characteristic equation of the actual aircraft and the desired closed loop characteristic equation are required.

The feedback gains which resulted from this process are shown on Table 8. Some of the gains are extremely large, such as those from the midwing accelerometers mounted at the side force surface. Also three of the states ($\dot{\eta}_1$, $\dot{\eta}_2$, $\dot{\eta}_3$) cannot be measured for feedback purposes. Therefore, other independent observations of the outputs had to be generated.

This was done by taking the sensors that yielded low feedback gains and filtering them. It was desired to keep the denominator of these new filtered sensors unchanged from the original sensor and to keep the order of the numerator from increasing. In order to accomplish this, the sensors were sent through first and second order low pass filters which canceled out one or two of the zeroes in the numerator. In this way the denominators were unchanged while the order of the numerators decreased by one or two.

It was decided to produce eight filtered sensor signals to replace the three $\dot{\eta}_i$ states and the sensors which produced the five highest feedback gains ($n_{z_{PILOT}}$, $n_{z_{CG}}$, $n_{z_{WING\ @\ FWD\ SFS}}$, $n_{z_{WING\ @\ AFT\ SFS}}$, α_{YANG}). Various sets of filtered sensors were devised. The first set used low pass filters on each sensor which canceled out its first or second lowest frequency zero. The next set used low pass filters which canceled out highest or second highest frequency zero. A third set used these higher frequency filters with an additional lead (.05s + 1) in order to shape the filter to amplify the sensed

TABLE 8

FULL STATE FEEDBACK GAINS
FOR OPTIMAL SOLUTION
$(q/r = 10^{31})$*

STATE	UNITS	GAIN
u	deg/m/sec	2.51
θ	deg/rad	- .090
$\dot{\eta}_1$	deg/1	- .801
$\dot{\eta}_2$	deg/1	- .828
$\dot{\eta}_3$	deg/1	- .430
$n_{z_{PILOT}}$	deg/g	20.8
$n_{z_{CG}}$	deg/g	143.0
$n_{z_{TAIL\ CONE}}$	deg/g	5.57
$n_{z_{WING\ TIP}}$	deg/g	.398
$n_{z_{WING\ @\ FWD\ SFS}}$	deg/g	179.0
$n_{z_{WING\ @\ AFT\ SFS}}$	deg/g	-145.0
$n_{z_{HORIZ.\ TAIL\ TIP}}$	deg/g	.137
q_{CG}	deg/deg/sec	4.45
α_{VANE}	deg/deg	78.2
δ_e	deg/deg	8.09

*Wide band actuator is assumed.

signals at the natural frequencies of the structural modes and attenuate them at higher frequencies.

None of the above three sets of filtered sensors yielded a set of feedback gains which were obviously better than any one of the others, although all gains were lower than those from the unfiltered set of sensors. A fourth set of filtered sensors was generated which was made up of the best sensors (ones which yielded lowest feedback gains) from each of the previous three sets. This set did yield feedback gains which were significantly lower than any of the other sets. None were higher than ten degrees per g. A final set of gains was calculated using a realistic model for the elevator, a first order actuator with a time constant of 1/30 second. Again all of the gains remained less than ten degrees per g.

A tabulation of the feedback gains obtained with the various sets of filtered sensors is shown on Table 9. The final set of filtered sensors are shown below:

$n_{z_{TAIL\ CONE}}$ (FIRST FILTER) $\qquad \dfrac{4.4}{s + 4.4}$

$n_{z_{TAIL\ CONE}}$ (SECOND FILTER) $\qquad \dfrac{(22)^2}{s^2 + (2)(.155)(22)s + (22)^2}$

$n_{z_{WING\ TIP}}$ (FIRST FILTER) $\qquad \dfrac{26.7}{s + 26.7}$

$n_{z_{WING\ TIP}}$ (SECOND FILTER) $\qquad \dfrac{(57)^2(.05s + 1)}{s^2 + (2)(.3)(57)s + (57)^2}$

$n_{z_{HORIZ.\ TAIL\ TIP}}$ (FIRST FILTER) $\qquad \dfrac{(61.8)^2}{s^2 + (2)(.077)(61.8)s + (61.8)^2}$

$n_{z_{HORIZ.\ TAIL\ TIP}}$ (SECOND FILTER) $\qquad \dfrac{(41)^2(.05s + 1)}{s^2 + (2)(.52)(41)s + (41)^2}$

q_{CG} (FIRST FILTER) $\qquad \dfrac{1.4}{s + 1.4}$

q_{CG} (SECOND FILTER) $\qquad \dfrac{(23)^2}{s^2 + (2)(.25)(23)s + (23)^2}$

TABLE 9

FEEDBACK GAINS FROM FILTERED SENSOR SETS

Sensor	Units	Low - Low Pass Filters	High - Low Pass Filters	High - Low Pass Filters Plus (.05s+1) Lead	Best Set of Filters	Best Set of Filters with Realistic $\delta_{e_{ACTUATOR}}$
u	deg/m/sec	- .142	.016	- .051	- .028	- .009
θ	deg/rad	- 8.96	.035	.003	- 1.26	- .168
$n_{z_{TAIL\ CONE}}$	deg/g	19.2	12.4	-16.3	9.57	- 1.68
$n_{z_{TAIL\ CONE\ (THROUGH\ 1st\ FILTER)}}$	deg/g	44.2	54.8	90.2	- 2.05	- .713
$n_{z_{TAIL\ CONE\ (THROUGH\ 2nd\ FILTER)}}$	deg/g	53.1	-66.9	-84.9	7.16	6.52
$n_{z_{WING\ TIP}}$	deg/g	- .874	-21.6	10.9	- 2.48	5.76
$n_{z_{WING\ TIP\ (THROUGH\ 1st\ FILTER)}}$	deg/g	.067	6.05	-10.6	- 1.03	- 7.16
$n_{z_{WING\ TIP\ (THROUGH\ 2nd\ FILTER)}}$	deg/g	-35.3	18.0	1.21	.925	- 1.87
$n_{z_{HOR.\ TAIL\ TIP}}$	deg/g	1.75	.548	1.84	.140	.035
$n_{z_{HOR.\ TAIL\ TIP\ (THROUGH\ 1st\ FILTER)}}$	deg/g	7.68	- .523*	- .535	.033	- .105

TABLE 9, CONT'D

Sensor	Units	Low - Low Pass Filters	High - Low Pass Filters	High - Low Pass Filters Plus (.05s+1) Lead	Best Set of Filters	Best Set of Filters with Realistic δ_e Actuator
$n_{z_{\text{HOR. TAIL TIP (THROUGH 2nd FILTER)}}}$	deg/g	6.27	.258	.254	- .019	.071
q_{CG}	deg/deg/sec	9.82	-88.5	-28.7	2.74	.695
$q_{CG_{\text{(THROUGH 1st FILTER)}}}$	deg/deg/sec	37.2	140.0	100.7	4.12	.382
$q_{CG_{\text{(THROUGH 2nd FILTER)}}}$	deg/deg/sec	-11.6	-52.1	-70.2	- 1.57	- .194
δ_e	deg/deg	21.3	- 2.63	8.74	4.47	1.48

An attempt was made at simplifying the above feedback system. This was done by eliminating sensors or network and then recomputing feedback gains from the reduced number of sensors by obtaining generalized inverses to the control law of Equation (6-24). A deletion of rows of the matrix T requires a control law computation using the following relationship

$$u = -(\Delta - \mathcal{D})(T^T T)^{-1} T^T X \tag{6-28}$$

where $(T^T T)^{-1} T^T$ is a generalized inverse of T. Weighted inverse solutions, using methods described in Section 4, could also be obtained. This type of approximate or suboptimal computation does not give an exact solution for the desired closed loop pole locations since the number of feedbacks is less than the number of degrees of freedom of the system. The few attempts at this technique yielded results that were not acceptable. Eliminating only a few feedbacks resulted in greatly increased gains and poor approximation to the desired pole locations. Unstable roots were sometimes generated. Tables 10 and 11 show the results of one of these trials in which one of the more important feedback paths was eliminated, the highly observable output of the first filter from the wing tip accelerometer.

Although time and money did not allow a complete investigation, it is felt that a sensitivity analysis of each of the feedback paths should prove quite useful. The feedback gain calculation of Equation (6-24) yields a column matrix of feedback gains as

$$K = -(\Delta - \mathcal{D})\, T^{-1}$$

where

$$K^T = [k_1 \quad k_2 \quad k_3 \quad \cdots \quad k_n] \tag{6-29}$$

In terms of the elements of this gain matrix, the closed loop characteristic polynomial is given by

$$\Delta(s) = \mathcal{D}(s) + \sum_{k=1}^{n} k_i \cdot N_i(s) \tag{6-30}$$

TABLE 10

FEEDBACK GAINS WITH REDUCED NUMBER OF SENSORS

Sensor	Full Complement of Sensors	One Sensor Eliminated
u	- .009	- .135
θ	- .168	- 9.53
$n_{z_{TAIL\ CONE}}$	- 1.68	50.7
$n_{z_{TAIL\ CONE\ (THROUGH\ 1st\ FILTER)}}$	- .713	42.8
$n_{z_{TAIL\ CONE\ (THROUGH\ 2nd\ FILTER)}}$	6.52	24.9
$n_{z_{WING\ TIP}}$	5.76	-19.5
$n_{z_{WING\ TIP\ (THROUGH\ 1st\ FILTER)}}$	- 7.16	Sensor Eliminated
$n_{z_{WING\ TIP\ (THROUGH\ 2nd\ FILTER)}}$	- 1.87	5.30
$n_{z_{HOR.\ TAIL\ TIP}}$	.035	.477
$n_{z_{HOR.\ TAIL\ TIP\ (THROUGH\ 1st\ FILTER)}}$	- .105	.174
$n_{z_{HOR.\ TAIL\ TIP\ (THROUGH\ 2nd\ FILTER)}}$	.071	- .156
q_{CG}	.695	8.30
$q_{CG\ (THROUGH\ 1st\ FILTER)}$	.382	38.7
$q_{CG\ (THROUGH\ 2nd\ FILTER)}$	- .194	- 9.86
δ_e	1.48	20.0

TABLE 11

CLOSED LOOP POLES WITH
REDUCED NUMBER OF SENSORS

Mode		With Full Complement of Sensors	With One Sensor Eliminated
Phugoid	ζ	.146	.146
	ω	.047	.046
Short Period	ζ	.679	.616
	ω	2.25	2.34
1st Wing Bending	ζ	.379	.333
	ω	20.9	22.4
1st Wing Torsion	ζ	.309	.456
	ω	33.5	28.6
1st Fuselage & Horizontal Tail Bending	ζ	.162	- .069
	ω	46.0	47.2
2nd Fuselage & Horizontal Tail Bending	ζ	.210	.330
	ω	52.1	57.5
2nd Wing Bending	ζ	.079	- .069
	ω	61.8	65.2

where $N_i(s)$ is the numerator polynomial of a sensor transfer function or the numerator polynomial of an observer output with respect to the control input. Using Equation (6-30), each of the feedback paths can be examined with respect to their effect on the closed loop characteristic equation. Feedback paths having negligible effect can be deleted from the control law, and the effect of this deletion can be exactly determined.

In summary, a single controller feedback control system was designed in which the basic flexible TIFS aircraft was made to respond as a more rigid structure. Realistic gains were calculated for feedback from the system's sensors which consisted of velocity, pitch attitude, pitch rate, and accelerometers at the tail cone, wing tip, and horizontal tail tip. In addition, feedback paths were also generated by passing the accelerometer and pitch rate signals through easily mechanizable filters.

Section VII

CONCLUSIONS AND RECOMMENDATIONS

7.1 CONCLUSIONS

The research performed in this program was done in response to a need for the development of criteria and methods for active control technology application. Active control technology is in its infancy and although the desirability for immediate application to existing aircraft is obvious, it has not been adequately demonstrated that the benefits are sufficient to offset the increased complexity that such systems will require.

There is much to be done in the area of active control technology development. A casual perusal of this report should be an adequate affirmation. Active control technology implies additional control surfaces on an aircraft and it is quite clear that much is yet to be learned about where these surfaces should be located, what their purposes should be, and how they should be driven to accomplish these purposes. Active control should not be attempted without first clearly defining the objectives and how they might best be accomplished. The technology is far from optimized.

Research and development in this area free of constraints relating to product development and to specific airframe configurations should be continued. Active control is feasible right now and for existing airframes, but the technology development will be narrowly restricted if limited to existing wide body jet airframe designs.

The problem areas in active control technology are many but there is great opportunity for substantial progress. The results in this report merely show that there do exist new avenues to be taken, new ways to more compactly and completely define the problem areas and seek viable and comprehensive solutions. The problems aren't all that difficult. Their solutions require only foresight and modest resources.

First, among the requirements for active control technology development is a real need for ways to accurately predict and continually improve the dynamical mathematical model of an airframe that shows significant aero-elastic characteristics. The FLEXSTAB program is a significant step in the right direction. But the accuracy of FLEXSTAB results could not be correlated or verified by flight tests of the TIFS airplane. There is reason to believe that FLEXSTAB may not be directly applicable to the peculiar TIFS configuration. If not, then either FLEXSTAB should be modified to be able to accept the high aspect ratio turboprop configurations like TIFS; or FLEXSTAB should be verified on airframe configurations more directly compatible with FLEXSTAB constraints. In either case, FLEXSTAB will have limited credibility until flight verification has been established. When this has been done, FLEXSTAB will be a powerful but preliminary tool for the control system designer to help him derive effective control laws for structural mode control, gust alleviation, flutter control and even maneuver load control. On problems of this complexity one should never put total reliance on a mathematical model obtained entirely by theoretic-analytical means. A prudent and safe approach requires flight test verification and a mathematical model derived from experimentation.

The procedure described in this report for the estimation of the aeroelastic equations of motion of an aircraft shows promise. The technique makes use of well established methods of system identification in a way that combines analytical predictions with experimental estimates so that the mathematical model can be continuously updated as more and more experimental results become available during the course of a flight test program. It is also the expectation that the model can be systematically improved using data that might initially be considered redundant. Equally important, this method of system identification avoids the overwhelming computational problems associated with attempts to use Least Squares, Maximum Likelihood or Minimum Variance methods to simultaneously come up with estimates for two or three hundred parameters. The procedure uses the classical "frequency sweep" input excitation customarily used for flutter analysis, so the near-impossible task of designing an optimal input that would enable each of the two or three hundred parameters to be independently identifiable is avoided.

Section IV of the report involves criteria for gust alleviation and shows that many different control law configurations, open loop, closed loop and hybrid combinations can be used. Only the most conceptually simple method was investigated in this program, but even this most simple approach led to a multitude of options and possible results. A control law that appeared to be both simple in concept and maximally effective was computed for TIFS. But, like a typical study program, all mechanization realities could either not be incorporated in the design or they could not be foreseen. Experimental flight test is required.

Maneuver load control is investigated next in the report. A systematic and unified approach has evolved to enable the designer to directly express the criterion in mathematical form, then come up with a family of candidate solutions that make optimal use of the available control surfaces and finally to simplify the most viable candidate solution for easy mechanization, at the same time avoiding any stability problems associated with control law simplification or suboptimal design procedures. It is felt that a flight test of these ideas is fully warranted now.

Criteria development was the most perplexing part of the structural mode control part of this program. Earlier investigations stressed mode suppression at particular airframe stations, as in the B-52 program (Reference 2, 3) rather than trying to define the more fundamental criteria problem of where to place the closed loop eigenvalues or poles of the system. A criterion for defining closed loop pole locations was evolved, independent of the airframe station, the sensors to be used in the control system design or the control surfaces to be used to suppress the structural modes. The result is a criterion that, when applied with a particular control configuration, will result in a controlled aircraft that uses the controllers to force the aircraft to behave more like a rigid airframe. This is in keeping with civil aircraft objectives of reducing structural motions throughout the wing and fuselage, rather than at select vehicle stations. The criterion, however, does not exclude a tradeoff for "point" modal suppression to relieve a particular airframe weak point. The merits of the criterion developed in this program relative to criteria used in the past have yet to be compared.

The method of identification of selected rows of a phase variable transformation associated with the vehicle instrumentation leads directly to methods for the construction of simplified observers that eliminate the need for complete state feedback in pole placement as specified by the criterion. Simple lag or lead-lag filters can be constructed that do not require interconnections among the measured outputs or a measurement of the control input. Networks with resonant peaks, the counterpart of notch networks, can be designed to control the modes with minimum feedback gain magnitudes. These networks tend to maximize mode controllability, in a sense the dual of a notch network, whose purpose is to minimize mode observability and therefore controllability. Observer construction in this fashion completes the unified design procedure of using phase variable transformations for system identification, criteria definition (analysis), and control law definition (synthesis).

The techniques of observer construction have been outlined only for a single controller system. Methods have not been developed yet to combine controllers in such a way to use the different control surfaces most effectively to accomplish mode suppression, but others (Reference 17) have contributed significantly to this problem. Theoretically, only one controller (or equivalent) can place all the poles, so additional surfaces can be used for other purposes, such as sensitivity minimization. It is not yet known how this can best be done or whether it would conflict with mode suppression requirements. Some preliminary ideas on how to incorporate sensitivity minimization into a feedback control system design have been given in Appendix F.

Much has been done toward the development of active control technology, but the work reported is only a substantial beginning. Experimental testing and parallel theoretical studies would insure continuous technology evolution and verification for direct application to existing wide body jets and optimum application to future aircraft.

7.2 RECOMMENDATIONS

1. A unified technique for large scale system identification, criteria definition and simplified observer construction has been outlined in this report. The ideas, particularly for large scale system identification, have only been partially developed and not completely verified by flight test. Because of the potential advantages afforded by this method, it is strongly recommended that more complete development and verification of these techniques be undertaken. The following is a partial listing of questions or tasks that warrant further investigation.

   a) Does a gradual and continuous transition occur between an analytically computed model and an experimentally determined model as more and more experimental data are used to replace the analytically determined model? Is there a better way to fuse the data than by direct replacement?

   b) Are experimental data really necessary at all? Are FLEXSTAB or other computer programs sufficiently accurate to provide a model that a control system designer can use to obtain control laws for structural mode or flutter suppression? It appears doubtful unless the control laws have been designed for substantial insensitivity. A minimal flight test or simulation program should answer some of these kinds of questions and such a program is recommended.

   c) By using frequency sweep inputs from more than one controller or force point input, a direct check is available on the accuracy of the identification results. A

phase variable transformation matrix can be identified for each input. The following relationship must be satisfied:

$$T_{\delta_1} F_o T_{\delta_1}^{-1} = T_{\delta_2} F_o T_{\delta_2}^{-1}$$

Because identification in the presence of noise is never exact, the above relationship can be used to define an error

$$e = F_o T_{\delta_1}^{-1} T_{\delta_2} - T_{\delta_1}^{-1} T_{\delta_2} F_o$$

By including a criterion to minimize this error (or a norm of the error), it should be possible to increase the accuracy of the identification process. Phase variable transformations can be added (or subtracted), i.e. the system matrix can be determined from the expression

$$F = (T_{\delta_1} + k T_{\delta_2}) F_o (T_{\delta_1} + k T_{\delta_2})^{-1}$$

where k is a positive or negative constant. A transfer function calculation

$$H(s) = \left[Is - \left(T_{\delta_1} + k T_{\delta_2}\right) F_o \left(T_{\delta_1} + k T_{\delta_2}\right)^{-1} \right]^{-1} G$$

will yield T_{δ_1} and T_{δ_2}. The differences between this calculation and the experimentally estimated phase variable transformation should clearly indicate whether T_{δ_1} and T_{δ_2} have been derived from the same dynamic system, and therefore whether or not they have been accurately estimated from the flight test results. It is recommended that the possibilities for increased system identification accuracy be investigated.

2. The criterion for structural mode control given in Section VI of this report is general – applicable to any aircraft. The criterion does not, however, consider important individual airframe characteristics, such as the relative amplitude of each of the normal mode variables for particular ways that the airframe can be excited, as by turbulence or by a control surface deflection. Further criterion development should be continued that will trade off relative amplitudes of deflection of the mode variables and minimize structural deflection at particular vehicle weak points.

3. The technique for the construction of simplified observers using phase variable transformations described in this report has been developed for single input systems only. It is certainly reasonable to expect that increased controllability would result from the use of multiple control surfaces for optimal structural mode and flutter control. It is recommended that further research be undertaken to develop these ideas for multiple control usage and to determine the sensitivity of the effectiveness of these observers to unknown or varying parameters.

4. A family of solutions to the gust alleviation problem was presented in Section IV. They progress from simple feedforward systems requiring direct gust measurements to more complex systems requiring gust measurements and feedback. Only the most simple was studied in this program. It is recommended that gust alleviation designs be computed using several of the solution techniques, compared in a simulation and finally flight tested. A number of potential problem areas exist when applied to real aircraft that were not included in the analysis. For instance, the level of gust alleviation depends upon the accuracy to which the control parameters and the gust effectiveness parameters, a subset of the

system matrix, are known. A sensitivity study and actual flight should be conducted to investigate these areas that may limit the effectiveness of gust alleviation.

5. The most direct and systematic design procedure outlined in this report is for maneuver load control. Calspan is of the opinion that this system can be programmed into TIFS and flight tested without significant modification to the command augmentation. It is recommended that this be done.

6. It was recognized early that the control system for an actively controlled airplane would be complex. A system that incorporates gust alleviation, maneuver load control and structural mode suppression can be designed in one complex entity, without necessarily being able to physically separate each functional component of the system. A subjective decision was made to design each of the functional activities of active control separately and in a way that they could be physically separable. In this way, the individual systems could be activated or shut down as required or desired, and the effectiveness of the systems separately or collectively evaluated. A failure in one system should not render the other two inoperable.

7. An alternate single entity gust alleviation, maneuver load control and structural mode control system should be designed to be able to evaluate the effectiveness of both of the two design approaches.

The recommendations listed above are general in that they address the major untouched areas of investigation. Each of the major areas contain imbedded minor areas that were passed by during the course of the investigation. It is clear that the technology of the use of active controls is in

its infancy. A theoretical and experimental research and technology development effort paralleling the immediate effort to apply the technology to wide body jets would be of considerable usefulness to NASA and to the United States.

Section VIII

LIST OF REFERENCES

1. Konar, A. F.; Stone, C. R.; Mahesh, J. K.; and Hank, M.: "Active Control Synthesis for Flexible Vehicles, Vol. I and II KONPAC", Honeywell Incorporated, AFFDL-TR-75-146, April 1976.

2. Burris, P. M.; and Bender, M. A.: "Aircraft Load Alleviation and Mode Stabilization (LAMS)", AFFDL-TR-68-163, November 1969.

3. Burris, P. M.; and Bender, M. A.: "Aircraft Load Alleviation and Mode Stabilization (LAMS) Flight Demonstration Test Analysis", AFFDL-TR-68-164, December 1969.

4. Stockdale, C. R.; and Poyneer, R. D.: "Control Configured Vehicle Ride Control System (CCVRCS)", Air Force Flight Dynamics Laboratory Report AFFDL-TR-73-83, July 1973.

5. Luenberger, D. G.: "Observers for Multivariable Systems", IEEE Transactions on Automatic Control, Vol. AC-11, pp 190-197, April 1966.

6. Andrisani, D.; Daughaday, H.; Dittenhauser, J.; and Rynaski, E.: "The Total In-Flight Simulator (TIFS)." NASA CR-158965, 1978.

7. Levy, E. C.: "Complex Curve Fitting", IEEE Transactions on Automatic Control, Vol. AC-4, May 1959.

8. Sanahanan, C. K.; and Koerner, J.: "Transfer Function Synthesis as a Ratio of Two Complex Polynomials", IEEE Transactions on Automatic Control, Vol. AC-8, January 1963.

9. Boeing Commercial Airplane Company and Boeing Computer Services, Inc.: "A Method for Predicting the Stability Characteristics of Control

Configured Vehicles", Vol. I "FLEXSTAB 2.01.00 Theoretical Description"; Air Force Flight Dynamics Laboratory Report No. TR-74-91, Vol. I, Nov. 1974.

10. Boeing Commercial Airplane Company and Boeing Computer Services, Inc.: "A Method for Predicting the Stability Characteristics of Control Configured Vehicles", Vol. II "FLEXSTAB 2.01.00 User's Manual"; Air Force Flight Dynamics Laboratory Report No. TR-74-91, Vol. II, Nov. 1974.

11. Lewis, T. O.; and Odell, P. L.: Estimation in Linear Models, Prentice-Hall, Inc., Chapter 1, 1971.

12. Anon.: Military Specification "Flying Qualities of Piloted Airplanes", MIL-F-8785B(ASG), 7 August 1969.

13. Rynaski, E. G.; and Weingarten, N. C.: "Flight Control Principles for Control Configured Vehicles", (Calspan Corporation Report No. TB-3052-F-1) AFFDL-TR-71-154, January 1972.

14. Kalman, R. E.; Englar, T.; and Bucy, R.: "Fundamental Study of Adaptive Control Systems", Vol. I and II, ASD-TR-61-27, March 1961 and March 1962.

15. Chang, S. S. L.: "Synthesis of Optimum Control System", McGraw-Hill Book Company, Inc., 1961.

16. Rynaski, E. G.; and Whitbeck, R. F.: "The Theory and Application of Linear Optimal Control", (Calspan Corporation Report No. IH-1943-F-1) AFFDL-TR-65-28, October 1965.

17. Adams, R. M.: "A Design of a Modal Controller for the B-52 Control Configured Vehicle (CCV)", Thesis, Air Force Institute of Technology, December 1975.

18. Rynaski, E. G.; Whitbeck, R. F.; and Wierwille, W. W.: "Optimal Control of a Flexible Launch Vehicle", (Calspan Corporation Report No. IH-2089-F-1) NASA CR-80772, July 1966.

19. Reynolds, P. A., et al.: "Capability of the Total In-Flight Simulator", (Calspan Report No. TB-3020-F-4) AFFDL-TR-72-39, July 1972.

20. Chen, R.T.N.; Eulrich, B. J.; and Lebacqz, J. V.: "Development of Advanced Techniques for the Identification of V/STOL Aircraft Stability and Control Parameters", Calspan Report No. BM-2820-F-1, August 1971.

APPENDIX A

EQUATIONS OF MOTION FOR TIFS OBTAINED BY USING FLEXSTAB PROGRAM

This appendix presents equations of motion, sensor equations, and loads equations for ACT TIFS with numerical coefficients for the climb, cruise, and landing conditions. The equations of motion and sensor equations were obtained as outputs of the linear system analysis program (LSA) of FLEXSTAB which is discussed in Reference 9. Stability and control derivatives which were computed in the SD & SS program of FLEXSTAB including the effects of aero-elasticity are also given. The load equations were based on an experimental version of AFLOADS (Reference 10), a program developed by the Air Force Flight Dynamics Laboratory for use with FLEXSTAB. It was pointed out in Reference 12 that the AFLOADS program and, in particular, the computation of torque had not yet been thoroughly verified.

Inputs to the FLEXSTAB program were prepared using geometric and mass parameters as discussed in Reference 6. The stiffness parameters in Reference 6 were "tweaked" in order to obtain a slightly better agreement between the computed zero airspeed frequencies and those measured in ground vibration tests as shown in Table A-1. All structural stiffnesses given in Reference 6 were multiplied by a factor of 1.177 except the wing torsional stiffnesses which were multiplied by a factor of 1.11.

Rigid body stability and control derivatives computed by FLEXSTAB were replaced by derivatives extracted from TIFS flight test data. The computed quasi-static derivatives were first corrected for aeroelastic effects. These modified aerodynamic terms are reflected in all FLEXSTAB outputs.

Assumptions Used in FLEXSTAB Modeling

In the formulation of a computationally practical mathematical model for the TIFS geometric and structural properties, many simplifying assumptions were made. This modeling task involved transforming an aircraft

TABLE A-1

TIFS MEASURED AND COMPUTED STRUCTURAL FREQUENCIES

ZERO AIRSPEED

Symbol ≠	Mode Characterization	FREQUENCY (HZ.)		
		Ground Vib. Test	FLEXSTAB – Basic Stiffnesses (Original Estimates)	FLEXSTAB – "Tweaked" Stiffnesses*
η_1	1st Wing Bending	3.3	3.02	3.28
η_2	1st Wing Torsion	4.9	4.65	5.01
η_3	Fus. & H.T. Bending (Inphase)	6.6	6.09	6.51
η_4	Fus. & H.T. Bending (180^{o} Phase Difference)	7.5	6.90	7.45
η_5	2nd Wing Bending	9.7	9.01	9.77
η_6	2nd Fus. & H.T. Bending	NA	15.10	16.31
η_7	Wing Outer Panel Mode	NA	17.25	18.33

*In order to improve agreement with ground vibration test results original estimates of wing torsional stiffnesses were multiplied by 1.11 and all other original stiffness estimates multiplied by 1.177.

≠The generalized coordinates for the symmetric structural modes are denoted η_1, η_2, η_3, ...

and wing with sweep-back, camber, twist, a double trapzoidal shape, taper, two dihedral angles, a complex structure, several airfoil shapes, engine nacelles, nonsymmetrical fuselage, side force surfaces, and an evaluation cockpit affixed on the front of a C-131 into a mathematical form compatible with a computer program, FLEXSTAB, designed to model sleek jet aircraft. The basic raw materials available for this modeling phase consisted of a complete Convair structural analysis, circa 1950, a detailed weight and balance of the C-131 and of the TIFS modifications, structural analysis of the TIFS modifications and complete design drawings of both the C-131 and the TIFS modifications.

A detailed discussion of the TIFS/FLEXSTAB mathematical model including both geometric and structural models as well as a complete listing of assumptions with discussion can be found in Reference 6. An abbreviated listing of assumptions follows.

Aerodynamic/Geometric Assumptions

1. Propeller slipstream effects as well as effects of the high velocity exhaust from the TIFS turboprop engine were not modeled. This assumption may have a measurable effect upon both the lift and moment characteristics of the resulting model and particularly on the direct lift flaps.

2. First order unsteady aerodynamic effects were included in the analysis but were neglected in determining the forces and moments due to control surface deflection.

3. The small side force surface fairing was ignored.

4. The engine nacelle was taken to be a closed body, i.e., flow through the nacelle was ignored. The TIFS engine, a turboprop, derives approximately 10% of its total thrust from flow through the engine.

5. The fuselage was represented with circular cross sections with the correct cross sectional area and area centroid locations even though the actual TIFS area distribution in the region of the evaluation cockpit fairing is nonsymmetrical. A similar approximation was made for the noncircular engine nacelles.

6. The only planar lifting surface represented with a thickness distribution was the wing.

Structural Assumptions

1. Fore and aft bending of the wing was ignored.

2. The wing elastic axis was assumed to be at 36.5% of the wing chord in accordance with the Convair structural analysis.

3. Twenty-two simple beam finite elements, each of constant stiffness, were used to represent the transverse bending and torsional stiffness distributions of the wing per side.

4. The wing was assumed to be effectively rigid inboard of the fuselage attachments. However, short beam segments were introduced at the spanwise location of the attachments in order to represent the slope changes due to bending of the wing carry-through structure.

5. The inertia properties of the wing were represented by twelve equivalent dumbbell masses per side.

6. The nacelle and engine isolators were assumed rigid.

7. The side force surfaces were assumed very stiff and rigidly attached to the wing.

8. Nineteen masses and twenty-two beam sections were used to represent the mass and stiffness distributions of the fuselage.

9. Nine simple beam finite elements were used to represent the transverse bending and torsional stiffness distributions of the horizontal tail per side.

10. The inertia properties of the horizontal tail were represented by nine equivalent dumbbell masses per side.

11. Control surface structural deflections were ignored and control surface rotations were assumed constant along the span of each control surface.

Outputs of LSA and AFLOADS Programs

The LSA program of FLEXSTAB provides system equations presented in the following form:

$$\left[\begin{matrix}\text{Coefficients of} \\ s^0 \text{ Terms}\end{matrix}\right]\left\{\chi_H\right\} + \left[\begin{matrix}\text{Coefficients of} \\ s^1 \text{ Terms}\end{matrix}\right]\left\{\dot{\chi}_H\right\} + \left[\begin{matrix}\text{Coefficients of} \\ s^2 \text{ Terms}\end{matrix}\right]\left\{\ddot{\chi}_H\right\} = 0 \quad \text{(A-1)}$$

where the components of the state vector $\{\chi_H\}$ are airplane rigid body motions, airplane elastic mode motions, control law variables, sensor outputs, controller deflections and applied gust velocity. These equations as obtained from LSA are homogeneous because the vector $\{\chi_H\}$ contains both output and input variables. The FLEXSTAB representation of TIFS did not actually include a control law although the vector $\{\chi_H\}$ included control law variables. The control law option of LSA was used merely as a convenient means for changing the units of the sensor outputs.

The components of the output vector $\{ L \}$ of the AFLOADS program are shear, bending moment, and torque and are given as a linear function of the components in $\{x_H\}$, $\{\dot{x}_H\}$ and $\{\ddot{x}_H\}$. The only load equations given in this memo are the shear, bending moment and torque about the elastic axis measured at the wing root (distance outboard of $\not\Leftarrow$ = 1.4427 m = 56.8 in).

Transformation of FLEXSTAB Equations of Motion to First Order Form

As discussed in the previous section, the system equations obtained from the LSA and AFLOADS programs involve second derivatives of the vector $\{x_H\}$. However, it was desired to have equations of motion for the TIFS airplane in the conventional first order form used in control system analysis in which separate state and control input vectors are used.

Thus the system vector $\{x_H\}$ was partitioned into a state vector and a control and gust input vector and the LSA equations were separated into equations of motion and sensor equations. The second derivative of any variable in the LSA equations could be eliminated by the simple expedient of introducing a new variable identically equal to its first derivative (e.g., if $y = \dot{\eta}_i$, then $\ddot{\eta}_i = \dot{y}$). The state vector from LSA was enlarged by the addition of these new variables and defining equations ($y = \dot{\eta}_i = \frac{d}{dt}(\eta_i)$ etc.) were added to the equations of motion. The enlarged state vector obtained in this manner was denoted by $\{x_o\}$ and the control and gust input vector by $\{U\}$. When these substitutions were made the equations of motion from the LSA equation took the following form,

$$[A_o]\{x_o\} + [A_1]\{\dot{x}_o\} + [A_2]\{U\} = 0 \qquad \text{(A-2)}$$

The vector of sensor outputs was adjoined to the load output vector to obtain an enlarged vector denoted by $\{y\}$. Then the sensor equations from LSA and the load equations from AFLOADS were written as a single vector equation in terms of $\{x_o\}$ and $\{U\}$.

$$\{y\} = \begin{Bmatrix} \text{SENSOR OUTPUTS} \\ \hline \text{LOADS} \end{Bmatrix} = \begin{bmatrix} [C] \\ \hline [LXI] \end{bmatrix} \{\dot{x}_o\} + \begin{bmatrix} [D] \\ \hline [LXO] \end{bmatrix} \{x_o\} + \begin{bmatrix} [O] \\ \hline [LG] \end{bmatrix} \{U\} \quad \text{(A-3)}$$

The equations from FLEXSTAB written in the form of Equations (A-2) and (A-3) were mechanized on the IBM 370 computer at Calspan. The numerical values of the matrix elements in Equations (A-2) and (A-3) were the same as the corresponding elements obtained from the LSA and AFLOADS programs except that matrices $[A_2]$ and $[LG]$ were modified so that control inputs would be expressed in degrees rather than in radians.

The standard form of the equations of motion was obtained by rearranging Equation (A-2) and pre-multiplying by the matrix $[A_1]^{-1}$. The state vector was then rearranged so that the components representing the deflection (η_i) in each elastic mode and its time derivative $(\dot{\eta}_i)$ would be adjacent. This rearrangement simplified the procedure for the reduction of the system to simpler subcases as discussed later. The resulting equations of motion could be written in the following standard form,

$$\{\dot{x}\} = [F]\{x\} + [G]\{U\} \quad \text{(A-4)}$$

where $\{x\}$ is the rearranged state vector. When the rearranged state vector was introduced into the output equations (Equation (A-3)), they could be written in the form,

$$\{y\} = [C]\{\dot{x}\} + [D]\{x\} + [E]\{U\} \quad \text{(A-5)}$$

The components of the rearranged state vector are,

$$\{x\}^T = [U, W, q, \theta, \eta_1, \dot{\eta}_1, \eta_2, \dot{\eta}_2, \eta_3, \dot{\eta}_3, \eta_4, \dot{\eta}_4, \eta_5, \dot{\eta}_5, \eta_6, \dot{\eta}_6, \eta_7, \dot{\eta}_7]$$

The equations are written for the body axis system and the velocities U and W are expressed in m/sec, pitch angle θ is in radians, $q = \dot{\theta}$ is in rad/sec, the structural mode deflections $\eta_1, \cdots, \eta_7$ are dimensionless and $\dot{\eta}_1, \cdots, \dot{\eta}_7$

have the dimensions sec^{-1}. The components of the control and gust input vector are,

$$\{U\}^T = [\delta_{sa}, \delta_z, \delta_e, w_g]$$

where controller angles are in degrees and the gust velocity is in m/sec. Components of the sensor and load output vector are as follows,

$$\{y\}^T = [n_{zp}, n_{zcg}, n_{zT}, n_{zWT}, n_{zFSF}, n_{zAST}, n_{zRHT}, q_{cg}, \alpha_v, S_R, BM_R, T_R]$$

Accelerations n_{zp}, etc. are in g's, pitching rate at the c.g. (q_{cg}) is in degrees/sec, angle of attack at vane (α_v) in degrees, root shear (S_R) in Newton's and root bending moment (BM_R) and root torque T_R in Newton meters. Tables A-2 and A-3 indicate the positions of the accelerometers and the α_v vane.

Numerical values for the elements of the matrices in Equations (A-4) and (A-5) are presented for the climb, cruise, and landing conditions. The consistency of this data with the original FLEXSTAB outputs was checked by comparing transfer function polynomials computed from Equations (A-4) and (A-5) with those computed in the LSA program of FLEXSTAB. The zeros and poles and coefficients of the transfer functions derived from Equations (A-4) and (A-5) agreed with the FLEXSTAB outputs to within 3 or 4 significant figures.

Quasistatic Elimination of Degrees of Freedom

Under certain circumstances, it is desirable to delete higher frequency structural modes from dynamic models yet to include the static effects of these modes. For instance, if modes with frequencies of 12 Hertz or higher are not of interest, then it may be useful to delete these modes from the equations of motion.

TABLE A-2

TIFS SENSORS AND C.G. LOCATION

Sensor (Output Symbol)	Vertical Location from Waterline (1)	Longitudinal Location from Fuselage Ref. (2)	Lateral Location from Buttock Line (3)
Radar altimeter antennas	0.0	654 (ave)	0.0
Attitude & Hdg. Gyro	+35.5	351	4 LBL
Angular Rate Gyro (q_{cg})	+44.5	370	3 LBL
Angular Accelerometer	+37	369	4 RBL
Linear Accelerometer at C.G. ($n_{z_{cg}}$)	+37	369	1 LBL
Linear Accel. at Sim.Cockpit (n_{z_p})	+ 3	- 36	0
α Vane (α_v)	+19	- 16	46 LBL
β Vane	-11	- 16	0
Static Pressure Source	+10	- 47	43 LBL
Dynamic Pressure Probe	+65	+ 78	45 LBL
TIFS c.g. Range	$\approx$ +36	370 to 379	0

(1) Waterline — Horizontal plane tangent to lower fuselage skin; measurement above waterline is positive.

(2) Fuselage Ref. — Extreme forward point of original aircraft nose. Distances aft of point are positive.

(3) Buttock Line — Vertical plane dissecting aircraft fore-to-aft, distances are measured to left (LBL) or right (RBL) of buttock line.

All stations named in inches (1 in. = 2.54 cm).

TABLE A-3

TIFS LINEAR ACCELEROMETERS

FOR VIBRATION MEASUREMENT *

Location on Airplane (Output Symbol)	Vertical Location Waterline	Longitudinal Location Fuselage Sta.	Lateral Location Buttock Line
Vertical Stabilizer	266	873	2 RBL
Right Wing Tip ($n_{z_{WT}}$)	≈ 70	418	610 RBL
Left Wing Tip	≈ 70	419	615 LBL
Right Wing at SFS -Fwd. Accel. ($n_{z_{FSF}}$)	≈ 33	379	358 RBL
Right Wing at SFS -Aft Accel. ($n_{z_{ASF}}$)	≈ 33	415	361 RBL
Right Horizontal Stab. ($n_{z_{RHT}}$)	55	860	232 RBL
Left Horizontal Stab.	55	860	232 LBL
Tail Cone ($n_{z_{TC}}$)	55	852	0

*All accelerometers measure vertical motion except the one mounted on the vertical stabilizer which measures lateral motion. All stations named in inches (1 in. = 2.54 cm).

Coefficients for equations obtained by quasistatic deletions are included for two cases. The first case involves deleting the two highest frequency modes, second fuselage bending (ω_n = 16.3 Hz) and a wing bending/torsion mode (ω_n = 18.3 Hz). The resulting state vector is of 14th order and is of the following form:

$$x^T = \left[u \;\; w \;\; q \;\; \theta \;\; \eta_1 \;\; \dot{\eta}_1 \;\; \eta_2 \;\; \dot{\eta}_2 \;\; \eta_3 \;\; \dot{\eta}_3 \;\; \eta_4 \;\; \dot{\eta}_4 \;\; \eta_5 \;\; \dot{\eta}_5\right]$$

The second case involved deleting three more highest frequency modes, the second wing bending mode (ω_n = 9.8 Hz), the first horizontal tail bending mode (ω_n = 7.5 Hz) and the first fuselage mode (ω_n = 6.5 Hz). The resulting state vector contains the first eight variables of the x vector above.

Stability and Control Derivatives

The nondimensional stability and control derivatives are a principal output of FLEXSTAB. Of importance as well are data showing the aeroelastic effects on these derivatives. This information is included in this appendix. The three flight conditions included, landing, climb and cruise, are identical to those of Reference 6. Data is presented in the stability axis system and is described in detail in Reference 9, Vol. 1 and the c.g. position is 28.7% MAC.

The pages labeled "Static Stability Derivatives" are now described. Data on these pages are appropriate for analyzing the case where all aeroelastic effects are treated quasistatically and structural mode responses are not retained as independent degrees of freedom. Column 2 labeled "RIGID" contains rigid derivatives computed by FLEXSTAB using finite element aerodynamics. The column entitled "ELASTIC INCREMENT" is the total aeroelastic correction to the corresponding derivative. The column "TOTAL" is the sum of columns 2 and 3 and represents the derivative corrected for static aeroelastic effects. The units of each derivative are described in the last column.

The pages labeled "DYNAMIC STABILITY DERIVATIVES" and "ACTIVE CONTROL DERIVATIVES" are similar to each other in form. The second column "RIGID COMPUTED" are those rigid derivatives computed internally by FLEXSTAB. The column labeled "RIGID OUTPUT" are those rigid derivatives input by the user in order to replace the rigid derivatives computed by FLEXSTAB. Data entered in this column are based on derivatives extracted from TIFS flight test data as mentioned previously. The measured derivatives were corrected for aeroelastic effects in order to obtain the required rigid derivative for input to FLEXSTAB. The column entitled "ELASTIC INCREMENT" is the aeroelastic correction only for modes which are not retained in the dynamic equations of motion. That is, if modes 1-7 are modeled dynamically, as was the case for TIFS, the elastic corrections in this column are for modes 8- ∞. The "TOTAL" column (Column 5) is the sum of columns 3 and 4. The derivatives of column 5 obtained in the SD&SS routine are dimensionalized in FLEXSTAB and passed to the LSA program for dynamic analysis.

The "ACTIVE CONTROL DERIVATIVE" pages describe derivatives for the three TIFS symmetric controllers, collective aileron ("AILS"), direct lift flap ("DLF"), and elevator ("ELVT"). Derivatives proportional to both surface deflection ("DS") and rate of deflection ("DS-DOT") are shown.

A direct comparison of the quasistatic stability and control derivatives extracted from TIFS flight test data using the Calspan Bayesian Maximum Liklihood Computer Program (BML) with those obtained from FLEXSTAB are shown in Table A-4. The c.g. position has been moved to 20.7% MAC, a position more like the flight test conditions. The parameter identification process used to obtain the BML results of Table A-4 is described in Reference 1.

TABLE A-4

COMPARISON OF BML IDENTIFIED QUASISTATIC STABILITY AND CONTROL DERIVATIVES WITH THOSE COMPUTED BY FLEXSTAB (Stiffnesses in FLEXSTAB were increased as noted in text, C.G. = .207$\bar{c}$)

	LANDING		CLIMB		CRUISE	
	FLEXSTAB	BML	FLEXSTAB	BML	FLEXSTAB	BML
C_{D_α}/deg	.0201	.0101	.0149	.00770	.00312	.00378
$C_{D_{\delta_e}}$/deg	.00145	-.00160	.000975	.00377	-.000022	.000239
$C_{D_{\delta_3}}$/deg	NA	.00164	.00133	.000321	.000388	.000153
C_{m_q}/rad	-40.1	-43.4	-40.2	-36.7	-41.1	-37.7
C_{m_α}/deg	-.0404	-.0204	-.0408	-.0201	-.0443	-.0176
$C_{m_{\delta_e}}$/deg	-.0549	-.0418	-.0521	-.0428	-.0487	-.0406
$C_{m_{\delta_3}}$/deg	NA	-.00279	-.0588	-.00362	-.00724	-.00387
$C_{m_{\dot{\alpha}}}$/rad	-14.3	-16.4	-14.6	-13.9	-17.8	-14.2
C_{L_α}	.101	.0950	.103	.0941	.111	.110
$C_{L_{\delta_e}}$	.0141	.00844	.0140	.0100	.0128	.0175
$C_{L_{\delta_3}}$	NA	.00982	.0230	.0173	.0227	.0156

NOTES:

1) BML and FLEXSTAB are not directly comparable at landing since flight tests from which BML results were derived were with $\delta_3 = \delta_F = 15^o$ while for FLEXSTAB $\delta_3 = \delta_F = 0^o$.

2) NA means data not presently available.

3) $C_{m_{\dot{\alpha}}}$ from FLEXSTAB is not corrected for change of c.g. position from .287 to .207$\bar{c}$.

COEFFICIENT MATRICES FOR ACT TIFS

EQUATIONS OF MOTION AND SENSOR AND LOAD EQUATIONS

(Seven independent structural modes)

LANDING

$$\dot{x} = Fx + Gu$$

$$y = Cx + Dx + Eu$$

$F =$

COLUMNS 1 THRU 10

9.697830-03	1.56635D-01	-8.32814D+00	-9.73278D+00	-1.29711D-03	-1.89514D-03	1.51038D-02	9.18292D-04	3.26900D-02	-1.28856D-04
-3.07996D-01	-8.53786D-01	6.74886D+01	-1.19568D+00	2.69437D-01	1.37653D-02	-5.88473D-01	-7.25865D-03	2.10706D-01	1.01829D-02
-3.73240D-03	-2.41218D-02	-1.31172D+00	5.80937D-03	1.34587D-02	3.86109D-05	-6.66174D-02	-2.08972D-03	1.85363D-01	2.13774D-03
0.0	0.0	1.000000+00	0.0	0.0	0.0	0.0	0.0	0.0	0.0
0.0	0.0	0.0	0.0	0.0	1.00000D+00	0.0	0.0	0.0	0.0
6.10799D+01	1.47286D+02	-4.09622D+02	7.82148D+00	-4.62921D+02	-6.34132D+00	7.81879D+01	1.47707D+00	1.29270D+02	-1.30499D+00
0.0	0.0	0.0	0.0	0.0	0.0	0.0	1.00000D+00	0.0	0.0
-1.78518D+01	-6.18138D+01	-5.25882D+02	1.38615D+00	1.54848D+01	1.93437D+00	-1.03498D+03	-3.57193D+00	6.91534D+01	1.90074D+00
0.0	0.0	0.0	0.0	0.0	0.0	0.0	0.0	0.0	1.00000D+00
9.90664D+00	6.38955D+01	8.43312D+02	-2.15115D+00	-1.31027D+01	-1.07035D+00	6.05420D+01	2.48541D+00	-1.81135D+03	-5.37092D+00
0.0	0.0	0.0	0.0	0.0	0.0	0.0	0.0	0.0	0.0
5.46522D+00	4.92749D+01	1.18645D+03	-4.16803D+00	1.76166D+00	1.22950D+00	5.06456D+01	2.15661D+00	-2.08912D+02	-2.99917D+00
0.0	0.0	0.0	0.0	0.0	0.0	0.0	0.0	0.0	0.0
-1.23715D+01	-3.32793D+01	-7.04855D+01	-6.58070D-01	7.01544D+00	2.31408D+00	-1.75306D+01	-1.36847D+00	-4.96854D+00	1.38682D+00
0.0	0.0	0.0	0.0	0.0	0.0	0.0	0.0	0.0	0.0
-3.69768D+00	-1.70166D+01	1.58759D+02	-1.29978D+00	3.93995D+00	5.44941D-01	-8.18039D+00	-1.81253D-01	-9.85743D+00	5.29210D-01
0.0	0.0	0.0	0.0	0.0	0.0	0.0	0.0	0.0	0.0
-2.46854D+01	-9.13560D+01	1.61152D+02	-4.86781D+00	3.99960D+01	2.52305D+00	-7.00826D+01	-2.17105D-01	-4.03663D+01	2.07237D+00

COLUMNS 11 THRU 18

-1.35810D-02	-2.84429D-05	1.32510D-02	3.04193D-04	-3.89533D-02	-2.40199D-04	-1.03323D-01	-1.03038D-03
5.70238D-01	3.45516D-03	-1.86792D-01	-8.76289D-04	3.35306D+00	-1.47934D-02	1.13042D+01	-3.85318D-02
3.62530D-02	2.45665D-03	2.85060D-02	3.01099D-04	4.05865D-01	-7.88209D-04	3.59484D-01	-2.67877D-03
0.0	0.0	0.0	0.0	0.0	0.0	0.0	0.0
0.0	0.0	0.0	0.0	0.0	0.0	0.0	0.0
-8.38535D+01	2.21070D+00	1.10493D+02	2.45361D+00	-3.98837D+02	1.54338D+00	-2.18720D+03	2.74387D+00
0.0	0.0	0.0	0.0	0.0	0.0	0.0	0.0
3.48428D+01	1.19635D+00	-4.47749D+01	-1.53539D+00	2.93544D+02	-2.20948D-01	6.20257D+02	-1.23008D+00
0.0	0.0	0.0	0.0	0.0	0.0	0.0	0.0
-2.24251D+01	-3.96698D+00	1.01696D+02	1.44469D+00	-2.78270D+02	8.62494D-01	-2.35519D+02	3.29768D+00
0.0	1.00000D+00	0.0	0.0	0.0	0.0	0.0	0.0
-2.17671D+03	-1.00248D+01	1.67164D+02	1.63632D-01	-1.73919D+02	9.22523D-01	6.81198D+02	1.47392D+00
0.0	0.0	0.0	1.00000D+00	0.0	0.0	0.0	0.0
1.12634D+01	-4.34663D-01	-3.75947D+03	-6.52438D+00	8.35585D+01	-2.28233D-01	3.53325D+02	-2.66201D-01
0.0	0.0	0.0	0.0	0.0	1.00000D+00	0.0	0.0
5.07482D+00	3.86309D-01	-5.84605D+01	-7.05570D-03	-1.03629D+04	-6.09667D+00	7.30380D+01	-1.15328D+00
0.0	0.0	0.0	0.0	0.0	0.0	0.0	1.00000D+00
5.12774D+01	-1.18865D+00	-6.55488D+01	-7.03826D-02	3.00770D+02	-3.10093D+00	-1.16230D+04	-1.51585D+01

$$G =$$

7.29586D-03	-5.38656D-03	2.53396D-02	8.10894D-02
-1.75884D-01	-1.25763D-01	-1.09030D-01	-9.11297D-01
-9.36982D-03	-4.00806D-03	-4.68933D-02	-3.32003D-02
0.0	0.0	0.0	0.0
0.0	0.0	0.0	0.0
6.20999D+01	4.69518D+01	-1.28246D+01	1.47780D+02
0.0	0.0	0.0	0.0
-3.07513D+01	-6.48365D+00	-3.06995D+01	-6.17852D+01
0.0	0.0	0.0	0.0
1.81202D+01	-2.02748D+01	5.21878D+01	6.38380D+01
0.0	0.0	0.0	0.0
-5.15738D+00	-1.04247D+01	5.86439D+01	4.91292D+01
0.0	0.0	0.0	0.0
-3.58915D+01	1.89255D+01	1.04060D+00	-3.33340D+01
0.0	0.0	0.0	0.0
2.56419D+00	6.45802D+00	1.45615D+01	-1.70983D+01
0.0	0.0	0.0	0.0
4.21879D-01	9.60380D+00	-4.71305D+00	-9.16730D+01

$$C =$$

COLUMNS 1 THRU 10

0.0	1.01900D-01	-1.08625D+00	0.0	0.0	8.21314D-04	0.0	1.75064D-03	0.0	-3.39429D-04
0.0	1.01900D-01	-3.75094D-02	0.0	0.0	3.02643D-04	0.0	-2.29581D-04	0.0	6.66324D-04
0.0	1.01900D-01	1.21159D+00	0.0	0.0	8.58304D-04	0.0	1.26865D-03	0.0	-7.22165D-04
0.0	1.01900D-01	8.98656D-02	0.0	0.0	-6.58274D-03	0.0	3.84469D-03	0.0	-2.45477D-03
0.0	1.01900D-01	-1.20344D-02	0.0	0.0	-2.03902D-03	0.0	3.23838D-04	0.0	-2.59030D-04
0.0	1.01900D-01	8.06946D-02	0.0	0.0	-2.13990D-03	0.0	6.71113D-04	0.0	3.59503D-04
0.0	1.01900D-01	1.23299D+00	0.0	0.0	1.34916D-03	0.0	3.72037D-03	0.0	-1.22280D-02
-6.92133D-05	-3.97976D-04	-1.62090D-03	0.0	-2.20761D-03	9.70018D-06	-9.78039D-04	-4.50288D-06	4.30463D-02	4.42152D-06
-5.84769D-05	-2.16647D-04	-8.12698D-04	0.0	6.48172D-03	3.42020D-06	1.32194D-02	-1.40277D-06	-2.32560D-03	2.03259D-06

COLUMNS 11 THRU 18

0.0	4.39597D-04	0.0	-5.29880D-04	0.0	1.36444D-03	0.0	-7.44481D-04
0.0	-3.19864D-04	0.0	7.03314D-04	0.0	1.00932D-04	0.0	1.00830D-04
0.0	1.23401D-03	0.0	-7.72198D-04	0.0	-8.02055D-04	0.0	3.11916D-05
0.0	2.60966D-03	0.0	9.15368D-03	0.0	-1.34610D-03	0.0	-1.65689D-03
0.0	-2.63310D-05	0.0	-1.79038D-03	0.0	1.26662D-03	0.0	2.77677D-03
0.0	-3.21494D-04	0.0	-1.56722D-03	0.0	2.04411D-04	0.0	-1.21465D-03
0.0	-2.27441D-02	0.0	3.07636D-03	0.0	6.67037D-03	0.0	-1.10256D-03
-1.55272D-03	-7.17916D-06	1.73664D-02	-4.12186D-07	2.15547D-01	-1.20608D-06	-6.60620D-02	-2.37376D-05
3.13561D-03	6.90440D-08	-3.51198D-03	4.42724D-08	8.29286D-03	-4.23779D-06	-4.23610D-03	-1.02724D-05

LANDING (Concl.)

D =

COLUMNS 1 THRU 10

0.0	0.0	-6.93430D+00	1.21872D-01	0.0	0.0	0.0	0.0	0.0	0.0
0.0	0.0	-6.93430D+00	1.21872D-01	0.0	0.0	0.0	0.0	0.0	0.0
0.0	0.0	-6.93430D+00	1.21872D-01	0.0	0.0	0.0	0.0	0.0	0.0
0.0	0.0	-6.93430D+00	1.21872D-01	0.0	0.0	0.0	0.0	0.0	0.0
0.0	0.0	-6.93430D+00	1.21872D-01	0.0	0.0	0.0	0.0	0.0	0.0
0.0	0.0	-6.93430D+00	1.21872D-01	0.0	0.0	0.0	0.0	0.0	0.0
0.0	0.0	-6.93430D+00	1.21872D-01	0.0	0.0	0.0	0.0	0.0	0.0
0.0	0.0	5.72958D+01	0.0	0.0	0.0	0.0	0.0	0.0	0.0
0.0	8.42000D-01	-8.54630D+00	0.0	0.0	0.0	0.0	0.0	0.0	0.0

COLUMNS 11 THRU 18

0.0	0.0	0.0	0.0	0.0	0.0	0.0	0.0
0.0	0.0	0.0	0.0	0.0	0.0	0.0	0.0
0.0	0.0	0.0	0.0	0.0	0.0	0.0	0.0
0.0	0.0	0.0	0.0	0.0	0.0	0.0	0.0
0.0	0.0	0.0	0.0	0.0	0.0	0.0	0.0
0.0	0.0	0.0	0.0	0.0	0.0	0.0	0.0
0.0	0.0	0.0	0.0	0.0	0.0	0.0	0.0
0.0	0.0	0.0	0.0	0.0	0.0	0.0	0.0
0.0	0.0	0.0	0.0	0.0	0.0	0.0	0.0

$$E = \left[\begin{array}{cccc} & & 0 & \\ \hline 0.0 & 0.0 & 0.0 & 8.42000D\text{-}01 \end{array}\right]$$

CLIMB

$$\dot{x} = Fx + Gu$$

$$y = C\dot{x} + Dx + Eu$$

F =

COLUMNS 1 THRU 10

4.68040D-03	1.17988D-01	-6.64165D+00	-9.77342D+00	-1.31070D-03	-1.47907D-03	1.38562D-02	6.97203D-04	3.14965D-02	-7.94412D-05
-2.79242D-01	-9.03753D-01	8.24070D+01	-7.96144D-01	2.50715D-01	1.45878D-02	-6.20682D-01	-7.58602D-03	1.47939D-01	1.11958D-02
-2.67146D-03	-2.54994D-02	-1.21659D+00	3.01745D-03	9.78989D-03	9.34103D-06	-6.72215D-02	-2.20061D-03	1.84985D-01	2.21272D-03
0.0	0.0	1.00000D+00	0.0	0.0	0.0	0.0	0.0	0.0	0.0
0.0	0.0	0.0	0.0	0.0	1.00000D+00	0.0	0.0	0.0	0.0
5.15389D+01	1.57683D+02	-4.62901D+02	4.74051D+00	-4.63616D+02	-6.71213D+00	8.49966D+01	1.52230D+00	1.48674D+02	-1.46592D+00
0.0	0.0	0.0	0.0	0.0	0.0	0.0	1.00000D+00	0.0	0.0
-1.44853D+01	-6.62632D+01	-5.66103D+02	8.15918D-01	1.41551D+01	2.05353D+00	-1.03862D+03	-3.69868D+00	6.65386D+01	2.02285D+00
0.0	0.0	0.0	0.0	0.0	0.0	0.0	0.0	0.0	1.00000D+00
6.31019D+00	6.88339D+01	9.16268D+02	-1.29867D+00	-1.04612D+01	-1.11837D+00	6.44633D+01	2.65646D+00	-1.81651D+03	-5.57991D+00
0.0	0.0	0.0	0.0	0.0	0.0	0.0	0.0	0.0	0.0
3.32392D+00	5.25134D+01	1.29533D+03	-2.54014D+00	5.23773D+00	1.38160D+00	5.30629D+01	2.31326D+00	-2.24242D+02	-3.15579D+00
0.0	0.0	0.0	0.0	0.0	0.0	0.0	0.0	0.0	0.0
-1.02604D+01	-3.59878D+01	-7.33570D+01	-4.11509D-01	7.62790D+00	2.48853D+00	-2.05936D+01	-1.46429D+00	-6.79665D+00	1.50107D+00
0.0	0.0	0.0	0.0	0.0	0.0	0.0	0.0	0.0	0.0
-2.05993D+00	-1.74955D+01	1.71955D+02	-7.77923D-01	4.05324D+00	5.59067D-01	-8.78853D+00	-1.78742D-01	-1.09053D+01	5.70350D-01
0.0	0.0	0.0	0.0	0.0	0.0	0.0	0.0	0.0	0.0
-1.79924D+01	-9.73581D+01	1.88032D+02	-2.94951D+00	3.78139D+01	2.66888D+00	-7.21702D+01	-1.75724D-01	-5.08943D+01	2.25873D+00

COLUMNS 11 THRU 18

-1.19153D-02	2.51621D-05	1.26467D-02	2.33854D-04	-3.53219D-02	-2.12204D-04	-9.80676D-02	-8.27572D-04
6.31144D-01	3.62841D-03	-2.08750D-01	-6.63581D-04	3.34891D+00	-1.70732D-02	1.09189D+01	-4.44704D-02
5.11171D-02	2.63097D-03	2.70028D-02	3.34891D-04	4.06106D-01	-9.40861D-04	3.26485D-01	-2.90620D-03
0.0	0.0	0.0	0.0	0.0	0.0	0.0	0.0
0.0	0.0	0.0	0.0	0.0	0.0	0.0	0.0
-8.38008D+01	2.44680D+00	1.18844D+02	2.59195D+00	-4.04437D+02	1.78438D+00	-2.18332D+03	3.46544D+00
0.0	0.0	0.0	0.0	0.0	0.0	0.0	0.0
4.60736D+01	1.28594D+00	-4.74310D+01	-1.62747D+00	3.05668D+02	-3.16483D-01	6.29104D+02	-1.45034D+00
0.0	0.0	0.0	0.0	0.0	0.0	0.0	0.0
-4.74159D+01	-4.29687D+00	9.54352D+01	1.51768D+00	-3.00855D+02	1.01768D+00	-2.52378D+02	3.60998D+00
0.0	1.00000D+00	0.0	0.0	0.0	0.0	0.0	0.0
-2.21510D+03	-1.06864D+01	1.44961D+02	1.23180D-01	-1.93414D+02	1.06053D+00	6.51427D+02	1.47134D+00
0.0	0.0	0.0	1.00000D+00	0.0	0.0	0.0	0.0
1.44918D+01	-4.73294D-01	-3.77215D+03	-6.77848D+00	9.41403D+01	-2.82547D-01	3.87752D+02	-3.92460D-01
0.0	0.0	0.0	0.0	0.0	1.00000D+00	0.0	0.0
8.46910D+00	4.15617D-01	-5.44706D+01	1.22729D-02	-1.03738D+04	-6.19773D+00	9.03728D+01	-1.28760D+00
0.0	0.0	0.0	0.0	0.0	0.0	0.0	1.00000D+00
5.37702D+01	-1.31778D+00	-6.73639D+01	-3.30639D-02	2.99454D+02	-3.43540D+00	-1.16826D+04	-1.62480D+01

$$G = \begin{bmatrix}
5.32961D-03 & 1.47417D-02 & -3.79965D-02 & 6.11628D-02 \\
-2.24304D-01 & -2.71938D-01 & -1.71839D-01 & -9.83667D-01 \\
-1.15772D-02 & 2.71629D-03 & -6.21409D-02 & -3.55983D-02 \\
0.0 & 0.0 & 0.0 & 0.0 \\
0.0 & 0.0 & 0.0 & 0.0 \\
7.97247D+01 & 6.09729D+01 & -1.65646D+01 & 1.58277D+02 \\
0.0 & 0.0 & 0.0 & 0.0 \\
-3.94191D+01 & -8.03691D+00 & -3.94722D+01 & -6.62205D+01 \\
0.0 & 0.0 & 0.0 & 0.0 \\
2.29804D+01 & -2.67466D+01 & 6.72718D+01 & 6.87514D+01 \\
0.0 & 0.0 & 0.0 & 0.0 \\
-7.20268D+00 & -1.40752D+01 & 7.56532D+01 & 5.23156D+01 \\
0.0 & 0.0 & 0.0 & 0.0 \\
-4.64722D+01 & 2.45198D+01 & 1.35489D+00 & -3.60529D+01 \\
0.0 & 0.0 & 0.0 & 0.0 \\
3.61768D+00 & 8.50597D+00 & 1.88698D+01 & -1.75931D+01 \\
0.0 & 0.0 & 0.0 & 0.0 \\
1.57465D+00 & 1.28307D+01 & -6.04132D+00 & -9.77376D+01
\end{bmatrix}$$

$C =$

COLUMNS 1 THRU 10

0.0	1.01900D-01	-1.08625D+00	0.0	0.0	8.21314D-04	0.0	1.74962D-03	0.0	-3.40550D-04
0.0	1.01900D-01	-3.75094D-02	0.0	0.0	3.02643D-04	0.0	-2.29784D-04	0.0	6.66018D-04
0.0	1.01900D-01	1.21159D+00	0.0	0.0	8.58406D-04	0.0	1.26764D-03	0.0	-7.22777D-04
0.0	1.01900D-01	8.98656D-02	0.0	0.0	-6.58172D-03	0.0	3.84367D-03	0.0	-2.45375D-03
0.0	1.01900D-01	-1.20344D-02	0.0	0.0	-2.03902D-03	0.0	3.24144D-04	0.0	-2.58520D-04
0.0	1.01900D-01	8.06946D-02	0.0	0.0	-2.13990D-03	0.0	6.71215D-04	0.0	3.59707D-04
0.0	1.01900D-01	1.23299D+00	0.0	0.0	1.35017D-03	0.0	3.71935D-03	0.0	-1.22280D-02
-5.75823D-05	-3.90872D-04	-1.70570D-03	0.0	-2.20589D-03	9.47672D-06	-9.98665D-04	-4.40089D-06	4.30177D-02	4.86040D-06
-3.99253D-05	-1.82699D-04	-7.16751D-04	0.0	5.35165D-03	2.80444D-06	1.09077D-02	-1.13804D-06	-1.92640D-03	1.85827D-06

COLUMNS 11 THRU 18

0.0	4.41635D-04	0.0	-5.30593D-04	0.0	1.37055D-03	0.0	-7.31744D-04
0.0	-3.19558D-04	0.0	7.03212D-04	0.0	1.01686D-04	0.0	1.02715D-04
0.0	1.23605D-03	0.0	-7.72810D-04	0.0	-7.97979D-04	0.0	4.07906D-05
0.0	2.60966D-03	0.0	9.15164D-03	0.0	-1.34508D-03	0.0	-1.65486D-03
0.0	-2.66672D-05	0.0	-1.78936D-03	0.0	1.26560D-03	0.0	2.77270D-03
0.0	-3.21596D-04	0.0	-1.56722D-03	0.0	2.03698D-04	0.0	-1.21669D-03
0.0	-2.27339D-02	0.0	3.07330D-03	0.0	6.66426D-03	0.0	-1.09339D-03
-1.54699D-03	-7.59742D-06	1.73549D-02	-1.77560D-07	2.15604D-01	-1.46734D-06	-6.58901D-02	-2.64076D-05
2.60074D-03	7.02847D-08	-2.90316D-03	8.44668D-08	6.87970D-03	-3.85975D-06	-3.42595D-03	-9.46167D-06

D =

COLUMNS 1 THRU 10

0.0	0.0	-8.39860D+00	8.05418D-02	0.0	0.0	0.0	0.0	0.0	0.0
0.0	0.0	-8.39860D+00	8.05418D-02	0.0	0.0	0.0	0.0	0.0	0.0
0.0	0.0	-8.39860D+00	8.05418D-02	0.0	0.0	0.0	0.0	0.0	0.0
0.0	0.0	-8.39860D+00	8.05418D-02	0.0	0.0	0.0	0.0	0.0	0.0
0.0	0.0	-8.39860D+00	8.05418D-02	0.0	0.0	0.0	0.0	0.0	0.0
0.0	0.0	-8.39860D+00	8.05418D-02	0.0	0.0	0.0	0.0	0.0	0.0
0.0	0.0	-8.39860D+00	8.05418D-02	0.0	0.0	0.0	0.0	0.0	0.0
0.0	0.0	5.72958D+01	0.0	0.0	0.0	0.0	0.0	0.0	0.0
0.0	6.95200D-01	-7.05628D+00	0.0	0.0	0.0	0.0	0.0	0.0	0.0

COLUMNS 11 THRU 18

0.0	0.0	0.0	0.0	0.0	0.0	0.0	0.0
0.0	0.0	0.0	0.0	0.0	0.0	0.0	0.0
0.0	0.0	0.0	0.0	0.0	0.0	0.0	0.0
0.0	0.0	0.0	0.0	0.0	0.0	0.0	0.0
0.0	0.0	0.0	0.0	0.0	0.0	0.0	0.0
0.0	0.0	0.0	0.0	0.0	0.0	0.0	0.0
0.0	0.0	0.0	0.0	0.0	0.0	0.0	0.0
0.0	0.0	0.0	0.0	0.0	0.0	0.0	0.0
0.0	0.0	0.0	0.0	0.0	0.0	0.0	0.0

E =

$$E = \begin{bmatrix} 0 \\ \hline 0.0 \quad 0.0 \quad 0.0 \quad 6.95200D\text{-}01 \end{bmatrix}$$

CRUISE

$$\dot{x} = Fx + Gu$$

$$\dot{y} = C\dot{x} + Dx + Eu$$

COLUMNS 1 THRU 10

-1.64346D-02	-8.70833D-04	1.46849D+00	-9.80567D+00	-1.83491D-04	-4.12051D-04	1.73899D-03	1.24766D-04	2.05239D-02	6.49670D-05
-1.55586D-01	-1.62920D+00	1.47953D+02	9.66105D-02	2.89603D-01	2.42226D-02	-1.21452D+00	-1.13488D-02	-1.10066D-01	2.10502D-02
-2.26752D-05	-4.60847D-02	-2.17733D+00	-3.08734D-04	-6.70590D-03	7.27566D-06	-1.32387D-01	-4.02734D-03	3.57790D-01	3.55432D-03
0.0	0.0	1.00000D+00	0.0	0.0	0.0	0.0	0.0	0.0	0.0
0.0	0.0	0.0	0.0	0.0	1.00000D+00	0.0	0.0	0.0	0.0
3.24890D+01	2.68619D+02	-9.48792D+02	-6.28318D-01	-4.96761D+02	-1.06495D+01	1.86143D+02	2.10963D+00	3.71936D+02	-3.23892D+00
0.0	0.0	0.0	0.0	0.0	0.0	0.0	1.00000D+00	0.0	0.0
-6.18369D+00	-1.18549D+02	-1.05903D+03	-9.50273D-02	1.56025D+01	3.48331D+00	-1.10438D+03	-5.26710D+00	1.17094D+02	3.51513D+00
0.0	0.0	0.0	0.0	0.0	0.0	0.0	0.0	0.0	1.00000D+00
-6.03307D+00	1.29875D+02	1.78838D+03	1.73784D-01	-1.24254D+00	-1.93882D+00	1.48707D+02	4.80550D+00	-1.98514D+03	-8.11869D+00
0.0	0.0	0.0	0.0	0.0	0.0	0.0	0.0	0.0	0.0
-3.97993D+00	1.01133D+02	2.56523D+03	3.54854D-01	3.10912D+01	2.38359D+00	1.23674D+02	4.44802D+00	-5.23156D+02	-5.19276D+00
0.0	0.0	0.0	0.0	0.0	0.0	0.0	0.0	0.0	0.0
-4.62710D+00	-6.65210D+01	-1.15570D+02	6.62215D-02	1.71777D+01	4.28405D+00	-5.71336D+01	-2.43832D+00	-2.19975D+01	2.69853D+00
0.0	0.0	0.0	0.0	0.0	0.0	0.0	0.0	0.0	0.0
4.06830D+00	-2.85314D+01	2.82788D+02	9.78161D-02	7.75852D+00	8.80708D-01	-2.01669D+01	-2.28706D-01	-2.18440D+01	1.03694D+00
0.0	0.0	0.0	0.0	0.0	0.0	0.0	0.0	0.0	0.0
1.24637D+00	-1.67602D+02	4.07533D+02	3.96790D-01	5.23726D+01	4.51321D+00	-1.39250D+02	-2.76629D-02	-1.47514D+02	4.36122D+00

COLUMNS 11 THRU 18

3.92854D-03	2.00622D-04	5.93581D-03	2.79790D-05	4.82610D-03	-2.11505D-04	8.93118D-03	-3.93176D-04
1.46022D+00	5.36520D-03	-5.49872D-01	-1.50148D-03	5.48679D+00	-3.82773D-02	1.56232D+01	-9.47545D-02
2.06328D-01	5.16856D-03	2.85423D-02	3.10210D-04	7.70858D-01	-2.79753D-03	3.67228D-01	-5.13918D-03
0.0	0.0	0.0	0.0	0.0	0.0	0.0	0.0
0.0	0.0	0.0	0.0	0.0	0.0	0.0	0.0
-1.39108D+02	4.77427D+00	2.56227D+02	4.21662D+00	-7.29448D+02	4.19945D+00	-3.73054D+03	1.06890D+01
0.0	0.0	0.0	0.0	0.0	0.0	0.0	0.0
1.62792D+02	2.44136D+00	-1.02325D+02	-2.81528D+00	6.35049D+02	-1.54835D+00	1.15327D+03	-3.80573D+00
0.0	0.0	0.0	0.0	0.0	0.0	0.0	0.0
-2.64197D+02	-7.88073D+00	1.31281D+02	2.69100D+00	-7.31100D+02	3.18887D+00	-6.05814D+02	7.35811D+00
0.0	1.00000D+00	0.0	0.0	0.0	0.0	0.0	0.0
-2.50246D+03	-1.74326D+01	1.15173D+02	3.72388D-01	-5.53973D+02	3.26627D+00	8.42576D+02	2.38517D+00
0.0	0.0	0.0	1.00000D+00	0.0	0.0	0.0	0.0
4.94270D+01	-8.50892D-01	-3.84989D+03	-9.21593D+00	2.41664D+02	-9.90824D-01	9.03369D+02	-2.01271D+00
0.0	0.0	0.0	0.0	0.0	1.00000D+00	0.0	0.0
3.66116D+01	6.36665D-01	-6.76431D+01	5.29541D-02	-1.03300D+04	-7.21217D+00	2.77196D+02	-2.85763D+00
0.0	0.0	0.0	0.0	0.0	0.0	0.0	1.00000D+00
1.11605D+02	-2.54239D+00	-1.32073D+02	4.60765D-03	5.26864D+02	-6.85155D+00	-1.08428D+04	-2.70073D+01

$$G = \begin{bmatrix}
-1.15592D-02 & 1.60052D-03 & -1.51220D-02 & 8.12422D-03 \\
-6.78184D-01 & -7.39938D-01 & -7.98038D-01 & -1.65215D+00 \\
-3.71450D-02 & 1.73937D-03 & -1.96116D-01 & -7.09147D-02 \\
0.0 & 0.0 & 0.0 & 0.0 \\
0.0 & 0.0 & 0.0 & 0.0 \\
2.38721D+02 & 1.88005D+02 & -4.57950D+01 & 2.69076D+02 \\
0.0 & 0.0 & 0.0 & 0.0 \\
-1.18811D+02 & -2.17669D+01 & -1.17076D+02 & -1.18659D+02 \\
0.0 & 0.0 & 0.0 & 0.0 \\
7.16529D+01 & -8.70162D+01 & 1.99167D+02 & 1.30016D+02 \\
0.0 & 0.0 & 0.0 & 0.0 \\
-1.70269D+01 & -5.39633D+01 & 2.23067D+02 & 1.01271D+02 \\
0.0 & 0.0 & 0.0 & 0.0 \\
-1.38337D+02 & 6.97680D+01 & 3.35393D+00 & -6.66118D+01 \\
0.0 & 0.0 & 0.0 & 0.0 \\
1.16695D+01 & 2.72383D+01 & 5.56083D+01 & -2.86122D+01 \\
0.0 & 0.0 & 0.0 & 0.0 \\
4.90542D+00 & 3.82684D+01 & -1.97028D+01 & -1.67923D+02
\end{bmatrix}$$

$G =$

COLUMNS 1 THRU 10

0.0	1.01900D-01	-1.08625D+00	0.0	0.0	8.21925D-04	0.0	1.73332D-03	0.0	-3.49619D-04
0.0	1.01900D-01	-3.75094D-02	0.0	0.0	3.02847D-04	0.0	-2.31721D-04	0.0	6.63573D-04
0.0	1.01900D-01	1.21159D+00	0.0	0.0	8.58711D-04	0.0	1.25541D-03	0.0	-7.27974D-04
0.0	1.01900D-01	8.98656D-02	0.0	0.0	-6.58172D-03	0.0	3.84265D-03	0.0	-2.45273D-03
0.0	1.01900D-01	-1.20344D-02	0.0	0.0	-2.03902D-03	0.0	3.27099D-04	0.0	-2.54444D-04
0.0	1.01900D-01	8.06946D-02	0.0	0.0	-2.13990D-03	0.0	6.72642D-04	0.0	3.61949D-04
0.0	1.01900D-01	1.23299D+00	0.0	0.0	1.35017D-03	0.0	3.70712D-03	0.0	-1.21974D-02
-3.54947D-05	-5.16521D-04	-2.62758D-03	0.0	-2.18698D-03	1.24733D-05	-1.18316D-03	-5.39153D-06	4.27999D-02	9.35067D-06
-1.17244D-05	-1.49710D-04	-6.64994D-04	0.0	2.94563D-03	2.12347D-06	5.95014D-03	-7.46062D-07	-1.08678D-03	1.99651D-06
0.0	-2.10300D+02	-3.30400D+02	0.0	0.0	-3.19100D+01	0.0	-2.94900D+01	0.0	-1.09300D+01
0.0	-1.57300D+03	-2.97500D+03	0.0	0.0	-2.35200D+02	0.0	-2.57300D+01	0.0	-2.46400D+01
0.0	-9.11000D+01	-1.05600D+02	0.0	0.0	5.46200D+00	0.0	-4.92100D+01	0.0	-5.82100D+01

COLUMNS 11 THRU 18

0.0	4.60996D-04	0.0	-5.36707D-04	0.0	1.42252D-03	0.0	-6.17310D-04
0.0	-3.17520D-04	0.0	7.02193D-04	0.0	1.08422D-04	0.0	1.19631D-04
0.0	1.25439D-03	0.0	-7.77803D-04	0.0	-7.60174D-04	0.0	1.26356D-04
0.0	2.61068D-03	0.0	9.14349D-03	0.0	-1.33285D-03	0.0	-1.63244D-03
0.0	-2.96733D-05	0.0	-1.78631D-03	0.0	1.25643D-03	0.0	2.73907D-03
0.0	-3.22615D-04	0.0	-1.56315D-03	0.0	1.97584D-04	0.0	-1.23605D-03
0.0	-2.26422D-02	0.0	3.04783D-03	0.0	6.62452D-03	0.0	-1.01278D-03
-1.48969D-03	-1.23530D-05	1.72632D-02	8.28497D-07	2.16406D-01	-4.53496D-06	-6.41713D-02	-5.21907D-05
1.49174D-03	1.87108D-08	-1.61526D-03	1.86496D-07	3.94637D-03	-4.35936D-06	-1.53075D-03	-1.07454D-05
0.0	-1.72600D+00	0.0	-1.75100D+01	0.0	-3.87500D+00	0.0	-8.24300D+00
0.0	-3.33500D+00	0.0	-6.68300D+01	0.0	-2.22000D+00	0.0	1.65800D+01
0.0	2.50900D+01	0.0	-8.79600D-01	0.0	8.85400D+00	0.0	8.71900D+00

D =

COLUMNS 1 THRU 10

0.0	0.0	-1.52646D+01	-9.85475D-03	0.0	0.0	0.0	0.0	0.0	0.0
0.0	0.0	-1.52646D+01	-9.85475D-03	0.0	0.0	0.0	0.0	0.0	0.0
0.0	0.0	-1.52646D+01	-9.85475D-03	0.0	0.0	0.0	0.0	0.0	0.0
0.0	0.0	-1.52646D+01	-9.85475D-03	0.0	0.0	0.0	0.0	0.0	0.0
0.0	0.0	-1.52646D+01	-9.85475D-03	0.0	0.0	0.0	0.0	0.0	0.0
0.0	0.0	-1.52646D+01	-9.85475D-03	0.0	0.0	0.0	0.0	0.0	0.0
0.0	0.0	-1.52646D+01	-9.85475D-03	0.0	0.0	0.0	0.0	0.0	0.0
0.0	0.0	5.72958D+01	0.0	0.0	0.0	0.0	0.0	0.0	0.0
0.0	3.82400D-01	-3.88136D+00	0.0	0.0	0.0	0.0	0.0	0.0	0.0
0.0	6.04500D+03	-9.40300D+03	0.0	-8.86400D+02	-1.46800D+02	2.34800D+03	-2.50500D+01	8.38600D+03	-3.00600D+01
0.0	6.07300D+04	5.61100D+03	0.0	-8.80300D+03	-2.03600D+03	3.18000D+04	3.56000D+02	7.22000D+04	-7.86800D+02
0.0	1.27300D+03	-4.94600D+03	0.0	3.39300D+01	2.90600D+01	3.85300D+02	-5.22400D+01	5.87900D+02	-8.85200D+01

COLUMNS 11 THRU 18

0.0	0.0	0.0	0.0	0.0	0.0	0.0	0.0
0.0	0.0	0.0	0.0	0.0	0.0	0.0	0.0
0.0	0.0	0.0	0.0	0.0	0.0	0.0	0.0
0.0	0.0	0.0	0.0	0.0	0.0	0.0	0.0
0.0	0.0	0.0	0.0	0.0	0.0	0.0	0.0
0.0	0.0	0.0	0.0	0.0	0.0	0.0	0.0
0.0	0.0	0.0	0.0	0.0	0.0	0.0	0.0
0.0	0.0	0.0	0.0	0.0	0.0	0.0	0.0
0.0	0.0	0.0	0.0	0.0	0.0	0.0	0.0
-8.42900D+02	1.10500D+02	2.99000D+03	6.43200D+00	-4.38300D+03	1.20900D+02	-3.33900D+04	3.46500D+02
-2.04900D+04	1.01900D+03	3.94700D+04	6.51800D+02	-9.96400D+04	1.10300D+03	-4.33100D+05	3.06600D+03
-7.10800D+02	3.14400D+01	-3.93300D+02	-4.24000D+01	3.83100D+02	1.14400D+02	3.70400D+03	4.45000D+02

E =

$$0$$

0.0	0.0	0.0	3.82400D-01
2.72446D+03	5.39307D+03	0.0	-6.04500D+03
4.59720D+04	4.09803D+04	0.0	-6.07300D+04
-2.50978D+03	-5.50128D+03	0.0	-1.27300D+03

COEFFICIENT MATRICES FOR ACT TIFS

EQUATIONS OF MOTION AND SENSOR AND LOAD EQUATIONS

(Five independent structural modes)

LANDING

$$\dot{x} = F'x + G'u$$
$$y = Ax + Bu$$

$F' =$

COLUMNS 1 THRU 10

9.93275D-03	1.57518D-01	-8.33021D+00	-9.73273D+00	-1.66949D-03	-1.91982D-03	1.57614D-02	9.20956D-04	3.30895D-02	-1.49457D-04
-3.33360D-01	-9.48826D-01	6.77015D+01	-1.20088D+00	3.09811D-01	1.64165D-02	-6.59667D-01	-7.53406D-03	1.67889D-01	1.23892D-02
-4.65027D-03	-2.76522D-02	-1.30033D+00	5.60551D-03	1.48637D-02	1.39117D-04	-6.91304D-02	-2.10375D-03	1.83709D-01	2.22356D-03
0.0	0.0	1.00000D+00	0.0	0.0	0.0	0.0	0.0	0.0	0.0
0.0	0.0	0.0	0.0	0.0	1.00000D+00	0.0	0.0	0.0	0.0
6.58945D+01	1.65250D+02	-4.46970D+02	8.79598D+00	-4.70632D+02	-6.84075D+00	9.17549D+01	1.52595D+00	1.37311D+02	-1.71880D+00
0.0	0.0	0.0	0.0	0.0	0.0	0.0	1.00000D+00	0.0	0.0
-1.92843D+01	-6.72146D+01	-5.12508D+02	1.08663D+00	1.77444D+01	2.08577D+00	-1.03898D+03	-3.58897D+00	6.66971D+01	2.02753D+00
0.0	0.0	0.0	0.0	0.0	0.0	0.0	0.0	0.0	1.00000D+00
1.05126D+01	6.62295D+01	8.35662D+02	-2.01600D+00	-1.40282D+01	-1.13687D+00	6.21987D+01	2.49482D+00	-1.81025D+03	-5.42779D+00
0.0	0.0	0.0	0.0	0.0	0.0	0.0	0.0	0.0	0.0
4.07658D+00	4.41861D+01	1.19348D+03	-4.43325D+00	4.04251D+00	1.36891D+00	4.66683D+01	2.14664D+00	-2.11125D+02	-2.88589D+00
0.0	0.0	0.0	0.0	0.0	0.0	0.0	0.0	0.0	0.0
-1.31564D+01	-3.62138D+01	-6.41572D+01	-8.17948D-01	8.26877D+00	2.39580D+00	-1.97382D+01	-1.37670D+00	-6.28609D+00	1.45467D+00

COLUMNS 11 THRU 14

-1.40585D-02	-1.93984D-05	1.40702D-02	3.04849D-04
6.22008D-01	2.43241D-03	-2.71257D-01	-9.47379D-04
3.80552D-02	2.43507D-03	2.41196D-02	2.98622D-04
0.0	0.0	0.0	0.0
0.0	0.0	0.0	0.0
-9.37400D+01	2.41773D+00	1.25416D+02	2.46718D+00
0.0	0.0	0.0	0.0
3.77405D+01	1.14424D+00	-5.00320D+01	-1.53937D+00
0.0	0.0	0.0	0.0
-2.36123D+01	-3.95329D+00	1.04640D+02	1.44632D+00
0.0	1.00000D+00	0.0	0.0
-2.17379D+03	-1.01002D+01	1.64210D+02	1.59620D-01
0.0	0.0	0.0	1.00000D+00
1.28705D+01	-4.67407D-01	-3.76199D+03	-6.52659D+00

$G' =$

7.28180D-03	-5.49812D-03	2.53231D-02	8.19753D-02
-1.74570D-01	-1.14129D-01	-1.08501D-01	-1.00667D+00
-9.25392D-03	-3.44984D-03	-4.64568D-02	-3.67438D-02
0.0	0.0	0.0	0.0
0.0	0.0	0.0	0.0
6.19076D+01	4.48580D+01	-1.25765D+01	1.65808D+02
0.0	0.0	0.0	0.0
-3.06521D+01	-5.77638D+00	-3.05168D+01	-6.72054D+01
0.0	0.0	0.0	0.0
1.80412D+01	-2.06483D+01	5.18845D+01	6.61807D+01
0.0	0.0	0.0	0.0
-5.17137D+00	-9.96016D+00	5.81485D+01	4.40231D+01
0.0	0.0	0.0	0.0
-3.58557D+01	1.92757D+01	1.02734D+00	-3.62789D+01

$A =$

COLUMNS 1 THRU 10

-3.36266D-03	-3.24614D-02	3.87664D-01	1.70890D-03	-3.37891D-01	-7.27082D-04	-1.72578D+00	-2.68590D-03	5.72064D-01	7.87639D-04
-1.29774D-02	-2.56780D-02	1.25603D-01	1.20425D-03	-1.20320D-01	-3.91930D-04	2.14306D-01	6.04439D-04	-1.10665D+00	-1.47710D-03
8.68896D-05	-3.89639D-02	-1.72598D+00	1.18391D-02	-3.23121D-01	-7.23709D-04	-1.36242D+00	-4.64966D-03	1.49378D+00	4.28875D-03
-6.77892D-01	-1.82415D+00	1.29545D+00	-6.78253D-02	3.31985D+00	8.30288D-02	-4.88355D+00	-3.79243D-02	3.22142D+00	3.96603D-02
-1.53794D-01	-4.08550D-01	5.92532D-01	-1.60449D-02	9.85487D-01	1.22641D-02	-5.71940D-01	-3.25402D-03	2.42241D-01	4.27450D-03
-1.65207D-01	-4.31286D-01	4.89357D-01	-1.61560D-02	1.03248D+00	1.31188D-02	-9.28125D-01	-4.24711D-03	-7.90202D-01	3.17736D-03
-2.84285D-01	-2.08413D+00	-4.17091D+01	1.45289D-01	-4.14012D-01	-9.48774D-03	-5.77676D+00	-9.82205D-02	2.75953D+01	1.45711D-01
8.88181D-04	2.30769D-03	5.72646D+01	1.24615D-03	-4.88684D-03	-2.30582D-03	5.89003D-03	-9.44544D-04	-5.82105D-03	4.30081D-02
3.48911D-04	8.43014D-01	-8.55846D+00	8.48871D-04	-1.74152D-03	6.44973D-03	2.09822D-03	1.32381D-02	-3.50590D-03	-2.34998D-03

COLUMNS 11 THRU 14

-9.43269D-01	-1.25885D-03	1.99165D+00	1.94808D-03
7.13556D-01	8.93315D-04	-2.60776D+00	-2.68523D-03
-2.59845D+00	-2.52290D-03	3.07782D+00	4.62224D-03
-4.66810D+00	-3.19814D-02	-3.53078D+01	-8.51050D-02
3.06595D-01	-2.21388D-03	6.40411D+00	5.67697D-03
9.62577D-01	-1.40296D-03	5.55305D+00	4.31219D-03
4.98933D+01	2.87391D-01	-1.66024D+01	-4.35209D-02
1.41088D-02	-1.48411D-03	2.34414D-03	1.74050D-02
-7.35924D-04	3.13101D-03	5.94949D-04	-3.49878D-03

$B =$

5.03505D-05	1.12642D-02	-1.69391D-02	-2.80271D-02
-3.21095D-03	6.38612D-03	1.05810D-02	-3.10913D-02
-6.47459D-03	3.09992D-03	-8.33593D-02	-5.54997D-02
-9.29984D-01	-1.28299D-01	-1.59835D-02	-1.83539D+00
-9.41762D-02	-1.33825D-01	-1.15460D-02	-4.15336D-01
-1.07240D-01	-1.46207D-01	-1.00247D-02	-4.38964D-01
-2.73007D-01	5.61468D-01	-2.15266D+00	-2.09634D+00
9.54183D-04	4.84798D-04	-5.63241D-05	2.35702D-03
3.34375D-04	1.47574D-04	1.69095D-04	8.43040D-01

CLIMB

$$\dot{x} = F'x + G'u$$

$$y = Ax + Bu$$

$F' =$

COLUMNS 1 THRU 10

4.83946D-03	1.18872D-01	-6.64386D+00	-9.77339D+00	-1.64398D-03	-1.50359D-03	1.44961D-02	6.99335D-04	3.19649D-02	-1.00546D-04
-2.96828D-01	-1.00113D+00	8.26434D+01	-7.99181D-01	2.87577D-01	1.72850D-02	-6.91405D-01	-7.81327D-03	9.64184D-02	1.35125D-02
-3.26216D-03	-2.89495D-02	-1.20441D+00	2.90302D-03	1.10203D-02	1.07093D-04	-6.96119D-02	-2.21272D-03	1.83111D-01	2.29933D-03
0.0	0.0	1.00000D+00	0.0	0.0	0.0	0.0	0.0	0.0	0.0
0.0	0.0	0.0	0.0	0.0	1.00000D+00	0.0	0.0	0.0	0.0
5.49991D+01	1.76688D+02	-5.05739D+02	5.32728D+00	-4.70876D+02	-7.23664D+00	9.88991D+01	1.56314D+00	1.58687D+02	-1.91414D+00
0.0	0.0	0.0	0.0	0.0	0.0	0.0	1.00000D+00	0.0	0.0
-1.55224D+01	-7.20721D+01	-5.50597D+02	6.32244D-01	1.63262D+01	2.21523D+00	-1.04280D+03	-3.71373D+00	6.34474D+01	2.16272D+00
0.0	0.0	0.0	0.0	0.0	0.0	0.0	0.0	0.0	1.00000D+00
6.76404D+00	7.14779D+01	9.07068D+02	-1.21122D+00	-1.14069D+01	-1.19320D+00	6.62993D+01	2.66559D+00	-1.81508D+03	-5.64612D+00
0.0	0.0	0.0	0.0	0.0	0.0	0.0	0.0	0.0	0.0
2.35813D+00	4.73956D+01	1.30286D+03	-2.69096D+00	7.27220D+00	1.52054D+00	4.91979D+01	2.30653D+00	-2.26887D+02	-3.03986D+00
0.0	0.0	0.0	0.0	0.0	0.0	0.0	0.0	0.0	0.0
-1.08796D+01	-3.94023D+01	-6.53759D+01	-5.17440D-01	8.92657D+00	2.58293D+00	-2.30828D+01	-1.47193D+00	-8.59925D+00	1.56194D+00

COLUMNS 11 THRU 14

-1.23991D-02	3.47450D-05	1.34128D-02	2.34088D-04
6.84508D-01	2.53862D-03	-2.90951D-01	-6.90279D-04
5.29748D-02	2.61034D-03	2.29226D-02	3.34447D-04
0.0	0.0	0.0	0.0
0.0	0.0	0.0	0.0
-9.42441D+01	2.67508D+00	1.33875D+02	2.59760D+00
0.0	0.0	0.0	0.0
4.92448D+01	1.22756D+00	-5.27647D+01	-1.62888D+00
0.0	0.0	0.0	0.0
-4.88408D+01	-4.28042D+00	9.85199D+01	1.51804D+00
0.0	1.00000D+00	0.0	0.0
-2.21225D+03	-1.07668D+01	1.42142D+02	1.21132D-01
0.0	0.0	0.0	1.00000D+00
1.63656D+01	-5.12963D-01	-3.77494D+03	-6.77946D+00

$G' =$

5.30315D-03	1.46026D-02	-3.80145D-02	6.20502D-02
-2.21563D-01	-2.56935D-01	-1.70899D-01	-1.08144D+00
-1.13881D-02	3.41875D-03	-6.15575D-02	-3.90630D-02
0.0	0.0	0.0	0.0
0.0	0.0	0.0	0.0
7.92693D+01	5.81930D+01	-1.62711D+01	1.77357D+02
0.0	0.0	0.0	0.0
-3.92217D+01	-7.07899D+00	-3.92135D+01	-7.20530D+01
0.0	0.0	0.0	0.0
2.28388D+01	-2.72788D+01	6.68445D+01	7.14065D+01
0.0	0.0	0.0	0.0
-7.17672D+00	-1.35064D+01	7.49956D+01	4.71784D+01
0.0	0.0	0.0	0.0
-4.63835D+01	2.50320D+01	1.34327D+00	-3.94810D+01

$A =$

COLUMNS 1 THRU 10

-4.17948D-03	-3.40552D-02	2.53522D-01	9.31978D-04	-3.38479D-01	-7.15330D-04	-1.72671D+00	-2.71453D-03	5.74746D-01	8.32016D-04
-1.38118D-02	-2.61433D-02	1.83213D-01	1.52675D-04	-1.21012D-01	-4.06067D-04	2.13909D-01	6.16439D-04	-1.10601D+00	-1.46215D-03
-2.30662D-04	-3.94103D-02	-1.56326D+00	5.94610D-03	-3.30516D-01	-7.66996D-04	-1.36106D+00	-4.78106D-03	1.48642D+00	4.36216D-03
-5.62201D-01	-1.95685D+00	1.70286D+00	-4.20523D-02	3.32088D+00	8.84491D-02	-4.98134D+00	-3.95495D-02	3.00867D+00	4.28932D-02
-1.29727D-01	-4.34536D-01	7.37742D-01	-1.02764D-02	9.81370D-01	1.28799D-02	-5.86438D-01	-3.27739D-03	1.95293D-01	4.66330D-03
-1.39896D-01	-4.58601D-01	6.47981D-01	-1.03953D-02	1.02835D+00	1.37763D-02	-9.43444D-01	-4.28849D-03	-8.38839D-01	3.57760D-03
-1.87500D-01	-2.23982D+00	-4.51046D+01	8.66256D-02	-5.30558D-01	-1.16773D-02	-5.90139D+00	-1.04782D-01	2.80122D+01	1.52682D-01
7.27722D-04	2.41978D-03	5.72581D+01	9.32552D-04	-4.77759D-03	-2.30888D-03	5.86719D-03	-9.65027D-04	-6.22396D-03	4.29762D-02
2.40098D-04	6.96109D-01	-7.06927D+00	5.45871D-04	-1.41943D-03	5.32377D-03	1.76445D-03	1.09243D-02	-3.16689D-03	-1.94891D-03

COLUMNS 11 THRU 14

-9.48095D-01	-1.25709D-03	1.99527D+00	1.98355D-03
7.13850D-01	9.17354D-04	-2.61225D+00	-2.71751D-03
-2.59634D+00	-2.54429D-03	3.06795D+00	4.79159D-03
-4.61953D+00	-3.46841D-02	-3.55292D+01	-8.88497D-02
3.19579D-01	-2.51779D-03	6.40548D+00	5.83634D-03
9.76989D-01	-1.70433D-03	5.55620D+00	4.43673D-03
5.11316D+01	3.07190D-01	-1.60545D+01	-4.43608D-02
1.51001D-02	-1.47140D-03	1.64397D-03	1.73940D-02
-7.27742D-04	2.59576D-03	3.45892D-04	-2.89188D-03

$B =$

-6.15895D-05	-4.44303D-03	-2.28761D-02	-3.06989D-02
-4.26021D-03	-3.32091D-03	1.04795D-02	-3.37821D-02
-7.58112D-03	2.61710D-03	-1.12326D-01	-5.94040D-02
-1.19534D+00	-1.75322D-01	-2.25920D-02	-1.97138D+00
-1.19501D-01	-1.84553D-01	-1.78917D-02	-4.43791D-01
-1.36234D-01	-1.99884D-01	-1.60632D-02	-4.68852D-01
-3.34139D-01	7.47823D-01	-2.77932D+00	-2.25393D+00
1.20331D-03	6.41972D-04	-5.27562D-05	2.47926D-03
3.53390D-04	1.65637D-04	2.05457D-04	6.96135D-01

CRUISE

$$\dot{x} = F'x + G'u$$

$$y = Ax + Bu$$

$F' =$

COLUMNS 1 THRU 10

-1.64315D-02	-1.02562D-03	1.46898D+00	-9.80567D+00	-1.35713D-04	-4.07826D-04	1.61219D-03	1.24626D-04	2.03893D-02	6.91449D-05
-1.51308D-01	-1.89056D+00	1.48718D+02	9.72476D-02	3.70574D-01	3.13287D-02	-1.42953D+00	-1.15276D-02	-3.38125D-01	2.80295D-02
3.32996D-04	-5.42699D-02	-2.14111D+00	-2.87042D-04	-4.23662D-03	2.36282D-04	-1.38917D-01	-4.04582D-03	3.50836D-01	3.78983D-03
0.0	0.0	1.00000D+00	0.0	0.0	0.0	0.0	0.0	0.0	0.0
0.0	0.0	0.0	0.0	0.0	1.00000D+00	0.0	0.0	0.0	0.0
3.16982D+01	3.29181D+02	-1.11489D+03	-7.74367D-01	-5.15583D+02	-1.22902D+01	2.36147D+02	2.13940D+00	4.24950D+02	-4.84081D+00
0.0	0.0	0.0	0.0	0.0	0.0	0.0	1.00000D+00	0.0	0.0
-5.77646D+00	-1.38574D+02	-9.96042D+02	-4.55916D-02	2.17824D+01	4.03007D+00	-1.12078D+03	-5.28541D+00	9.96881D+01	4.05593D+00
0.0	0.0	0.0	0.0	0.0	0.0	0.0	0.0	0.0	1.00000D+00
-6.40497D+00	1.41659D+02	1.74399D+03	1.43656D-01	-4.83939D+00	-2.26442D+00	1.58236D+02	4.82396D+00	-1.97501D+03	-8.44703D+00
0.0	0.0	0.0	0.0	0.0	0.0	0.0	0.0	0.0	0.0
-4.08697D+00	8.97408D+01	2.58232D+03	3.80319D-01	3.47086D+01	2.68477D+00	1.14033D+02	4.45728D+00	-5.33345D+02	-4.21097D+00
0.0	0.0	0.0	0.0	0.0	0.0	0.0	0.0	0.0	0.0
-4.40977D+00	-8.13931D+01	-7.35004D+01	1.02268D-01	2.17929D+01	4.68764D+00	-6.93920D+01	-2.44697D+00	-3.49967D+01	3.09367D+00

COLUMNS 11 THRU 14

4.04059D-03	1.98819D-04	5.79081D-03	2.80099D-05
1.64492D+00	2.04802D-03	-7.83171D-01	-1.46271D-03
2.13125D-01	5.12616D-03	1.86397D-02	3.14423D-04
0.0	0.0	0.0	0.0
0.0	0.0	0.0	0.0
-1.80990D+02	5.59853D+00	3.07937D+02	4.21035D+00
0.0	0.0	0.0	0.0
1.77306D+02	2.20924D+00	-1.21130D+02	-2.81123D+00
0.0	0.0	0.0	0.0
-2.73342D+02	-7.78082D+00	1.43896D+02	2.68683D+00
0.0	1.00000D+00	0.0	0.0
-2.49575D+03	-1.76586D+01	1.08442D+02	3.70107D-01
0.0	0.0	0.0	1.00000D+00
5.98178D+01	-1.04689D+00	-3.86286D+03	-9.21408D+00

$G' =$

-1.15492D-02	1.64642D-03	-1.51101D-02	7.96913D-03
-6.63975D-01	-6.67714D-01	-7.93065D-01	-1.91403D+00
-3.60771D-02	5.19263D-03	-1.92570D-01	-7.91176D-02
0.0	0.0	0.0	0.0
0.0	0.0	0.0	0.0
2.35992D+02	1.72348D+02	-4.38806D+01	3.29756D+02
0.0	0.0	0.0	0.0
-1.17499D+02	-1.58064D+01	-1.15480D+02	-1.38724D+02
0.0	0.0	0.0	0.0
7.05093D+01	-9.12345D+01	1.96205D+02	1.41824D+02
0.0	0.0	0.0	0.0
-1.72323D+01	-5.23927D+01	2.18796D+02	8.98583D+01
0.0	0.0	0.0	0.0
-1.37602D+02	7.37373D+01	3.23767D+00	-8.15131D+01

$A =$

COLUMNS 1 THRU 10

2.98313D-03	-6.78004D-02	1.92844D-01	-2.78703D-04	-3.37656D-01	-6.67064D-04	-1.70885D+00	-2.50120D-03	5.69931D-01	8.19843D-04
-1.05415D-02	-5.04585D-02	1.48908D-01	-1.12024D-04	-1.22199D-01	-5.35827D-04	2.10833D-01	9.17269D-04	-1.10781D+00	-1.56534D-03
7.91893D-03	-7.69430D-02	-2.88543D+00	-7.22244D-04	-3.52653D-01	-6.45586D-04	-1.43641D+00	-6.89204D-03	1.67663D+00	5.96560D-03
-2.81495D-01	-3.75397D+00	4.99975D+00	6.52609D-03	3.81625D+00	1.55015D-01	-6.74407D+00	-5.84984D-02	7.15021D-01	8.68275D-02
-7.23168D-02	-8.01842D-01	1.47388D+00	1.39175D-03	1.05749D+00	2.16907D-02	-9.11803D-01	-4.20574D-03	-2.91680D-01	1.07766D-02
-8.12146D-02	-8.45101D-01	1.34575D+00	1.42746D-03	1.10835D+00	2.32089D-02	-1.28714D+00	-5.50140D-03	-1.33652D+00	9.94016D-03
1.63598D-01	-4.33669D+00	-8.79136D+01	-1.15655D-02	-1.24327D+00	-1.70521D-02	-8.87651D+00	-1.90089D-01	3.74009D+01	2.39685D-01
4.91329D-04	6.12084D-03	5.72003D+01	2.85890D-04	-7.18468D-03	-2.42925D-03	1.01051D-02	-1.12338D-03	-7.89313D-03	4.26775D-02
8.05567D-05	3.83791D-01	-3.90033D+00	9.93001D-05	-1.16868D-03	2.90808D-03	1.94911D-03	5.97230D-03	-3.31456D-03	-1.12318D-03
-6.61382D+02	3.00109D+02	1.32090D+03	3.96158D-01	1.42918D+04	4.34255D+01	2.79422D+04	4.89556D+01	1.54306D+04	3.01873D+01
-6.70137D+03	-1.26419D+03	-4.82182D+02	2.43285D+00	1.07680D+05	2.42627D+02	1.39556D+04	5.25686D+01	2.81485D+04	2.21592D+01
7.45964D+02	4.08637D+03	-1.18501D+04	-9.58347D+00	-2.73565D+03	-4.26228D+01	5.06360D+04	5.41788D+01	9.95598D+04	4.98098D+01

COLUMNS 11 THRU 14

-9.92391D-01	-1.78706D-03	2.01600D+00	2.27375D-03
7.16798D-01	9.08689D-04	-2.61060D+00	-3.03900D-03
-2.48517D+00	-1.67172D-03	3.09096D+00	5.99318D-03
-3.23890D+00	-6.42781D-02	-3.79602D+01	-1.28507D-01
6.28847D-01	-6.17203D-03	6.11288D+00	6.10717D-03
1.30411D+00	-5.35481D-03	5.23658D+00	4.23168D-03
6.08689D+01	5.13822D-01	-1.60739D+01	-7.37336D-02
2.37003D-02	-1.30179D-03	1.65499D-03	1.73437D-02
-1.48592D-03	1.48220D-03	4.17959D-04	-1.60056D-03
5.16862D+03	5.92657D+00	6.32212D+04	8.64743D+01
2.04366D+04	4.23489D+01	2.31690D+05	2.82758D+02
-5.73164D+04	-3.74742D+01	5.01225D+03	-1.99674D+01

$B =$

3.09082D-03	8.74805D-03	-7.73345D-02	-4.29274D-02
-1.19731D-02	-4.50435D-03	2.87755D-03	-5.17204D-02
-2.21477D-02	9.74712D-03	-3.67681D-01	-1.09014D-01
-3.55174D+00	-5.01447D-01	-1.33488D-01	-3.76416D+00
-3.58480D-01	-5.31642D-01	-8.89951D-02	-8.04988D-01
-4.08432D-01	-5.78442D-01	-8.47610D-02	-8.50620D-01
-1.11834D+00	2.63632D+00	-8.14294D+00	-4.37454D+00
4.77344D-03	2.42134D-03	1.26000D-04	6.20592D-03
8.27101D-04	3.04879D-04	6.36364D-04	3.83812D-01
4.57079D+02	1.60496D+02	2.48589D+03	-1.17895D+04
1.82384D+03	-2.47807D+03	9.47424D+03	-1.22727D+05
2.12284D+02	2.24175D+02	-4.02399D+02	1.54896D+03

COEFFICIENT MATRICES FOR ACT TIFS

EQUATIONS OF MOTION AND SENSOR AND LOAD EQUATIONS

(Two independent structural modes)

LANDING

$$\dot{x} = F'x + G'u$$

$$y = A'x + Bu$$

$$F' = \begin{bmatrix}
1.00535D-02 & 1.58341D-01 & -8.32250D+00 & -9.73274D+00 & -1.93058D-03 & -1.94104D-03 & 1.65568D-02 & 9.48704D-04 \\
-3.30807D-01 & -9.30173D-01 & 6.80955D+01 & -1.20222D+00 & 3.09647D-01 & 1.66000D-02 & -6.41502D-01 & -6.69319D-03 \\
-3.66704D-03 & -2.06908D-02 & -1.19813D+00 & 5.32369D-03 & 1.36160D-02 & 7.22508D-05 & -6.23661D-02 & -1.83370D-03 \\
0.0 & 0.0 & 1.00000D+00 & 0.0 & 0.0 & 0.0 & 0.0 & 0.0 \\
0.0 & 0.0 & 0.0 & 0.0 & 0.0 & 1.00000D+00 & 0.0 & 0.0 \\
6.61228D+01 & 1.67450D+02 & -4.33850D+02 & 8.79964D+00 & -4.71664D+02 & -6.91195D+00 & 9.40744D+01 & 1.58725D+00 \\
0.0 & 0.0 & 0.0 & 0.0 & 0.0 & 0.0 & 0.0 & 1.00000D+00 \\
-1.86958D+01 & -6.37353D+01 & -4.62404D+02 & 9.50744D-01 & 1.72272D+01 & 2.04146D+00 & -1.03579D+03 & -3.44961D+00
\end{bmatrix}$$

$$G' = \begin{bmatrix}
7.51702D-03 & -5.74833D-03 & 2.59284D-02 & 8.27983D-02 \\
-1.72889D-01 & -1.19319D-01 & -8.88827D-02 & -9.88067D-01 \\
-7.89854D-03 & -5.47824D-03 & -4.03243D-02 & -2.97906D-02 \\
0.0 & 0.0 & 0.0 & 0.0 \\
0.0 & 0.0 & 0.0 & 0.0 \\
6.23852D+01 & 4.42741D+01 & -1.08944D+01 & 1.68008D+02 \\
0.0 & 0.0 & 0.0 & 0.0 \\
-2.96941D+01 & -6.88911D+00 & -2.77338D+01 & -6.37299D+01
\end{bmatrix}$$

$$A = \begin{bmatrix}
-8.14799D-03 & -4.63581D-02 & 1.40271D-01 & 2.47504D-03 & -3.40463D-01 & -4.89947D-04 & -1.73365D+00 & -3.42557D-03 \\
-9.26789D-03 & -2.86986D-02 & 2.44316D-02 & 1.61143D-03 & -1.15659D-01 & -8.71703D-04 & 2.03238D-01 & 6.59081D-04 \\
-5.11727D-03 & -5.69888D-02 & -2.40601D+00 & 1.45753D-02 & -3.34926D-01 & -1.56356D-03 & -1.37424D+00 & -5.91774D-03 \\
-5.41187D-01 & -1.44396D+00 & 9.75087D-01 & -5.44258D-02 & 3.20385D+00 & 5.50464D-02 & -4.67252D+00 & -2.45580D-02 \\
-1.74545D-01 & -4.56609D-01 & 7.53937D-01 & -1.83326D-02 & 9.98700D-01 & 1.64454D-02 & -5.91866D-01 & -5.01353D-03 \\
-1.88048D-01 & -4.97554D-01 & 5.26021D-01 & -1.83965D-02 & 1.05353D+00 & 1.78583D-02 & -9.66843D-01 & -6.54165D-03 \\
-1.85760D-02 & -1.31499D-01 & -3.77829D+00 & 2.13395D-02 & -5.23916D-01 & 5.03331D-05 & -3.86886D+00 & -1.36353D-02 \\
8.62489D-04 & 2.30405D-03 & 5.72691D+01 & 1.22454D-03 & -4.79797D-03 & -2.29044D-03 & 5.93181D-03 & -9.41539D-04 \\
3.26440D-04 & 8.42871D-01 & -8.56043D+00 & 8.54034D-04 & -1.71539D-03 & 6.45167D-03 & 1.96342D-03 & 1.32326D-02
\end{bmatrix}$$

$$B = \begin{bmatrix}
-9.78346D-03 & 1.80947D-02 & -2.27544D-02 & -4.19046D-02 \\
8.37659D-03 & 3.02770D-03 & -4.47458D-03 & -3.40890D-02 \\
-1.13133D-02 & 1.04647D-02 & -1.02449D-01 & -7.34273D-02 \\
-5.43158D-01 & -3.30583D-01 & -4.75936D-02 & -1.45434D+00 \\
-1.54343D-01 & -1.04600D-01 & 4.66076D-03 & -4.63535D-01 \\
-1.71681D-01 & -1.11966D-01 & -7.61069D-03 & -5.05378D-01 \\
-5.36619D-02 & 1.51894D-02 & -1.76655D-01 & -1.47845D-01 \\
8.19945D-04 & 5.17252D-04 & 1.18144D-04 & 2.35246D-03 \\
2.98460D-04 & 1.91729D-04 & 5.21545D-05 & 8.42897D-01
\end{bmatrix}$$

CLIMB

$$\dot{x} = F'x + Gu$$

$$y = Ax + Bu$$

$$F' = \begin{bmatrix}
4.90799D-03 & 1.19749D-01 & -6.63527D+00 & -9.77340D+00 & -1.86270D-03 & -1.52474D-03 & 1.53299D-02 & 7.28824D-04 \\
-2.95292D-01 & -9.82880D-01 & 8.30632D+01 & -7.99996D-01 & 2.89071D-01 & 1.75685D-02 & -6.73735D-01 & -6.96609D-03 \\
-2.64991D-03 & -2.12739D-02 & -1.08757D+00 & 2.72050D-03 & 1.01445D-02 & 4.76781D-05 & -6.22507D-02 & -1.91472D-03 \\
0.0 & 0.0 & 1.00000D+00 & 0.0 & 0.0 & 0.0 & 0.0 & 0.0 \\
0.0 & 0.0 & 0.0 & 0.0 & 0.0 & 1.00000D+00 & 0.0 & 0.0 \\
5.51281D+01 & 1.79791D+02 & -4.81751D+02 & 5.31556D+00 & -4.71934D+02 & -7.32132D+00 & 1.02033D+02 & 1.65484D+00 \\
0.0 & 0.0 & 0.0 & 0.0 & 0.0 & 0.0 & 0.0 & 1.00000D+00 \\
-1.51190D+01 & -6.82585D+01 & -4.92511D+02 & 5.41725D-01 & 1.60034D+01 & 2.17744D+00 & -1.03931D+03 & -3.55992D+00
\end{bmatrix}$$

$$G' = \begin{bmatrix}
5.58839D-03 & 1.42784D-02 & -3.72320D-02 & 6.29273D-02 \\
-2.20420D-01 & -2.63137D-01 & -1.46850D-01 & -1.06325D+00 \\
-9.74282D-03 & 6.84072D-04 & -5.33482D-02 & -3.13999D-02 \\
0.0 & 0.0 & 0.0 & 0.0 \\
0.0 & 0.0 & 0.0 & 0.0 \\
8.00276D+01 & 5.71674D+01 & -1.33475D+01 & 1.80460D+02 \\
0.0 & 0.0 & 0.0 & 0.0 \\
-3.80655D+01 & -8.55930D+00 & -3.54598D+01 & -6.82454D+01
\end{bmatrix}$$

$$A = \begin{bmatrix}
-8.38683D-03 & -4.88084D-02 & -1.04618D-02 & 1.38061D-03 & -3.41169D-01 & -4.64958D-04 & -1.73564D+00 & -3.49934D-03 \\
-9.83256D-03 & -2.92602D-02 & 7.37098D-02 & 4.04399D-04 & -1.17429D-01 & -9.27646D-04 & 2.03379D-01 & 6.80814D-04 \\
-5.14395D-03 & -5.81241D-02 & -2.29000D+00 & 7.56796D-03 & -3.43077D-01 & -1.67646D-03 & -1.37396D+00 & -6.12186D-03 \\
-4.51279D-01 & -1.54776D+00 & 1.24551D+00 & -3.36367D-02 & 3.19802D+00 & 5.83508D-02 & -4.74057D+00 & -2.54567D-02 \\
-1.47366D-01 & -4.88622D-01 & 9.01287D-01 & -1.16735D-02 & 9.96804D-01 & 1.74238D-02 & -6.12838D-01 & -5.21497D-03 \\
-1.58421D-01 & -5.32423D-01 & 6.78102D-01 & -1.17694D-02 & 1.05091D+00 & 1.89225D-02 & -9.89619D-01 & -6.79501D-03 \\
-1.51578D-02 & -1.37514D-01 & -3.75768D+00 & 1.15684D-02 & -5.35707D-01 & 6.26249D-05 & -3.87321D+00 & -1.40769D-02 \\
7.08629D-04 & 2.41780D-03 & 5.72632D+01 & 9.18820D-04 & -4.67300D-03 & -2.29171D-03 & 5.90948D-03 & -9.61369D-04 \\
2.27462D-04 & 6.95972D-01 & -7.07120D+00 & 5.48705D-04 & -1.40173D-03 & 5.32546D-03 & 1.63602D-03 & 1.09190D-02
\end{bmatrix}$$

$$B = \begin{bmatrix}
-1.27502D-02 & 4.42009D-03 & -3.00181D-02 & -4.54254D-02 \\
-1.08713D-02 & -7.57124D-03 & -8.85434D-03 & -3.68702D-02 \\
-1.38223D-02 & 1.22379D-02 & -1.36008D-01 & -7.79907D-02 \\
-6.96367D-01 & -4.35911D-01 & -6.82041D-02 & -1.56122D+00 \\
-1.97860D-01 & -1.46162D-01 & 1.39982D-03 & -4.98051D-01 \\
-2.20048D-01 & -1.54836D-01 & -1.45077D-02 & -5.42853D-01 \\
-6.80015D-02 & 1.93808D-02 & -2.30651D-01 & -1.57236D-01 \\
1.02837D-03 & 6.80292D-04 & 1.80103D-04 & 2.47604D-03 \\
3.14783D-04 & 2.17078D-04 & 6.94755D-05 & 6.95998D-01
\end{bmatrix}$$

CRUISE

$$\dot{x} = F'x + G'u$$

$$y = Ax + Bu$$

$$F' = \begin{bmatrix}
-1.65070D-02 & 3.06548D-04 & 1.48795D+00 & -9.80567D+00 & -1.24328D-04 & -4.20431D-04 & 3.14863D-03 & 1.71382D-04 \\
-1.51001D-01 & -1.86263D+00 & 1.49903D+02 & 9.74402D-02 & 3.92071D-01 & 3.30725D-02 & -1.39300D+00 & -9.66886D-03 \\
-1.02015D-03 & -2.66527D-02 & -1.68846D+00 & -2.36938D-04 & -2.35980D-03 & 1.19005D-04 & -1.06854D-01 & -3.00555D-03 \\
0.0 & 0.0 & 1.00000D+00 & 0.0 & 0.0 & 0.0 & 0.0 & 0.0 \\
0.0 & 0.0 & 0.0 & 0.0 & 0.0 & 1.00000D+00 & 0.0 & 0.0 \\
3.01789D+01 & 3.47471D+02 & -9.52826D+02 & -7.67920D-01 & -5.18228D+02 & -1.26900D+01 & 2.57094D+02 & 2.65461D+00 \\
0.0 & 0.0 & 0.0 & 0.0 & 0.0 & 0.0 & 0.0 & 1.00000D+00 \\
-6.13572D+00 & -1.25616D+02 & -7.64116D+02 & -1.83590D-02 & 2.33242D+01 & 4.00224D+00 & -1.10599D+03 & -4.75977D+00
\end{bmatrix}$$

$$G' = \begin{bmatrix}
-1.11041D-02 & 8.31781D-04 & -1.29932D-02 & 9.30281D-03 \\
-6.73908D-01 & -6.86143D-01 & -7.11660D-01 & -1.88605D+00 \\
-2.77875D-02 & -1.19551D-02 & -1.46397D-01 & -5.14676D-02 \\
0.0 & 0.0 & 0.0 & 0.0 \\
0.0 & 0.0 & 0.0 & 0.0 \\
2.42739D+02 & 1.61877D+02 & -1.77220D+01 & 3.48064D+02 \\
0.0 & 0.0 & 0.0 & 0.0 \\
-1.12438D+02 & -2.43935D+01 & -9.45008D+01 & -1.25749D+02
\end{bmatrix}$$

$$A = \begin{bmatrix}
-1.09228D-04 & -9.29883D-02 & -2.62983D-01 & -3.31216D-04 & -3.43001D-01 & -2.52254D-04 & -1.73160D+00 & -3.78878D-03 \\
-4.78740D-03 & -5.44646D-02 & -3.76327D-02 & -1.45017D-04 & -1.22308D-01 & -1.40490D-03 & 1.96203D-01 & 1.03436D-03 \\
1.58911D-03 & -8.14169D-02 & -3.81266D+00 & -8.95138D-04 & -3.78634D-01 & -2.35833D-03 & -1.43911D+00 & -8.32267D-03 \\
-2.37685D-01 & -2.96185D+00 & 3.19380D+00 & 5.03680D-03 & 3.54020D+00 & 1.02282D-01 & -6.09361D+00 & -3.70174D-02 \\
-7.89171D-02 & -9.39070D-01 & 1.72374D+00 & 1.63705D-03 & 1.10429D+00 & 3.05529D-02 & -1.02665D+00 & -7.91880D-03 \\
-8.41763D-02 & -1.02000D+00 & 1.39926D+00 & 1.68621D-03 & 1.16441D+00 & 3.32271D-02 & -1.44466D+00 & -1.01100D-02 \\
1.35608D-03 & -2.19192D-01 & -6.19047D+00 & -1.32262D-03 & -5.76190D-01 & 1.21990D-03 & -4.02663D+00 & -1.87519D-02 \\
4.90773D-04 & 6.04348D-03 & 5.72150D+01 & 2.88863D-04 & -6.78607D-03 & -2.38422D-03 & 1.01700D-02 & -1.11150D-03 \\
9.21398D-05 & 3.83528D-01 & -3.90415D+00 & 9.89183D-05 & -1.17497D-03 & 2.91067D-03 & 1.65064D-03 & 5.96278D-03 \\
-7.87074D+02 & 9.50204D+01 & 1.67896D+04 & 3.76137D+00 & 1.46800D+04 & 1.10174D+02 & 2.80955D+04 & 4.97661D+01 \\
-7.07302D+03 & -3.89665D+03 & 3.58816D+04 & 1.34109D+01 & 1.09242D+05 & 5.24807D+02 & 1.24366D+04 & -5.55108D+00 \\
4.80755D+02 & 9.49759D+03 & 1.39586D+04 & -1.20793D+01 & -3.97640D+03 & -2.40790D+02 & 5.63336D+04 & 1.98273D+02
\end{bmatrix}$$

$$B = \begin{bmatrix}
-3.38648D-02 & 3.38376D-02 & -9.18600D-02 & -6.81631D-02 \\
3.19381D-02 & -1.47931D-02 & -5.04962D-02 & -5.57097D-02 \\
-3.50513D-02 & 2.39794D-02 & -3.83747D-01 & -1.13527D-01 \\
-2.10087D+00 & -1.23016D+00 & -3.32166D-01 & -2.97088D+00 \\
-6.00065D-01 & -4.07824D-01 & -6.55319D-02 & -9.42411D-01 \\
-6.65982D-01 & -4.33692D-01 & -1.09973D-01 & -1.02575D+00 \\
-1.92015D-01 & 4.34746D-02 & -6.27278D-01 & -2.51869D-01 \\
4.05547D-03 & 2.53645D-03 & 1.04117D-03 & 6.12858D-03 \\
7.18834D-04 & 4.72603D-04 & 2.36919D-04 & 3.83549D-01 \\
-1.36925D+03 & 6.57253D+02 & 4.29631D+03 & -1.19953D+04 \\
-5.89514D+03 & 5.55265D+02 & 1.36569D+04 & -1.25264D+05 \\
4.46145D+03 & -3.36275D+03 & 4.63197D+03 & 6.96607D+03
\end{bmatrix}$$

ACT TIFS STABILITY DERIVATIVES

AND ELASTIC INCREMENTS

STATIC STABILITY DERIVATIVES

	RIGID	ELASTIC INCREMENT	TOTAL	UNITS
CL(0)	.326523	-.007018	.319505	
CD(0)	.009236	-.000100	.009135	
CM(0)	.069187	-.006898	.062290	
CL(U)	1.990966	-.006629	1.984337	(1/RAD)
CD(U)	.283147	-.001024	.282124	(1/RAD)
CM(U)	-.958211	-.037439	-.995650	(1/RAD)
CL(ALPHA)	.100592	.000260	.100852	(1/DEG)
CD(ALPHA)	.020053	.000032	.020084	(1/DEG)
CM(ALPHA)	-.031751	-.000523	-.032274	(1/DEG)
CL(Q)	15.387961	-.151795	15.236166	(1/RAD)
CD(Q)	1.348552	-.018733	1.329819	(1/RAD)
CM(Q)	-39.523980	.579412	-38.944568	(1/RAD)
CL(DE)	.014856	-.000770	.014087	(1/DEG)
CD(DE)	.001548	-.000094	.001454	(1/DEG)
CM(DE)	-.057258	.003487	-.053771	(1/DEG)
CL(THRUST)	.000001	-.000000	.000001	(1/NEWTON)
CD(THRUST)	-.000014	-.000000	-.000014	(1/NEWTON)
CM(THRUST)	.000001	.000000	.000001	(1/NEWTON)

TIFS, CASE 1, LANDING

* DYNAMIC STABILITY DERIVATIVES *

	RIGID COMPUTED	RIGID OUTPUT	ELASTIC INCREMENT	TOTAL	UNITS
CL(U)	1.990966	1.940000	.008964	1.948964	(1/RAD)
CD(U)	.283147	.169000	.001116	.170116	(1/RAD)
CM(U)	-.058211	-.115000	-.021790	-.136790	(1/RAD)
CL(ALPHA)	.100592	.094771	.000787	.095558	(1/DEG)
CD(ALPHA)	.020053	.010071	.000099	.010169	(1/DEG)
CM(ALPHA)	-.031751	-.019897	-.001852	-.021749	(1/DEG)
CL(Q)	15.387961	.185000	.323030	.508030	(1/RAD)
CD(Q)	1.348552	.022800	.039954	.062754	(1/RAD)
CM(Q)	-39.523980	-44.100000	-1.252093	-45.352093	(1/RAD)
CY(BETA)	.000000	.000000	.000000	.000000	(1/DEG)
CL(BETA)	.000000	.000000	.000000	.000000	(1/DEG)
CN(BETA)	.000000	.000000	.000000	.000000	(1/DEG)
CY(P)	.000000	.000000	.000000	.000000	(1/RAD)
CL(P)	.000000	.000000	.000000	.000000	(1/RAD)
CN(P)	.000000	.000000	.000000	.000000	(1/RAD)
CY(R)	.000000	.000000	.000000	.000000	(1/RAD)
CL(R)	.000000	.000000	.000000	.000000	(1/RAD)
CN(R)	.000000	.000000	.000000	.000000	(1/RAD)
CL(A-DOT)	-2.734997	.000000	.026678	.026678	(1/RAD)
CD(A-DOT)	-.403823	.000000	.003868	.003868	(1/RAD)
CM(A-DOT)	-14.040751	-16.100000	-.260362	-16.360362	(1/RAD)
CL(Q-DOT)	-17.115815	.000000	-.368164	-.368164	(1/RAD)
CD(Q-DOT)	-2.337752	.000000	-.045969	-.045969	(1/RAD)
CM(Q-DOT)	-21.069772	.000000	1.199494	1.199494	(1/RAD)
CY(R-DOT)	.000000	.000000	.000000	.000000	(1/RAD)
CL(R-DOT)	.000000	.000000	.000000	.000000	(1/RAD)
CN(R-DOT)	.000000	.000000	.000000	.000000	(1/RAD)
CY(P-DOT)	.000000	.000000	.000000	.000000	(1/RAD)
CL(P-DOT)	.000000	.000000	.000000	.000000	(1/RAD)
CN(P-DOT)	.000000	.000000	.000000	.000000	(1/RAD)
CY(R-DOT)	.000000	.000000	.000000	.000000	(1/RAD)
CL(R-DOT)	.000000	.000000	.000000	.000000	(1/RAD)
CN(R-DOT)	.000000	.000000	.000000	.000000	(1/RAD)

TIFS, CASE 1, LANDING

****
* ACTIVE CONTROL DERIVATIVES *
****

* SYMMETRICALLY DEFLECTED CONTROLS *

*NAME	RIGID COMPUTED	RIGID OUTPUT	ELASTIC INCREMENT	TOTAL	UNITS
		CONTROL 1 = AILS			
CL(DS)	.012626	.012626	-.000048	.012578	(1/DEG)
CD(DS)	.000755	.000755	-.000006	.000749	(1/DEG)
CM(DS)	-.005329	-.005329	-.000043	-.005372	(1/DEG)
CL(DS-DOT)	-1.669640	-1.669640	-.019954	-1.689594	(1/RAD)
CD(DS-DOT)	-.221047	-.221047	-.002507	-.223554	(1/RAD)
CM(DS-DOT)	1.304015	1.304015	.045146	1.350161	(1/RAD)
		CONTROL 2 = DLF			
CL(DS)	.023604	.010000 *	-.000160	.009840	(1/DEG)
CD(DS)	.001775	.001670 *	-.000021	.001649	(1/DEG)
CM(DS)	-.003323	-.006550 *	.000367	-.006183	(1/DEG)
CL(DS-DOT)	-2.771764	-2.771764	.032642	-2.739121	(1/RAD)
CD(DS-DOT)	-.379529	-.379529	.004012	-.375517	(1/RAD)
CM(DS-DOT)	-.919782	-.919782	-.155576	-1.075358	(1/RAD)
		CONTROL 3 = ELVT			
CL(DS)	.014856	.009240	-.000144	.009096	(1/DEG)
CD(DS)	.001948	-.001900	-.000018	-.001918	(1/DEG)
CM(DS)	-.057258	-.045500	.000557	-.044943	(1/DEG)
CL(DS-DOT)	-1.137668	-1.137668	-.033833	-1.171501	(1/RAD)
CD(DS-DOT)	-.150253	-.150253	-.004204	-.154457	(1/RAD)
CM(DS-DOT)	2.078389	2.078389	.123741	2.202129	(1/RAD)

*Note: These numbers were obtained from quasistatic derivatives obtained from in-flight parameter identification but were corrected only for the static effects of modes higher than 7. As a result, they are not truly rigid derivatives. The additional required corrections were made for the equations of motion in Table A-4.

TIFS, CASE 2, CLIMB, M = .246

STATIC STABILITY DERIVATIVES

	RIGID	ELASTIC INCREMENT	TOTAL	UNITS
CL(A)	.329428	-.009241	.320187	
CD(A)	.005332	-.000131	.005202	
CM(A)	.070229	-.008920	.061309	
CL(U)	1.554454	-.012745	1.541709	(1/RAD)
CD(U)	.157754	-.001298	.156456	(1/RAD)
CM(U)	-.032534	-.035219	-.067753	(1/RAD)
CL(ALPHA)	.102331	.000345	.102675	(1/DEG)
CD(ALPHA)	.031852	.000027	.031880	(1/DEG)
CM(ALPHA)	-.031854	-.000695	-.032550	(1/DEG)
CL(Q)	15.525168	-.198466	15.326702	(1/RAD)
CD(Q)	.934771	-.016154	.918617	(1/RAD)
CM(Q)	-39.797308	.750716	-39.046592	(1/RAD)
CL(DE)	.014004	-.000106	.013898	(1/DEG)
CD(DE)	.001155	-.000180	.000975	(1/DEG)
CM(DE)	-.057701	.004532	-.053168	(1/DEG)
CL(THRUST)	.000000	-.000000	.000000	(1/NEWTON)
CD(THRUST)	-.000013	-.000000	-.000013	(1/NEWTON)
CM(THRUST)	.000001	.000000	.000001	(1/NEWTON)

TIFS, CASE 2, CLIMB, M = . 248

DYNAMIC STABILITY DERIVATIVES

	RIGID COMPUTED	RIGID OUTPUT	ELASTIC INCREMENT	TOTAL	UNITS
CL(U)	1.554454	1.660000	.006400	1.666400	(1/RAD)
CD(U)	.157754	.102000	.000522	.102522	(1/RAD)
CM(U)	-.332534	-.074100	-.015342	-.089442	(1/RAD)
CL(ALPHA)	.1-233	.093899	.001044	.094943	(1/DEG)
CD(ALPHA)	.014652	.007645	.000087	.007732	(1/DEG)
CM(ALPHA)	-.031854	-.019373	-.002453	-.021826	(1/DEG)
CL(Q)	15.525168	.242000	.430456	.672456	(1/RAD)
CD(Q)	.934771	.019700	.035130	.054830	(1/RAD)
CM(Q)	-39.7973c8	-37.630000	-1.661632	-39.291632	(1/RAD)
CY(BETA)	.000000	.000000	.000000	.000000	(1/DEG)
C1(BETA)	.000000	.000000	.000000	.000000	(1/DEG)
CN(BETA)	.000000	.000000	.000000	.000000	(1/DEG)
CY(P)	.000000	.000000	.000000	.000000	(1/RAD)
C1(P)	.000000	.000000	.000000	.000000	(1/RAD)
CN(P)	.000000	.000000	.000000	.000000	(1/RAD)
CY(R)	.000000	.000000	.000000	.000000	(1/RAD)
C1(R)	.000000	.000000	.000000	.000000	(1/RAD)
CN(R)	.000000	.000000	.000000	.000000	(1/RAD)
CL(A-DOT)	-2.982322	-2.982322	.035639	-2.946684	(1/RAD)
CD(A-DOT)	-.311418	-.311418	.002597	-.308821	(1/RAD)
CM(A-DOT)	-14.29?997	-14.290997	-.348690	-14.639686	(1/RAD)
CL(Q-DOT)	-17.890862	-17.890862	-.499799	-18.390661	(1/RAD)
CD(Q-DOT)	-1.688645	-1.688645	-.041366	-1.730011	(1/RAD)
CM(Q-DOT)	-2 .940744	-2 .940744	1.623837	-19.316907	(1/RAD)
CY(B-DOT)	.000000	.000000	.000000	.000000	(1/RAD)
C1(B-DOT)	.000000	.000000	.000000	.000000	(1/RAD)
CN(B-DOT)	.000000	.000000	.000000	.000000	(1/RAD)
CY(P-DOT)	.000000	.000000	.000000	.000000	(1/RAD)
C1(P-DOT)	.000000	.000000	.000000	.000000	(1/RAD)
CN(P-DOT)	.000000	.000000	.000000	.000000	(1/RAD)
CY(R-DOT)	.000000	.000000	.000000	.000000	(1/RAD)
C1(R-DOT)	.000000	.000000	.000000	.000000	(1/RAD)
CN(R-DOT)	.000000	.000000	.000000	.000000	(1/RAD)

TIFS, CASE 2, CLIMB, M = . 246

ACTIVE CONTROL DERIVATIVES

SYMMETRICALLY DEFLECTED CONTROLS

NAME	RIGID COMPUTED	RIGID OUTPUT	ELASTIC INCREMENT	TOTAL	UNITS
		CONTROL 1 - AILS			
CL(DS)	.012741	.012741	-.000064	.012677	(1/DEG)
CD(DS)	.000561	.000561	-.000006	.000555	(1/DEG)
CM(DS)	-.005359	-.005359	-.000058	-.005416	(1/DEG)
CL(DS-DOT)	-1.725530	-1.725530	-.026906	-1.752435	(1/RAD)
CD(DS-DOT)	-.155731	-.155731	-.002248	-.157980	(1/RAD)
CM(DS-DOT)	1.322656	1.322656	.061802	1.384457	(1/RAD)
		CONTROL 2 - DLF			
CL(DS)	.023831	.018089 *	-.000212	.017877	(1/DEG)
CD(DS)	.001313	.000340 *	-.000019	.000321	(1/DEG)
CM(DS)	-.003354	-.004100 *	.000488	-.003612	(1/DEG)
CL(DS-DOT)	-2.870586	-2.870586	.043818	-2.826769	(1/RAD)
CD(DS-DOT)	-.272614	-.272614	.003541	-.268473	(1/RAD)
CM(DS-DOT)	-.967414	-.967404	-.208374	-1.175778	(1/RAD)
		CONTROL 3 - ELVT			
CL(DS)	.015004	.011660	-.000193	.010807	(1/DEG)
CD(DS)	.001055	.003900	-.000016	.003884	(1/DEG)
CM(DS)	-.057700	-.048000	.000743	-.047257	(1/DEG)
CL(DS-DOT)	-1.183523	-1.183523	-.046057	-1.229580	(1/RAD)
CD(DS-DOT)	-.106416	-.106416	-.003785	-.110201	(1/RAD)
CM(DS-DOT)	2.153215	2.153215	.167894	2.321110	(1/RAD)

*Note: These numbers were obtained from quasistatic derivatives obtained from in-flight parameter identification but were corrected only for the static effects of modes higher than 7. As a result, they are not truly rigid derivatives. The additional required corrections were made for the equations of motion in Table A-4.

TIFS, CASE 3, CRUISE, M = .456

STATIC STABILITY DERIVATIVES

	RIGID	ELASTIC INCREMENT	TOTAL	UNITS
CL(0)	.353030	-.030932	.322098	
CD(0)	.005981	-.000420	.005561	
CM(0)	.078810	-.025598	.053213	
CL(U)	.558372	-.074308	.484065	(1/RAD)
CD(U)	.013286	-.000091	.013195	(1/RAD)
CM(U)	-.002847	-.000736	-.003582	(1/RAD)
CL(ALPHA)	.110246	.001190	.111435	(1/DEG)
CD(ALPHA)	.003137	-.000013	.003124	(1/DEG)
CM(ALPHA)	-.032885	-.002465	-.035350	(1/DEG)
CL(Q)	16.450197	-.609684	15.840513	(1/RAD)
CD(Q)	.010879	.005419	.016298	(1/RAD)
CM(Q)	-42.026620	2.204323	-39.822297	(1/RAD)
CL(DE)	.015891	-.003091	.012800	(1/DEG)
CD(DE)	-.000055	.000033	-.000022	(1/DEG)
CM(DE)	-.061318	.013651	-.047668	(1/DEG)
CL(THRUST)	-.000000	-.000000	-.000000	(1/NEWTON)
CD(THRUST)	-.000001	.000000	-.000001	(1/NEWTON)
CM(THRUST)	.000000	.000000	.000000	(1/NEWTON)

TIFS, CASE 3, CRUISE, M = .456

DYNAMIC STABILITY DERIVATIVES

	RIGID COMPUTED	RIGID OUTPUT	ELASTIC INCREMENT	TOTAL	UNITS
CL(U)	.558372	.598000	-.022986	.575014	(1/RAD)
CD(U)	.013286	.063500	.000132	.063632	(1/RAD)
CM(U)	-.002847	-.042600	.059787	.017187	(1/RAD)
CL(ALPHA)	.110246	.108559	.003654	.112213	(1/DEG)
CD(ALPHA)	.003137	.003805	-.000026	.003778	(1/DEG)
CM(ALPHA)	-.032885	-.013649	-.008750	-.022398	(1/DEG)
CL(Q)	16.450197	.738500	1.565133	2.303633	(1/RAD)
CD(Q)	.010879	-.006080	-.014333	-.020413	(1/RAD)
CM(Q)	-42.026620	-40.400000	-6.035934	-46.435934	(1/RAD)
CY(BETA)	.000000	.000000	.000000	.000000	(1/DEG)
C1(BETA)	.000000	.000000	.000000	.000000	(1/DEG)
CN(BETA)	.000000	.000000	.000000	.000000	(1/DEG)
CY(P)	.000000	.000000	.000000	.000000	(1/RAD)
C1(P)	.000000	.000000	.000000	.000000	(1/RAD)
CN(P)	.000000	.000000	.000000	.000000	(1/RAD)
CY(R)	.000000	.000000	.000000	.000000	(1/RAD)
C1(R)	.000000	.000000	.000000	.000000	(1/RAD)
CN(R)	.000000	.000000	.000000	.000000	(1/RAD)
CL(A-DOT)	-5.070958	.000000	.137929	.137929	(1/RAD)
CD(A-DOT)	-.045024	.000000	-.002513	-.002513	(1/RAD)
CM(A-DOT)	-16.460042	-12.800000	-1.368064	-14.168064	(1/RAD)
CL(Q-DOT)	-23.981556	.000000	-2.086441	-2.086441	(1/RAD)
CD(Q-DOT)	-.081740	.000000	.016880	.016880	(1/RAD)
CM(Q-DOT)	-19.811921	.000000	6.847757	6.847757	(1/RAD)
CY(B-DOT)	.000000	.000000	.000000	.000000	(1/RAD)
C1(B-DOT)	.000000	.000000	.000000	.000000	(1/RAD)
CN(B-DOT)	.000000	.000000	.000000	.000000	(1/RAD)
CY(P-DOT)	.000000	.000000	.000000	.000000	(1/RAD)
C1(P-DOT)	.000000	.000000	.000000	.000000	(1/RAD)
CN(P-DOT)	.000000	.000000	.000000	.000000	(1/RAD)
CY(R-DOT)	.000000	.000000	.000000	.000000	(1/RAD)
C1(R-DOT)	.000000	.000000	.000000	.000000	(1/RAD)
CN(R-DOT)	.000000	.000000	.000000	.000000	(1/RAD)

TIFS, CASE 3, CRUISE, M = .456

****
* *
* ACTIVE CONTROL DERIVATIVES *
* *
****

* SYMMETRICALLY DEFLECTED CONTROLS *

NAME	RIGID COMPUTED	RIGID OUTPUT	ELASTIC INCREMENT	TOTAL	UNITS
		CONTROL 1 - AILS			
CL(DS)	.013731	.013731	-.000218	.013513	(1/DEG)
CD(DS)	.000150	.000150	.000000	.000150	(1/DEG)
CM(DS)	-.005798	-.005798	-.000234	-.006031	(1/DEG)
CL(DS-DOT)	-2.157571	-2.157571	-.106154	-2.263724	(1/RAD)
CD(DS-DOT)	.001071	.001071	.000755	.001825	(1/RAD)
CM(DS-DOT)	1.469189	1.469189	.240093	1.709282	(1/RAD)
		CONTROL 2 - DLF			
CL(DS)	.025615	.016500 *	-.000742	.015758	(1/DEG)
CD(DS)	.000329	.000151 *	.000003	.000154	(1/DEG)
CM(DS)	-.003513	-.005480 *	.001804	-.003676	(1/DEG)
CL(DS-DOT)	-3.643238	-3.643238	.170608	-3.472629	(1/RAD)
CD(DS-DOT)	-.014563	-.014563	-.001727	-.016290	(1/RAD)
CM(DS-DOT)	-1.414440	-1.414440	-.817938	-2.232378	(1/RAD)
		CONTROL 3 - ELVT			
CL(DS)	.015891	.020700	-.000720	.019980	(1/DEG)
CD(DS)	-.000055	.000207	.000006	.000213	(1/DEG)
CM(DS)	-.061318	-.054600	.002781	-.051819	(1/DEG)
CL(DS-DOT)	-1.536890	-1.536890	-.196812	-1.733702	(1/RAD)
CD(DS-DOT)	.001549	.001549	.001706	.003254	(1/RAD)
CM(DS-DOT)	2.804017	2.804017	.721217	3.525235	(1/RAD)

*Note: These numbers were obtained from quasistatic derivatives obtained from in-flight parameter identification but were corrected only for the static effects of modes higher than 7. As a result, they are not truly rigid derivatives. The additional required corrections were made for the equations of motion in Table A-4.

APPENDIX B

ESTIMATION OF TIFS STABILITY AND CONTROL DERIVATIVES FROM FLIGHT DATA

Data for parameter identification purposes was obtained on flights 487 and 488 of the TIFS. While both flights were flown with the general purpose cockpit, flight 487 was flown with the side force surfaces removed. This unusual combination was flown in order to determine whether the side force surfaces have an adverse effect upon the aileron effectiveness. Table B-1 summarizes the flight data conditions.

Two types of inputs were applied. The first was a single controller input (either elevator or DLF) consisting of a series of doublets. The period of the first two doublets was selected to be equal to that of the short period mode (5 seconds) while a third doublet was of shorter duration (2 seconds). The second type input consisted of two elevator doublets followed by two direct lift flap doublets each with doublet periods of 5 seconds. Input time histories are included in the identification results shown later in this appendix.

While advanced estimation techniques have the advantage of using many data points and considering all parameters simultaneously, it is nonetheless useful to verify results obtained with simpler methods. One such method uses the initial response of the vehicle to a step input to determine control effectiveness terms.

Specifically the direct lift flap, elevator and aileron effectiveness can be computed as follows:

$$C_{L_{\delta_3}} = \frac{-C_{L_{trim}} \Delta n_3 - C_{L_\alpha} \Delta \alpha}{\Delta \delta_3}$$

TABLE B-1

FLIGHT CONDITIONS

FLIGHT/ RECORD	INPUT TYPE	INDICATED AIRSPEED km/hr	INDICATED ALTITUDE m	FOWLER FLAP deg	DLF deg	REMARKS	ESTIMATED C.G.,% MAC
CLIMB							
487/8	δ_z	278 - 285	1950	0	-3.5 ± 5		20.7
9	δ_z	278	1950	0	-3.5 ± 10	Exceeded safety trip	20.7
10	δ_z	274 - 285	1920 - 1950	0	-3.5 ± 8		20.7
11	δ_e	271 - 284	1950 - 2010	0	-3.5	δ_e ± 1.25	20.7
12	δ_e, δ_z	267 - 296	1950 - 2030	0	-3.5 ± 8°	δ_e ± 1.25	20.7
LANDING							
487/21	δ_z	245	2070	15	+15 ± 8		20.7
22	δ_z	243 - 246	2010 - 2040	15	15 ± 5		20.7
23	δ_e	235 - 245	2010 - 2040	15	15	δ_e ± 1.25	20.7
CRUISE							
488/6	δ_z	447	2800	0	-3.5 ± 3		22.15
7	δ_e	445 - 462	2790 - 2840	0	-3.5	δ_e ± .65	22.15
8	δ_e, δ_z	445 - 450	2870 - 2840	0	-3.5 ± 3	δ_e ± .65	22.15
AILERON DATA							
487/6	δ_a	278	1980	0	0	Climb	20.7
7	δ_a	278	1980	0	0	Climb	20.7
20	δ_a	278	2070	15	15	Landing	20.7

NOTES: 1) Flight 487 flown with SFS removed.
2) Both flights flown with General Purpose Canopy.

$$C_{m_{\delta_e}} = \frac{I_{yy}}{\bar{q} S c} \frac{1}{\Delta \delta_e} \left[\dot{q} - M'_q q \right]$$

$$C_{\ell_{\delta_a}} = \frac{I_{xz}}{\bar{q} S b} \frac{1}{\Delta \delta_a} \left[\dot{p} - L'_p p \right]$$

where

$C_{L_{trim}}$	=	trim lift coefficient, Table B-2
C_{L_α}	=	lift curve slope = .105/degree
I_{yy}	=	721,286 kg-m^2
I_{xz}	=	290,345 kg-m^2 for aircraft minus side force surfaces
$\bar{q}$	=	dynamic pressure, kg/m^2, Table B-2
S	=	wing area = 85.5 m^2
c	=	mean aerodynamic chord = 2.90 m
b	=	wing span = 32.2 m
M'_q	=	coupled damping in pitch = $K\left[C_{m_q} + C_{m_{\dot{\alpha}}}\right]$, Table B-2
L'_p	=	coupled damping in roll = $K\left[C_{\ell_p} + \frac{I_{xz}}{I_{xx}} C_{n_p}\right]$, Table B-2

The angular acceleration $\dot{q}$ and $\dot{p}$ are determined from the initial slopes of q and p time histories when a rapid step input is applied. The Δn_z is the maximum deflection from trim. The step inputs were electronically generated and filtered through a first order filter with time constant of τ = .1 sec..

The results of these computations are shown in Table B-3 and some important differences exist between the "identified" results and predictions of Reference 19. The flap effectiveness as reported in Reference 19 is derived from static flight testing techniques and exhibits a highly nonlinear behavior (Figure B-1). The nonlinearity is skew symmetric about δ_z = -3.5°.

---

19. Reynolds, P. A., et al.: "Capability of the Total In-Flight Simulator" Calspan Report No. TB-3020-F-4, July 1972. Also AFFDL TR-72-39.

TABLE B-2

CONSTANTS FOR SIMPLIFIED IDENTIFICATION

Records	$C_{l_{trim}}$	$\bar{q}$ (kg/m^2)	M'_q *	L'_p *
LANDING	.980	287.	-1.13	-2.99
CLIMB	.773	370.	-1.35	-3.40
CRUISE	.281	1049.	-2.09	No data

*Data is calculated from nondimensional derivatives of Reference 5.

TABLE B-3

RESULTS OF SIMPLIFIED IDENTIFICATION OF CONTROL EFFECTIVENESS

	$C_{l_{\delta_z}}$		$C_{m_{\delta_e}}$		$C_{l_{\delta_a}}$	
	Identified	Ref. 13	Identified	Ref. 13	Identified	Ref. 13
LANDING ($\delta_z = 15^o \pm 5$)	+.010	+.0086	-.040	-.036	-.043	-.097
CLIMB ($\delta_z = -3.5^o \pm 5$)	+.015	.034	-.041	-.036	-.043	-.097
CRUISE ($\delta_z = -3.5^o \pm 3$)	+.019	+.034	-.041	-.036	~	-.097

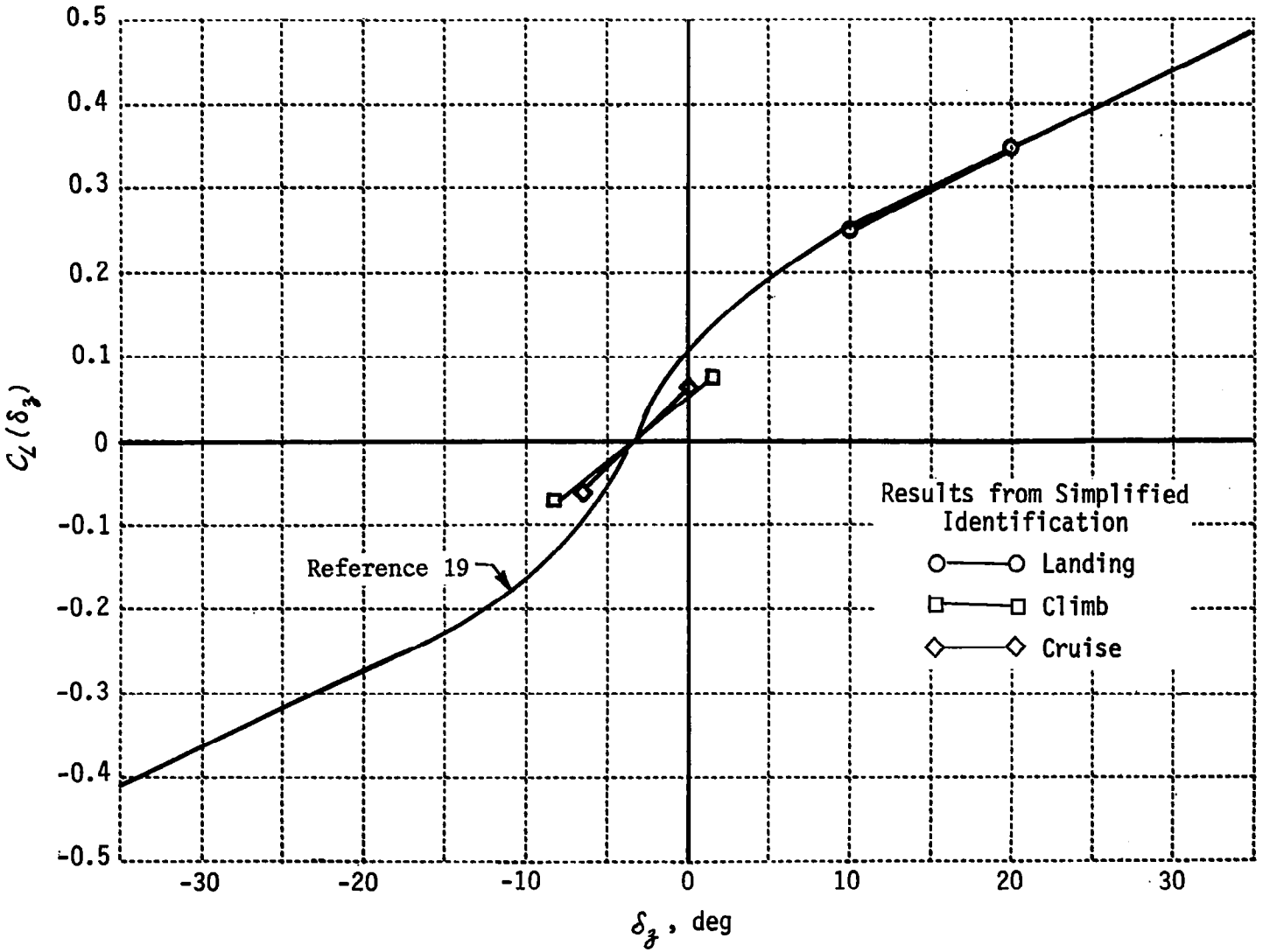

Figure B-1 FLAP EFFECTIVENESS USING SIMPLIFIED IDENTIFICATION

While excellent agreement exists between the "identified" linear flap effectiveness and the nonlinear curve at $\delta_{3_{trim}} = 15^{o}$, this is not the case at $\delta_{3_{trim}} = -3.5^{o}$. The identified linear flap effectiveness was much reduced when compared to the best straight line faired through the nonlinear curve in the region $\delta_3 = -3.5 \pm 5^{o}$. More will be said on this matter.

The elevator effectiveness (Table B-3) is "identified" (-.041) to be 14% larger than that of Reference 9 (-.036). However, the "identified" value agrees well with the Convair predicted elevator effectiveness (-.040) for the CV-340 airplane.

The effectiveness of the aileron as identified (-.043) is only 44% as large as in Reference 5 (-.097). The identified value adds evidence to confirm an earlier parameter identification result using the Calspan BML technique in which the aileron effectiveness was determined to be -.036. These differences have yet to be resolved since the Convair 340 has nearly identical ailerons as the TIFS. The only substantial aerodynamic difference between the CV-340 and the TIFS is the side force surfaces but recall that the side force surfaces were removed for this flight. A third parameter identification result using analog matching has determined the aileron effectiveness to be -.042. While it is not known why the Convair 340 data should differ so substantially from the TIFS, it is clear that the aileron effectiveness is less than half of that predicted for the Convair.

In order to determine both stability and control derivatives of the TIFS, the Calspan Bayesian Maximum Likelihood Identification program (Reference 20) was utilized. This technique is essentially a locally iterated extended Kalman filter. The mathematical model employed is linear in both state and measurement system models and is shown in Tables B-4 and B-5.

---

20. Chen, R.T.N., Eulrich, B. J. and Lebacqz, J. V.: "Development of Advanced Techniques for the Identification of V/STOL Aircraft Stability and Control Parameters", Calspan Report No. BM-2820-F-1, AD-730121, August 1971.

TABLE B-4

MATHEMATICAL MODELS

A. Longitudinal equations of motion

$$\Delta\dot{V} = D_V \Delta V + D_q q + D_\theta \Delta\theta + D_\alpha \Delta\alpha + D_{\delta_e} \Delta\delta_e + D_{\delta_z} \Delta\delta_z + D_o$$

$$\dot{q} = M'_V \Delta V + M'_q q + M'_\theta \Delta\theta + M'_\alpha \Delta\alpha + M'_{\delta_e} \Delta\delta_e + M'_{\delta_z} \Delta\delta_z + M_o'$$

$$\Delta\dot{\theta} = q$$

$$\Delta\dot{\alpha} = Z_V \Delta V + (1 + Z_q) q + Z_\theta \Delta\theta + Z_\alpha \Delta\alpha + Z_{\delta_e} \Delta\delta_e + Z_{\delta_z} \Delta\delta_z + Z_o$$

where $\Delta V = V - V_t$ (m/sec) $\Delta\delta_e = \delta_e - \delta_{e_t}$ (deg)

$\Delta\theta = \theta - \theta_t$ (deg) $\Delta\delta_z = \delta_z - \delta_{z_t}$ (deg)

$\Delta\alpha = \alpha - \alpha_t$ (c - y)

and subscript t implies reference on trim condition.

B. Measurement system model

$$\Delta V_m = \Delta V + V_b \quad \text{(m/sec)}$$

$$q_m = q + q_b \quad \text{(deg/sec)}$$

$$\Delta\theta_m = \Delta\theta + \theta_b \quad \text{(deg)}$$

$$\alpha_{V_m} = \Delta\alpha - \frac{\ell_{xV}}{V_t} q + \alpha_b \quad \text{(deg)}$$

$$n_{x_{cg_m}} = \sin\alpha_t (\Delta\dot{V} - D_\theta \Delta\theta) + \frac{\cos\alpha_t V_r}{57.3} (\Delta\dot{\alpha} - q - Z_\theta \Delta\theta) + n_{x_b} \quad \text{(m/sec}^2\text{)}$$

$$n_{z_{cg_m}} = \cos\alpha_t (\Delta\dot{V} - D_\theta \Delta\theta) - \frac{\sin\alpha_t V_r}{57.3} (\Delta\dot{\alpha} - q - Z_\theta \Delta\theta) + n_{z_b} \quad \text{(m/sec}^2\text{)}$$

$$\dot{q}_m = \dot{q} + \dot{q}_b$$

$$n_{z_{ps_m}} = \sin\alpha_t (\Delta\dot{V} - D_\theta \Delta\theta) - \frac{\sin\alpha_t V_r}{57.3} (\Delta\dot{\alpha} - q - Z_\theta \Delta\theta) + n_{z_b} \quad \text{(m/sec}^2\text{)}$$

TABLE B-5

DEFINITIONS OF LONGITUDINAL PARAMETERS

PARAMETER	UNITS	DEFINITIONS
D_V	$\frac{1}{sec}$	$-\frac{1}{m}\rho V_t S C_{D_t} + \frac{1}{m}\frac{\partial T_x}{\partial V}\cos\alpha_t$
D_α	$\frac{m}{sec^2\text{-}deg}$	$-\frac{1}{m}\frac{\bar{q}}{57.3} S C_{D_\alpha} + \frac{g}{57.3}\cos\gamma_t - \frac{T_x}{57.3m}\sin\alpha_t$
D_θ	$\frac{m}{sec^2\text{-}deg}$	$-\frac{g}{57.3}\cos\gamma_t$
D_{δ_z}	$\frac{m}{sec^2\text{-}deg}$	$-\frac{\bar{q}S}{57.3}\frac{\bar{q}S}{57.3} C_{D_{\delta_z}}$
Z_V	$\frac{deg}{m/sec}$	$57.3\left[-\frac{\rho S}{m} C_{L_t} \frac{\partial T_x}{\partial V}\sin\frac{\alpha_t}{V_t m}\right] \approx -\frac{2(57.3)}{V_t^2} g\cos\alpha_t$
Z_α	$\frac{1}{sec}$	$-\frac{1}{mV_t}\bar{q}S C_{L_\alpha} + \frac{g}{V_t}\sin\gamma_t - \frac{T_x}{mV_t}\cos\alpha_t \approx -\frac{1}{mV_t}\bar{q}S C_{L_\alpha}$
Z_θ	$\frac{1}{sec}$	$-\frac{g}{V_t}\sin\gamma_t$
Z_{δ_e}	$\frac{1}{sec}$	$-\frac{1}{mV_t}\bar{q}S C_{L_{\delta_e}}$
Z_{δ_z}	$\frac{1}{sec}$	$-\frac{1}{mV_t}\bar{q}S C_{L_{\delta_z}}$
M'_V	$\frac{deg}{sec\text{-}m}$	$M_V + M_{\dot\alpha} Z_V = 57.3\frac{\bar{q}SC}{I_{yy}}\left(\frac{2}{V_t} C_{m_t} + \frac{dC_m}{\partial V}\right) + \frac{gT}{I_{yy}}\frac{\partial T}{\partial V}\ 57.3 + M_{\dot\alpha} Z_V$
M'_q	$\frac{1}{sec}$	$M_q + M_{\dot\alpha} = \frac{\bar{q}SC}{I_{yy}}\frac{C}{2V_t}\left(C_{mq} + C_{m_{\dot\alpha}}\right)$
M'_α	$\frac{1}{sec^2}$	$M_\alpha + M_{\dot\alpha} Z_\alpha = \frac{\bar{q}SC}{I_{yy}}\left[C_{m_\alpha} - \frac{SCP}{4m} C_{m_{\dot\alpha}} C_{L_\alpha}\right]$
M'_θ	$\frac{1}{sec^2}$	$M_{\dot\alpha} Z_\theta$
M'_{δ_e}	$\frac{1}{sec^2}$	$M_{\delta_e} + M_{\dot\alpha} Z_{\delta_e} \approx \frac{\bar{q}SC}{I_{yy}} C_{m_{\delta_e}}$
M_{δ_z}	$\frac{1}{sec^2}$	$M_{\delta_z} + M_{\dot\alpha} Z_{\delta_\alpha} = \frac{\bar{q}SC}{I_{yy}}\left[C_{m_{\delta_z}} - \frac{SCP}{4m} C_{m_{\dot\alpha}} C_{L_{\delta_z}}\right]$

Required inputs are variance estimates of the states of the aircraft and unknown parameters as well as the initial values of the states and parameters. For this study the variance estimates were made sufficiently large so as to have no impact upon the final identified results. Initial parameter estimates in all cases were from Reference 19 and are shown in Column 2 of Tables B-6, B-7, and B-8. The root mean square measurement noise on the six measurements used for the identification are shown in Table B-9.

A summary of the BML identification results is shown in Tables B-6, B-7 and B-8 for the three flight conditions in Table B-1. At each flight condition several records were reduced with several resulting estimates of the same dimensional derivatives. These several estimates were combined in a weighted average to form the last column of the above-mentioned tables. The averaging was performed as follows:

$$\tilde{x} = \left[\sum_{i=1}^{n} \frac{x_i}{\sigma_i^2}\right]\left[\sum_{i=1}^{n} \frac{1}{\sigma^2}\right]^{-1}$$

where

$\tilde{x}$ = weighted average assuming the x_i are independent

x_i = the ith estimate of x

σ_i^2 = the variance of the ith estimate

n = number of estimates

$\left[\sum_{i=1}^{n} \frac{1}{\sigma_i^2}\right]^{-1}$ = the variance of the estimate $\tilde{x}$

The combined estimates were then nondimensionalized and presented in Table B-10 (cruise data was converted to a c.g. of 207$\bar{c}$). Table B-11 shows the nondimensional derivatives as predicted for these flight conditions by Reference 19. Direct comparison between these tables is useful. To aid in this comparison, Figure B-2 contains these nondimensional data plotted versus angle of attack.

TABLE B-6

PARAMETER IDENTIFICATION RESULTS
Flight Condition #1, Landing Configuration

V_t = 75 m/sec δ_{s_t} = +15°
H = 2,040 m δ_{F_t} = +15°
W = 23,810 kg
c.g. ≈ 20.7 % MAC
Flight 487
No SFS

$\alpha_t \approx 4.8°$

Parameter Name	Prior Estimate	BML Estimate Rec.21-4	BML RMS (σ) Rec.21-4	BML Estimate Rec.22-4	BML RMS Rec.22-4	BML Estimate Rec.23-2	BML RMS Rec.23-2	Combined BML Estimate
D_V	-.027	-.0337	.00257	+.0405	.00210	+.0116	.000785	+.0114
$D_\alpha (.3048)^{-1}$	.26	.254	.00403	+.152	.00653	+.221	.00204	+.222
$D_{\delta_e} (.3048)^{-1}$	0.	~	~	~	~	+.0532	.00201	+.0532
$D_{\delta_s} (.3048)^{-1}$	-.0244	-.0523	.000393	-.0592	.000623	~	~	-.0543
M'_V (.3048)	-.0114	+.0334	.00261	+.00794	.00244	+.00433	.000707	+.00644
M_q	-1.16	-1.88	.0149	-1.66	.0207	-1.05	.00384	-1.12
M'_α	-.682	-1.14	.00429	-1.20	.00639	-.751	.00274	-.903
M'_{δ_e}	-1.92	~	~	~	~	-2.30	.00447	-2.30
M'_{δ_s}	+.0979	-.157	.000975	-.152	.00135	~	~	-.155
Z_V (.3048)	-.0609	-.0479	.00183	-.0789	.00134	-.0539	.000548	-.0568
Z_α	-.823	-.701	.00286	-.645	.00488	-.763	.00159	-.741
Z_{δ_e}	-.0928	~	~	~	~	-.0642	.00166	-.0642
Z_{δ_s}	-.0663	-.0794	.000307	-.0706	.000485	~	~	-.0769
$\Delta\delta_s$		± 8°		± 5°				

TABLE B-7

PARAMETER INDENTIFICATION RESULTS

Flight Condition #2, Climb
V_t = 85.9 m/sec δ_{3_t} = -3.5°
H = 1,980 m δ_{F_t} = 0°
W = 24,770 kg
C.G. = 20.7% Flight 487, No SFS $\alpha_t \approx 6.4°$

Parameter Name	Prior Estimate	BML Estimate Rec.8-1	BML RMS Rec.8-1	BML Estimate Rec.10-1	BML RMS Rec.10-1	BML Estimate Rec.11-3	BML RMS Rec.11-3	BML Estimate Rec.12-4	BML RMS Rec.12-4	BML Estimate Rec.12-5	BML RMS Rec.12-5	Combined Estimate
D_V	-.0184	+.00189	.000401	-.0747	.000292	-.0665	.000531	-.0266	.000137	~	~	-.0337
D_α (.3048)$^{-1}$	.305	.149	.00348	+.198	.00225	.254	.00181	.277	.00166	~	~	.242
D_{δ_e}(.3048)$^{-1}$	0	~	~	~	~	~	~	-.155	.00236	~	~	-.155
D_{δ_3}(.3048)$^{-1}$	-.0819	-.0257	.000645	-.0256	.000405	~	~	+.00314	.000393	~	~	-.0132
M'_V (.3048)	-.00448	+.0396	.000734	-.00655	.000418	-.0275	.000619	-.0349	.000196	+.0452	.00144	-.0251
M'_q	-1.32	-1.18	.00803	-.609	.00491	-1.33	.00367	-1.07	.00296	-1.14	.00668	-1.08
$M'_{\dot\alpha}$	-1.29	-1.15	.00256	-1.17	.00189	-1.10	.00249	-1.27	.00152	-1.21	.00424	-1.20
M'_{δ_e}	-2.48	~	~	~	~	-3.22	.00464	-2.92	.00424	-2.94	.00864	-3.04
M'_{δ_3}	-.00765	-.238	.000983	-.163	.000615	~	~	-.228	.000328	~	~	-.216
Z_V (.3048)	-.0475	-.0772	.000400	-.0755	.000253	-.0376	.000487	-.0646	.000145	-.0453	.00135	-.0663
Z_α	-.897	-.842	.00239	-.834	.00160	-.811	.00139	-.761	.00114	-.858	.00298	-.799
Z_{δ_e}	-.102	~	~	~	~	-.0859	.00168	-.0748	.00183	-.139	.00326	-.0882
Z_{δ_3}	-.288	-.177	.000502	-.147	.000312	~	~	-.138	.000267	~	~	-.147
$\Delta\delta_3$		± 5°		± 8°				± 8°		± 8°		

TABLE B-8

PARAMETER IDENTIFICATION RESULTS

Flight Condition #3, High Speed, Cruise
V_t = 146 m/sec δ_z = -3.9° ± 3°
H = 2,820 m δ_{F_t} = 0°
W = 24,040 kg Flight 488
C.G.= 22.15% SFS Installed $\alpha_t \approx 1.1°$

Parameter Name	Prior Estimate	BML Estimate Rec.6-1	BML RMS (σ) Rec.6-1	BML Estimate Rec. 7-1	BML RMS Rec.7-1	BML Estimate Rec.8-1*	BML RMS Rec.8-1*	BML Estimate Rec.8-2*	BML RMS Rec.8-2*	Combined BML Estimate
D_V	-.0220	-.0242	.000770	-.0330	.000684	-.0292	.000237	-.0577	.00134	-.0299
$D_\alpha(.3048)^{-1}$	+.303	.132	.00583	+.128	.00355	+.130	.00344	+.144	.00409	.133
$D_{\delta e}(.3048)^{-1}$	0	~	~	-.0246	.00464	-.00621	.00567	-.0560	.00620	-.0270
$D_{\delta_z}(.3048)^{-1}$	-.0831	-.0189	.00122	~	~	-.0161	.00105	~	~	-.0173
$M'_V(.3048)$	-.0155	+.0869	.00191	+.00709	.00103	+.0197	.000654	+.0286	.00191	+.0220
M'_q	-2.02	-2.00	.0123	-1.73	.00850	-1.59	.00764	-1.77	.0118	-1.72
M'_α	-1.43	-2.53	.00669	-2.27	.00611	-2.36	.00454	-2.24	.00716	-2.35
$M'_{\delta e}$	-6.28	~	~	-7.61	.0185	-7.44	.0182	-7.77	.0267	-7.57
M'_{δ_z}	+.336	-.693	.00288	~	~	-.573	.00131	~	~	-.594
$Z_V(.3048)$	-.0172	-.0219	.000898	-.0276	.000699	-.0134	.000443	-.0156	.00122	-.0179
Z_α	-1.41	-1.32	.00367	-1.52	.00268	-1.52	.00246	-1.53	.00309	-1.49
$Z_{\delta e}$	-.160	~	~	-.251	.00337	-.213	.00395	-.242	.00425	-.237
Z_{δ_z}	-.453	-.199	.000697	~	~	-.224	.000711	~	~	-.211

*Record 8-1 contains 39.5 seconds of data and δ_e and δ_z inputs. Record 8-2 contains only the first 20.1 seconds of the Record 8-1 data and only δ_e inputs.

TABLE B-9

ROOT MEAN SQUARE MEASUREMENT ERROR

Measurement	RMS
ΔV	.037 m/sec
q	.02 deg/sec
$\Delta\theta$	.02 deg
$\Delta\alpha_{cg}$	.03 deg
$n_{z_{cg}}$	.049 m/sec^2
$n_{x_{cg}}$	.012 m/sec^2

TABLE B-10

TIFS NONDIMENSIONAL DERIVATIVE SUMMARY –
IDENTIFIED USING BML TECHNIQUE

c.g. = .207$\bar{c}$

	LANDING	CLIMB	CRUISE*
C_{D_α} /deg	.0101	.00770	.00378
$C_{D_{\delta_e}}$ /deg	-.00160	.00377	.000239
$C_{D_{\delta_\gamma}}$ /deg	.00164	.000321	.000153
C_{m_q} /rad**	-43.4	-36.7	-37.7
C_{m_α} /deg	-.0204	-.0201	-.0176
$C_{m_{\delta_e}}$ /deg	-.0418	-.0428	-.0406
$C_{m_{\delta_\gamma}}$ /deg	-.00279	-.00362	-.00387
$C_{m_{\dot{\alpha}}}$ /rad**	-16.4	-13.9	-14.2
C_{L_α} /deg	.0950	.0941	.110
$C_{L_{\delta_e}}$ /deg	.00844	.0100	.0175
$C_{L_{\delta_\gamma}}$ /deg	.00982	.0173	.0156
α deg	4.79	6.36	1.07

* Note the c.g. has been changed from .2215$\bar{c}$ to .207$\bar{c}$.

** Separation of $C_{m_{\dot{\alpha}}}$ and C_{m_q} is based on a ratio of $\frac{45}{17}$ between them.

TABLE B-11

TIFS NONDIMENSIONAL DERIVATIVE SUMMARY

Source: Reference 5

c.g. = .207$\bar{c}$

	LANDING***	CLIMB	CRUISE*
C_{D_α} /deg	.00899	.00614	.00239
$C_{D_{\delta_e}}$ /deg	0	0	0
$C_{D_{\delta_\gamma}}$ /deg	.000735	.00199	.000773
C_{m_q} /rad	-45.	-45.	-45.
C_{m_α} /deg	-.0170	-.0225	-.0137
$C_{m_{\delta_e}}$ /deg	-.0357	-.0357	-.0358
$C_{m_{\delta_\gamma}}$ /deg	+.00138	-.00157	-.000023**
$C_{m_{\dot{\alpha}}}$ /rad	-17.	-17.	-17.
C_{L_α} /deg	.105	.105	.105
$C_{L_{\delta_e}}$ /deg	.0120	.012	.012
$C_{L_{\delta_\gamma}}$ /deg	.00859	.034	.034
α deg	4.09	6.01	1.47

* Note c.g. has been changed from .2215$\bar{c}$ to .207$\bar{c}$.

** The effect of changing c.g. position was large enough to change the sign of this parameter.

*** This flight condition differs from the others in that both Fowler and Direct Lift Flaps are deflected. Derivatives which are not functions of δ_γ and δ_F are C_{L_α}, $C_{L_{\delta_e}}$, C_{m_q}, $C_{m_{\dot{\alpha}}}$, $C_{m_{\delta_e}}$.

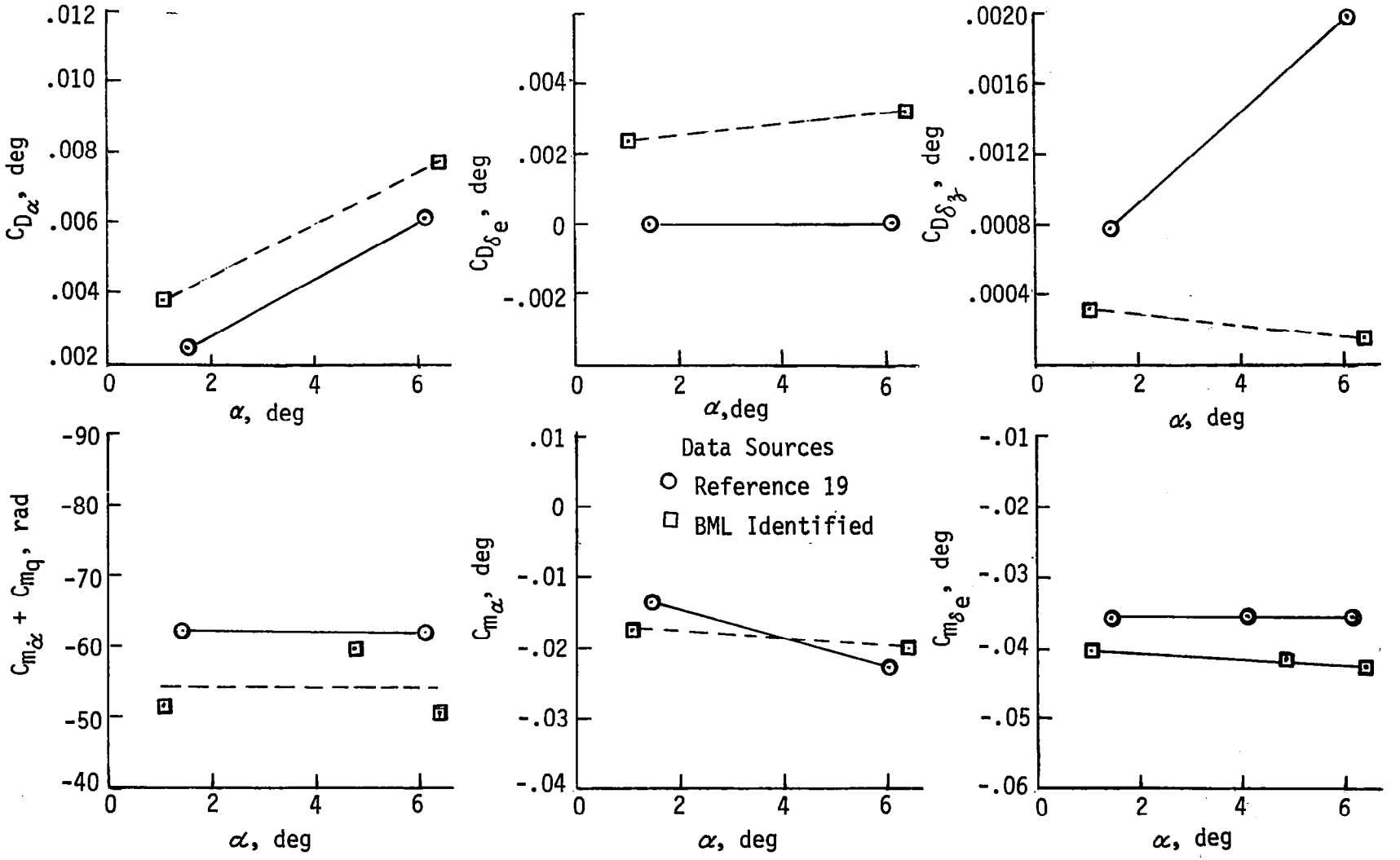

Figure B-2 NONDIMENSIONAL DERIVATIVES VERSUS ANGLE OF ATTACK, c.g. = .207$\bar{c}$

The trends discussed earlier in this appendix for elevator and DLF effectiveness are again confirmed with the BML results. For the DLF, this is shown clearly by comparison of Figure B-3 with Figure B-1.

It is believed that the BML parameter estimates are more accurate than the estimates derived from Reference 19. As evidence to support this belief, an integration of the equations of motion (Table B-4) using the prior estimates (Reference 19) was performed along with a similar integration using the combined BML estimates (Table B-8). In this computation the known measured time history of the control deflection is used as the forcing function to the equations of motion and the resulting integrated responses are overplotted on the actual measured aircraft response to the same input. Over-plots of this form will be called "final integrations" throughout the remainder of this section.

Results for Flight 488, Record 8 (cruise configuration) are shown in Figure B-4a, b, c. Figure B-4a shows the measured input sequence, elevator doublets first followed by DLF doublets. Figure B-4b shows the results for the prior estimates and B-4c for the BML combined estimates. The superiority of the combined BML estimates is readily apparent. Other examples of other records and flight conditions would show similar results.

In the course of the identification process, it was observed at the landing and climb configurations that the mathematical model being used in the identification process was less capable of accurately matching then measured responses when the DLF was the forcing function as compared to the elevator forcing function. This can be seen by comparing Figures B-5 and B-6. Figure B-5 shows for an elevator input the final integration from Record 23-2 (the -2 denotes second attempt at identification of this record). Excellent time history matches are observed. However, the matches for the DLF input at the same flight condition are substantially poorer, Figure B-6.

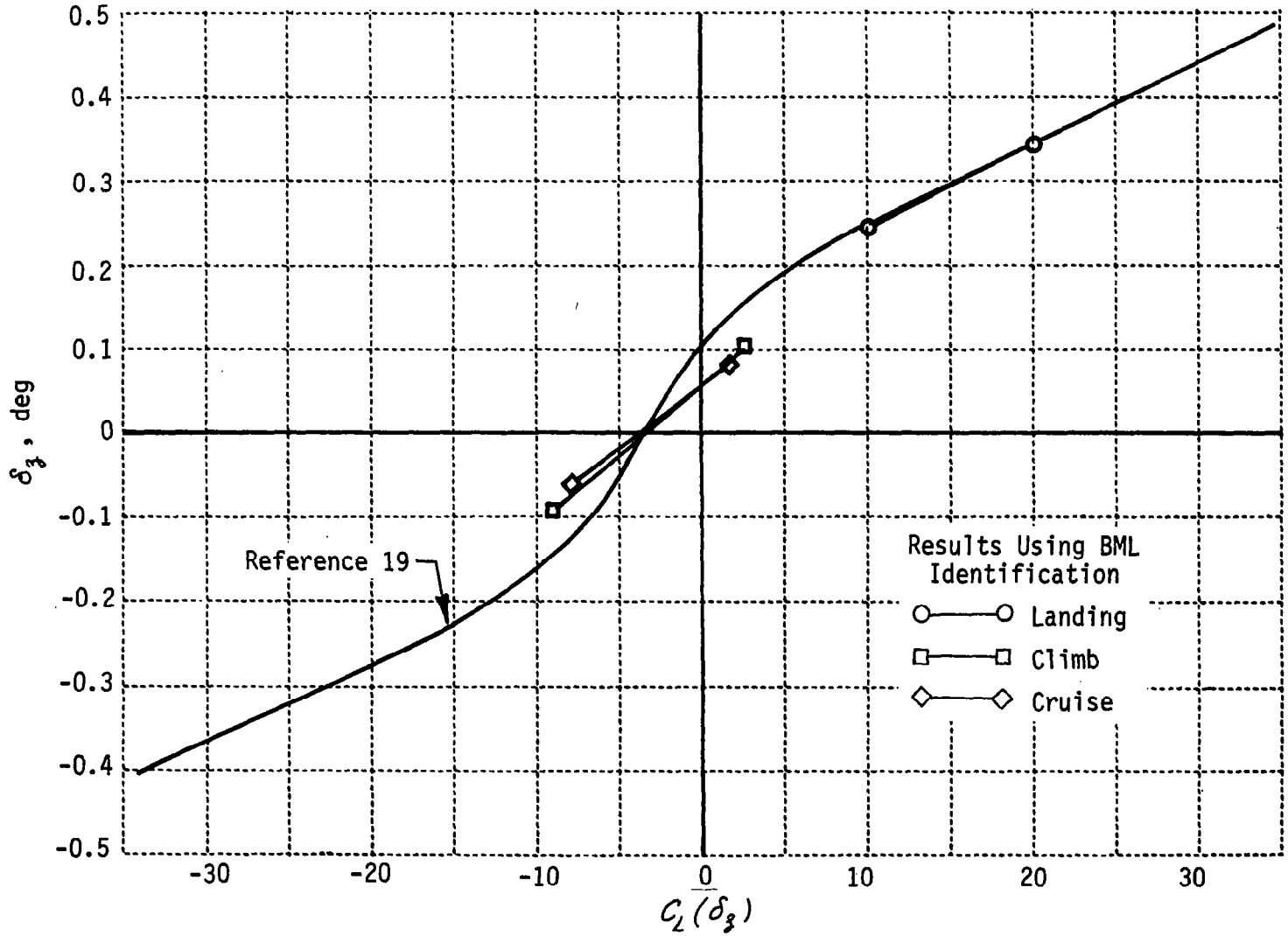

Figure B-3 FLAP EFFECTIVENESS USING BML IDENTIFICATION

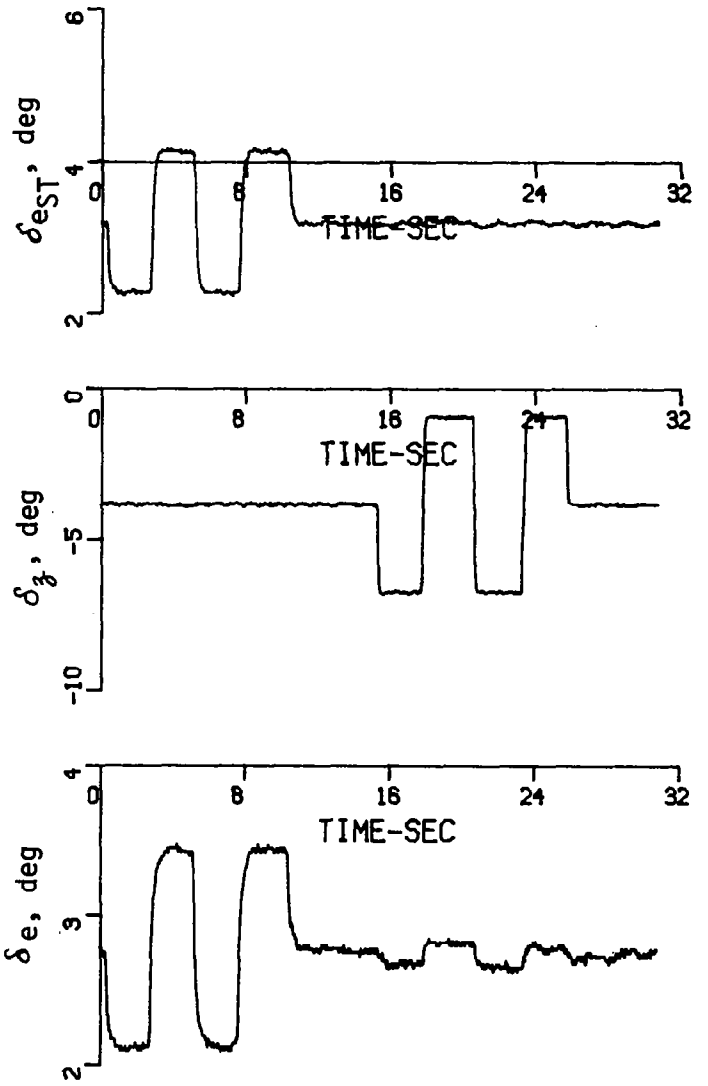

Figure B-4 FINAL INTEGRATION USING VARIOUS ESTIMATES, FLIGHT 488, RECORD 8
a) Input Sequence

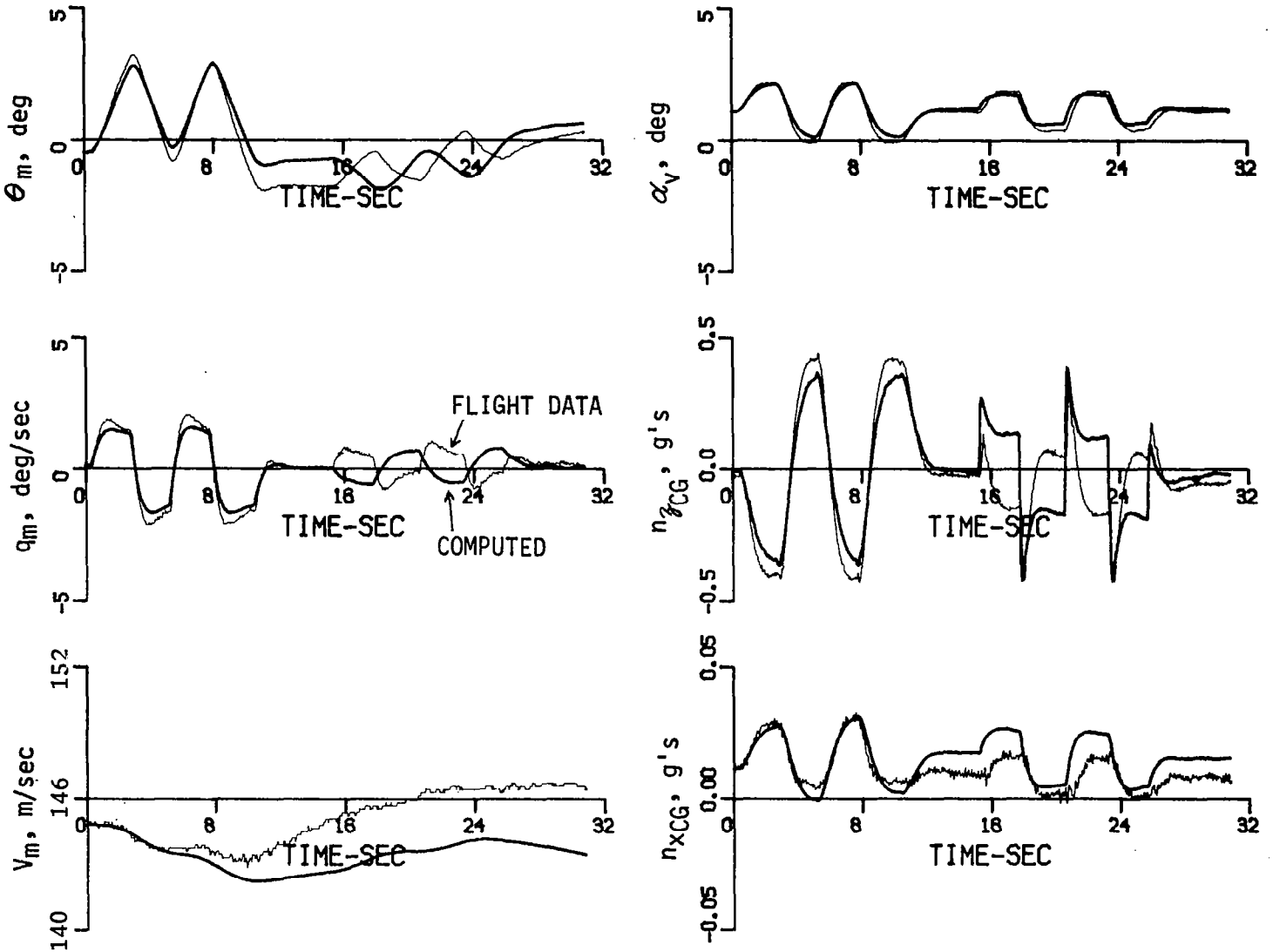

Figure B-4 FINAL INTEGRATION USING VARIOUS ESTIMATES, FLIGHT 488, RECORD 8
b) Using Stability and Control Derivatives from Reference 19.

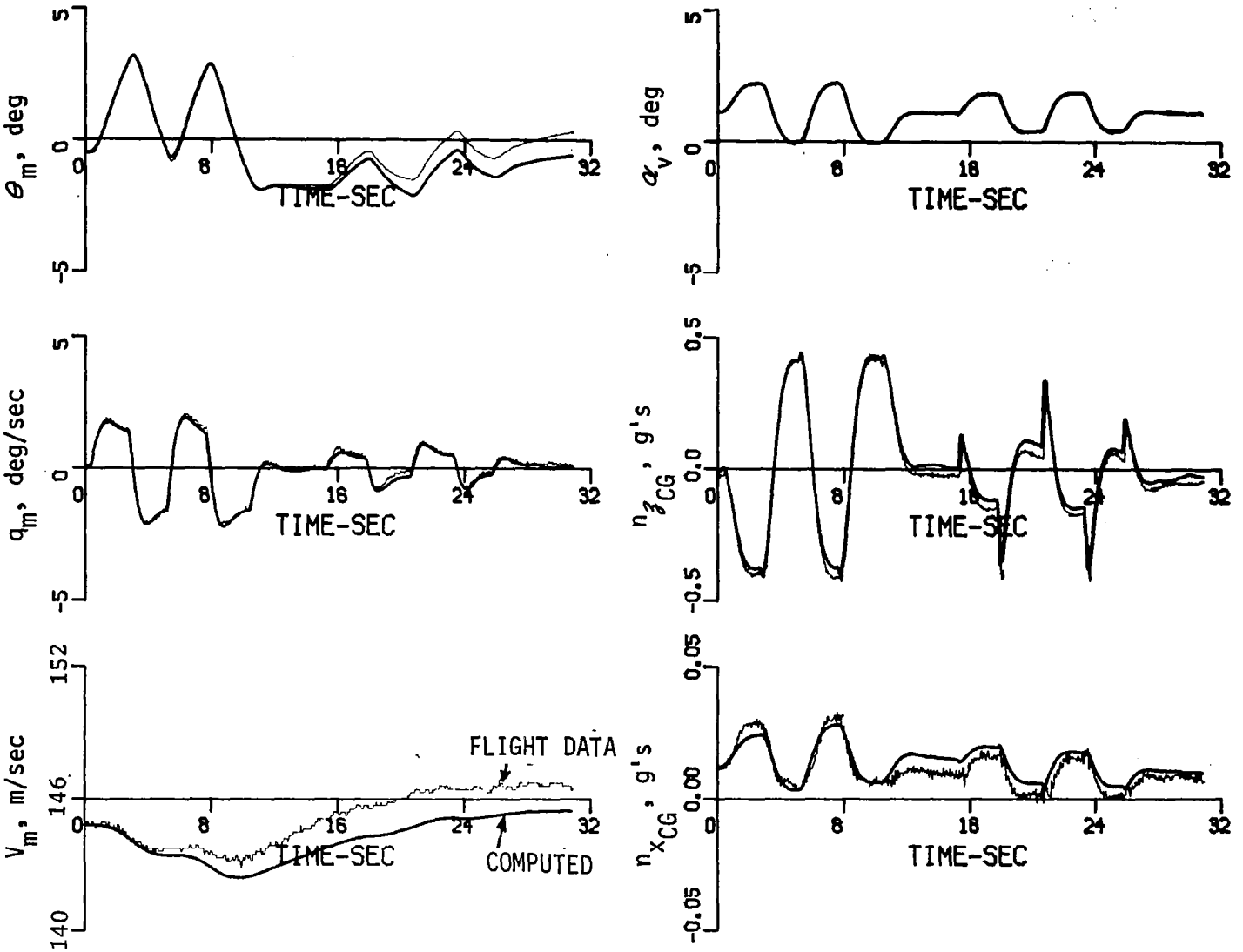

Figure B-4 FINAL INTEGRATION USING VARIOUS ESTIMATES, FLIGHT 488, RECORD 8
c) Using Identified Stability and Control Derivatives
(BML Combined Estimate, Cruise Configuration, Table B-8)

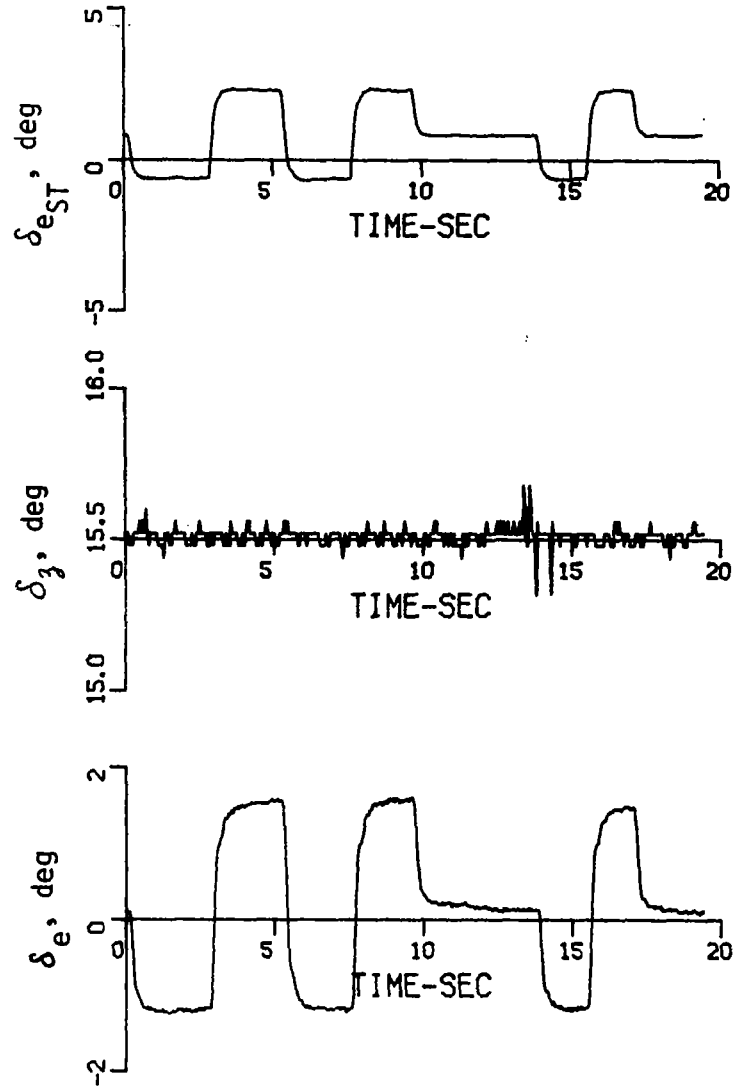

Figure B-5 FINAL INTEGRATION, LANDING CONFIGURATION, RECORD 23-2, ELEVATOR INPUT
a) Input Sequence

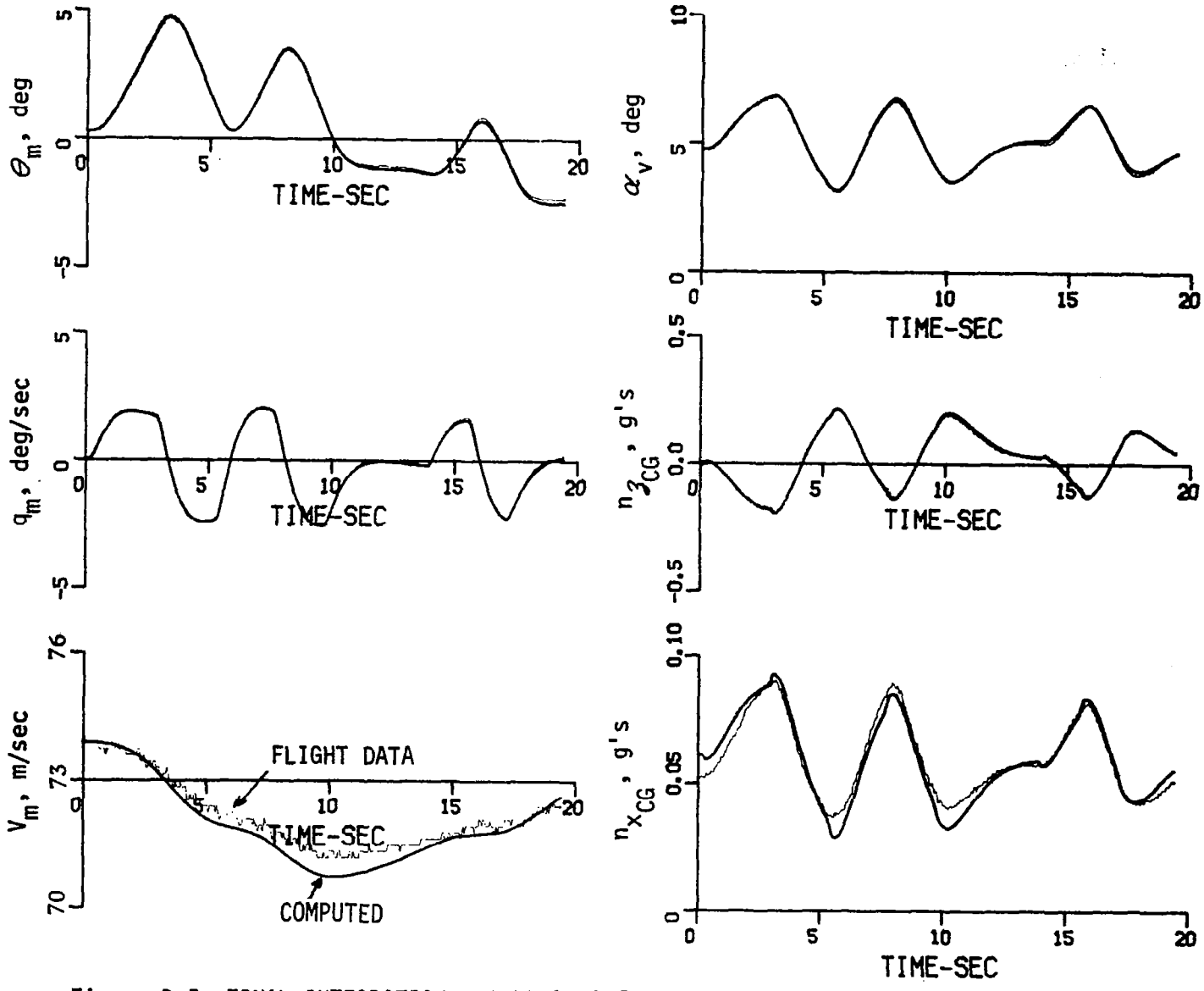

Figure B-5 FINAL INTEGRATION, LANDING CONFIGURATION, RECORD 23-2, ELEVATOR INPUT
b) Measurement Time Histories, Computed Using BML Identified Derivatives vs. Measured

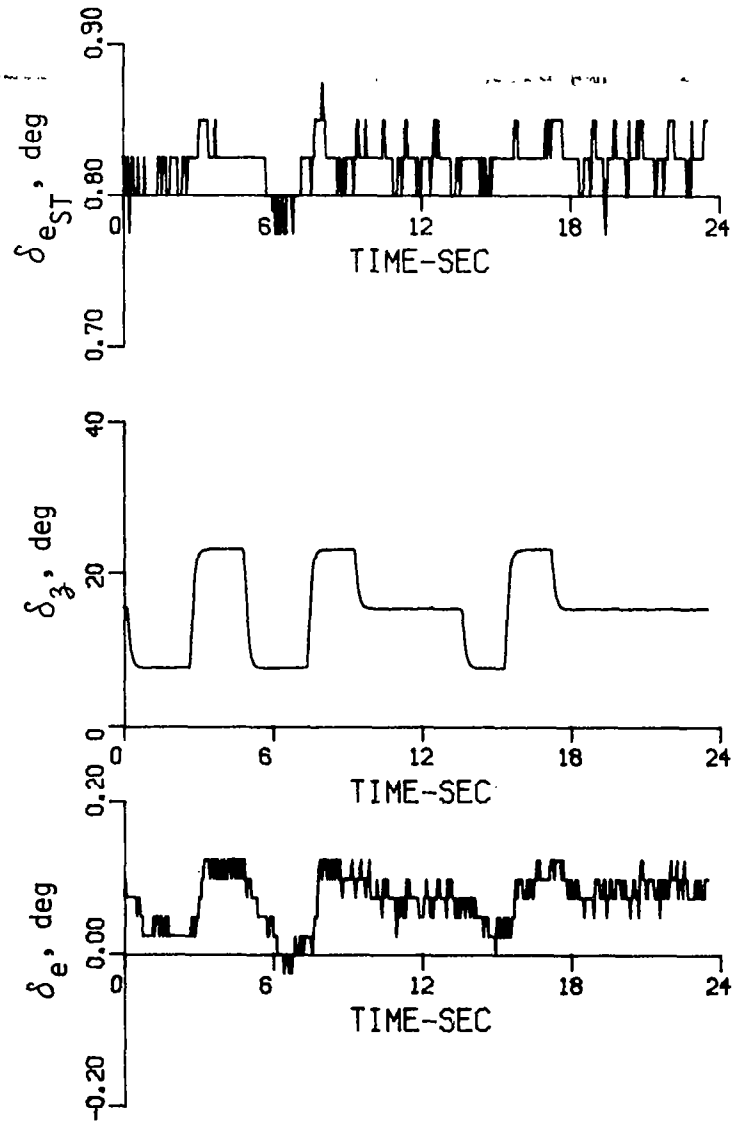

Figure B-6 FINAL INTEGRATION, LANDING CONFIGURATION, RECORD 21-4, DLF INPUT
a) Input Sequence

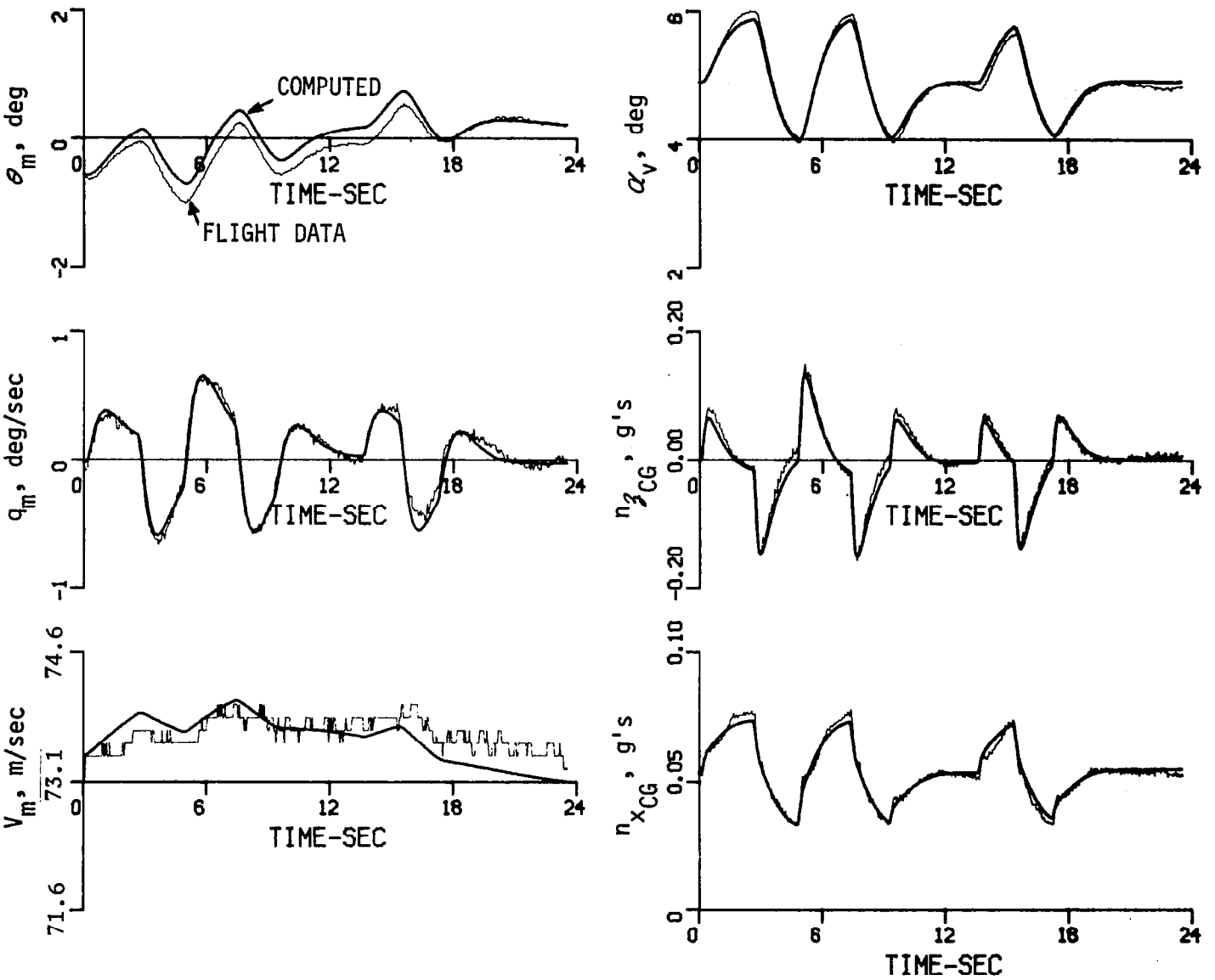

Figure B-6 FINAL INTEGRATION, LANDING CONFIGURATION, RECORD 21-4, DLF INPUT
b) Measurement Time Histories, Computed Using BML Identified Derivatives vs. Derivatives vs. Measured

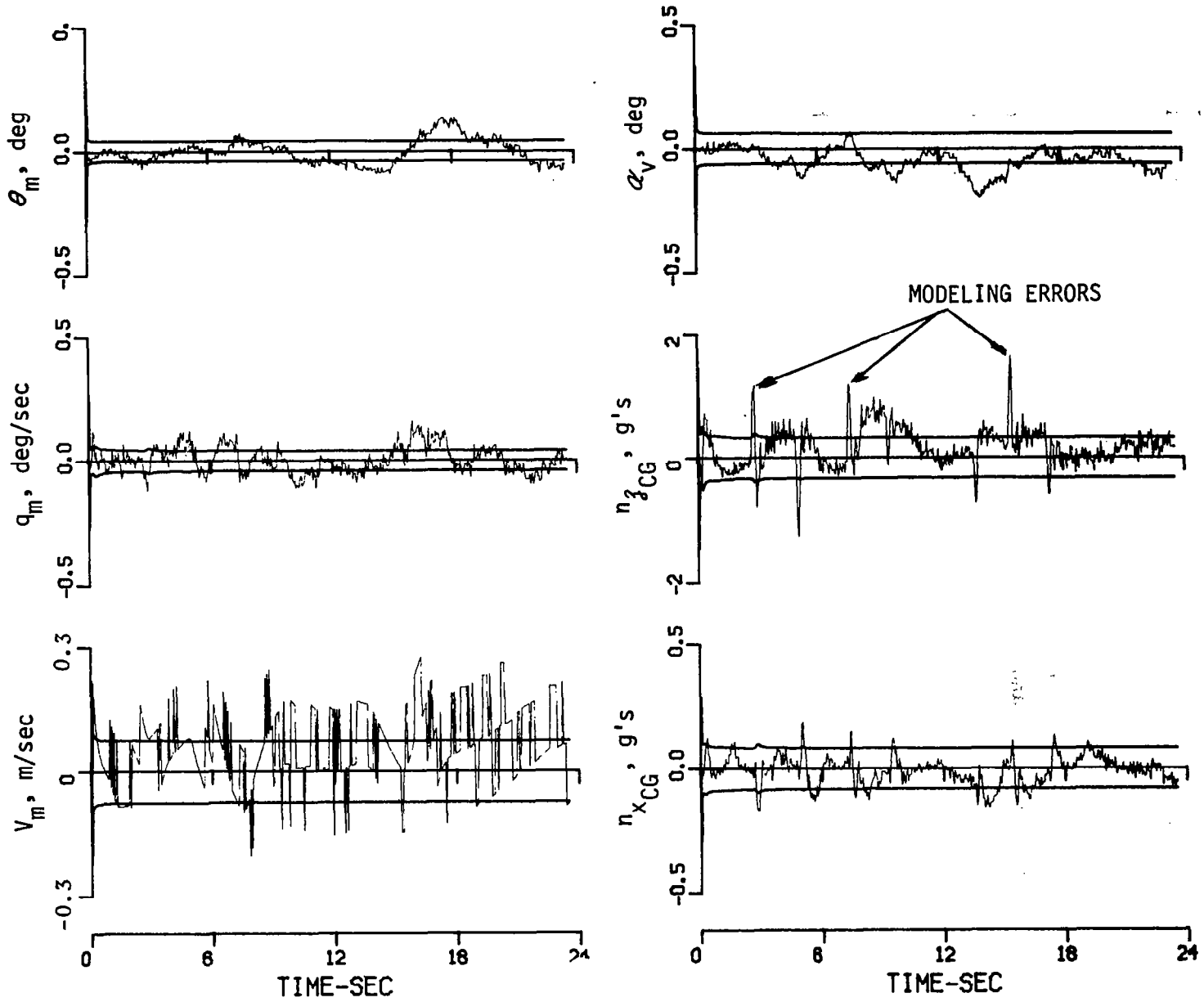

Figure B-6 FINAL INTEGRATION, LANDING CONFIGURATION, RECORD 21-4, DLF INPUT
c) Residuals of Kalman Filter

Several explanations for this are possible. As has been shown earlier, the DLF has a nonlinear control effectiveness and this fact may be the cause of the discrepancies observed in Figure B-6. Confirmation of this effect can be seen in the residuals of the Kalman filter. The residuals are a time history of the difference between the measured data (e.g., $n_{z_{cg}}$) and the filtered conditional estimate of that measurement. The residuals should appear gaussian white and zero mean and deviations from this appearance are an indication of one of many possible forms of modeling errors. In Figure 6c, the residuals are included to show the jumps in the $n_{z_{cg}}$ residual at each change in DLF position. This is a clear indication that the DLF effectiveness is a function of DLF deflection. Although it was possible to have identified the nonlinearity directly, this was not attempted because the length of time the DLF was other than zero plus or minus a constant was very small.

Another possible explanation is that the downwash field leaving the DLF takes a finite time to reach the tail where it will then introduce a delayed pitching moment into the aircraft. This type of phenomenon is clearly not adequately modeled. Since the time delay would be less at the high speed cruise configuration, better modeling at cruise configuration (as observed) would result.

Appendix C

COMPARISON OF COMPUTED AND MEASURED STRUCTURAL MODE FREQUENCIES AND RESPONSES OF THE TIFS AIRPLANE

Experimental and analytical approaches have been combined in the development of a dynamic model of the TIFS airplane for use in active control design as described in Section III of the main body of the report.

The analytical approach has involved defining the basic geometric, mass, and stiffness properties of TIFS for use in preparing inputs for the FLEXSTAB computer program (Reference 9). FLEXSTAB was then used to compute normal vibration modes, equations of motion, and frequency responses of the TIFS airplane to control and turbulence inputs. Some experimental results were incorporated in the computer inputs although the FLEXSTAB solutions are considered an analytical result. The computed stiffness parameters were modified slightly on the basis of frequencies measured in ground vibration tests and quasi-static rigid body derivatives identified from flight data were used as direct inputs to the computer program.

The experimental method for determining an aeroelastic model of TIFS started with frequency response data measured in flight using sinusoidal control inputs. The response of TIFS to turbulence was also measured. Section III describes how transfer functions were derived from the flight data and how these transfer functions were used in obtaining equations of motion.

An exact agreement should not be expected between the FLEXSTAB and flight test results because of simplifications used in formulating the structural model and use of the FLEXSTAB aerodynamic analysis beyond its strict range of applicability. Therefore equations of motion developed for TIFS have been based on flight test data in so far as possible. Some comments are included concerning possible explanations for differences between theoretical and experimental results but a detailed analysis of these differences has not been undertaken.

C.1 LIMITATIONS OF THE ANALYTICALLY DERIVED DATA

It is recognized that assumptions made in the development of FLEXSTAB restricted the validity of the aerodynamic theory to comparatively low reduced frequencies. Consequently, FLEXSTAB could not be expected to make accurate predictions of the aerodynamic forces associated with responses in the higher frequency modes of TIFS. Also, the Internal Structural Influence Coefficient Program (ISIC) of FLEXSTAB which was used in the analysis placed limitations on the structural modes which could be modeled. In particular, it was not possible to include degrees of freedom to represent motions of the engine sprung mass on its vibration isolators and fore and aft bending motions of the wing although they would be expected to introduce natural frequencies in the frequency range of interest.

Although a reasonably good agreement has been obtained between computed and measured frequencies for the TIFS airplane, only limited mode shape data was available from ground vibration test results. These results showed the computed node lines for the various vibration modes were in general agreement with those found in the vibration tests. However, it would be necessary to make additional response measurements in ground vibration tests to ensure the detailed accuracy of the computed modes. Errors in the modal description of the airplane can lead to errors in the computed effectiveness of the control surfaces in exciting the various structural modes. These errors would not be the same for all vibration modes and could cause distortion of the frequency responses.

C.2 DISCUSSION OF RESULTS

C.2.1 Zero Airspeed Vibration Frequencies

Table A-1 of Appendix A lists structural vibration frequencies of the TIFS airplane measured in ground vibration tests and frequencies computed by the FLEXSTAB Normal Modes Program using basic stiffnesses as originally estimated. In order to obtain a better agreement between measured frequencies

and those computed for the original structural model, frequency computations were also made using corrected or "tweaked" stiffnesses. The original wing torsional stiffnesses were multiplied by a factor of 1.11 while all other original stiffness estimates were multiplied by 1.177. The computed zero airspeed frequencies which were based on the "tweaked" stiffnesses are also presented in Table A-1 and are found to be in close agreement with the ground vibration test results. Measured frequencies were not available for the 6th and 7th modes for comparison with the computed values.

C.2.2 Variation of Structural Frequencies and Damping Ratios with Airspeed

Aerodynamic forces introduce couplings between the zero airspeed modes and result in changes in the natural frequencies and damping ratios of the structural modes with airspeed. The computed variations in these quantities with airspeed and are shown in Tables C-1 and C-2 for structural modes computed using basic stiffnesses and "tweaked" stiffnesses respectively. The basic stiffness results given in Table C-1 were computed by the SD & SS program of FLEXSTAB which does not include the effect of structural damping. Corresponding results for the "tweaked" stiffness case are presented in Table C-2. It is possible to include structural damping in modal computations carried out by the LSA program of FLEXSTAB. A structural damping ratio, ζ_{struct} = .025 (structural damping coefficient $g = 2\zeta_{struct} = .05$) was assumed on the basis of the ground vibration test results and included in modal frequency and damping ratio computations with the LSA program. The results of those computations are included in Table C-2. It was found that structural damping had a negligible effect on the frequencies of the structural modes and increased the damping ratio for each mode by approximately .025, the value of the assumed structural damping ratio.

The computed effect of the aerodynamic forces as presented in Table C-2 indicates both increases and decreases in modal frequencies with airspeed. In particular the frequency of mode 7 (the wing outer panel mode) decreases so rapidly with airspeed that it drops below that of mode 6 (2nd fuselage and horizontal tail bending) at the cruise condition. The computations

TABLE C-1

COMPUTED TIFS STRUCTURAL FREQUENCIES (f_n) AND DAMPING RATIOS (ζ_n) AS A FUNCTION OF AIRSPEED

BASIC STIFFNESSES (Original Estimates)

FLIGHT CONDITION			ZERO AIRSPEED		LANDING		CLIMB		CRUISE	
TRUE AIRSPEED (km/hr)			0		245.2		296.9		539.6	
Sym. Mode No.	Mode Characterization at Zero Airspeed	$\zeta_{(structct)}^{*} = g/2$	f_n (Hz)	ζ_n	f_n (Hz)	ζ_n	f_n (Hz)	ζ_n	f_n (Hz)	ζ_n
1	1st Wing Bending	0	3.02	0	3.21	.1394	3.21	.1489	3.45	.2515
2	1st Wing Torsion	0	4.65	0	4.76	.0348	4.77	.0374	4.88	.0794
3	Fus. & H. T. Bending (approximately in-phase)	0	6.09	0	6.29	.0143	6.28	.0156	6.17	.0159
4	Fus. & H. T. Bending (approx. 180° out-of-phase)	0	6.90	0	6.89	.118	6.96	.1258	7.72	.212
5	2nd Wing Bending	0	9.01	0	8.99	.0322	9.00	.0345	9.08	.0599
6	2nd Fus. & H. T. Bending	0	15.10	0	15.02	.0045	15.03	.0050	15.09≠	.0096
7	Wing Outer Panel Mode	0	17.25	0	16.16	.0424	16.19	.0467	15.37≠	.0918

* Structural damping assumed zero in all computations.

≠ Aerodynamic coupling in the cruise condition caused the order of the frequencies of modes 6 and 7 to be interchanged.

TABLE C-2

COMPUTED TIFS STRUCTURAL FREQUENCIES (f_n) AND DAMPING RATIOS (ζ_n) AS A FUNCTION OF AIRSPEED "TWEAKED" STIFFNESSES

FLIGHT CONDITION			ZERO AIRSPEED		LANDING		CLIMB		CRUISE	
TRUE AIRSPEED (km/hr)			0		245.2		296.9		539.6	
Sym. Mode No.	Mode Characterization at Zero Airspeed	ζ_{struct}* = g/2	f_n (Hz.)	ζ_n	f_n (Hz)	ζ_n	f_n (Hz)	ζ_n	f_n (Hz)	ζ_n
1	1st Wing Bending	0.0	3.28	0	3.47	.128	3.47	.1369	3.69	.229
		0.025				.154		.1626		.255
2	1st Wing Torsion	0.0	5.01	0	5.12	.0305	5.12	.0327	5.24	.0676
		0.025				.0556		.0578		.0925
3	Fus. & H. T. Bending (approximately in-phase)	0.0	6.51	0	6.72	.0156	6.71	.0170	6.60	.0199
		0.025				.041		.0423		.0453
4	Fus. & H. T. Bending (approximately 180° out-of-phase)	0.0	7.45	0	7.44	.1085	7.52	.116	8.30	.1954
		0.025				.1326		.140		.2177
5	2nd Wing Bending	0.0	9.77	0	9.75	.0296	9.76	.0317	9.84	.0547
		0.025				.0545		.0566		.0794
6	2nd Fus. & H. T. Bending	0.0	16.31	0	16.22	.0063	16.23	.0069	16.32‡	.0108
		0.025				.0312		.0312		.0357
7	Wing Outer Panel Mode	0.0	18.33	0	17.11	.0418	17.14	.0461	16.28‡	.0931
		0.025				.0656		.0702		.1179

*Modal frequencies were the same to three significant figures assuming structural damping ratios of ζ_{struct} = 0 and .025.

‡Aerodynamic couplings in the cruise condition caused the order of the frequencies of modes 6 and 7 to be interchanged.

indicate mode 3 (which at zero airspeed is characterized by approximately in-phase bending of the aft fuselage and horizontal tail) to be comparatively lightly damped. An even lower damping ratio was computed for mode 6 (2nd fuselage and horizontal tail bending).

Table C-3 presentes a comparison of computed and measured structural mode frequencies and damping ratios for the landing and cruise conditions. The computed data is that given previously for the case of "tweaked" stiffnesses and an assumed structural damping ratio of $\zeta_{struct} = .025$. The measured data were based on transfer functions giving the best fit to frequency response data measured in flight as described in Appendix D.

The computed and measured frequencies are all found to agree within a few percent at both the landing and cruise conditions. In general, the measured trends of frequency variation with airspeed are as predicted. However, the measured frequency for mode 3 increased in going from the landing to the cruise condition while the computations indicated a decrease in frequency.

The largest discrepancy between measured and computed frequencies is found for mode 2 (1st wing torsion) at the landing condition and may in part be due to simplifications in the structural modeling. The raw frequency response data (e.g. Figure C-13a) indicate that two structural modes are present in the neighborhood of 5 Hz. One of these which has a frequency below 5 Hz has a comparatively small effect on the measured responses. This mode was not identified in Appendix D by the transfer functions giving the best fit to the flight data. A peak in the raw data due to a second mode is seen to occur above 5 Hz and its frequency for the landing condition as obtained from the best fit transfer functions was found to be 5.52 Hz. The identification procedure of Appendix D represented the structural mode transfer functions as 10th order numerator polynomials in s over 10th order denominator polynomials and it is possible the peak below 5 Hz might have also been identified if higher order polynomials had been used. On the other hand a fre-

TABLE C-3

COMPARISON OF COMPUTED AND MEASURED
STRUCTURAL MODE FREQUENCIES AND DAMPING RATIOS

FLIGHT CONDITION		LANDING				CRUISE			
TRUE AIRSPEED (km/hr)		245.2		250 (245 IAS)		539.6		517 (448 IAS)	
Sym. Mode No.	Mode Characterization at Zero Airspeed	Computed*		Measured‡		Computed*		Measured‡	
		f_n (Hz)	ζ_n	f_n (Hz)	ζ_n	f_n (Hz)	ζ_n	f_n (Hz)	ζ_n
1	1st Wing Bending	3.47	.154	3.30	.085	3.69	.255	3.55	.145
2	1st Wing Torsion	5.12	.056	5.52	.046	5.24	.093	5.51	.060
3	Fus. and H. T. Bending (approximately in-phase)	6.72	.041	6.67	.047	6.60	.045	6.88	.062
4	Fus. and H. T. Bending (approximately 180° out-of-phase)	7.44	.133	7.68	.038	8.30	.218	7.89	.060
5	2nd Wing Bending	9.75	.055	9.60	.044	9.84	.079	9.90	.062

* Structural damping ratio, $\zeta_{struct} = .025$, assumed in computing eigenvalues. "Tweaked" stiffnesses used in computations.

‡ Based on denominators of transfer functions giving best fit to frequency response data measured in flight.

quency of 4.9 Hz was measured for the first wing torsional mode in the ground vibration tests and no other symmetric mode in this frequency range was identified.

Data in Table C-3 shows that the modal damping ratios as derived from frequency responses measured in flight are in general lower than those found from the FLEXSTAB computations. Again results for mode 3 are an exception and show the computed damping ratios at the landing and cruise conditions to be respectively 87% and 73% of the measured damping ratios. Variations in the magnitudes of the computed damping ratios for the different modes were greater than for the measured damping ratios.

Changes in frequency and damping ratio with airspeed as indicated by the Table C-3 data include the effects of the aerodynamic couplings between modes as well as the aerodynamic stiffening and damping of each mode individually. Further insight into these total changes can be obtained by considering data in Table C-4 which show the variations in modal frequencies and damping ratios with airspeed as computed with and without aerodynamic coupling between modes.

It can be seen from Table C-3 that the measured damping ratios for mode 1 (1st wing bending) were approximately 55% of the computed values. However, the higher computed damping ratios do not appear to be associated with modal coupling because results in Table 5 show little sensitivity of mode 1 damping ratio to aerodynamic coupling.

The measured damping ratios for the 1st wing torsion mode (mode 2) were 82 and 65% of the computed values for the landing and cruise conditions, respectively. The measured damping ratios for mode 5 (2nd wing bending) were approximately 80% of the computed values and did not seem to be appreciably affected by aerodynamic coupling between modes. However, Table C-4 data suggests that aerodynamic coupling was responsible for the low computed damping ratios for mode 3. On the other hand, aerodynamic coupling is found to give a significant increase in the computed damping ratio for mode 4.

TABLE C-4

COMPARISON OF FREQUENCIES AND DAMPING RATIOS OF STRUCTURAL MODES COMPUTED WITH AND WITHOUT AERODYNAMIC COUPLINGS, CRUISE CONDITION *

Mode No.	Characterization	Aero. Coupling Included		Aero. Coupling Neglected	
		f_n (Hz)	ζ_n	f_n (Hz)	ζ_n
1	1st Wing Bending	3.72	.254	3.56	.241
2	1st Wing Torsion	5.12	.099	5.19	.083
3	Fus. & H.T. Bending	6.70	.041	7.16	.093
4	Fus. & H.T. Bending	8.23	.219	7.90	.169
5	2nd Wing Bending	9.77	.078	9.81	.073

*Based on computer run 2-13-76. "Tweaked" stiffnesses slightly different than used in computing data in Table 3.

C.2.3 Effect of Aerodynamic Coupling on Structural Mode Shapes Computed in Forward Flight

The natural structural mode shapes of the TIFS airplane at zero airspeed were computed by the Normal Modes Program of FLEXSTAB assuming no structural damping. In forward flight these zero airspeed modes are damped and coupled together by aerodynamic forces resulting in a new set of forward flight modes which have complex eigenvalues and eigenfunctions. It is found that the aerodynamic couplings between modes made the mode shapes in forward flight significantly different from the corresponding zero airspeed modes. Table C-5 shows the relative amplitudes of the contributions of the zero airspeed structural modes in the natural strucural modes computed for the cruise condition. These data were based on modal computation outputs from the SD & SS program of FLEXSTAB which included aerodynamic forces but neglected structural damping. (Both aerodynamic and structural damping were included in the modal calculations for TIFS carried out by the LSA program of FLEXSTAB and presented in Appendix A). The contributions of the rigid body modes and the sixth and seventh zero airspeed elastic modes were comparatively small and are not included in Table C-5.

This procedure involves assuming the relative deflections and relative accelerations to be proportional for the response in a particular mode and neglects the effects of the quasi-static responses in structural modes higher than the seventh which are introduced implicitly in the results by the use of the Residual-Elastic Option of FLEXSTAB.

It can be seen from an examination of Table C-5 that motion in the first structural mode at the cruise condition is primarily due to the zero airspeed first wing bending mode (η_1) while motions in the fifth cruise structural mode are primarily due to the zero airspeed second wing bending mode (η_2).

On the other hand wing tip motion in the zero airspeed first wing bending (η_1) and first wing torsion (η_2) modes are of approximately equal importance in the second structural mode at the cruise condition.

TABLE C-5

RELATIVE AMPLITUDES OF CONTRIBUTIONS OF ZERO AIRSPEED MODES TO COMPUTED MOTIONS IN STRUCTURAL MODES AT THE CRUISE CONDITION

Cruise Mode No. (Freq.)	Zero Airspeed Mode		Relative Amplitudes of Motion in Cruise Condition Modes due to Zero Airspeed Struct. Modes*			
	General Coord.	Characterization	Pilot Sta. Accel.	Wing Tip Accel.	Tail Cone Accel.	Stab. Tip Accel.
1	η_1	1st Wing Bend.	13.48 -j 1.62	-108.00 +j12.97	14.08 -j 1.69	22.15 -j 2.66
	η_2	1st Wing Torsion	- .44 +j 4.20	- .98 +j 9.30	- .32 +j 3.04	- .94 +j 8.98
(3.69 Hz)	η_3	Fus. & H.T. Bend.	.04 +j .17	.26 +j 1.21	.08 +j .36	1.30 +j 6.02
	η_4	Fus. & H.T. Bend.	.07 +j .34	.38 +j 1.92	.18 +j .92	- 3.29 -j16.65
	η_5	2nd Wing Bend.	- .05 -j .28	.85 +j 4.67	- .07 -j .40	.28 +j 1.55
	Σ		13.10 +j 2.81	-107.49 +j30.07	13.95 +j 2.23	19.50 -j 2.76
2	η_1	1st Wing Bend.	1.13 -j 2.57	- 9.05 +j20.60	1.18 -j 2.69	1.86 -j 4.22
	η_2	1st Wing Torsion	3.48 +j 9.84	7.72 +j21.81	2.52 +j 7.13	7.45 +j21.05
(5.24 Hz)	η_3	Fus. & H.T. Bend.	.29 -j .39	2.07 -j 2.72	.61 -j .81	10.28 -j13.55
	η_4	Fus. & H.T. Bend.	.12 +j .11	.69 +j .64	.33 +j .31	- 6.02 -j 5.55
	η_5	2nd Wing Bend.	- .15 +j .09	2.54 -j 1.67	- .22 +j .14	.84 -j .56
	Σ		4.87 +j 7.08	3.97 +j38.66	4.42 +j 4.08	14.41 -j 2.83
3	η_1	1st Wing Bend.	+ 1.86 +j 2.48	- 14.93 -j19.86	+ 1.95 +j 2.59	3.06 +j 4.07
	η_2	1st Wing Torsion	- 1.62 -j .85	- 3.58 -j 1.88	- 1.17 -j .61	- 3.46 -j 1.81
(6.6 Hz)	η_3	Fus. & H.T. Bend.	.74 +j 2.45	5.20 +j17.20	1.54 +j 5.10	25.84 +j85.49
	η_4	Fus. & H.T. Bend.	1.05 +j 1.82	5.93 +j10.31	2.85 +j 4.96	-51.41 -j89.45
	η_5	2nd Wing Bend.	- .21 -j .16	3.68 +j 2.90	- .31 -j .25	1.23 +j .97
	Σ		1.82 j 5.74	- 3.70 +j 8.67	4.86 11.79	-24.74 -j .73
4	η_1	1st Wing Bend.	- .31 +j .21	+ 2.50 -j 1.65	- .33 +j .21	- .51 +j .34
	η_2	1st Wing Torsion	.07 +j 1.39	.16 +j 3.07	.05 +j 1.00	.15 +j 2.96
(8.3 Hz)	η_3	Fus. & H.T. Bend.	.13 +j .84	.88 +j 5.91	.26 +j 1.75	4.38 +j29.39
	η_4	Fus. & H.T. Bend.	- .88 -j 1.93	- 4.99 -j10.94	- 2.40 -j 5.26	43.27 +j94.90
	η_5	2nd Wing Bend.	- .08 +j .06	1.27 -j 1.00	- .11 +j .09	.42 -j .33
	Σ		- 1.07 +j .57	- .18 -j 4.61	- 2.53 -j 2.21	47.71 +j127.26
5	η_1	1st Wing Bend.	- 4.18 -j .78	33.51 +j 6.28	- 4.37 -j .82	- 6.87 -j 1.29
	η_2	1st Wing Torsion	5.68 +j 4.09	12.60 +j 9.08	4.12 +j 2.97	12.15 +j 8.76
(9.84 Hz)	η_3	Fus. & H.T. Bend.	1.64 +j 1.19	11.50 +j 8.36	3.42 +j 2.49	57.19 +j 41.58
	η_4	Fus. & H.T. Bend.	- 1.43 -j .99	- 8.11 -j 5.62	- 3.90 -j 2.70	70.31 +j 48.75
	η_5	2nd Wing Bend.	-20.76 +j13.33	353.84 -j227.22	-30.09 +j19.32	117.90 -j 75.71
	Σ		-19.05 +j16.84	403.34 -j209.12	-30.82 +j21.26	250.68 +j 22.09

*Relative amplitudes have not been normalized and the comparatively small contributions of the rigid body modes and modes η_6 and η_7 have not been indicated.

The effect of the aerodynamic coupling of the zero airspeed modes is particularly evident in the case of the third cruise condition structural mode. It is found that the fourth zero airspeed mode (η_4) contributes more than the third zero airspeed mode (η_3) to motion of the stabilizer tip in the third structural mode at the cruise condition. Furthermore, it can be seen that the third zero airspeed mode (η_3) has a significant effect on the computed motion in the fourth structural mode at the cruise condition.

C.2.4 Frequency Responses with DLF Excitation

Measured and computed frequency response data obtained with DLF excitation at the cruise condition are presented on Figures C-1 to C-4 while corresponding responses for the landing condition are presented on Figures C-5 to C-8. The measured responses were derived from data obtained in TIFS ACT Flights 488 and 489 and were the basis for modeling of the flexible characteristics of TIFS from flight test data as discussed in Appendix D.

The computed frequency responses were obtained from the LSA program of FLEXSTAB. These responses are based on equations of motion generated by FLEXSTAB which are presented in first order form in Appendix A. Computed stiffness data required as inputs to FLEXSTAB were corrected slightly on the basis of ground vibration test results as discussed previously. Measured rigid body stability derivatives (Appendix B) were input as parameters in the equations of motion used in the frequency response computations. A comparison of actual flight test conditions with corresponding conditions used in the FLEXSTAB computations is given in Table C-6.

Figure C-9 shows the computed modal contributions ($n_{z_{WT}}$) of the first five zero airspeed modes to the frequency response of the wing tip accelerometer at the cruise condition. (The stiffness parameters used in obtaining Figure C-9 were slightly different from those used in computing the responses shown on Figures C-1 to C-8).

TABLE C-6

COMPARISON OF ACTUAL FLIGHT TEST CONDITIONS WITH CONDITIONS USED IN FLEXSTAB COMPUTATIONS

Figure	Nominal Flight Cond.	TIFS/ACT Flight Number	FLEXSTAB Run Date	Control Input	Altitude (m)	Indicated Airspeed (km/hr)
1	Cruise	488	---	δ_3	2,900	448
	"	---	2-3-76	"	3,050	467
2	"	488	---	"	2,900	448
	"	---	2-3-76	"	3,050	467
3	"	488	---	"	2,900	448
	"	---	2-3-76	"	3,050	467
4	"	488	---	"	2,900	448
	"	---	2-3-76	"	3,050	467
5	Landing	489	---	"	460	245
	"	---	2-23-76	"	60	"
6	"	489	---	"	460	"
	"	---	2-23-76	"	60	"
7	"	489	---	"	460	"
	"	---	2-23-76	"	60	"
8	"	489	---	"	460	"
	"	---	2-23-76	"	60	"
9	Cruise	---	2-13-76	"	3,050	467
10	Landing	489	---	δ_e	490	245
	"	---	2-23-76	"	60	"
11	"	489	---	"	490	"
	"	---	2-23-76	"	60	"
12	"	489	---	"	490	"
	"	---	2-23-76	"	60	"
13	"	489	---	"	490	"
	"	---	2-23-76	"	60	"
14	"	489	---	"	490	"
	"	---	2-23-76	"	60	"

The curves on Figure C-9 indicate the presence of couplings between the zero airspeed modes which were used as generalized coordinates in the analysis. This effect was discussed previously with respect to mode shape data in Table C-5. Figure C-9 suggests that the couplings have a comparatively small effect on the computed responses near the natural frequencies for modes 1 and 5 but have a pronounced effect on the frequency responses in the frequency range of modes 2, 3, and 4.

Computations of first wing bending mode (mode 1) responses to DLF excitation at approximately 3.5 Hz far exceed the measured responses at all accelerometer positions. The flight identification of rigid body derivatives (Appendix B) showed the rigid body aerodynamic control forces due to DLF deflection to be less than the theoretical predictions and a similar result might be expected at the comparatively low natural frequency of the first wing bending mode (mode 1). However, there is also a discrepancy between the shapes of the computed and measured amplitude ratio curves near 3.5 HZ. The wing tip accelerometer responses presented on Figures C-2a and C-6a indicate the computed resonance peak to be broader than the measured ones. It does not appear possible to explain this difference on the basis of an incorrect coupling between modes because a comparison of Figure C-2a and Figure C-9 indicates that the computed total response near 3.5 Hz is almost entirely due to the first mode response.

In general the best agreement between computed and measured responses due to DLF excitation is found close to the second wing bending frequency (approximately 9.8 Hz). The Table C-5 data discussed previously indicates the aerodynamic coupling between the zero airspeed modes to have a small effect on the response at most accelerometer locations, but tended to make the stabilizer tip motion somewhat longer. It is found that the greatest discrepancies between computed and measured responses of 9.8 Hz are for stabilizer tip motions suggesting that they might be associated with the modal coupling terms.

Figures C-1a and C-5a show large responses were computed for the pilot station at 5 Hz (the first wing torsional frequency) while the corresponding responses measured in flight are small. Evidently the direct lift flap excites smaller torsional motions of the TIFS wing than predicted theoretically. Several factors which might explain this discrepancy have not yet been explored. As mentioned previously neglect in the analysis of engine vibration isolator deflections and the fore and aft bending motions of the wing might have caused inaccuracies in the computed torsional mode shape which in turn could have led to an overprediction of the generalized forces exciting the first wing torsion mode.

Large discrepancies exist between the computed and flight responses at approximately 6.8 Hz which is near the natural frequency of the third symmetric mode found in forward flight (see Figures C-1a, C-3a, C-5a, and C-7a). It will be remembered that aerodynamic coupling between the zero airspeed modes resulted in a low computed damping ratio for this mode as shown in Table C-4. Also data in Table C-5 computed for the cruise condition indicated that aerodynamic couplings cause all of the first five zero airspeed structural modes to contribute significantly to deflections in mode 3 at the cruise condition. Furthermore, Figure C-9 shows how all zero airspeed modes contribute to the although it has been characterized by in-phase bending of the aft fuselage and stabilizer tip. This wing torsional motion produces large lift forces which in particular tend to produce large response in the first wing bending mode (η_1). It can be seen by referring to Figure C-9 that the computed wing tip acceleration due to first mode response is greater at 6.0 Hz than at the first mode resonance frequency (3.6 Hz).

The computed responses on Figure C-1 to C-8 do not show large resonant responses in the range from 7.4 to 8.3 due to mode 4 response. For example, it is noted on Figure C-9 that there is no peak in the curve for mode 4 near the fourth mode natural frequency of 8.3 Hz. The peak in this mode 4 response which occurs at approximately 6.3 Hz is caused by coupling with mode 3.

The absence of peaks in the computed mode 4 responses near the mode 4 natural frequency similar to those found in the measured data may in part be due to the fact that the computed mode 4 damping ratio was approximately 3.5 times the measured damping ratio.

Most computed and measured phase data obtained with direct lift flap excitation are in general agreement. However, differences are noted in the phase plots for the tail cone (Figures C-3b and C-7b) and for the stabilizer tip (Figures C-4b and C-8b). The computed phase angle lag for the tail cone is larger than measured for frequencies above 4 Hz while the measured phase angle lag for stabilizer tip acceleration is greater than the computed angle in this range.

C.2.5 Frequency Response with Elevator Excitation

Figures C-10 to C-14 present measured and computed frequency responses obtained with elevator excitation for the landing condition. In general, a somewhat better agreement between measured and computed results were obtained with elevator excitation than with direct lift flap excitation.

The computed and measured responses due to elevator excitation are small near the resonance frequency of the first wing bending mode (approximately 3.3 Hz). This would be expected because there is comparatively small motion at the tail in the first bending mode resulting in small generalized forces due to elevator deflections. However, it should be noted that a good agreement exists between the amplitude ratios and phase angles of the tip accelerometer responses shown on Figures C-12a and C-12b in the range from 3 to 3.3 Hz. At higher frequencies the computed response is distorted by the presence of the computed wing torsional mode response.

The flight test data shows that the wing torsional mode (mode 2) could be excited by elevator inputs. The wing torsional mode resonance is most evident in the frequency response of the accelerometer at the pilot's station (Figure C-10a). The measured peak amplitude of this resonance peak at 5.6 Hz. The amplitude ratio for the corresponding computed resonance peak at 5.2 Hz

exceeds the measured amplitude ratio by a factor of 2. The fact that there is a narrow torsional peak at 5.6 Hz in the flight response obtained with elevator inputs suggests that the absence of significant wing torsion peaks with direct lift flap inputs was due to small effectiveness in exciting the torsional mode rather than that the torsional response was reduced by some effect not accounted for in the analysis.

The distortion of the measured torsion peak on Figure C-10a and measured peaks above and below 5 Hz on Figure C-11a and C-13a suggest that there are modes present involving wing torsional motion as discussed previously. The theoretical model only accounts for one of these peaks. Differences in the amplitudes of the computed and measured responses in the neighborhood of 5 Hz might be associated with this approximation in the theoretical model.

High computed resonance peaks found near 6.9 Hz with elevator excitation result from the response in mode 3 (i.e., the mode which is characterized at zero airspeed by in-phase motion of the aft fuselage and stabilizer tip). Corresponding peaks are also apparent in the measured flight responses. The amplitudes of the computed and measured responses to elevator inputs at 6.9 Hz are in good agreement at accelerometers located at the pilot station, c.g., and wing tip as shown on Figures C-10a, C-11a amd C-12a, but the computed responses are higher by a factor of approximately 2 at the tail cone and stabilizer tip (see Figures C-13a and C-14a).

The computed responses do not show a separate peak close to 7.44 Hz which can be associated with mode 4 (i.e., the mode which is characterized at zero airspeed by out-of-phase motion of the aft fuselage and stabilizer tip). However, a separate resonance peak corresponding to mode 4 can be seen in the flight data and is particularly evident in Figure 14a at approximately 7.8 Hz. It will be remembered that the computed damping ratio for mode 4 at bending was ζ = .133 while the measured damping ratio was only ζ = .038 which might explain why the effect of mode 4 is more evident in the experimental response

data. The large computed aerodynamic coupling between modes 3 and 4 caused the high computed damping ratio for mode 4 and may have been responsible for some distortion of the frequency response curves in the region of the third and fourth mode resonances.

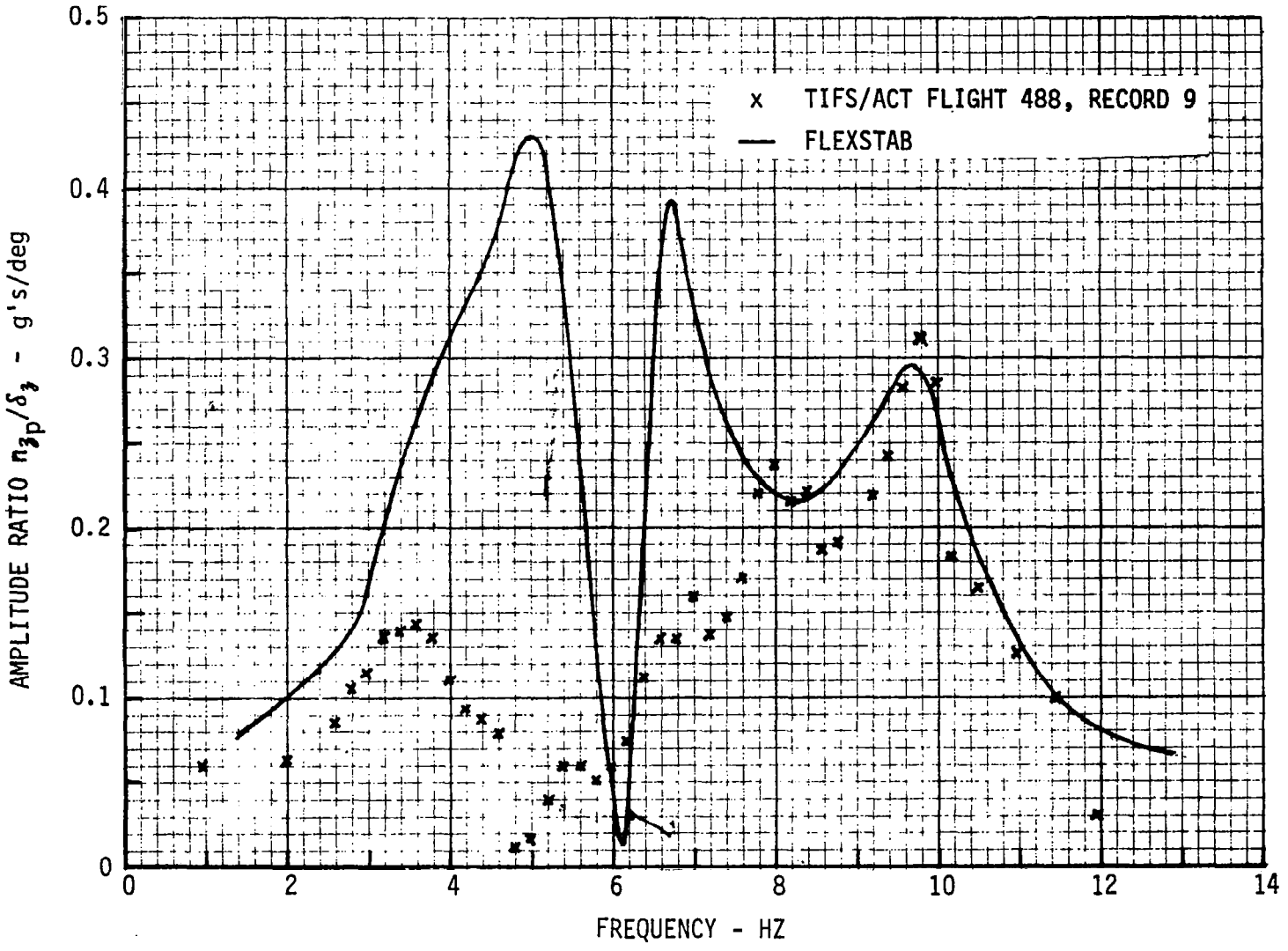

Figure C-1a FREQUENCY RESPONSE, PILOT ACCELERATION (n_{z_p})/DLF DEFLECTION (δ_z) CRUISE CONDITION

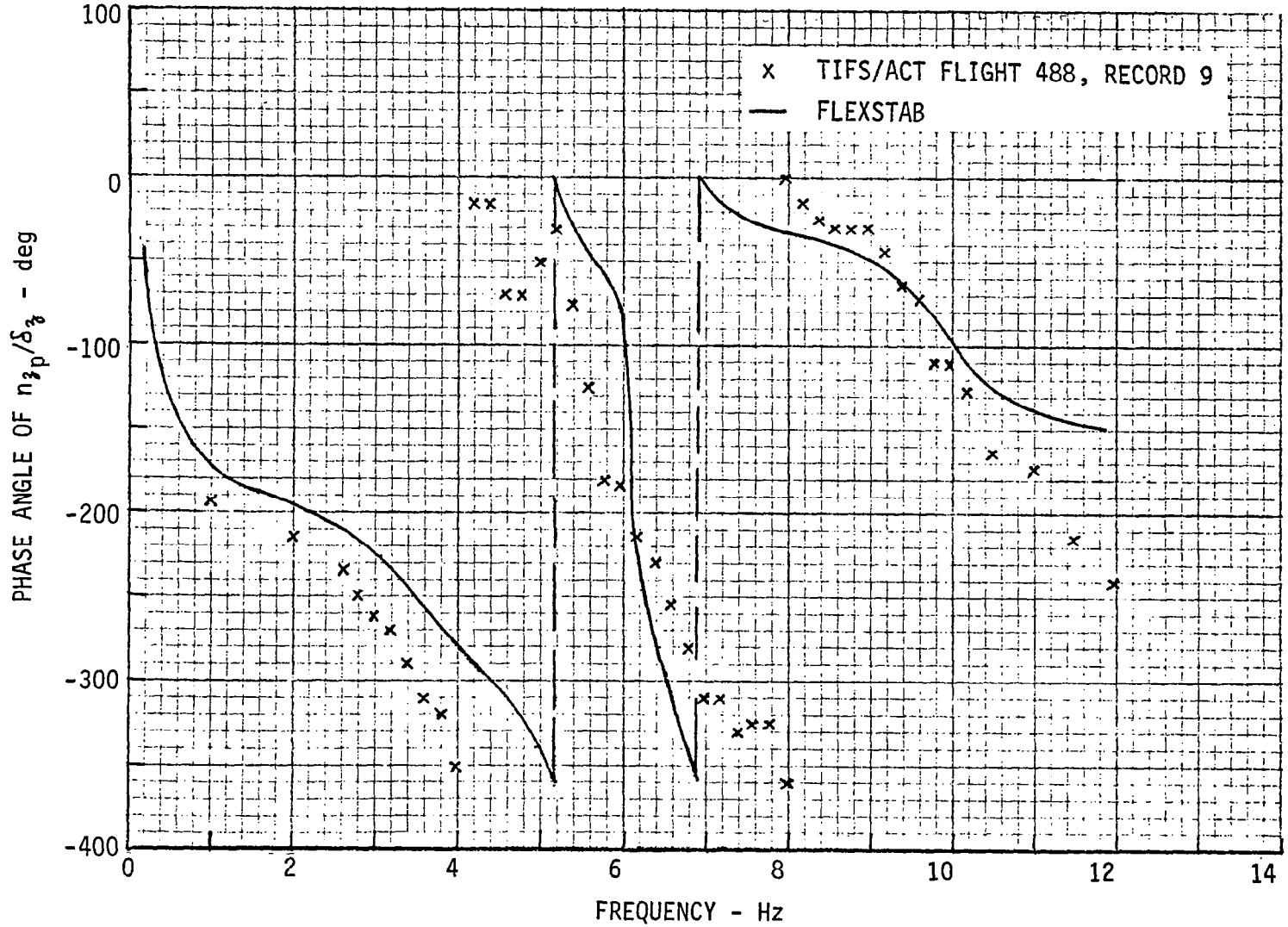

Figure C-1b FREQUENCY RESPONSE, PILOT ACCELERATION (n_{z_p})/DLF DEFLECTION (δ_z) CRUISE CONDITION

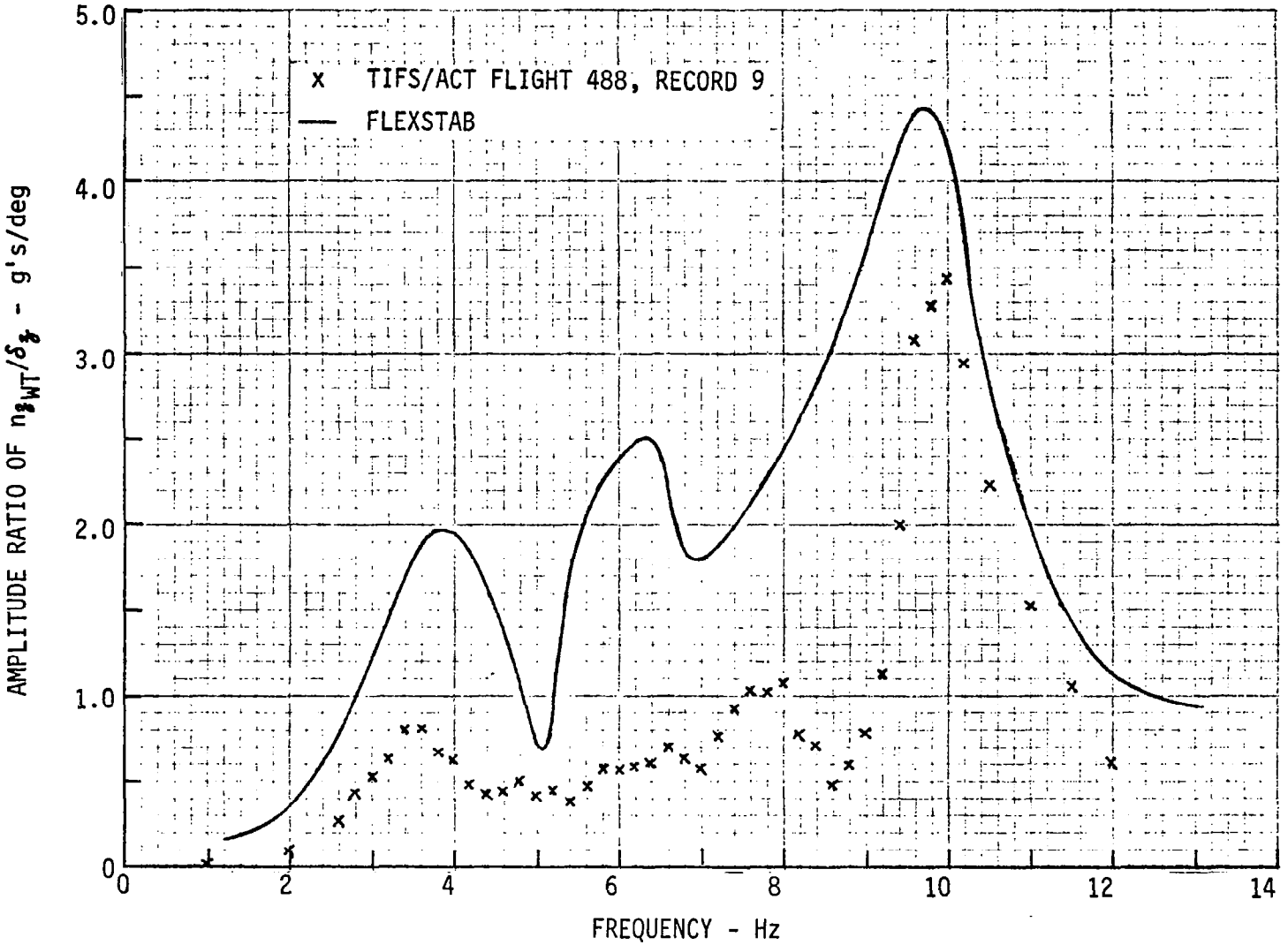

Figure C-2a FREQUENCY RESPONSE, WING TIP ACCELERATION ($n_{z_{WT}}$)/DLF-DEFLECTION (δ_z) CRUISE CONDITION

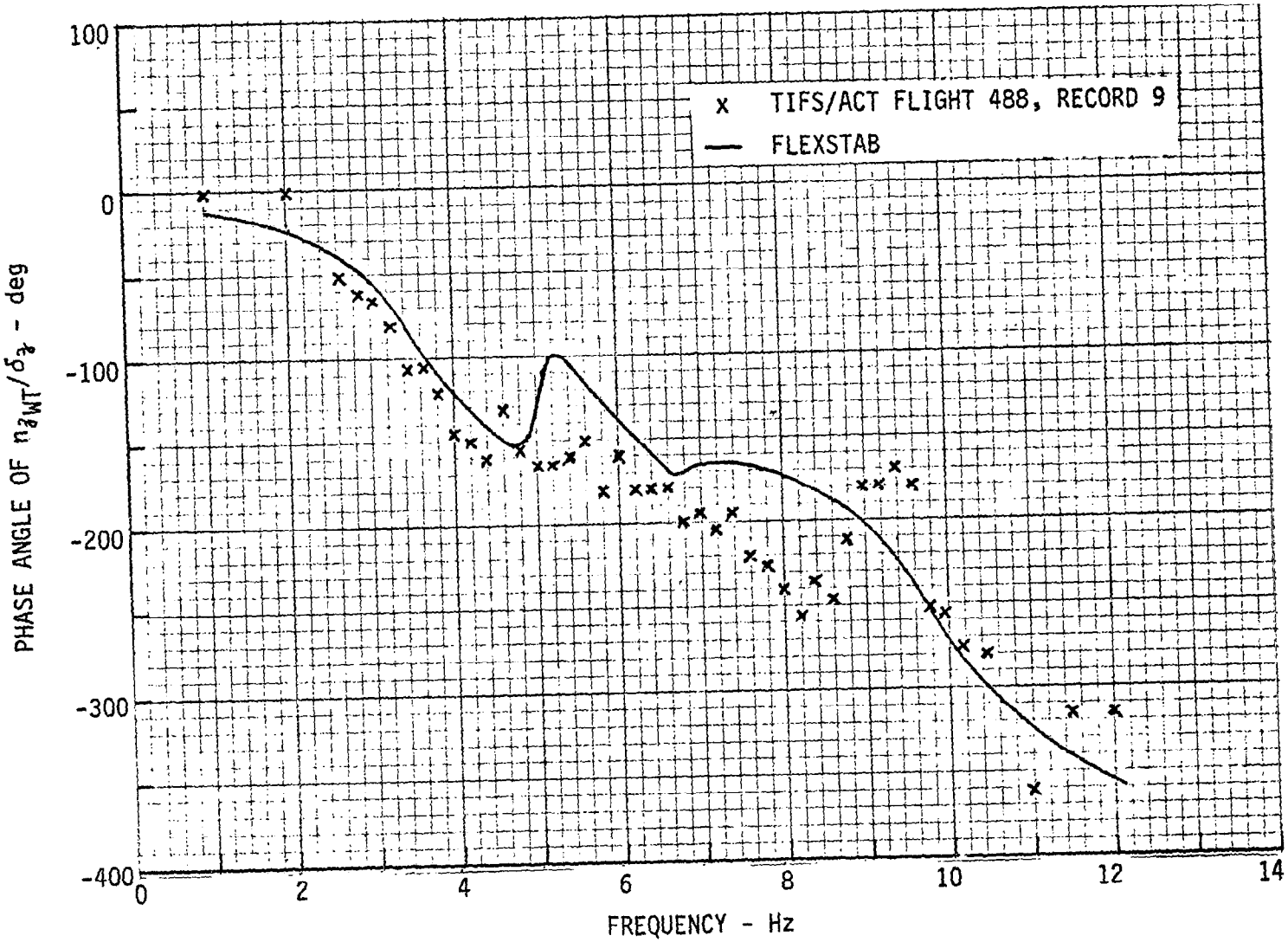

Figure C-2b FREQUENCY RESPONSE, WING TIP ACCELERATION ($n_{z_{WT}}$)/DLF DEFLECTION (δ_z)
CRUISE CONDITION

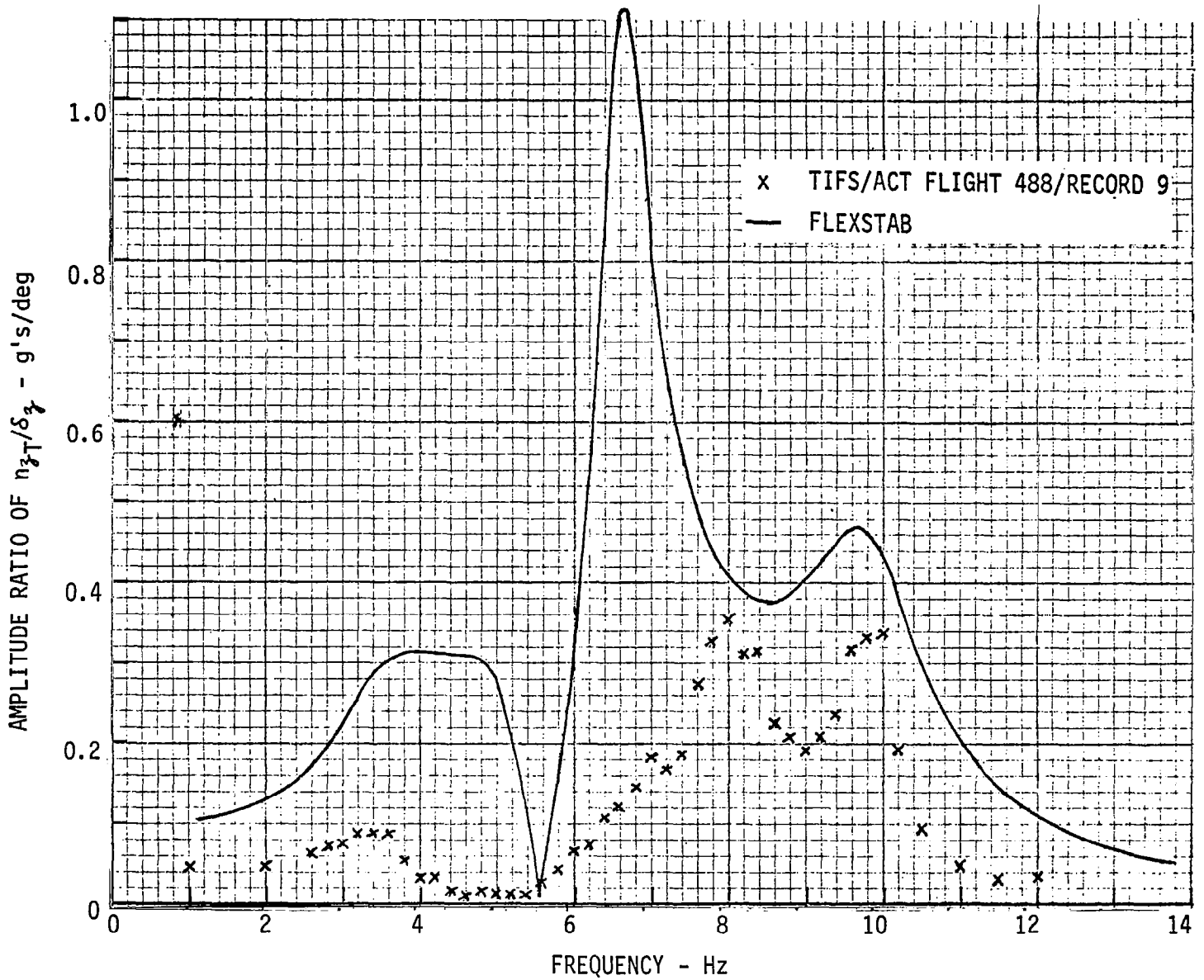

Figure C-3a FREQUENCY RESPONSE, TAIL CONE ACCELERATION (n_T)/DLF DEFLECTION ( )
CRUISE CONDITION

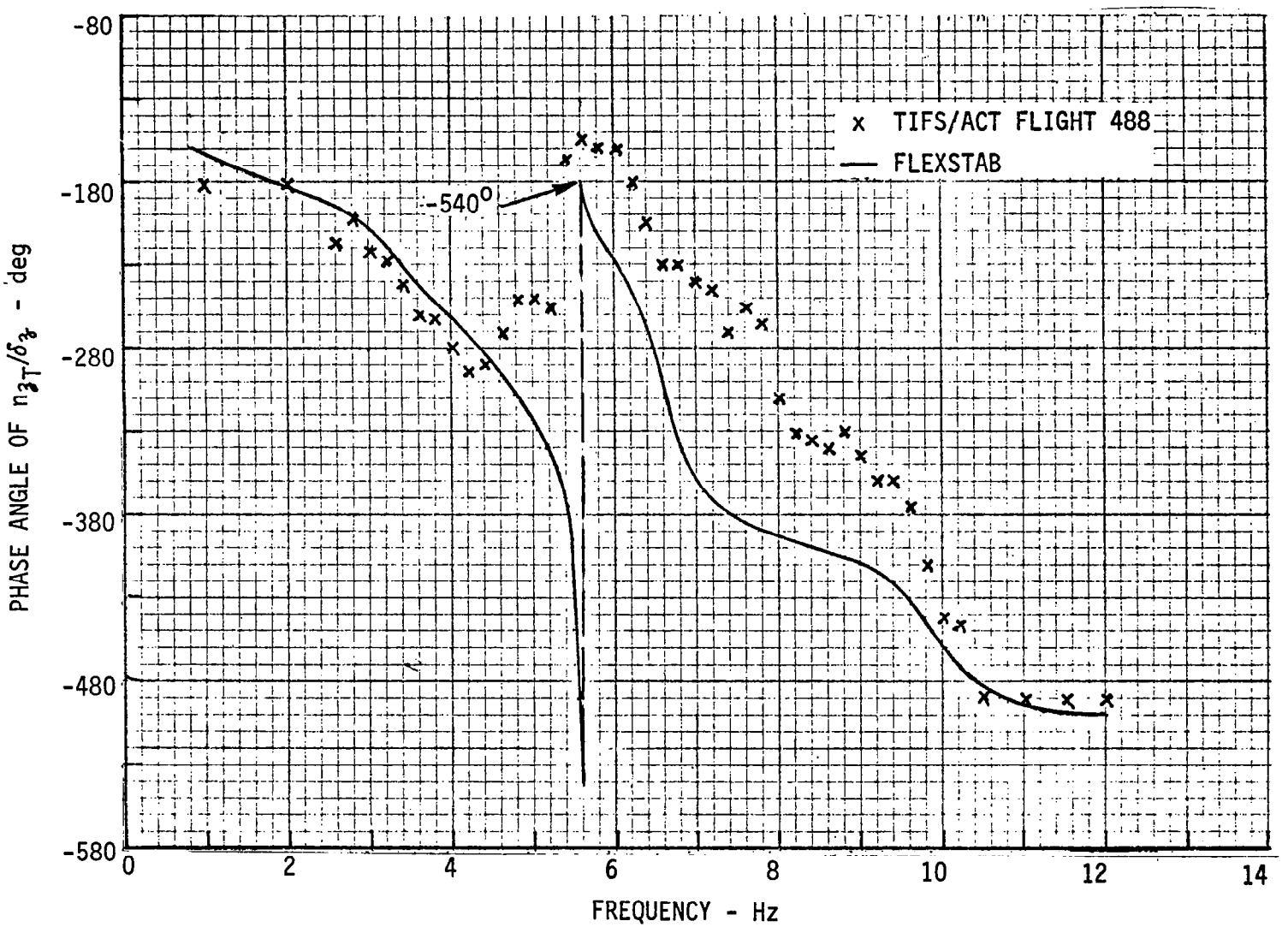

Figure C-3b FREQUENCY RESPONSE, TAIL CONE ACCELERATION (n_{z_T})/DLF DEFLECTION (δ_{z_f}) CRUISE CONDITION

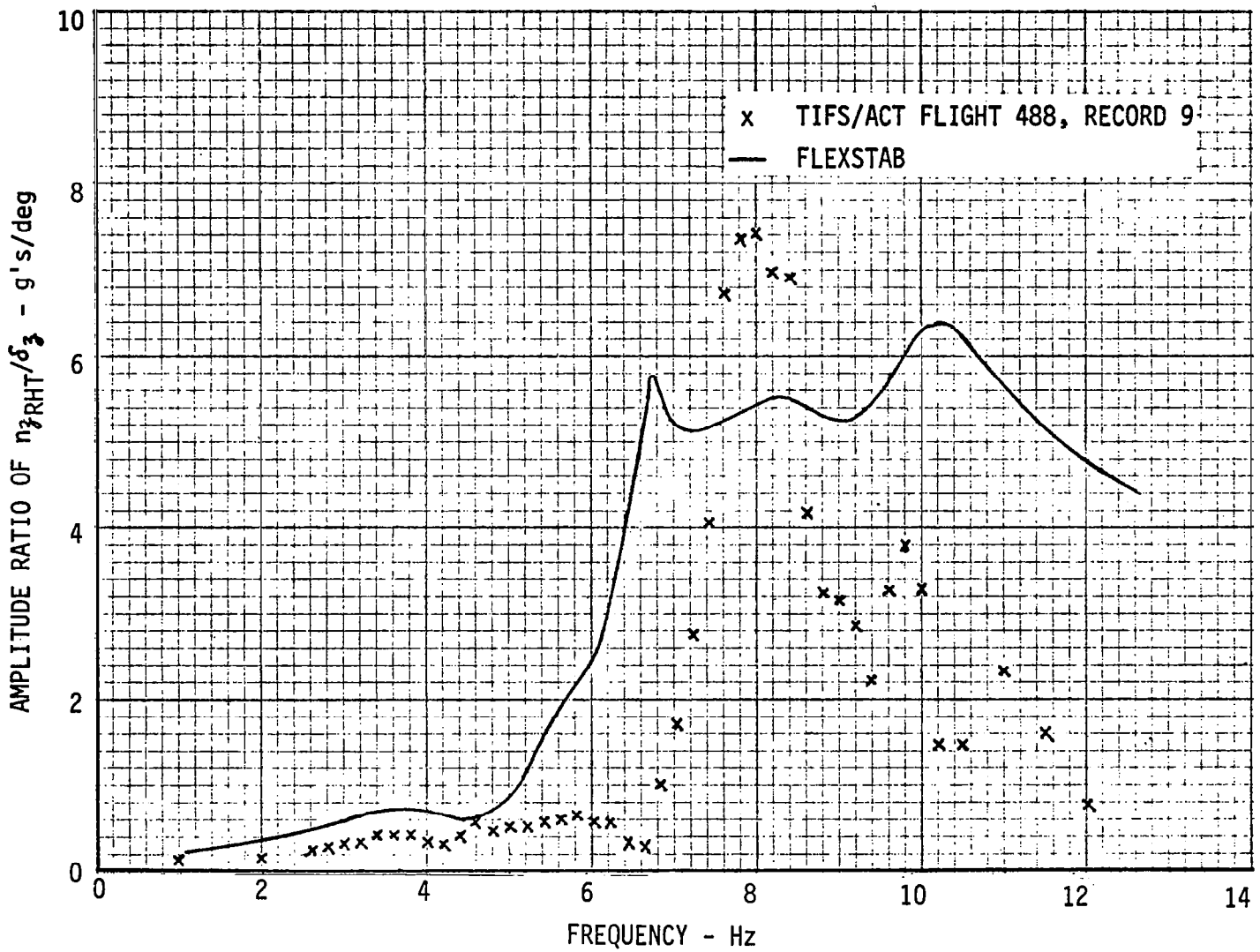

Figure C-4a FREQUENCY RESPONSE, STABILIZER TIP ACCELERATION ($n_{z_{RHT}}$)/DLF DEFLECTION (δ_z) CRUISE CONDITION

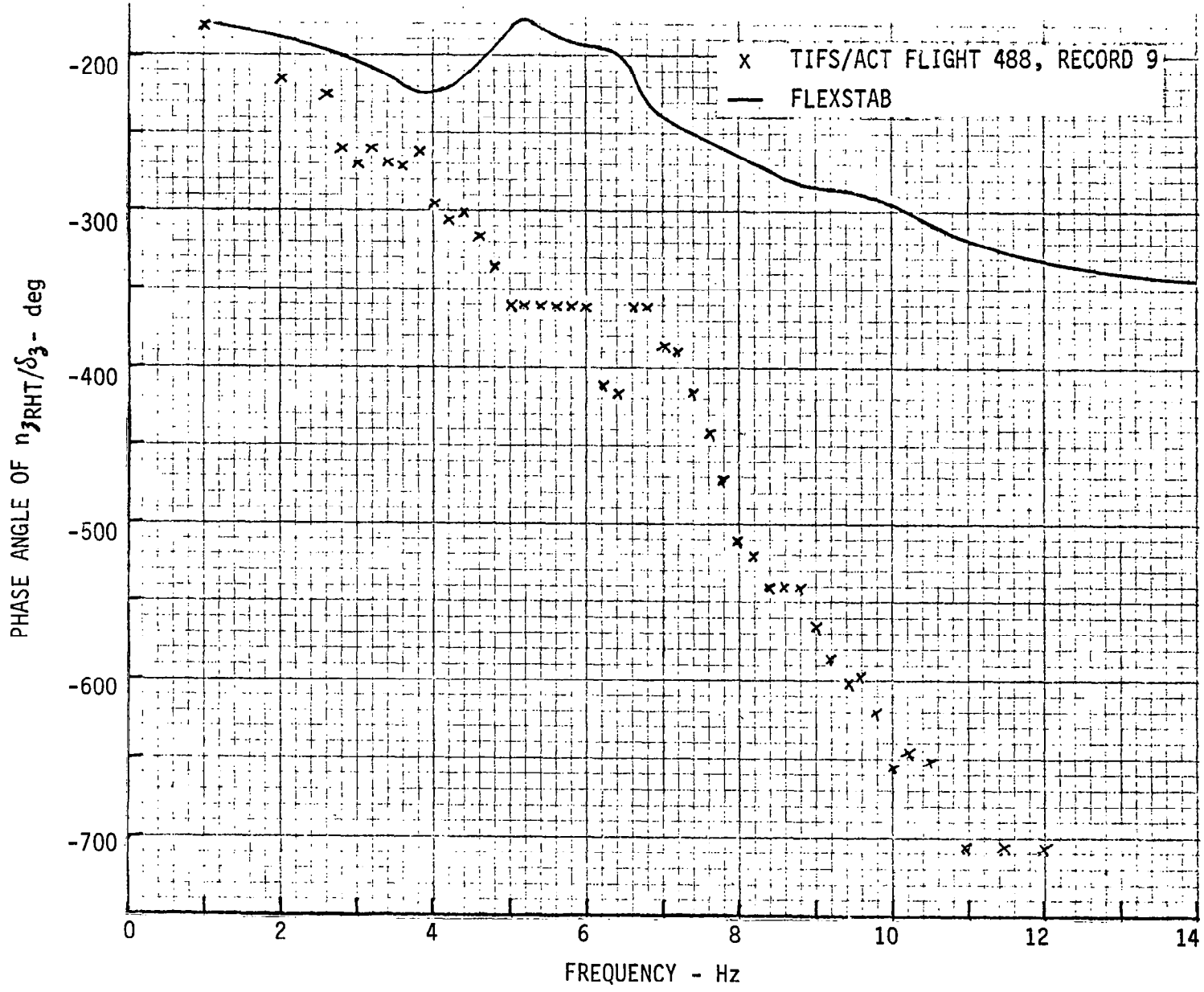

Figure C-4b FREQUENCY RESPONSE, STABILIZER TIP ACCELERATION ($n_{z_{RHT}}$)/DLF DEFLECTION (δ_z) CRUISE CONDITION

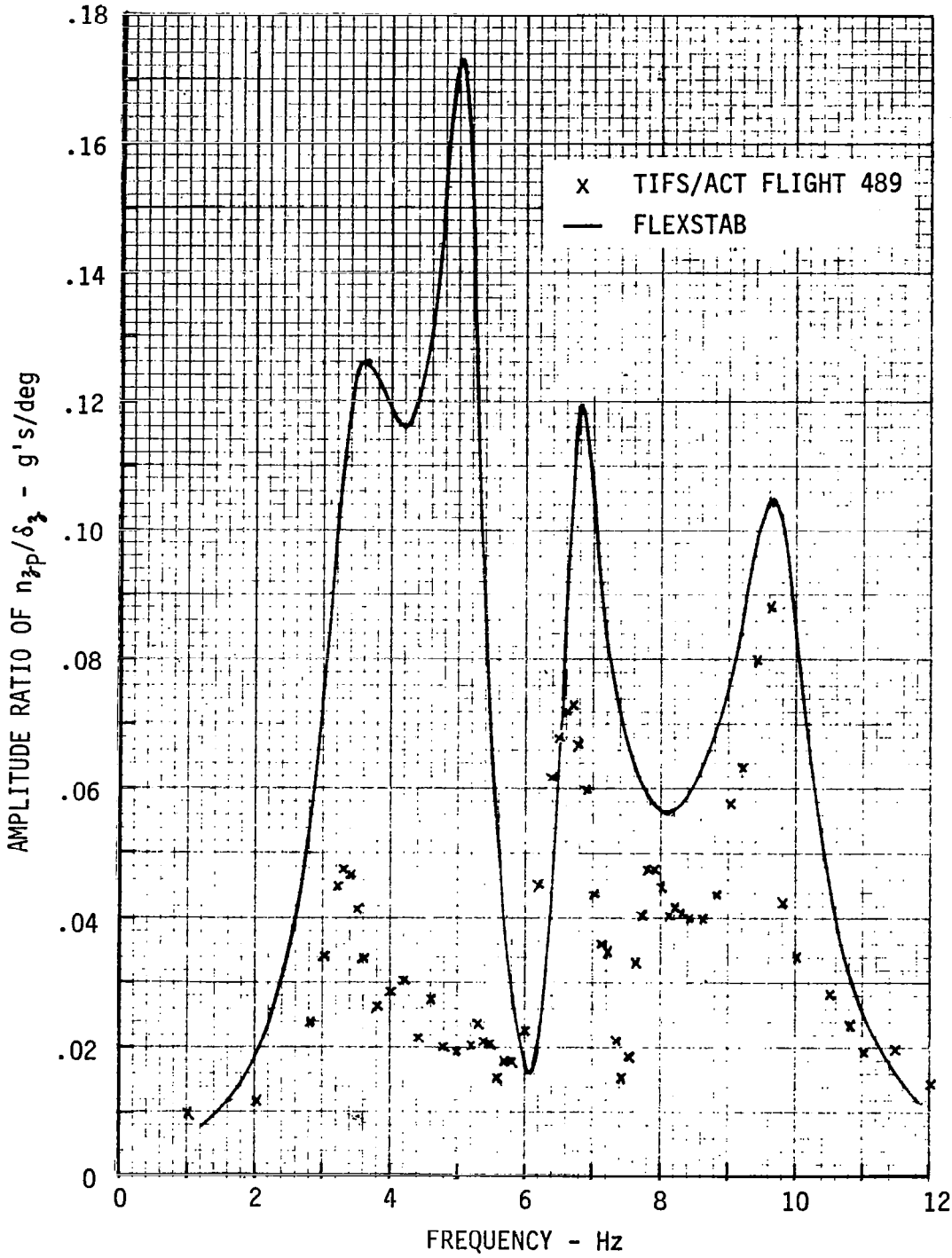

Figure C-5a FREQUENCY RESPONSE, PILOT ACCELERATION (n_{z_p})/DLF DEFLECTION (δ_z) LANDING CONDITION

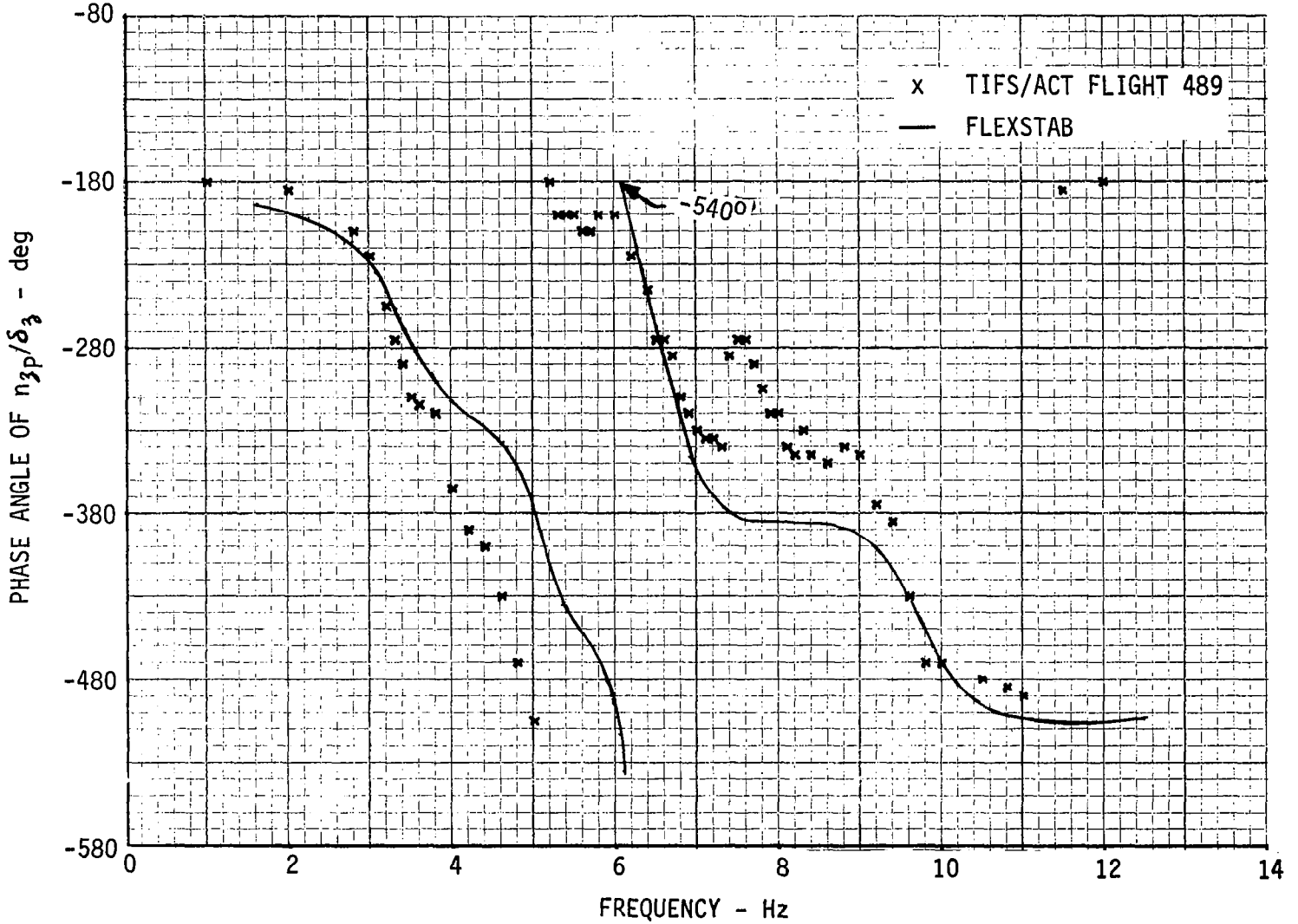

Figure C-5b FREQUENCY RESPONSE, PILOT ACCELERATION (n_{z_p})/DLF DEFLECTION (δ_z) LANDING CONDITION

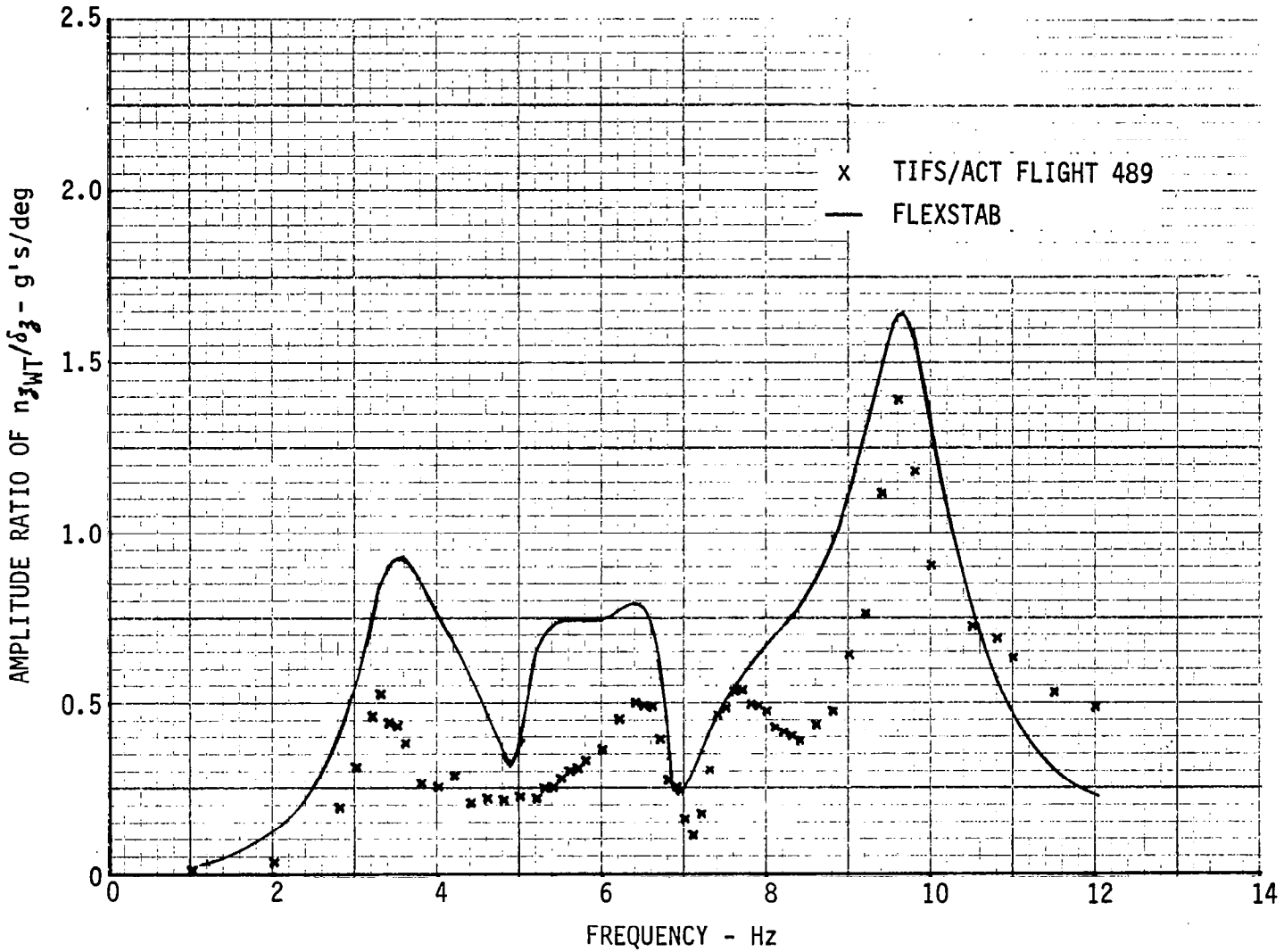

Figure C-6a FREQUENCY RESPONSE, WING TIP ACCELERATION ($n_{z_{WT}}$)/DLF DEFLECTION (δ_z) LANDING CONDITION

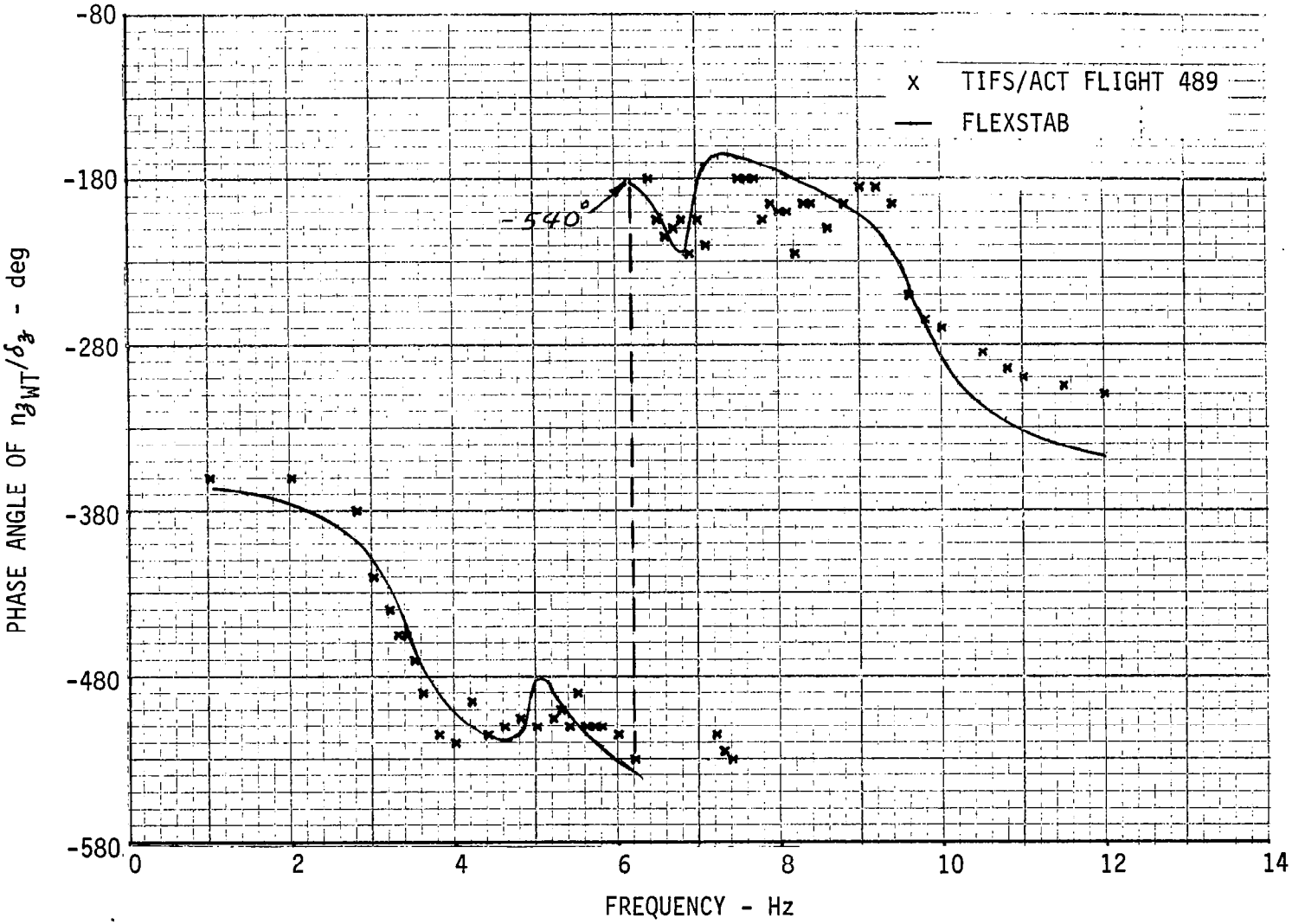

Figure C-6b FREQUENCY RESPONSE, WING TIP ACCELERATION ($n_{z_{WT}}$)/DLF DEFLECTION (δ_z)
LANDING CONDITION

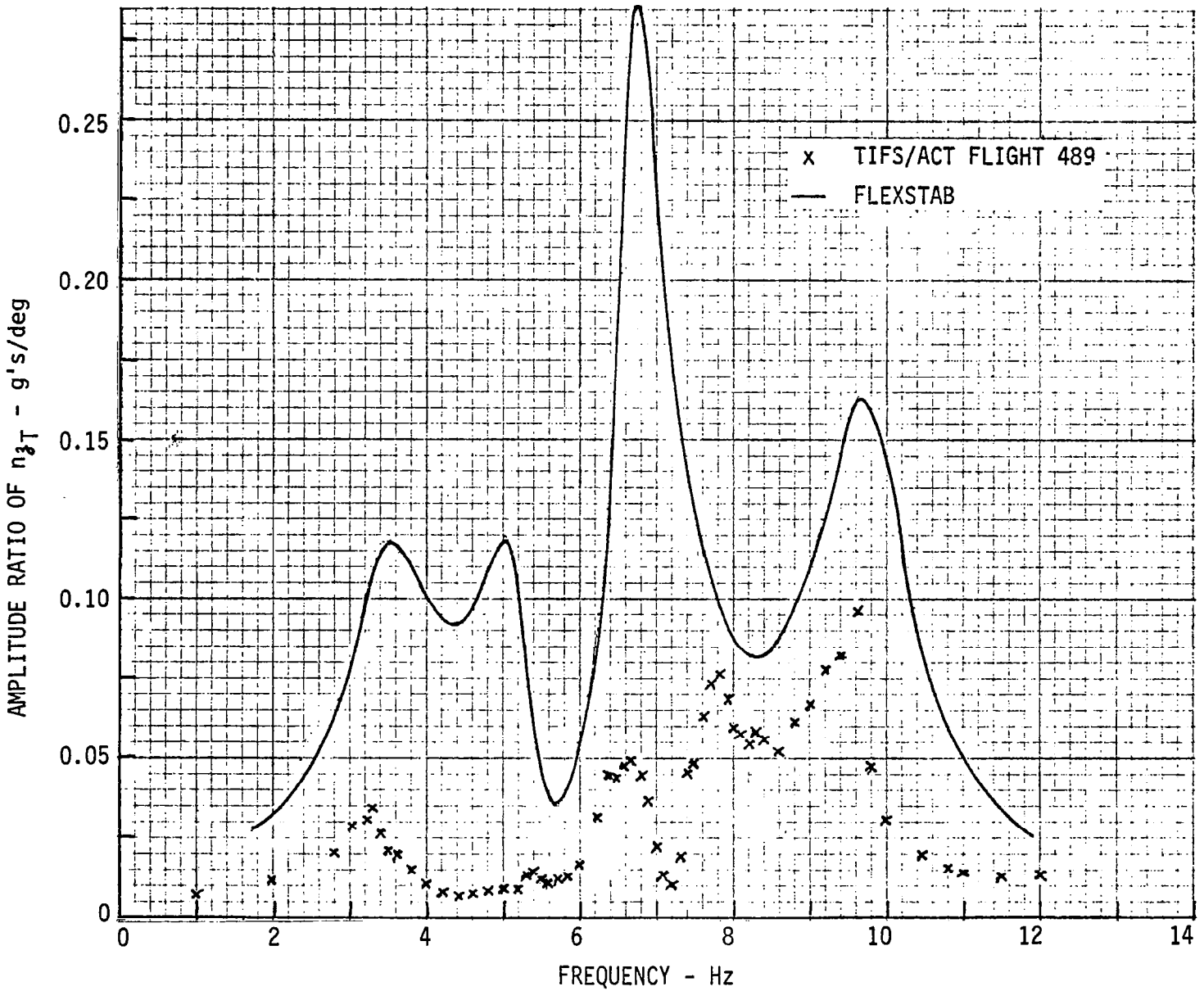

Figure C-7a FREQUENCY RESPONSE, TAIL CONE ACCELERATION (n_{z_T})/DLF DEFLECTION (δ_z) LANDING CONDITION

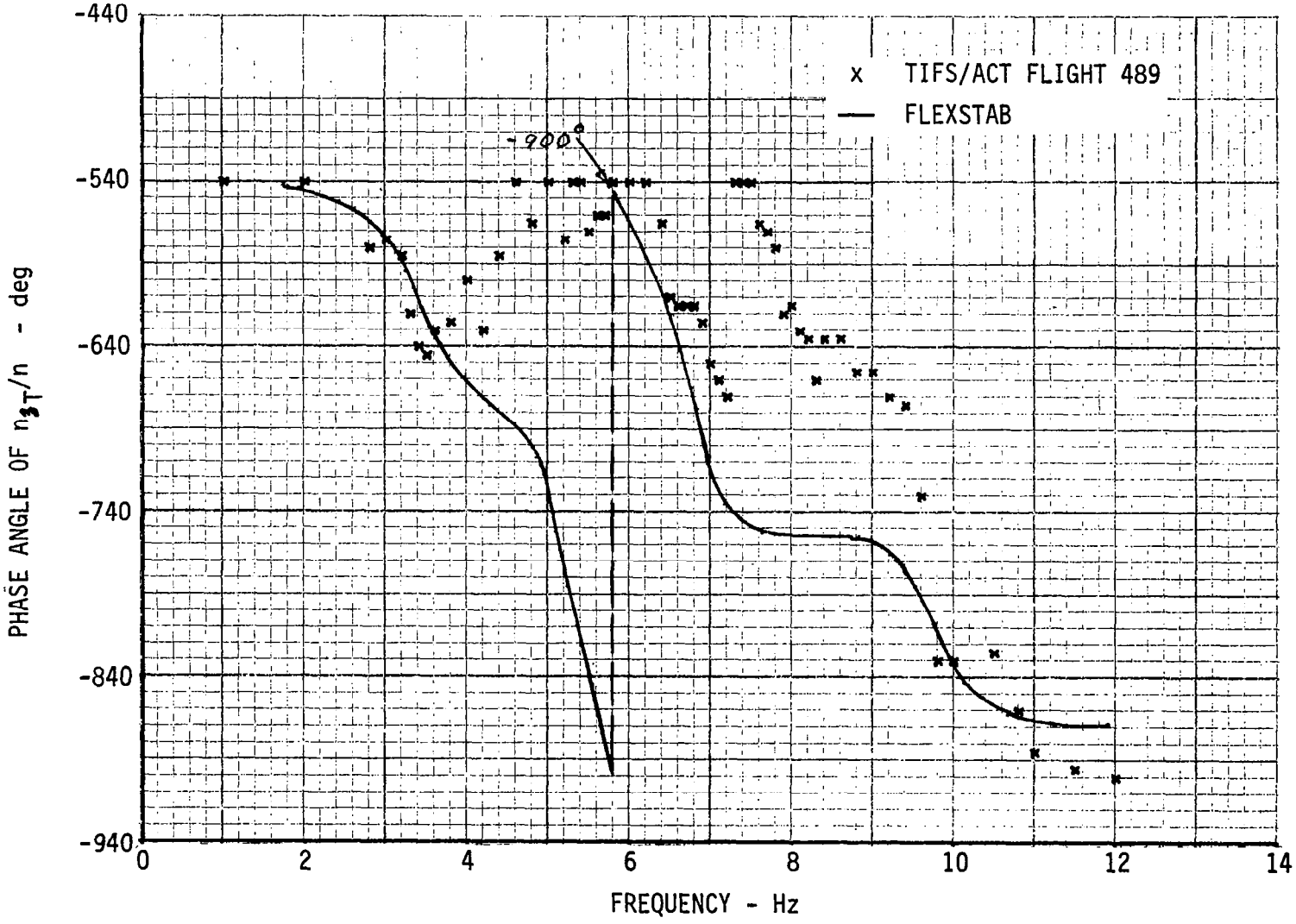

Figure C-7b FREQUENCY RESPONSE, TAIL CONE ACCELERATION (n_{z_T})/DLF DEFLECTION (δ_z) LANDING CONDITION

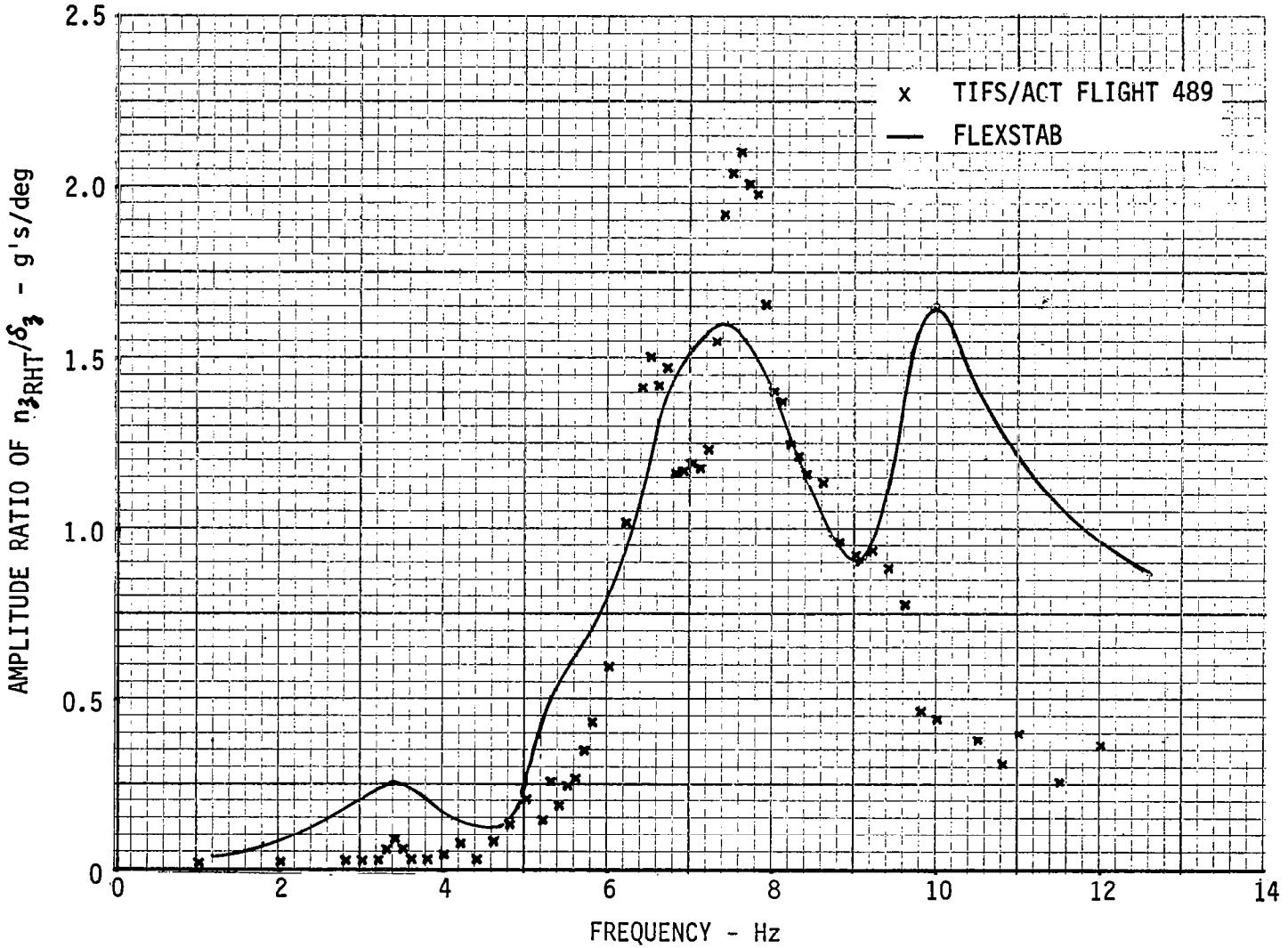

Figure C-8a FREQUENCY RESPONSE, STABILIZER TIP ACCELERATION ($n_{z_{RHT}}$)/DLF DEFLECTION (δ_z) LANDING CONDITION

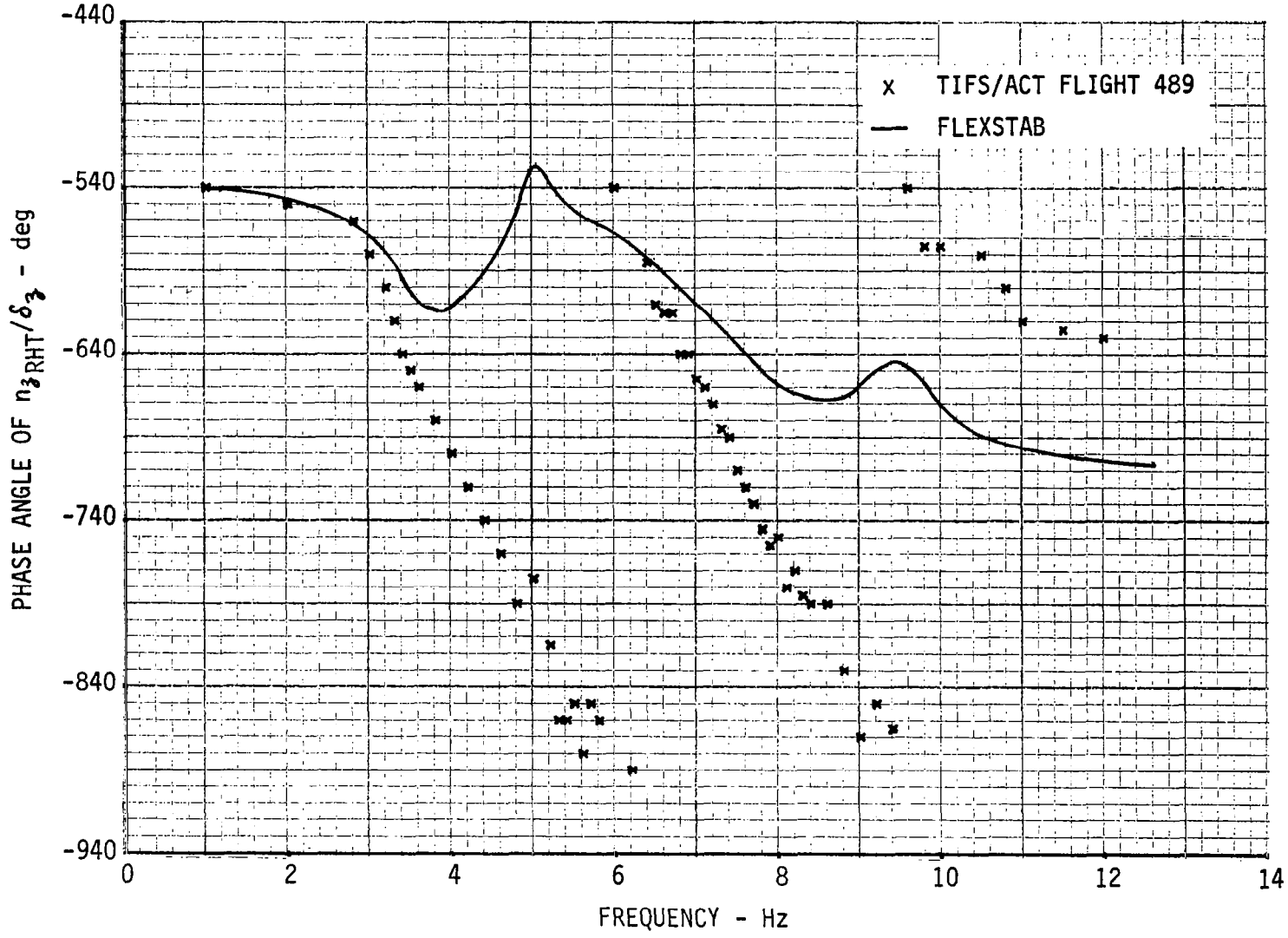

Figure C-8b FREQUENCY RESPONSE, STABILIZER TIP ACCELERATION ($n_{3_{RHT}}$)/DLF DEFLECTION (δ_3) LANDING CONDITION

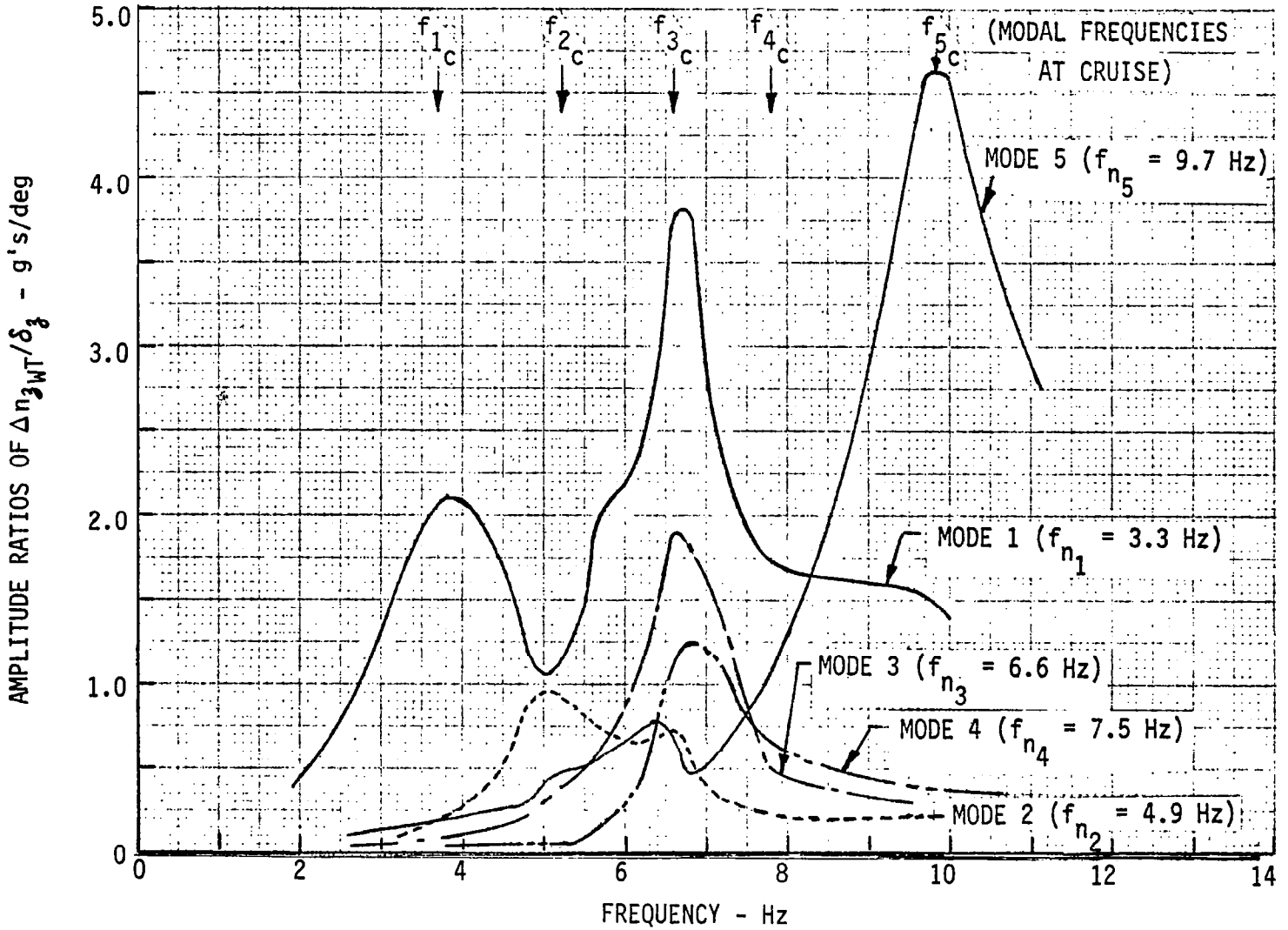

Figure C-9 MODAL CONTRIBUTIONS TO COMPUTED RESPONSES, WING TIP ACCELERATION ($\Delta n_{3_{WT}}$)/DLF DEFLECTION (δ_3), CRUISE CONDITION

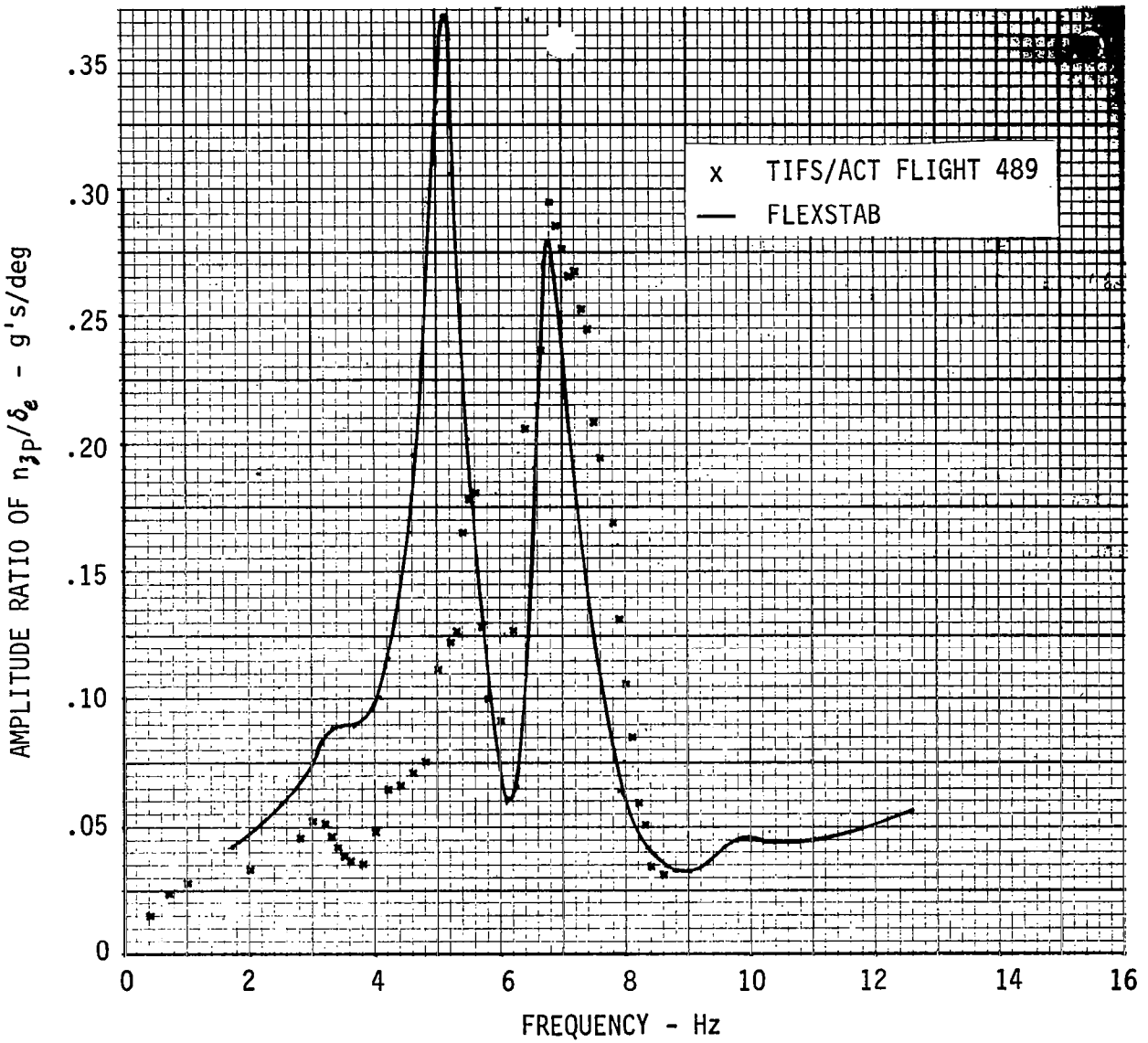

Figure C-10a FREQUENCY RESPONSE, PILOT ACCELERATION (n_{zp})/ELEVATOR DEFLECTION (δ_e) LANDING CONDITION

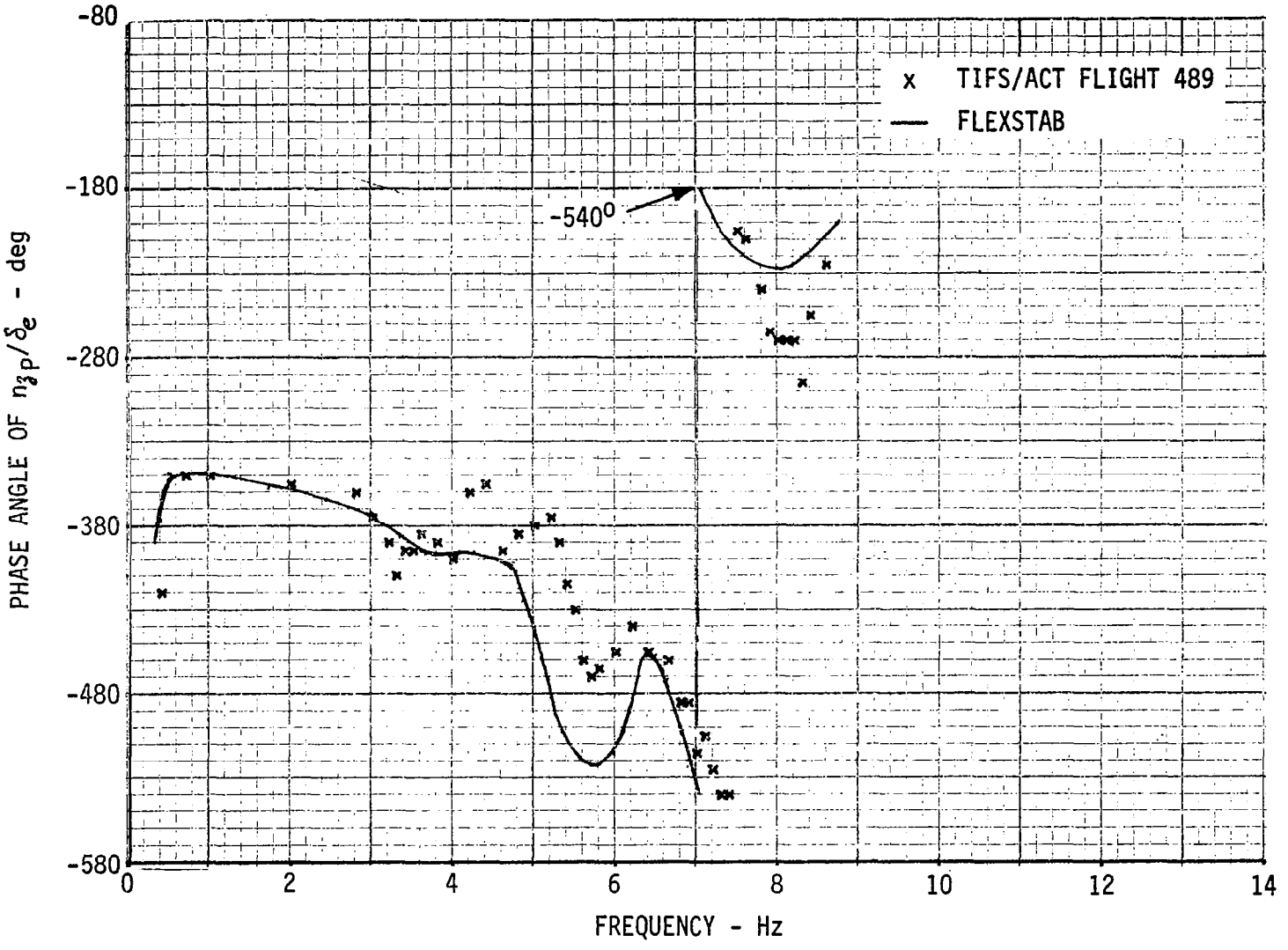

Figure C-10b FREQUENCY RESPONSE, PILOT ACCELERATION (n_{z_p})/ELEVATOR DEFLECTION (δ_e) LANDING CONDITION

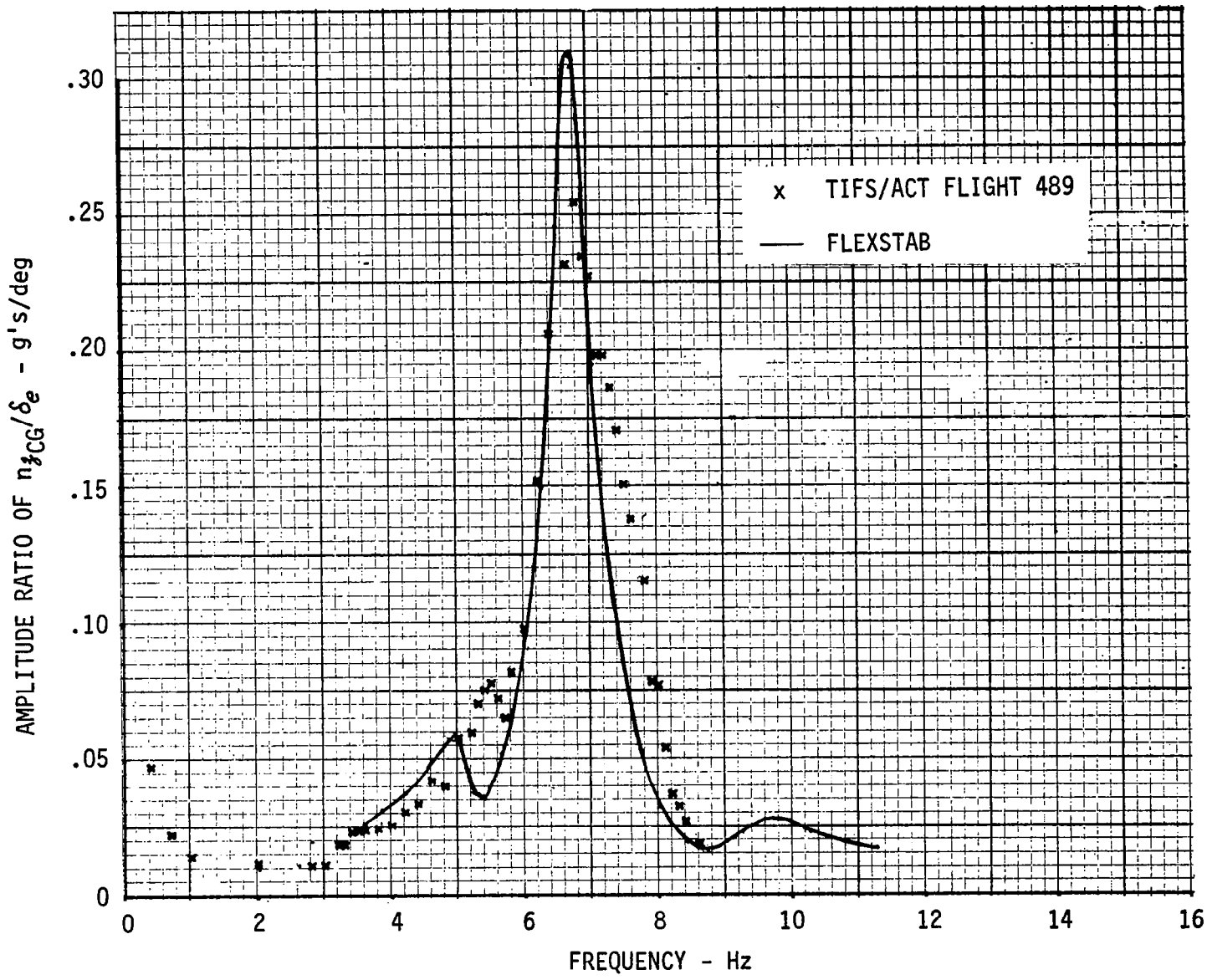

Figure C-11a FREQUENCY RESPONSE, C.G. ACCELERATION ($n_{z_{CG}}$)/ELEVATOR DEFLECTION (δ_e) LANDING CONDITION

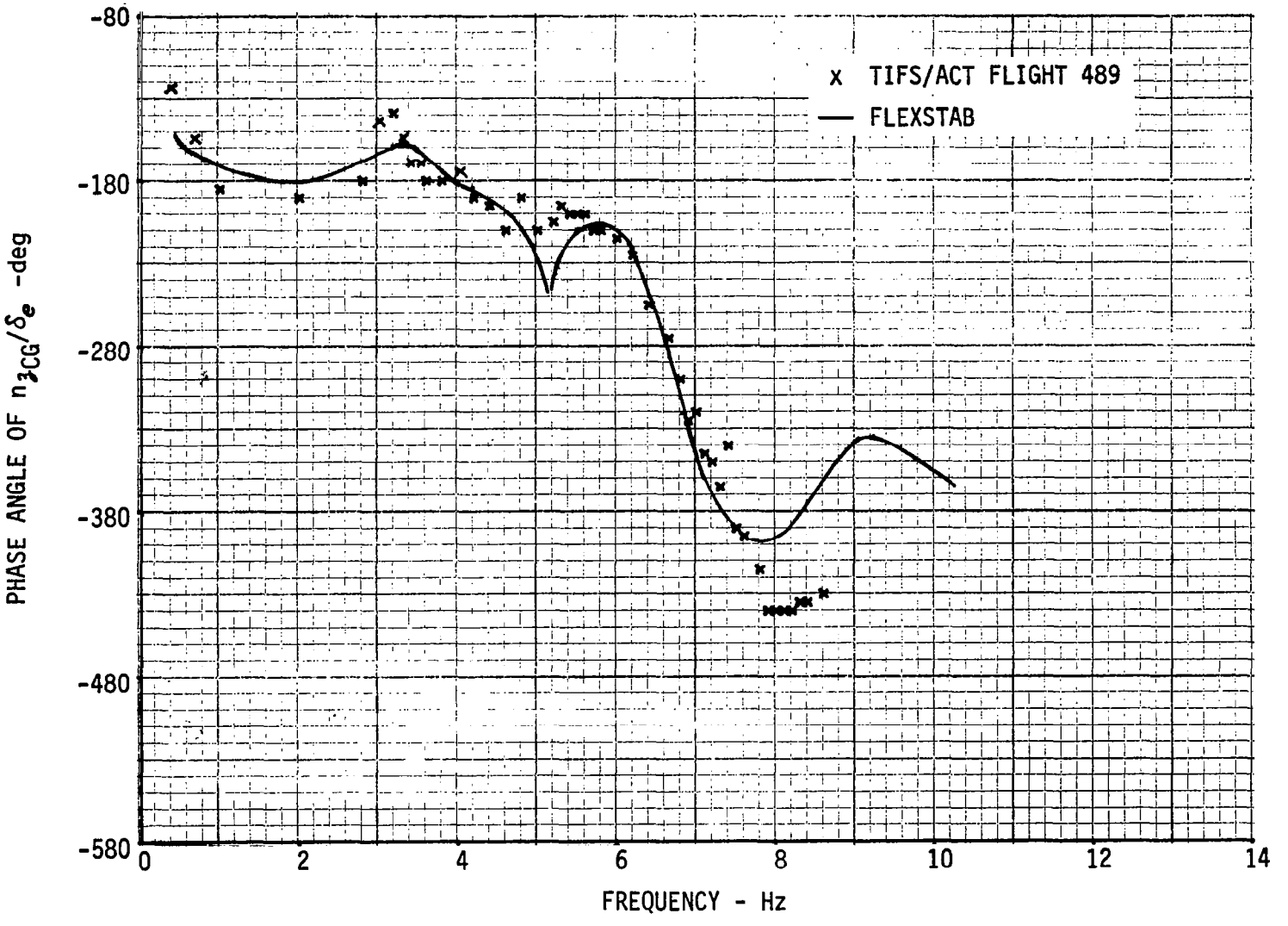

Figure C-11b FREQUENCY RESPONSE, C.G. ACCELERATION ($n_{z_{CG}}$)/ELEVATOR DEFLECTION (δ_e) LANDING CONDITION

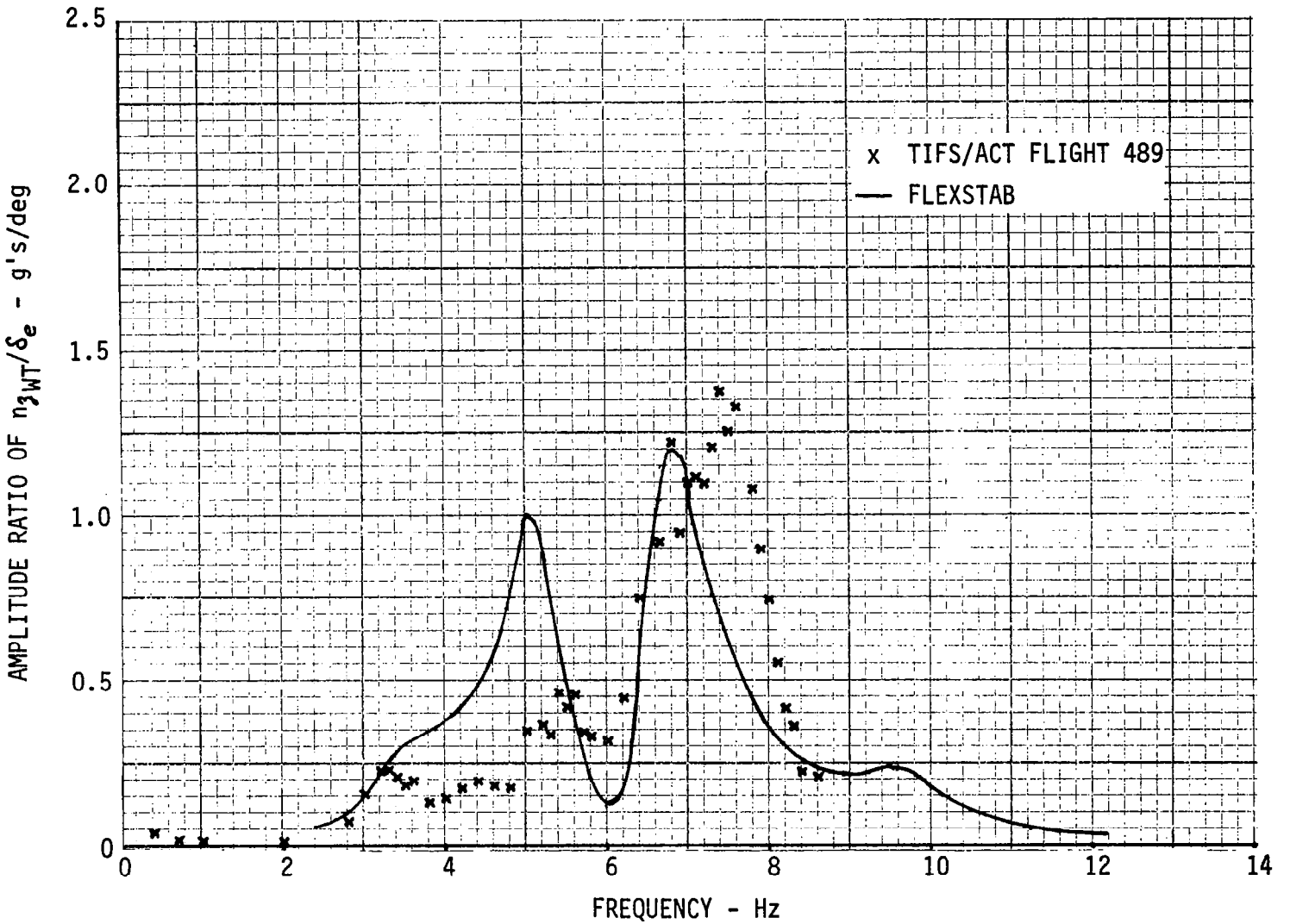

Figure C-12a FREQUENCY RESPONSE, WING TIP ACCELERATION ($n_{z_{WT}}$)/ELEVATOR DEFLECTION (δ_e) LANDING CONDITION

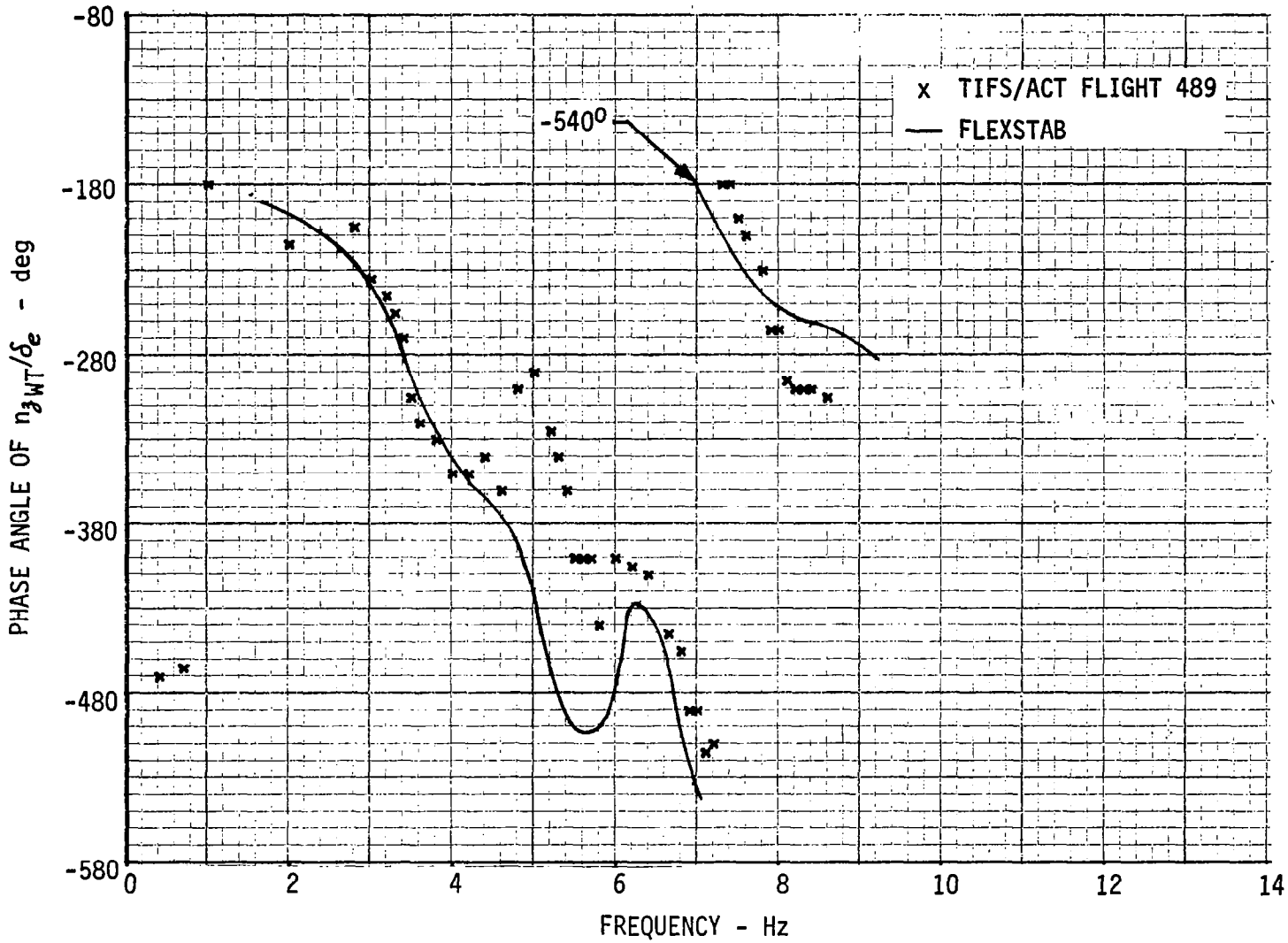

Figure C-12b FREQUENCY RESPONSE, WING TIP ACCELERATION ($n_{z_{WT}}$)/ELEVATOR DEFLECTION (δ_e) LANDING CONDITION

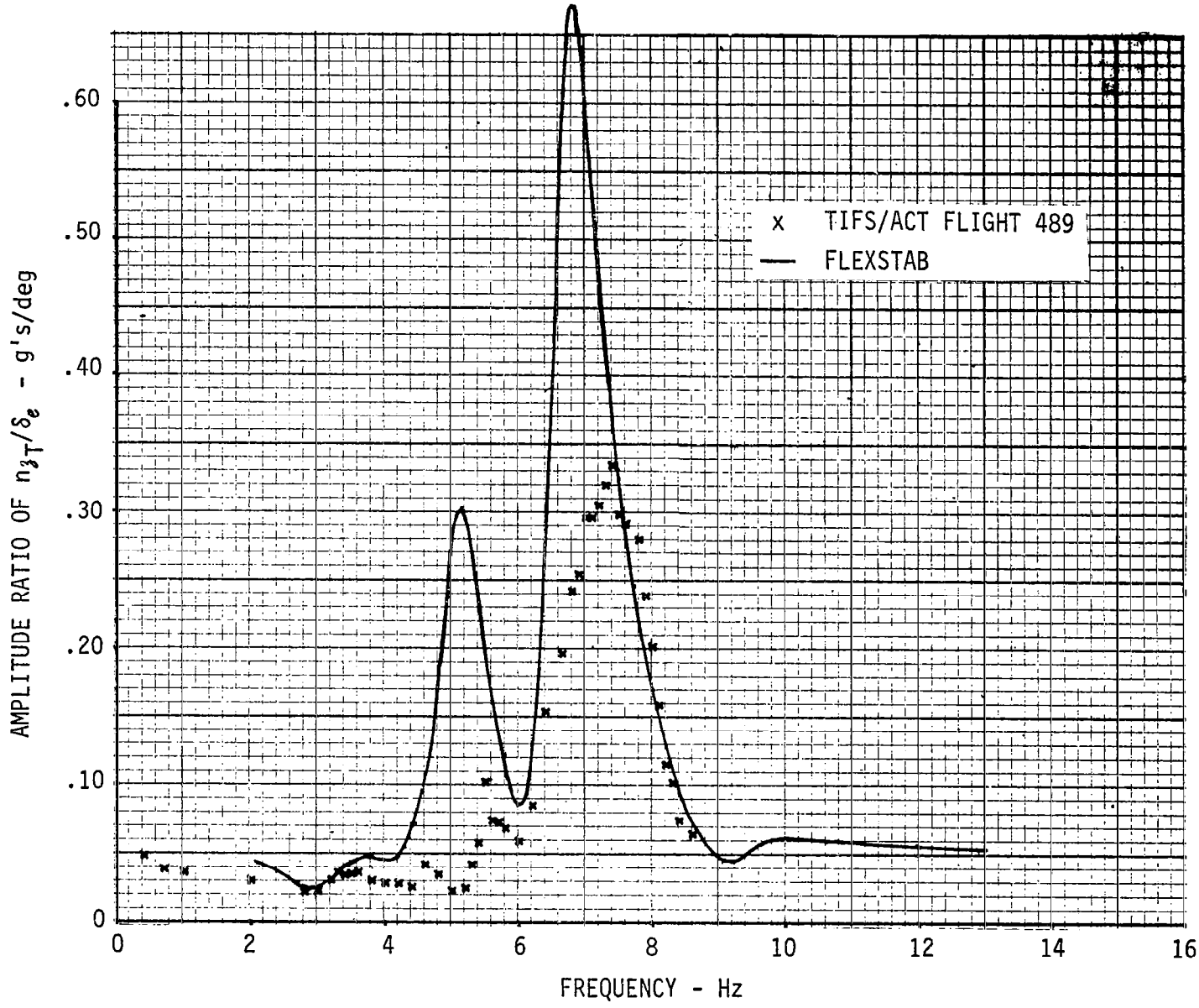

Figure C-13a FREQUENCY RESPONSE, TAIL CONE ACCELERATION (n_{z_T})/ELEVATOR DEFLECTION (δ_e) LANDING CONDITION

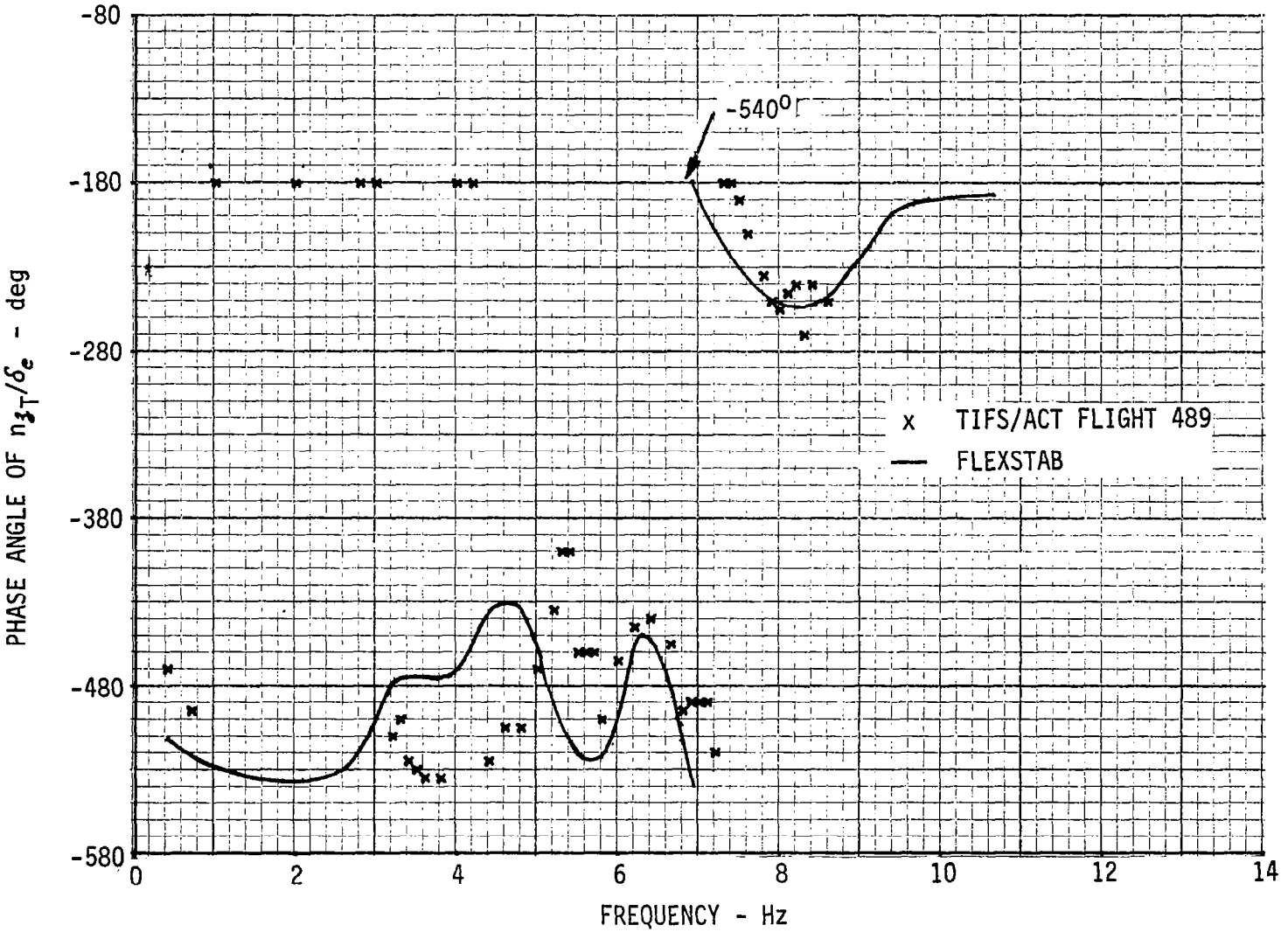

Figure C-13b FREQUENCY RESPONSE, TAIL CONE ACCELERATION (n_{z_T})/ELEVATOR DEFLECTION (δ_e) LANDING CONDITION

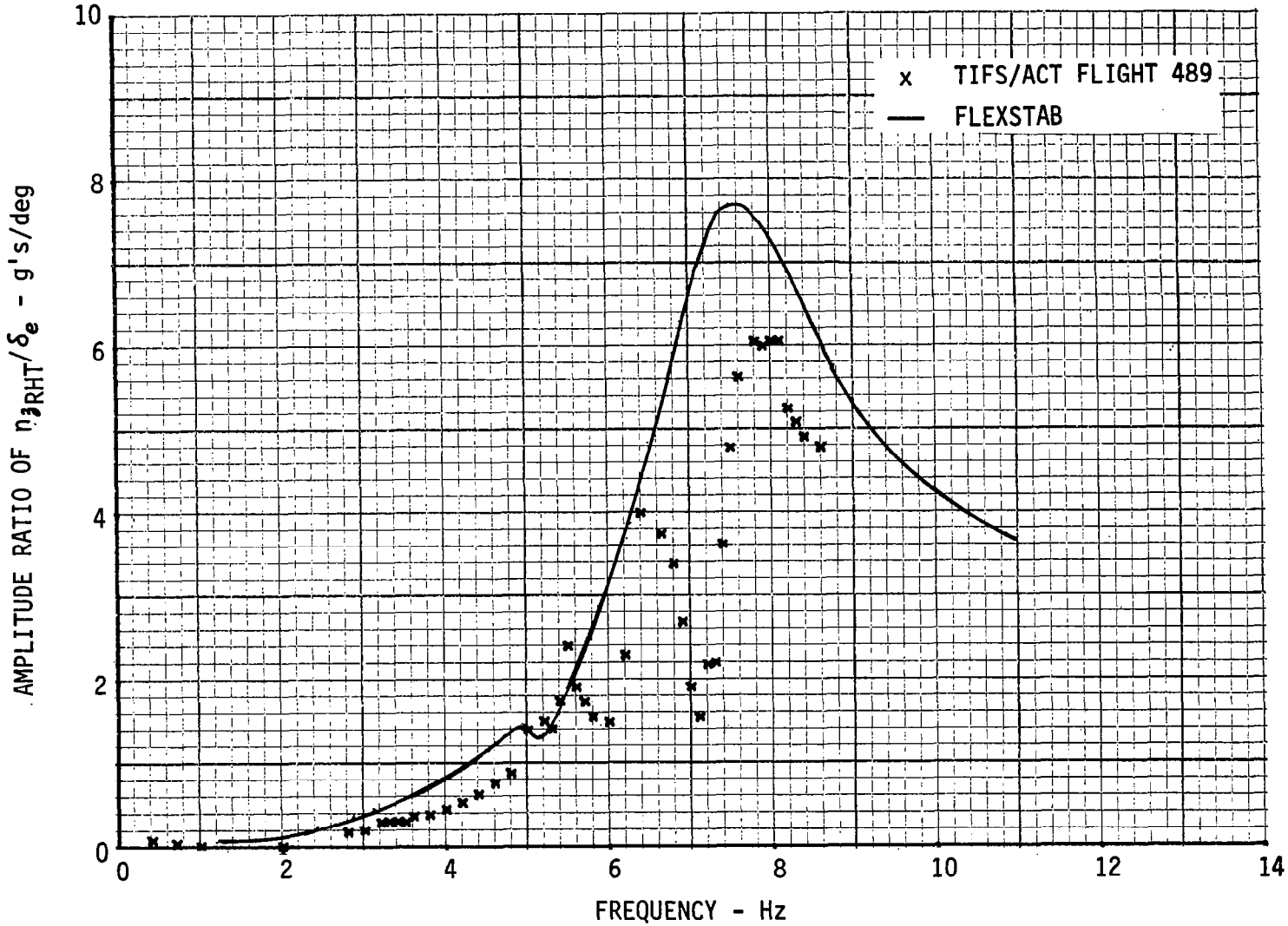

Figure C-14a FREQUENCY RESPONSE, STABILIZER TIP DEFLECTION ($n_{z_{RHT}}$)/ELEVATOR DEFLECTION (δ_e) LANDING CONDITION

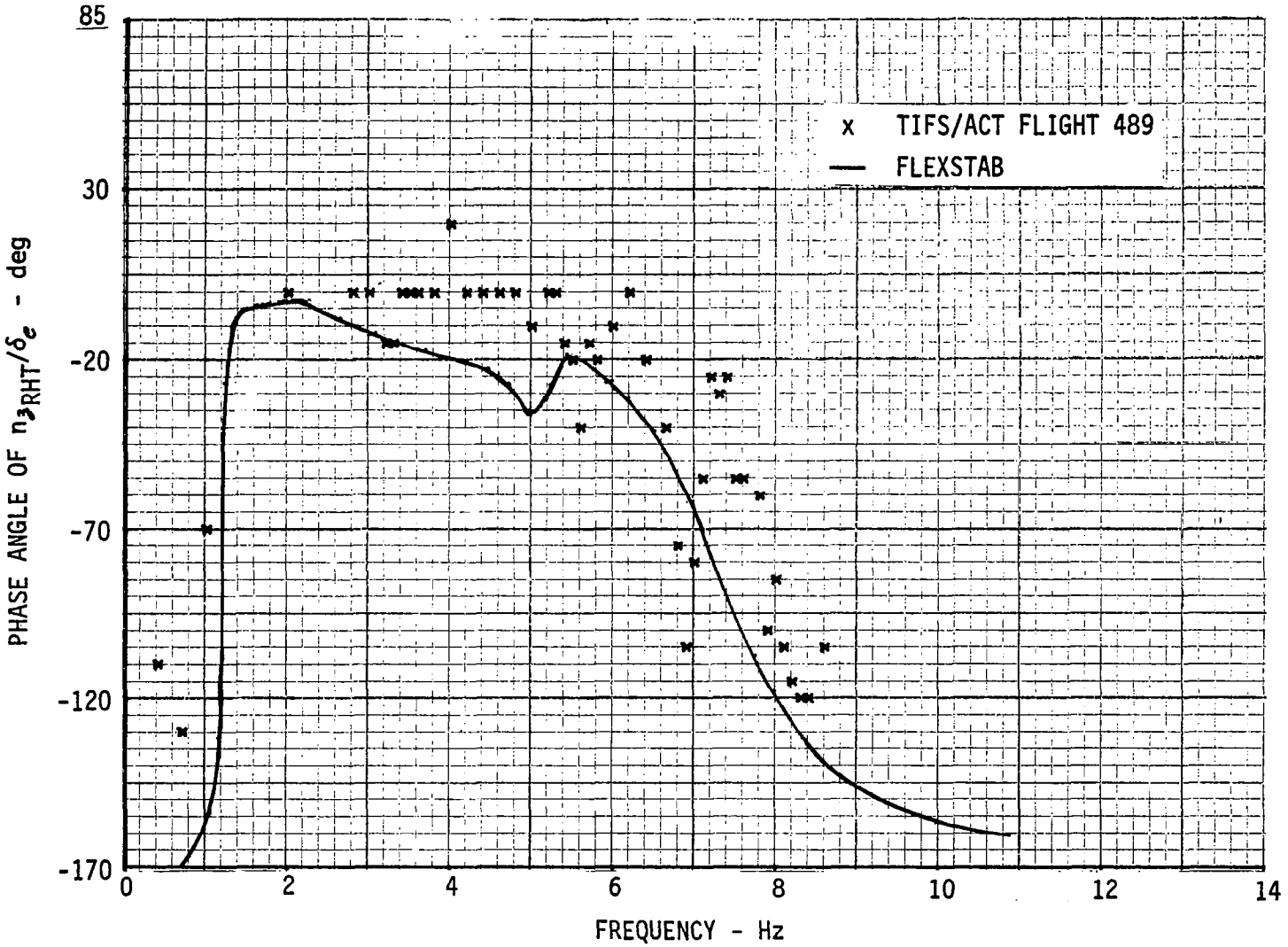

Figure C-14b FREQUENCY RESPONSE, STABILIZER TIP DEFLECTION ($n_{3_{RHT}}$)/ELEVATOR DEFLECTION (δ_e) LANDING CONDITION

APPENDIX D

MODELING OF THE FLEXIBLE CHARACTERISTICS OF TIFS FROM FLIGHT TEST DATA

This appendix describes the method by which a flexible model for the TIFS airplane was obtained from flight test data. This appendix also shows how that analytical model was combined with rigid body characteristics obtained from FLEXSTAB calculations to produce complete aircraft transfer functions.

Flight test data were obtained by exciting the TIFS with oscillatory inputs from the direct lift flaps and elevator. The surfaces were oscillated at specific frequencies from 1.0 to 12.0 Hz, which is the flexible region of interest. The amplitude and frequency of the oscillations were controlled by electronic oscillator inputs into the surface command amplifiers. It was attempted to keep the amplitudes high enough to get good data from each of the sensors, but at certain frequencies the amplitude had to be limited. Linearity was assumed in the data with the different amplitude excitations. This was verified in flight when the input amplitude was changed while holding the frequency fixed.

The accelerometer responses at various stations on the aircraft and control surface position were recorded. Figure D-1 is a sample of an unfiltered Brush recording of the digitally recorded data. From these servo command input oscillations and output accelerometer recordings, frequency response plots (amplitude ratio and phase) were generated. Every signal except the pilot and C.G. accelerometer responses had identical filtering (a 17 Hz low pass recording filter) which did not affect the relative phase and amplitude ratio with respect to each other. The pilot and C.G. accelerometer responses, however, had an additional 13.5 Hz, ζ = .9 low pass filter and the C.G. accelerometer an additional 17.2 Hz, ζ = .7 notch filter. The phase lag and amplitude ratio loss due to these filters were taken out of the recorded data before these signals were analyzed.

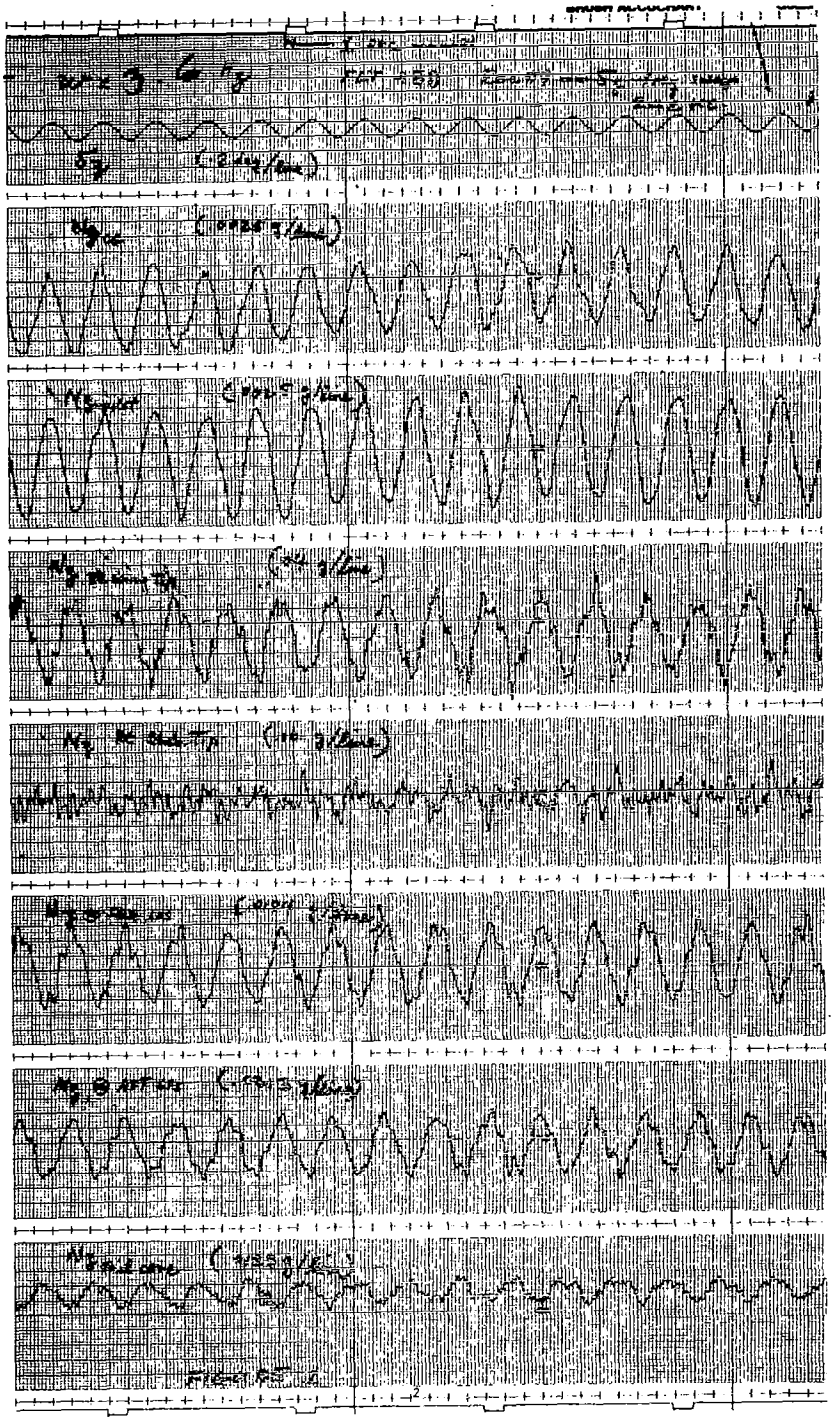

Figure D-1 TYPICAL FLIGHT RECORD

The frequency response plots obtained from the flight data in the range of 1 to 12 Hz contained some effects from the rigid body modes below 1 Hz. Before these curves were finally analyzed, these rigid body effects were extracted from the data. This was accomplished by forming polynomials in with the lower frequency (less than 1 Hz) poles and zeros obtained from FLEXSTAB 14th order models (Appendix A) and calculating the rigid body phase and amplitude ratio effects at the measured frequency points. It should be noted that most of the derivatives that went into determining the short period mode in FLEXSTAB were obtained from in-flight identification. New phase values were obtained by subtracting this rigid body phase effect from the original measure phase. New amplitude ratio values were obtained by dividing the rigid body amplitude ratio into the original measured amplitude ratio. This left data that was only a function of the higher frequency modes. Once these final frequency response plots were obtained, a least squares curve fitting technique based on the method presented in References 9 and 10 was used to estimate transfer functions which yielded the observed frequency responses.

Good flight data was obtained at the 448 km/hr cruise condition with direct lift flap excitation and at the 245 km/hr landing approach condition with the direct lift flap and elevator oscillatory inputs. The amplitudes of these inputs were approximately:

δ_{ζ}	(448 km/hr)	0.5 to 1.5 degrees peak to peak
δ_{ζ}	(245 km/hr)	1.0 to 4.0 degrees peak to peak
δ_{e}	(245 km/hr)	0.5 to 2.0 degrees peak to peak

Curve fittings with 10th order numerator polynomials in S and 10th order denominators were performed for each of the transfer functions. The 10th order model was chosen since previous ground vibration and past and present flight tests on TIFS indicated five structural modes in the frequency range of interest. For each flight condition, an identical denominator should have been identified for each sensor transfer function. However, since they did vary slightly from one another, a single denominator was established by the following technique. The factored out ω's and ζ's for each of the

denominator modes from all sensors at one flight condition were taken and averaged. The resulting averaged ω and ζ for each mode were then used to obtain the final denominator polynomial. With this new denominator the curve fitting program was used again. However, only the numerator polynomials were identified with the denominator held fixed. The steady state gain was also held fixed at its known value from FLEXSTAB. Typical results from this technique are shown in Figures D-2 to D-17. Included are all of the 448 km/hr δ_z transfer functions and one of the 245 km/hr δ_e transfer functions.

The flexible airplane transfer functions identified from the modified flight data then were combined with the rigid body transfer functions from the FLEXSTAB computations along with actuator dynamics to obtain the full transfer functions. The steady state gain from FLEXSTAB was used when the rigid and flexible polynomial fractions were multiplied to form the full transfer function. Two sets of transfer functions were obtained, one with second order approximations of the actuator dynamics:

$$\frac{\delta_z}{\delta_{z_c}} = \frac{2524}{s^2 + 100.5s + 2524}$$

$$\frac{\delta_e}{\delta_{e_c}} = \frac{840}{s^2 + 42s + 900}$$

and another set with first order approximations:

$$\frac{\delta_z}{\delta_{z_c}} = \frac{35.1}{s + 35.1}$$

$$\frac{\delta_e}{\delta_{e_c}} = \frac{28.0}{s + 30.0}$$

In addition to data from six accelerometer locations, the pitch rate response data, q, was also reduced to obtain its transfer functions.

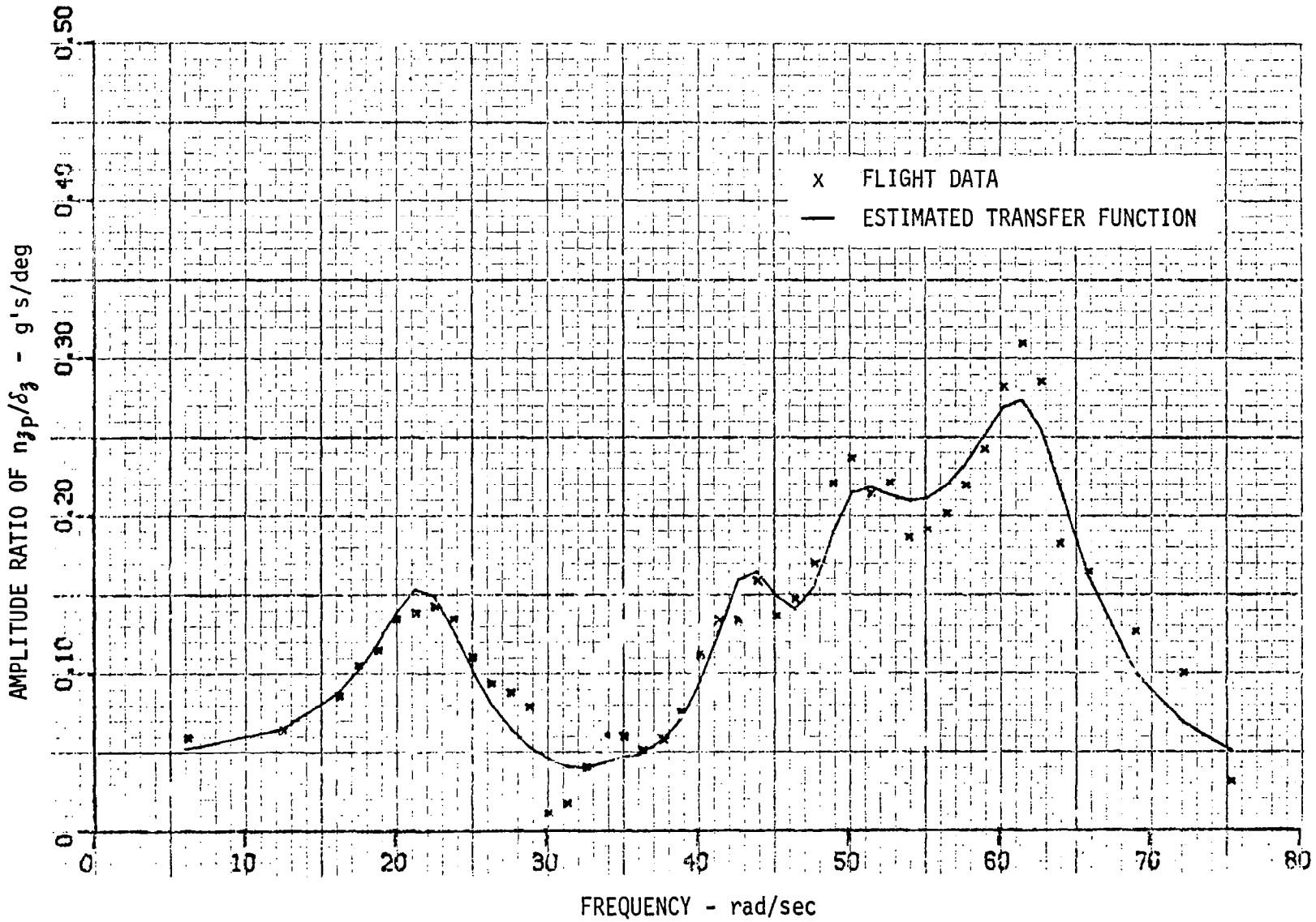

Figure D-2 FREQUENCY RESPONSE, PILOT ACCELERATION (n_{z_p})/ DLF DEFLECTION (δ_z)

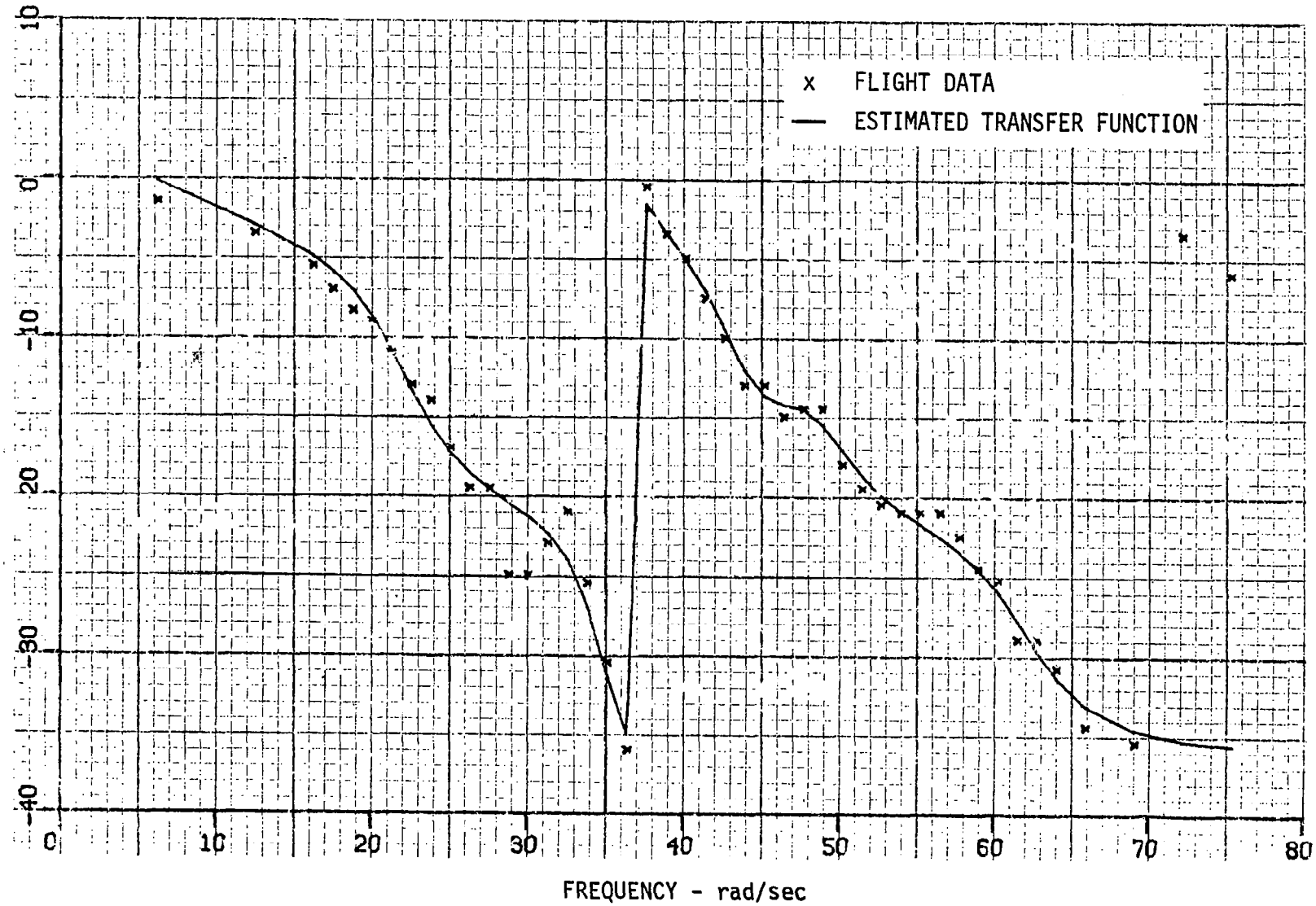

Figure D-3 FREQUENCY RESPONSE, PILOT ACCELERATION (n_{z_p})/DLF DEFLECTION (δ_z)

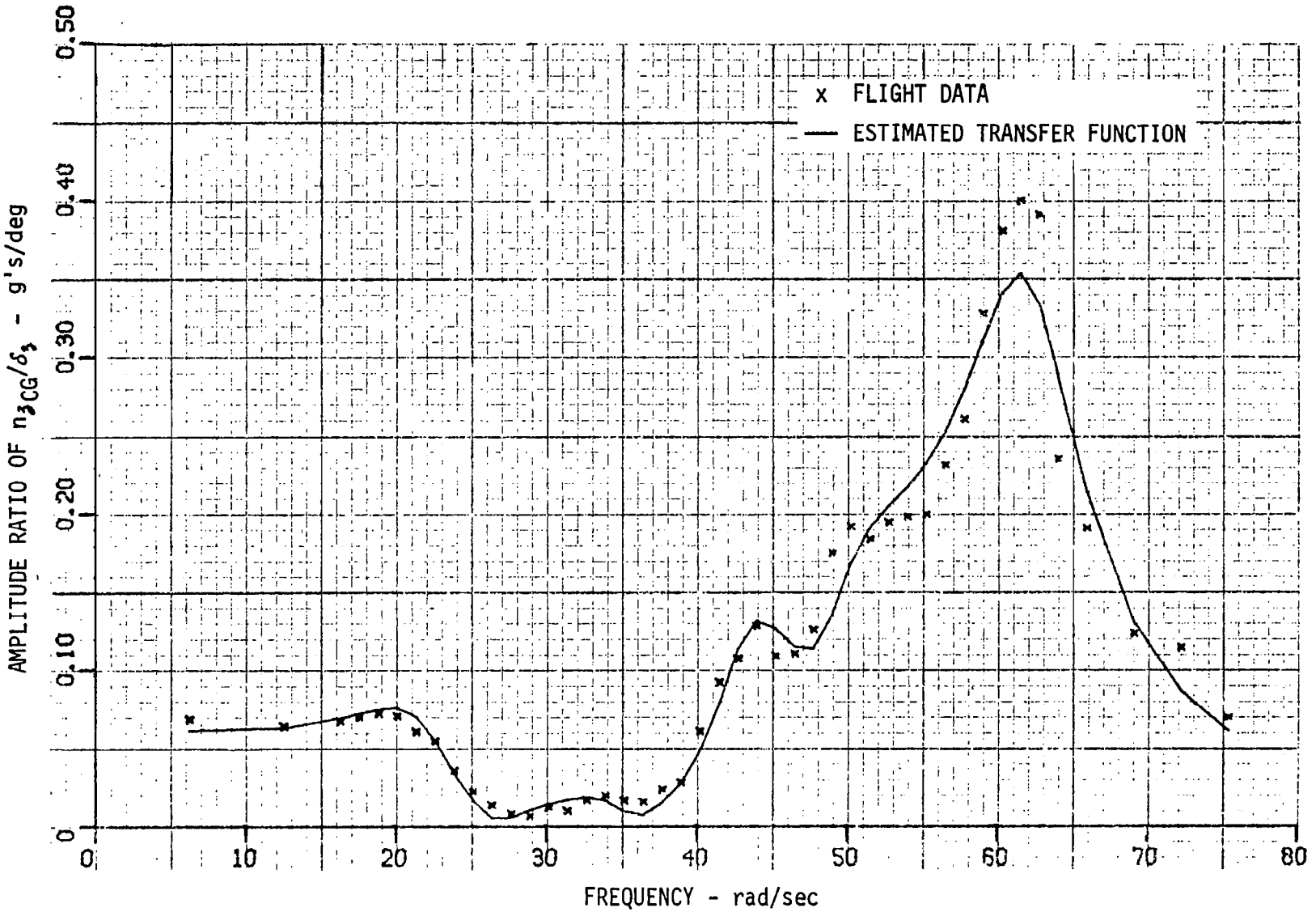

Figure D-4 FREQUENCY RESPONSE, C.G. ACCELERATION ($n_{z_{CG}}$)/DLF DEFLECTION (δ_z)

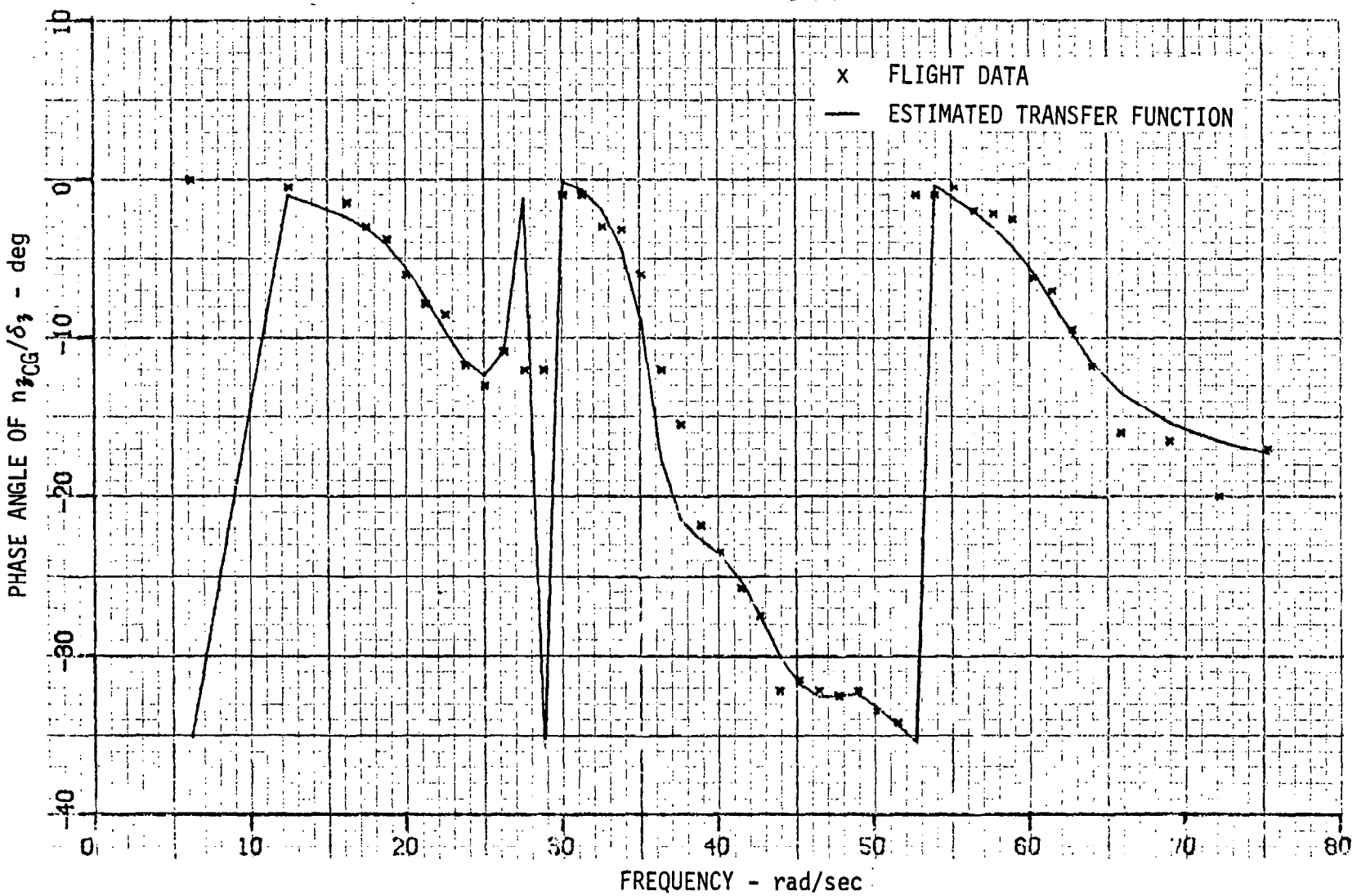

Figure D-5 FREQUENCY RESPONSE, C.G. ACCELERATION ($n_{z_{CG}}$)/ DLF DEFLECTION (δ_z)

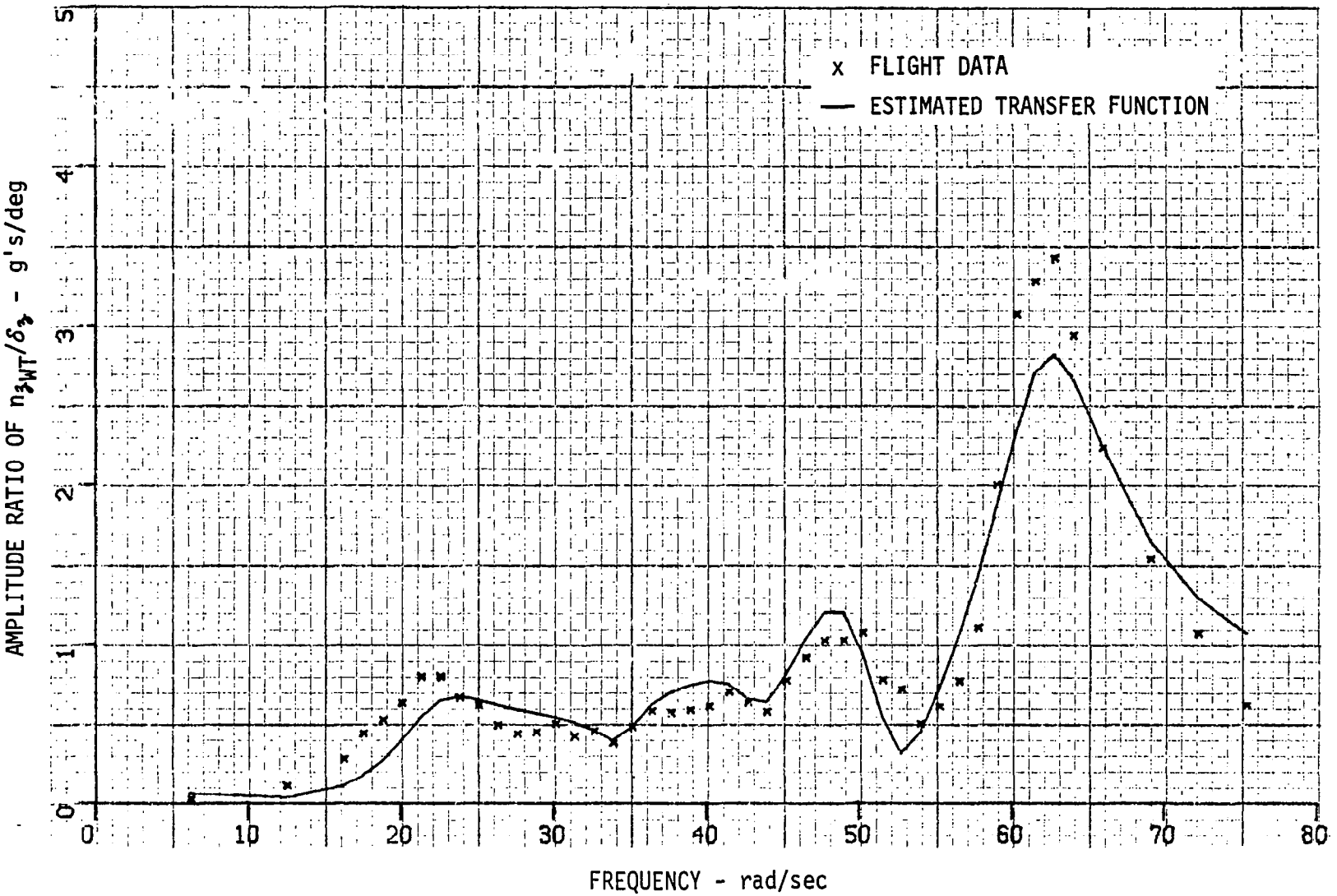

Figure D-6 FREQUENCY RESPONSE, WING TIP ACCELERATION ($n_{z_{WT}}$)/DEFLECTION (δ_z)

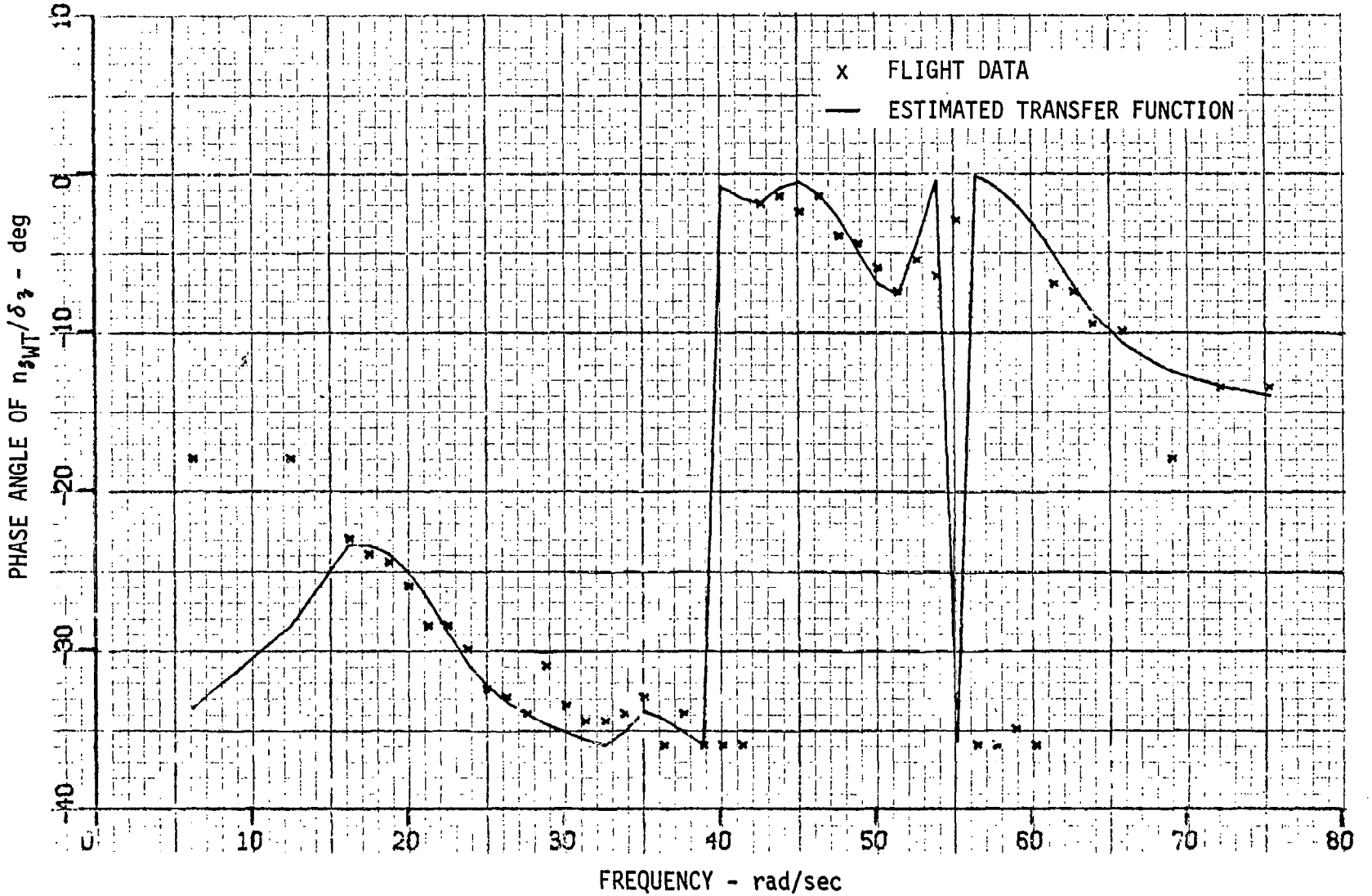

Figure D-7 FREQUENCY RESPONSE, WING TIP ACCELERATION ($n_{z_{WT}}$)/DEFLECTION (δ_z)

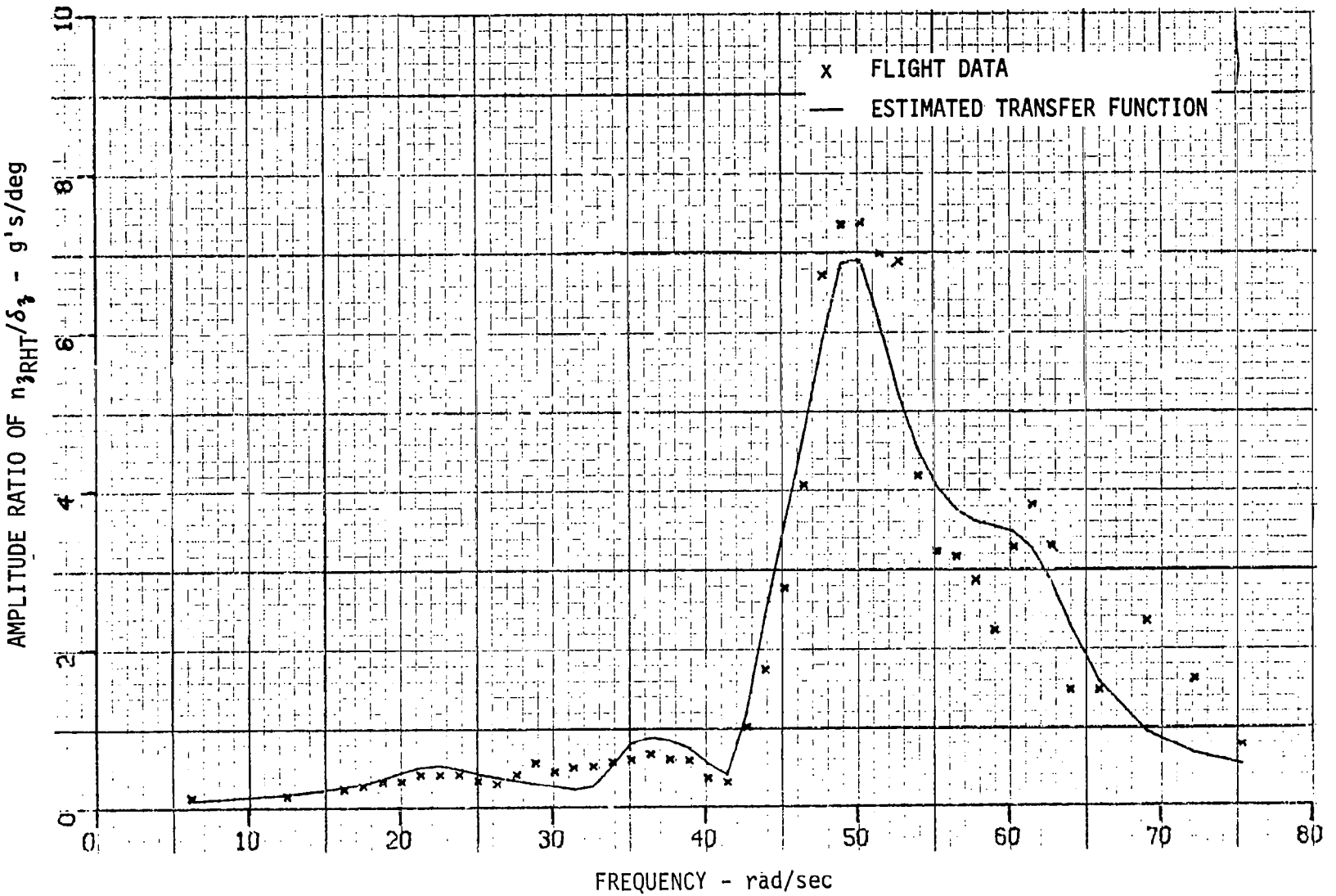

Figure D-8 FREQUENCY RESPONSE, STABILIZER TIP ACCELERATION ($n_{z_{RHT}}$)/ DLF DEFLECTION (δ_3)

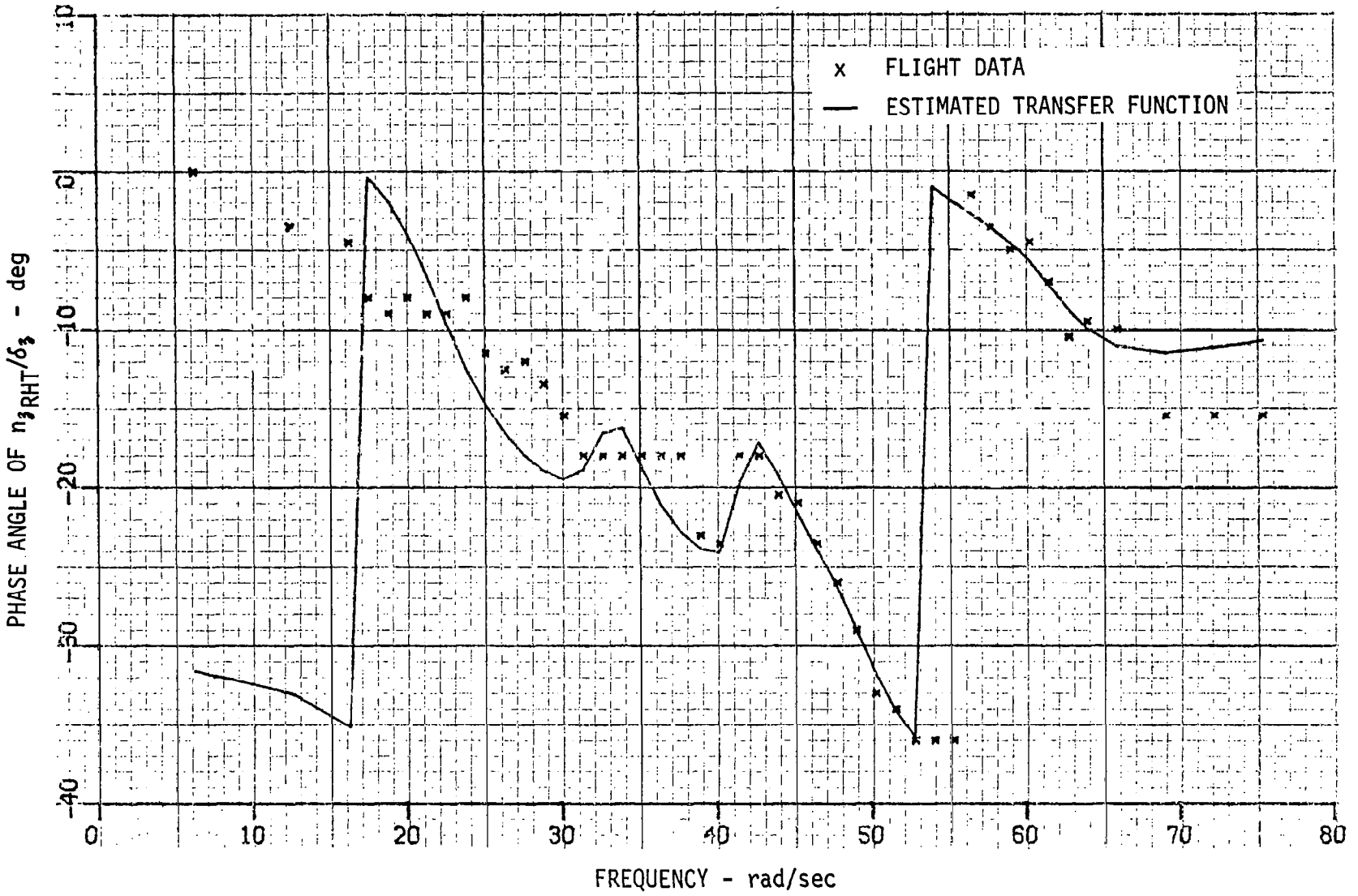

Figure D-9 FREQUENCY RESPONSE, STABILIZER TIP ACCELERATION ($n_{z_{RHT}}$)/DEFLECTION (δ_z)

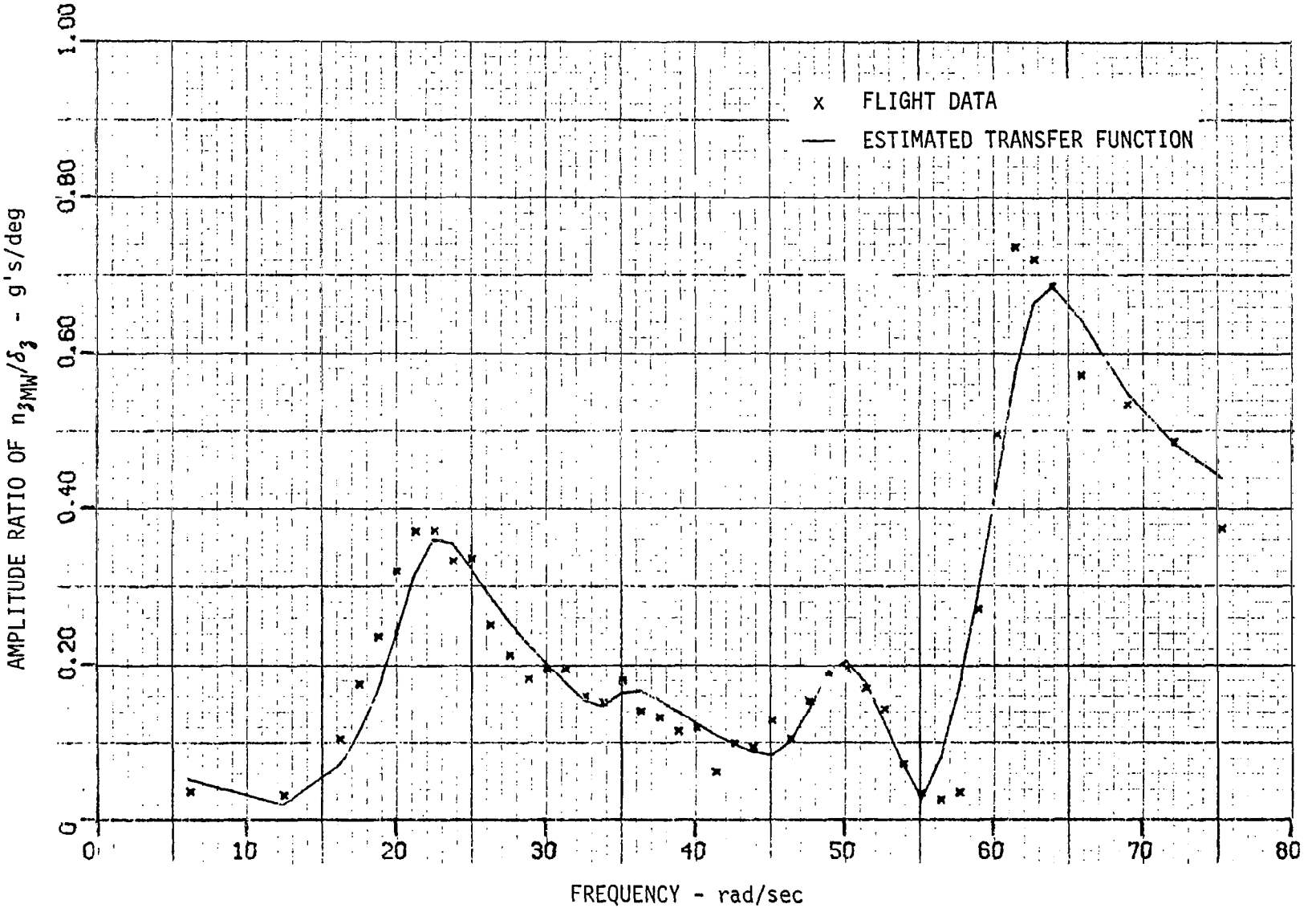

Figure D-10 FREQUENCY RESPONSE, MID WING ACCELERATION((n_{3MW})/ DEFLECTION (δ_3)

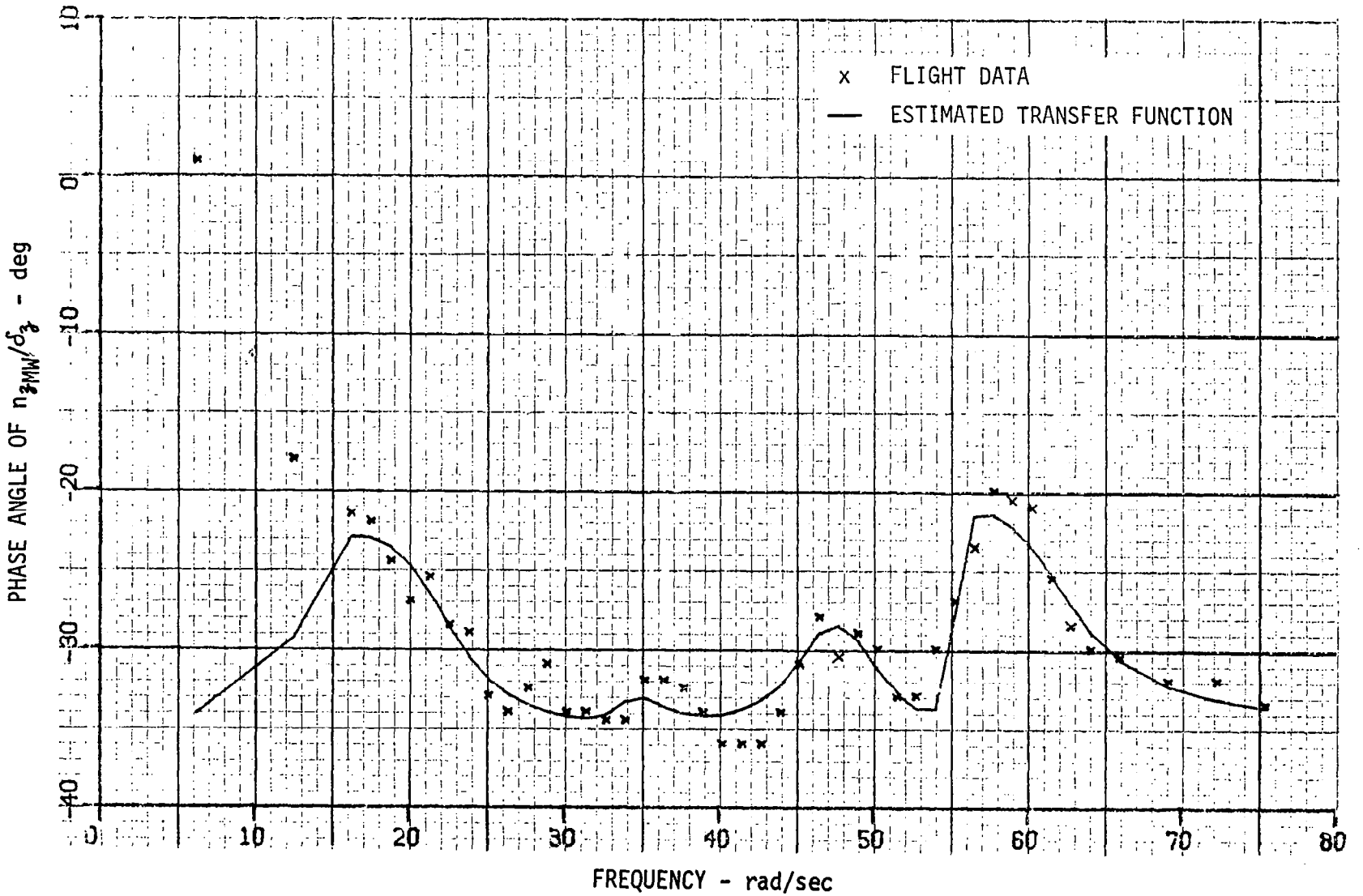

Figure D-11 FREQUENCY RESPONSE, MID WING ACCELERATION ($n_{z_{MW}}$)/DLF DEFLECTION (δ_z)

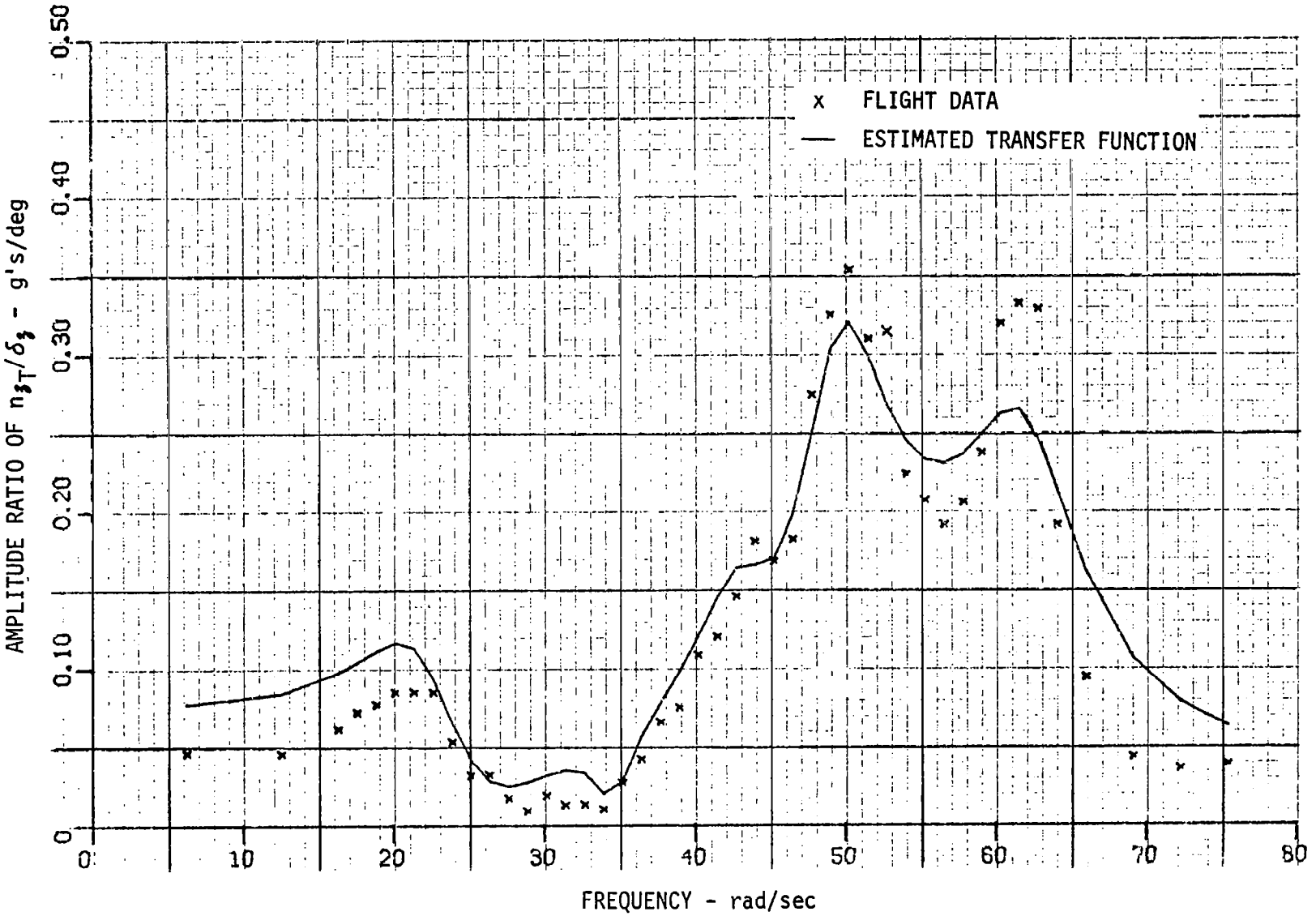

Figure D-12 FREQUENCY RESPONSE, TAIL CONE ACCELERATION (n_{z_T})/ DLF DEFLECTION (δ_z)

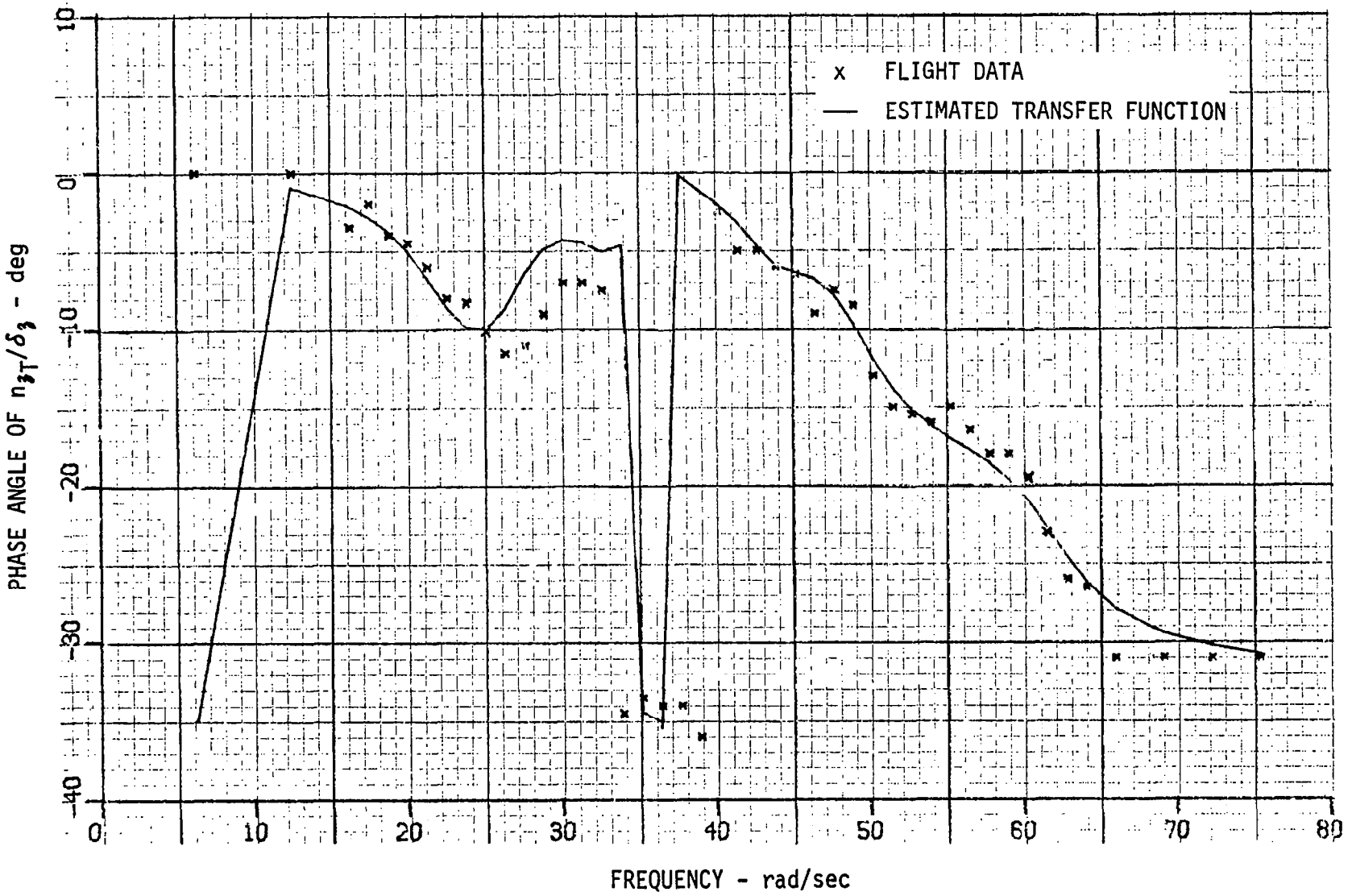

Figure D-13 FREQUENCY RESPONSE, TAIL CONE ACCELERATION (n_{z_T})/DLF DEFLECTION (δ_z)

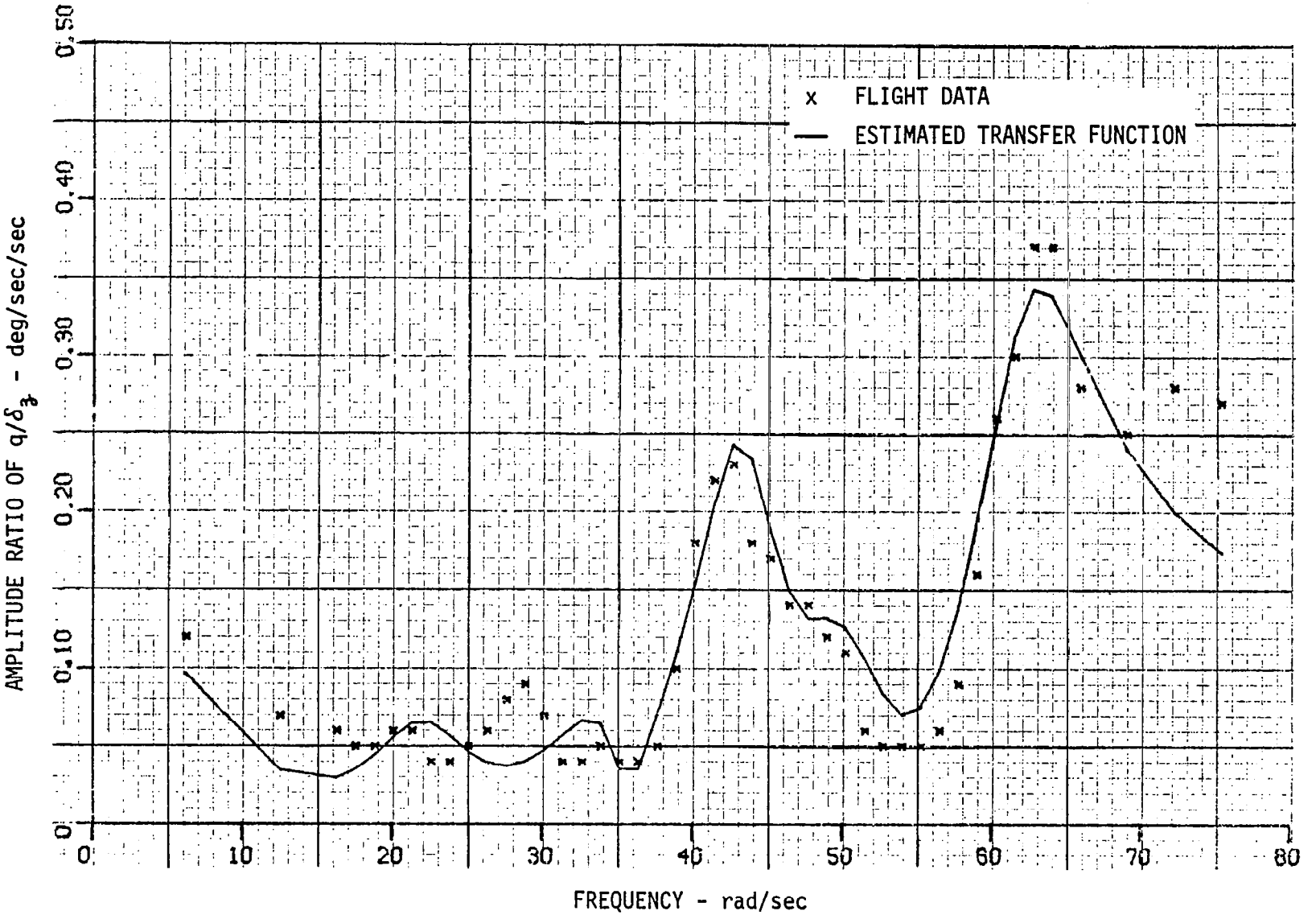

Figure D-14 FREQUENCY RESPONSE, PITCH RATE (q)/DLF DEFLECTION (δ_3)

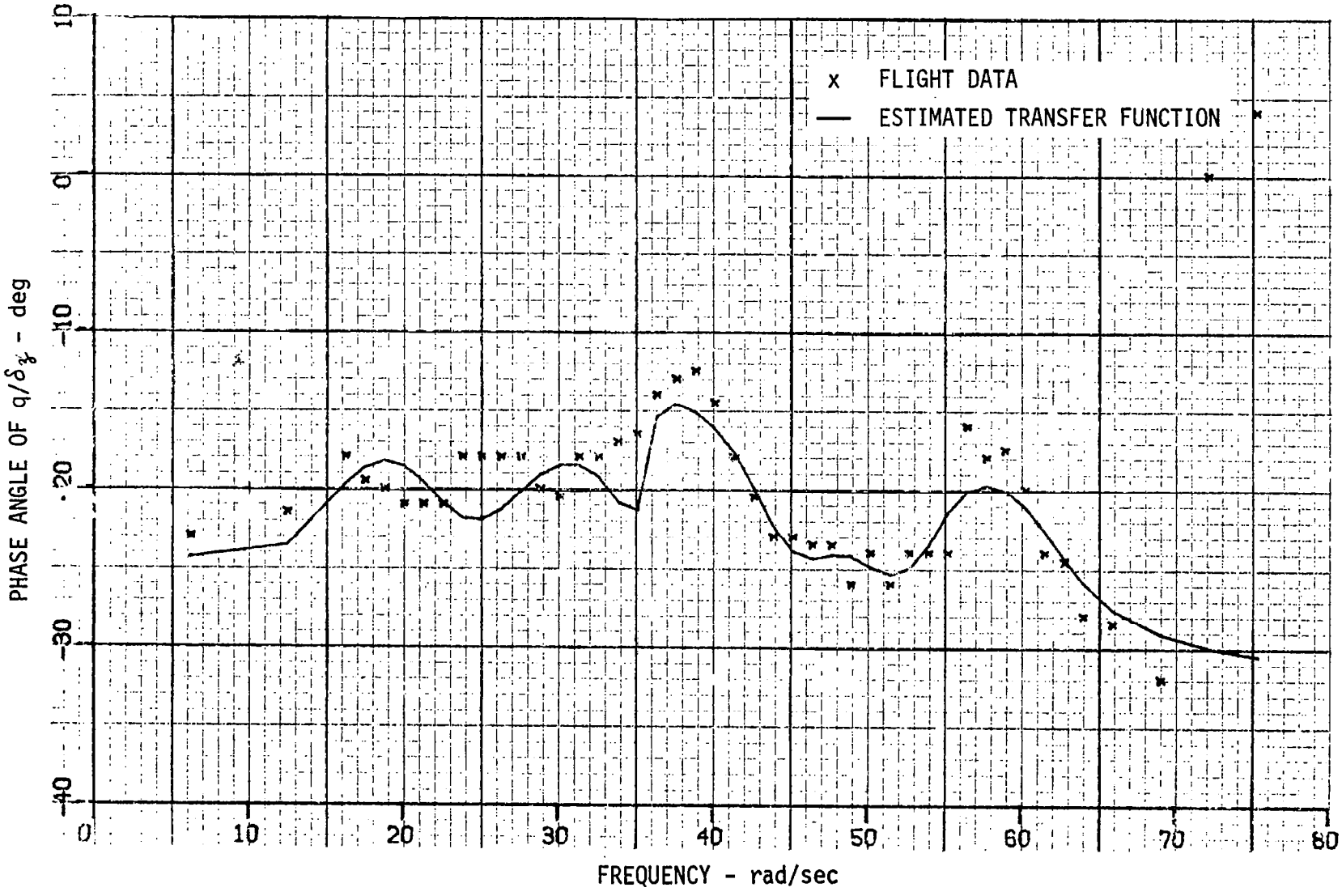

Figure D-15 FREQUENCY RESPONSE, PITCH RATE (q)/DLF DEFLECTION (δ_z)

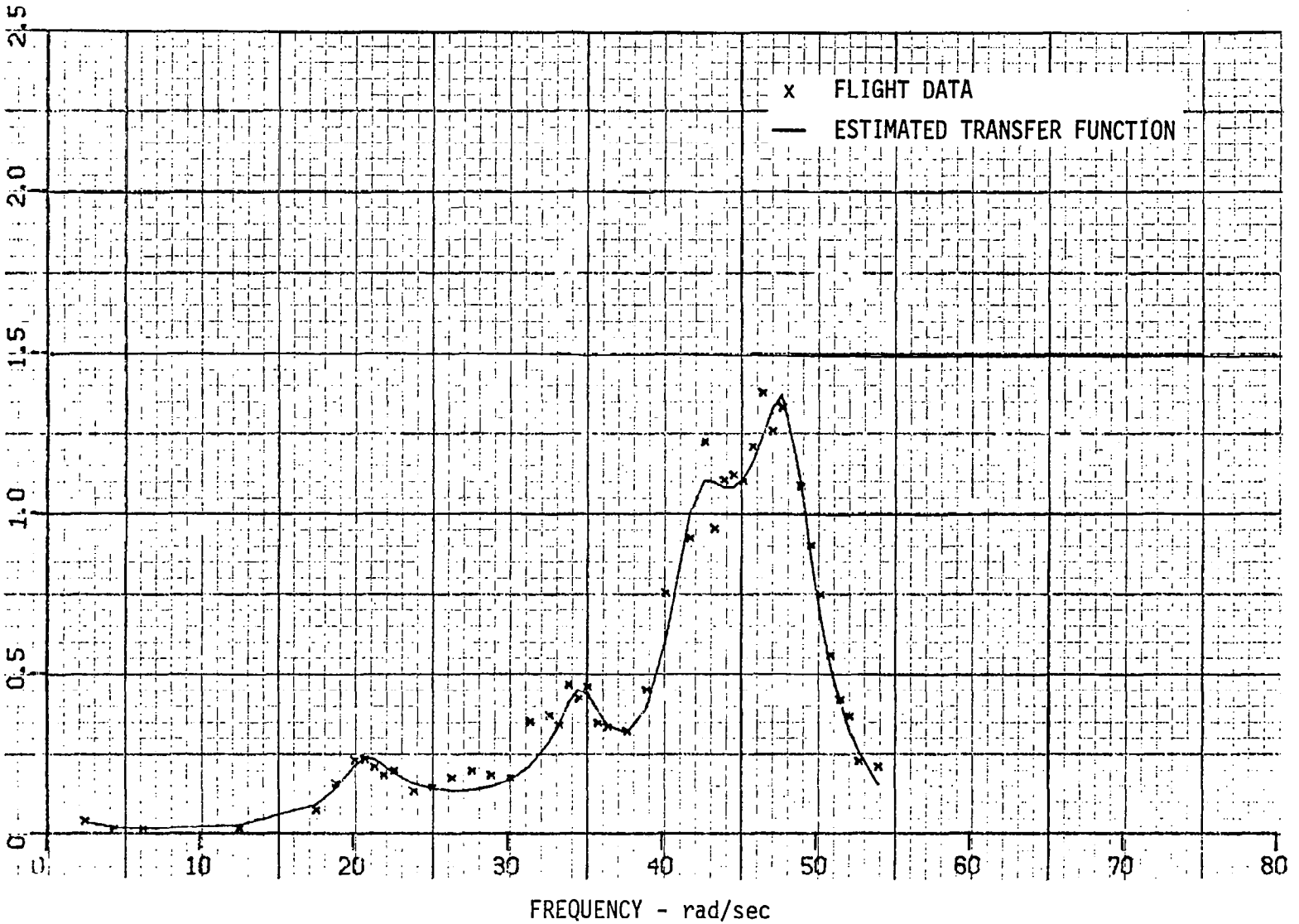

Figure D-16 FREQUENCY RESPONSE, WING TIP ACCELERATION ($n_{z_{WT}}$)/ELEVATOR DEFLECTION (δ_e)

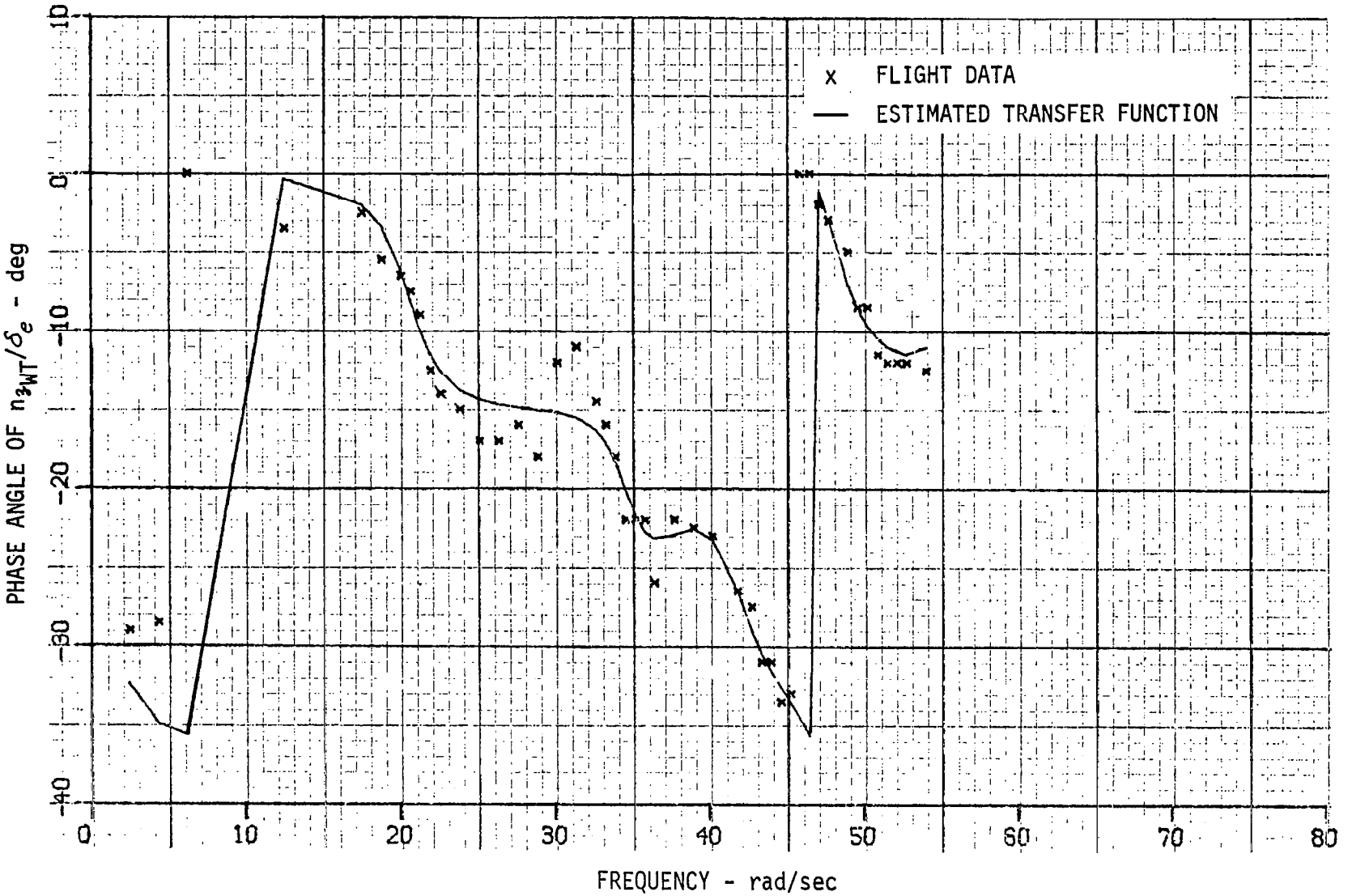

Figure D-17 FREQUENCY RESPONSE, WING TIP ACCELERATION ($n_{z_{WT}}$)/ ELEVATOR DEFLECTION (δ_e)

Transfer Functions

The following transfer functions were obtained: (The units are g's. deg. deg/sec). X, Y, Z locations for these accelerometers can be found in Reference 6.

448 km/hr

$n_{z_{pilot}}/\delta_{z_c}$
$n_{z_{CG}}/\delta_{z_c}$
$n_{z_{wing\ tip}}/\delta_{z_c}$
$n_{z_{mid\ wing}}/\delta_{z_c}$
$n_{z_{stabilizer\ tip}}/\delta_{z_c}$
$n_{z_{tail\ cone}}/\delta_{z_c}$
q/δ_{z_c}

} two sets - with first order δ_z/δ_{z_c}
with second order δ_z/δ_{z_c}

245 km/hr

$n_{z_{pilot}}/\delta_{z_c}$
$n_{z_{CG}}/\delta_{z_c}$
$n_{z_{wing\ tip}}/\delta_{z_c}$
$n_{z_{mid\ wing}}/\delta_{z_c}$
$n_{z_{stabilizer\ tip}}/\delta_{z_c}$
$n_{z_{tail\ cone}}/\delta_{z_c}$
q/δ_z

} two sets - with first order δ_z/δ_{z_c}
with second order δ_z/δ_{z_c}

245 km/hr

$n_{z_{pilot}}/\delta_{z_c}$
$n_{z_{CG}}/\delta_{z_c}$
$n_{z_{wing\ tip}}/\delta_{z_c}$
$n_{z_{stabilizer\ tip}}/\delta_{z_c}$
$n_{z_{tail\ cone}}/\delta_{z_c}$
q/δ_{z_c}

} two sets - with first order δ_z/δ_{z_c}
with second order δ_z/δ_{z_c}

(The mid wing accelerometer located near the forward wing spar at the side force surface was not excited enough with the elevator to obtain good data).

All of these complete transfer functions are presented below without actuator dynamics.

COMBINED RIGID AND FLEXIBLE

TRANSFER FUNCTIONS WITHOUT ACTUATOR DYNAMICS

NUMERATORS

TIFS/ACT PILOT/DZ 448 km/hr

CN=	1.19023D+10	S^0 0.0	8.54944D+12	S^1 0.0	1.10935D+15	S^2 0.0	-8.53749D+14	S^3 0.0
	-4.45477D+14	S^4 0.0	7.56776D+12	S^5 0.0	-9.50271D+11	S^6 0.0	1.97680D+10	S^7 0.0
	-7.38660D+08	S^8 0.0	1.53185D+07	S^9 0.0	-2.71714D+05	S^{10} 0.0	3.86237D+03	S^{11} 0.0
	-6.53636D+01	S^{12} 0.0	7.28737D-02	S^{13} 0.0	-9.93810D-03	S^{14} 0.0		

TIFS/ACT CG/DZ 448 km/hr

CN=	1.19023D+10	0.0	8.50146D+12	0.0	1.10154D+15	0.0	-9.07484D+14	0.0
	-5.92805D+14	0.0	-6.40131D+12	0.0	-2.03218D+12	0.0	-1.15414D+10	0.0
	-2.50436D+09	0.0	-7.09081D+06	0.0	-1.36202D+06	0.0	-8.71244D+02	0.0
	-3.07103D+02	0.0	2.66140D-01	0.0	-1.90327D-02	0.0		

TIFS/ACT WING TIP/DZ 448 km/hr

CN=	1.19023D+10	0.0	9.17418D+12	0.0	1.18919D+15	0.0	-9.55680D+14	0.0
	-6.84340D+14	0.0	-3.25395D+13	0.0	-5.13759D+12	0.0	-9.25245D+10	0.0
	-5.86357D+09	0.0	-7.74597D+07	0.0	-9.50483D+05	0.0	-2.20378D+04	0.0
	9.35121D+02	0.0	-1.49944D+00	0.0	2.67278D-01	0.0		

TIFS/ACT MID WING/DZ 448 km/hr

CN=	1.19023D+10	0.0	8.64180D+12	0.0	1.11971D+15	0.0	-9.07134D+14	0.0
	-6.28323D+14	0.0	-2.41357D+13	0.0	-5.17120D+12	0.0	-7.83555D+10	0.0
	-9.45272D+09	0.0	-8.34407D+07	0.0	-6.95694D+06	0.0	-3.52805D+04	0.0
	-2.25373D+03	0.0	-5.09665D+00	0.0	-2.66572D-01	0.0		

TIFS/ACT STAB TIP/DZ 448 km/hr

CN=	1.19023D+10	0.0	8.46265D+12	0.0	1.09616D+15	0.0	-8.13403D+14	0.0
	-7.99968D+14	0.0	-8.91684D+13	0.0	-5.69781D+11	0.0	-3.04314D+11	0.0
	5.97136D+07	0.0	-3.48439D+08	0.0	-1.71674D+05	0.0	-1.50150D+05	0.0
	-6.26460D+01	0.0	-1.90061D+01	0.0	3.80174D-02	0.0		

TIFS/ACT TAIL CONE/DZ 448 km/hr

CN=	1.19023D+10	0.0	8.60463D+12	0.0	1.11350D+15	0.0	-1.01426D+15	0.0
	-7.47076D+14	0.0	-7.00408D+12	0.0	-2.30552D+12	0.0	-7.73128D+09	0.0
	-2.49084D+09	0.0	-5.42215D+05	0.0	-1.19791D+06	0.0	1.69792D+03	0.0
	-2.76998D+02	0.0	3.49055D-01	0.0	-2.90006D-02	0.0		

TIFS/ACT Q/DZ 448 km/hr

CN=	0.0	0.0	-6.95213D+13	0.0	-4.32699D+15	0.0	-7.14759D+15	0.0
	-2.21542D+14	0.0	-4.66892D+13	0.0	-4.26971D+11	0.0	-6.80977D+10	0.0
	2.16676D+08	0.0	-6.75635D+07	0.0	7.44077D+05	0.0	-2.18090D+04	0.0
	4.11552D+02	0.0	-2.42456D+00	0.0	6.69551D-02	0.0		

DENOMINATOR 448 km/hr

CD=	1.19023D+14	0.0	8.13678D+14	0.0	5.43716D+16	0.0	3.37463D+16	0.0
	1.15970D+16	0.0	3.92367D+14	0.0	4.72112D+13	0.0	8.79189D+11	0.0
	6.45069D+10	0.0	7.44536D+08	0.0	3.85969D+07	0.0	2.64098D+05	0.0
	1.03357D+04	0.0	3.27080D+01	0.0	1.00000D+00	0.0		

NUMERATORS

S/ACT PILOT/DZ 245 km/hr			
-1.48624D+11 S^0 0.0	-1.23282D+12 S^1 0.0	1.03694D+14 S^2 0.0	-5.82045D+13 S^3 0.0
-3.51953D+13 S^4 0.0	-1.85795D+11 S^5 0.0	4.70420D+09 S^6 0.0	1.46820D+08 S^7 0.0
1.47858D+08 S^8 0.0	7.24329D+05 S^9 0.0	1.57883D+05 S^{10} 0.0	4.57364D+02 S^{11} 0.0
5.53280D+01 S^{12} 0.0	7.51333D-02 S^{13} 0.0	5.56191D-03 S^{14} 0.0	

TIFS/ACT CG/DZ 245 km/hr							
CN= -1.48624D+11	0.0	-1.22917D+12	0.0	1.02513D+14	0.0	-7.55300D+13	0.0
-6.80194D+13	0.0	-9.31697D+11	0.0	-2.36628D+11	0.0	-2.19658D+09	0.0
-3.19844D+08	0.0	-1.96558D+06	0.0	-1.96384D+05	0.0	-6.44878D+02	0.0
-4.91925D+01	0.0	-4.99145D-02	0.0	-3.15456D-03	0.0		

TIFS/ACT WING TIP/DZ 245 km/hr							
CN= -1.48624D+11	0.0	-1.25821D+12	0.0	1.02385D+14	0.0	-6.02353D+13	0.0
-9.13952D+13	0.0	-1.73987D+13	0.0	-1.45299D+12	0.0	-7.16863D+10	0.0
-2.13042D+09	0.0	-8.25802D+07	0.0	-7.89279D+05	0.0	-3.55850D+04	0.0
8.27029D+01	0.0	-5.03070D+00	0.0	5.91267D-02	0.0		

TIFS/ACT MID WING/DZ 245 km/hr							
CN= -1.48624D+11	0.0	-1.22353D+12	0.0	1.02513D+14	0.0	-8.09444D+13	0.0
-6.74148D+13	0.0	8.71305D+11	0.0	-8.47004D+11	0.0	-4.76638D+08	0.0
-1.74384D+09	0.0	-2.67245D+06	0.0	-1.39589D+06	0.0	-1.82330D+03	0.0
-4.87043D+02	0.0	-3.57861D-01	0.0	-6.18077D-02	0.0		

TIFS/ACT STAB TIP/DZ 245 km/hr							
CN= -1.48624D+11	0.0	-1.22055D+12	0.0	1.01311D+14	0.0	-1.01943D+14	0.0
-9.22391D+13	0.0	8.96834D+12	0.0	3.24290D+10	0.0	3.32438D+10	0.0
7.94001D+08	0.0	3.72441D+07	0.0	1.06213D+06	0.0	1.45066D+04	0.0
4.54669D+02	0.0	1.29116D+00	0.0	6.43416D-02	0.0		

TIFS/ACT TAIL CONE/DZ 245 km/hr							
CN= -1.48624D+11	0.0	-1.22949D+12	0.0	1.00926D+14	0.0	-9.38559D+13	0.0
-1.06226D+14	0.0	-2.18329D+12	0.0	-3.61753D+11	0.0	-5.27097D+09	0.0
-4.15154D+08	0.0	-4.28610D+06	0.0	-2.05514D+05	0.0	-1.27495D+03	0.0
-4.62335D+01	0.0	-9.24926D-02	0.0	-4.32312D-03	0.0		

TIFS/ACT Q/DZ 245 km/hr							
CN= 0.0	0.0	-6.98477D+13	0.0	-8.59361D+14	0.0	-1.76143D+15	0.0
-4.95808D+13	0.0	-1.39754D+13	0.0	-1.56939D+11	0.0	-3.25604D+10	0.0
-1.61469D+08	0.0	-3.04055D+07	0.0	-4.43950D+04	0.0	-1.18830D+04	0.0
9.42873D+00	0.0	-1.61857D+00	0.0	3.98447D-03	0.0		

DENOMINATOR 245 km/hr							
CD= 2.12320D+14	0.0	3.07773D+14	0.0	1.39217D+16	0.0	1.53079D+16	0.0
8.00141D+15	0.0	1.92939D+14	0.0	3.55929D+13	0.0	4.70738D+11	0.0
5.19491D+10	0.0	4.28726D+08	0.0	3.32013D+07	0.0	1.62802D+05	0.0
9.54914D+03	0.0	2.15905D+01	0.0	1.00000D+00	0.0		

NUMERATORS

TIFS/ACT PILOT/DE 245 km/hr

CN= -1.25906D+12 S^0 0.0	-3.91615D+13 S^1 0.0	1.52923D+15 S^2 0.0	1.71511D+14 S^3 0.0
2.69468D+14 S^4 0.0	2.55143D+12 S^5 0.0	9.41943D+11 S^6 0.0	2.51898D+09 S^7 0.0
1.00577D+09 S^8 0.0	-1.26663D+06 S^9 0.0	4.68191D+05 S^{10} 0.0	-1.60317D+03 S^{11} 0.0
1.10760D+02 S^{12} 0.0	-3.21930D-01 S^{13} 0.0	1.18294D-02 S^{14} 0.0	

TIFS/ACT CG/DE 245 km/hr

CN= -1.25906D+12	0.0	-3.91412D+13	0.0	1.51840D+15	0.0	-6.40489D+13	0.0
-4.72865D+13	0.0	-9.95268D+11	0.0	-1.72875D+11	0.0	-5.59708D+08	0.0
-5.26882D+07	0.0	1.50722D+06	0.0	1.20875D+05	0.0	1.19363D+03	0.0
7.66204D+01	0.0	2.10772D-01	0.0	1.21863D-02	0.0		

TIFS/ACT WING TIP/DE 245 km/hr

CN= -1.25906D+12	0.0	-3.93376D+13	0.0	1.52519D+15	0.0	-1.17186D+14	0.0
-3.41482D+13	0.0	-8.24174D+11	0.0	4.28943D+11	0.0	2.14464D+09	0.0
9.28576D+08	0.0	-7.26249D+05	0.0	8.18994D+05	0.0	-2.03547D+03	0.0
3.70026D+02	0.0	-4.41160D-01	0.0	6.07712D-02	0.0		

TIFS/ACT STAB TIP/DE 245 km/hr

CN= -1.25906D+12	0.0	-3.91287D+13	0.0	1.51156D+15	0.0	-4.73899D+14	0.0
-4.15679D+14	0.0	2.45632D+13	0.0	-4.84560D+12	0.0	3.27689D+10	0.0
-1.51407D+10	0.0	-5.18375D+07	0.0	-1.62357D+07	0.0	-7.05063D+04	0.0
-6.73630D+03	0.0	-1.91630D+01	0.0	-9.10437D-01	0.0		

TIFS/ACT TAIL CONE/DE 245 km/hr

CN= -1.25906D+12	0.0	-3.91298D+13	0.0	1.50614D+15	0.0	-3.52377D+14	0.0
-4.29049D+14	0.0	-5.57915D+12	0.0	-2.03389D+12	0.0	-1.55140D+10	0.0
-3.18612D+09	0.0	-1.57815D+07	0.0	-2.16877D+06	0.0	-6.40636D+03	0.0
-6.56227D+02	0.0	-8.48492D-01	0.0	-7.25200D-02	0.0		

TIFS/ACT Q/DE 245 km/hr

CN= 0.0	0.0	-5.92371D+14	0.0	-1.30316D+16	0.0	-1.75154D+16	0.0
-4.49433D+14	0.0	-7.09228D+13	0.0	-1.42624D+12	0.0	-8.74923D+10	0.0
-1.72248D+09	0.0	-4.40059D+07	0.0	-1.02568D+06	0.0	-9.73880D+03	0.0
-3.02263D+02	0.0	-8.19934D-01	0.0	-3.47044D-02	0.0		

DENOMINATOR 245 km/hr

CD= 2.12320D+14	0.0	3.07773D+14	0.0	1.39217D+16	0.0	1.53079D+16	0.0
8.00141D+15	0.0	1.92939D+14	0.0	3.55929D+13	0.0	4.70738D+11	0.0
5.19491D+10	0.0	4.28726D+08	0.0	3.32013D+07	0.0	1.62802D+05	0.0
9.54914D+03	0.0	2.15905D+01	0.0	1.00000D+00	0.0		

FACTORED 448 km/hr DENOMINATOR

REAL	IMAG	$-2\zeta\omega$	ω^2	ζ	ω (rad/sec)
-3.85690D+00	6.20841D+01	-7.71380D+00	3.86932D+03	6.20042D-02	6.22038D+01
-2.77343D+00	-4.94847D+01	-5.94685D+00	2.45758D+03	5.99796D-02	4.95739D+01
-2.68109D+00	-4.31455D+01	-5.36217D+00	1.86872D+03	6.20210D-02	4.32287D+01
-2.07701D+00	-3.45577D+01	-4.15402D+00	1.19855D+03	5.99945D-02	3.46200D+01
-3.23429D+00	-2.20697D+01	-6.46858D+00	4.97531D+02	1.45000D-01	2.23054D+01
-1.52440D+00	-1.66174D+00	-3.04881D+00	5.08518D+00	6.75999D-01	2.25504D+00
-6.86174D-03	-4.64946D-02	-1.37235D-02	2.20883D-03	1.46000D-01	4.69982D-02

FACTORED 245 km/hr DENOMINATOR

REAL	IMAG	$-2\zeta\omega$	ω^2	ζ	ω (rad/sec)
-2.65409D+00	6.02610D+01	-5.30818D+00	3.63843D+03	4.40006D-02	6.03194D+01
-1.83232D+00	-4.82135D+01	-3.66465D+00	2.32790D+03	3.79770D-02	4.82483D+01
-1.59460D+00	-3.46429D+01	-3.18920D+00	1.20267D+03	4.59609D-02	3.46796D+01
-1.97178D+00	-4.18717D+01	-3.94355D+00	1.75713D+03	4.70386D-02	4.19181D+01
-1.76250D+00	-2.06596D+01	-3.52499D+00	4.29926D+02	8.50024D-02	2.07347D+01
-9.77349D-01	-9.09663D-01	-1.95470D+00	1.78270D+00	7.32000D-01	1.33518D+00
-2.60758D-03	-1.24380D-01	-5.21516D-03	1.54771D-02	2.09601D-02	1.24407D-01

Appendix E

EXPLICIT-IMPLICIT MODEL-FOLLOWING RELATIONSHIPS

The maneuver load control system of Section V formulated the problem first as a feedback or an implicit model-following system with wing root beinding moment and torsion tradeoffs. The system was then transformed into feedforward, command augmentation or explicit model-following systems. This appendix will show how this transformation was accomplished, the equivalency and relationships between the two methods of control system synthesis and also some of the characteristics, advantages and disadvantages of each method of control system synthesis.

Consider the two block diagrams below that schematically show the feedforward and feedback model following configurations.

If the aircraft under control is given by

$$\dot{x}_p = F_p x_p + G_p u_p \tag{E-1}$$

and the model is given by

$$x_m = F_m x_m + G_m u_c \tag{E-2}$$

then the control law for feedforward model following is given by

$$u_p = K_1 x_m + K_2 u_c \tag{E-3}$$

and for feedback model following

$$u_p = K_2 u_m - K_1 x_p \tag{E-4}$$

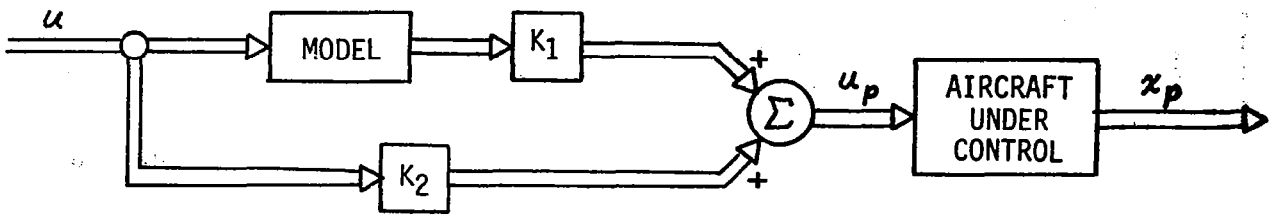

FEEDFORWARD OR EXPLICIT MODEL FOLLOWING

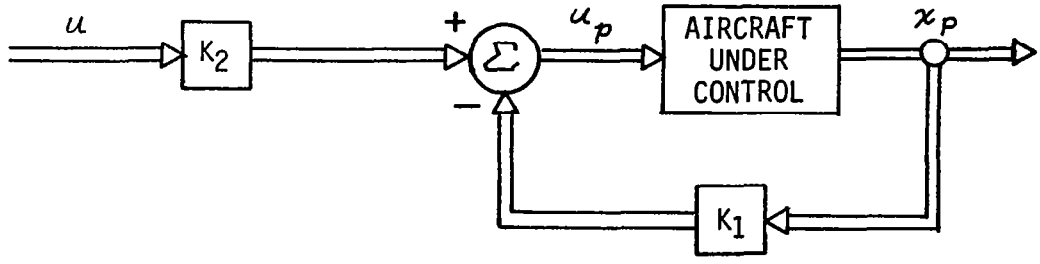

FEEDBACK OR IMPLICIT MODEL FOLLOWING

Figure E-1 MODEL FOLLOWING CONFIGURATIONS

The matrices of gains for both Equations (E-3) and (E-4) are given by

$$K_2 = (G_p^T G_p)^{-1} G_p^T G_m \qquad \text{(E-5)}$$

$$K_1 = (G_p^T G_p)^{-1} G_p^T (F_m - F_p) \qquad \text{(E-6)}$$

The gain matrices of Equations (E-5) and (E-6) are a function of the model dynamics and the aircraft dynamics, and feedback is not required to theoretically obtain exact model following. It is a relatively simple matter to switch from one configuration to the other. The maneuver load control system was mechanized as a feedforward system so that the feedback gains could be used for purposes other than maneuver load control; specifically for structural mode suppression.

An even more advantageous model-following configuration is shown in Figure E-2 below.

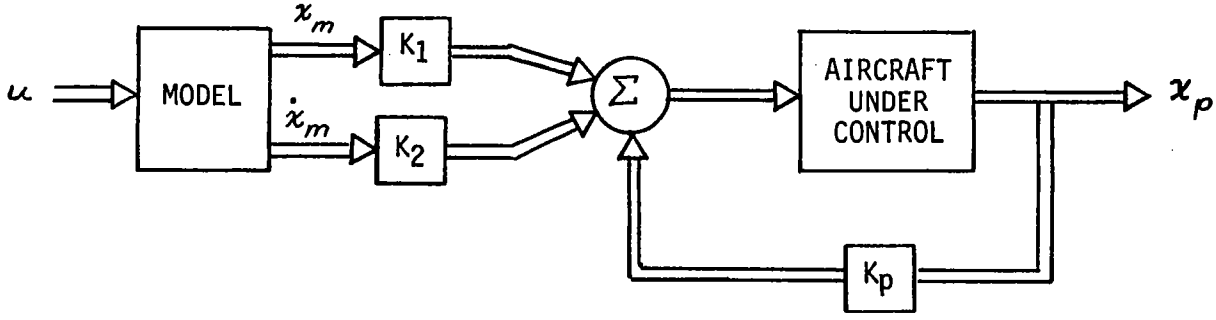

Figure E-2 IMPROVED MODEL-FOLLOWING CONFIGURATION

The matrix of gains is given by

$$K_1 = (G_p^T G_p)^{-1} G_p^T \tag{E-7}$$

$$K_2 = -(G_p^T G_p)^{-1} G_p^T (F_p - G_p K_p) \tag{E-8}$$

which shows that model following can be accomplished independently of the model dynamic characteristics and for any feedback configuration.

The model-following configuration shown above can only be obtained if the number of independent control variables is equal to the number of degrees of freedom of motion of the aircraft. In maneuver load control applications, this may not be a problem because an actively controlled airplane can generally be assumed to have more than the usual compliment of active surfaces, and perhaps even a redundancy of independent ways to control the aircraft.

E.1 NUMBER OF CONTROLLERS LESS THAN NUMBER OF DEGREES OF FREEDOM

Although less likely to happen for an aircraft using active control technology, a feedback design can be partially cast into a feedforward configuration if the number of control surfaces directly commanded by the pilot is less than the number of degrees of freedom of motion of the vehicle.

To do this the equations of motion of the aircraft and the model are partitioned as

$$\begin{bmatrix} \dot{x}_1 \\ \dot{x}_2 \end{bmatrix} = \left[\begin{array}{c|c} F_{11} & F_{12} \\ \hline F_{12} & F_{22} \end{array}\right] \begin{bmatrix} x_1 \\ x_2 \end{bmatrix} + \begin{bmatrix} G_1 \\ G_2 \end{bmatrix} u \qquad \text{Aircraft} \qquad \begin{matrix} \text{(E-9a)} \\ \text{(E-9b)} \end{matrix}$$

$$\begin{bmatrix} \dot{x}_{1m} \\ \dot{x}_{2m} \end{bmatrix} = \left[\begin{array}{c|c} F_{11m} & F_{12m} \\ \hline F_{21m} & F_{22m} \end{array}\right] \begin{bmatrix} x_{1m} \\ x_{2m} \end{bmatrix} + \begin{bmatrix} G_{1m} \\ G_{2m} \end{bmatrix} u_m \qquad \text{Model} \qquad \begin{matrix} \text{(E-10a)} \\ \text{(E-10b)} \end{matrix}$$

The objective is to define a control law such that $x_2(t) = x_{2m}(t)$. The control matrix partition G_2 is of rank equal to the number of available independent control surfaces. Assume a control law of the form

$$u = K_1 \dot{x}_{2m} + K_2 x_{2m} + K_3 x_1 \tag{E-11}$$

Substituting Equation (E-11) into Equation (E-9b) yields

$$\dot{x}_2 = (F_{21} + G_2 K_3) x_1 + F_{22} x_2 + G_2 K_1 \dot{x}_{2m} + G_2 K_2 x_{2m} \tag{E-12}$$

By taking the Laplace transform of both sides of Equation (E-11) the conditions for model following become immediately apparent.

$$(Is - F_{22}) x_2(s) = (F_{21} + G_2 K_3) x_1(s) + G_2 K_1 Is + G_2 K_2) x_{2m}(s) \tag{E-13}$$

The model-following requirements are satisfied if the following conditions are satisfied:

$$F_{21} + G_2 K_3 = 0 \qquad K_3 = -(G_2^T G_2)^{-1} G_2^T F_{21} \tag{E-14a}$$

$$G_2 K_2 = -F_{22} \qquad K_2 = -(G_2^T G_2)^{-1} G_2^T F_{22} \tag{E-14b}$$

$$G_2 K_1 = I \qquad K_1 = (G_2^T G_2)^{-1} G_2^T \tag{E-14c}$$

Equations (E-14) show that feedback is required to formulate a model following or command augmentation system if exact model following is desired for some of the states and if the number of control surfaces is less than the number of degrees of freedom of motion of the aircraft under control. The feedback is not from the model-following states, but instead is from those states not expected to follow the model. The stability of the model-following system shown above is determined by the roots of $|Is - F_{22}| = 0$ and $|Is - F_{11} + G_1 K_3| = 0$, but considerable freedom exists in selecting feedback for stability and other purposes.

E.2 OPTIMAL FEEDFORWARD MODEL FOLLOWING

Optimal model following can yield a wide range of solutions depending upon the performance index chosen. A typical performance index is

$$V = \min_{u} \int_{0}^{\infty} \left[(\dot{y}_p - \dot{y}_m) Q (\dot{y}_p - \dot{y}_m) + u' R u \right] dt \qquad \text{(E-15)}$$

subject to the constraint of the differential equations of motion of the plant and the model, an uncontrollable part of the state

$$\begin{bmatrix} \dot{x}_p \\ \dot{x}_m \end{bmatrix} = \begin{bmatrix} F_p & 0 \\ 0 & F_m \end{bmatrix} \begin{bmatrix} x_p \\ x_m \end{bmatrix} \begin{bmatrix} G_p \\ 0 \end{bmatrix} u \qquad \text{(E-16)}$$

and $$y = H(x - \dot{x}_m) \qquad \text{(E-17)}$$

Substituting Equation (E-17) into Equation (E-15) yields the performance index

$$V = \min_{u} \int_{0}^{\infty} (\dot{x}^T H' Q H \dot{x} + u^T R u) dt \qquad \text{(E-18)}$$

which yields a Lagrangian

$$\mathcal{L} = x^T F^T H^T Q H F x + 2 x^T F^T H^T Q H G u + u^T (R + G^T H^T Q H G) u + \lambda^T (-\dot{x} + F x + G u) \qquad \text{(E-19)}$$

The Euler-Lagrange equations become

$$\lambda + F^T \lambda + F^T H^T Q H G u + F^T H^T Q H F x = 0 \qquad \text{(E-20)}$$

$$(R + G^T H^T Q H G) u + G^T H^T Q H F x + G^T \lambda = 0 \qquad \text{(E-21)}$$

and from Equation (E-21) the control law can be obtained,

$$u = -(R + G^T H^T Q H G)^{-1} G^T \left[\lambda + H^T Q H F x\right] \qquad \text{(E-22)}$$

From Equations (E-20), (E-21), and (E-16), and with some mathematical manipulation, the steady state Riccati equations can be obtained.

$$0 = F_p^T (I - \hat{Q} G_p \hat{R}^{-1} G_p^T) P_{11} + P_{11} F_p (I - G_p \hat{R}^{-1} G_p^T \hat{Q}) - P_{11} G_p \hat{R}^{-1} G_p^T P_{11} + F_p^T \hat{Q} \left[I - G_p \hat{R}^{-1} G_p^T \hat{Q}\right] F_p \qquad \text{(E-23)}$$

$$0 = F_p^T (I - \hat{Q} G_p \hat{R}^{-1} G_p^T) P_{12} + P_{11} F_p G_p \hat{R}^{-1} G^T \hat{Q} + P_{12} F_m - P_{11} G_p \hat{R}^{-1} G_p^T P_{12} - F_p^T \hat{Q} \left[I - G_p \hat{R}^{-1} G^T \hat{Q}\right] F_m \qquad \text{(E-24)}$$

where $\hat{Q} = H^T Q H$

$\hat{R} = R + G^T H^T Q H G$

and the control law becomes

$$u = -\hat{R}^{-1} G_p^T (P_{11} x + P_{12} x_m + QFx - Q F_m x_m) \qquad \text{(E-25)}$$

This control law resembles Equation (E-6) with the modification that $\hat{R}$ is a guaranteed invertible matrix and P_{11} and P_{12} represent feedback and feedforward increments to the gains that minimize the difference between the plant and model responses. If the model part of the Equation (E-16) had a control term, i.e.

$$\dot{x}_m = F_m x_m + G_m u_m$$

then the optimal control law would have been

$$u = -\hat{R}^{-1} G_p^T (P_{11} x + P_{12} x_m + QFx - QF_m x_m) - \hat{R}^{-1} G_p^T G_m u_m \qquad \text{(E-26)}$$

Then control law would then have even more closely resembled the "exact" model-following situation.

The implicit or the equivalent explicit model-following control technique provides an effective tool for control system design if the ideal or the model, which serves as design objective, can be properly or accurately formulated. The versatility of the resulting configuration, which can be often mechanized as either a feedforward or feedback system, allows for considerable design flexibility.

Appendix F

FEEDBACK FOR SENSITIVITY MINIMIZATION

It isn't enough to design a control system, feedback or feedforward, to accomplish a desired result without considering the sensitivity of this design to the real environment, such as changes in flight conditions and imperfectly known stability and control derivatives and their variations.

The minimization of the sensitivity of control system designs has usually been treated as an interesting but secondary sideline in the design of flight control systems. Instead of trying to minimize sensitivity, the trend has been to adaptive systems, gain programming or other techniques that complicate and reduce the reliability of a flight control system. However, zero or minimum sensitivity designs are possible. The technical content of this report shows that there are alternate ways to satisfy a particular flight control requirement, there is no uniqueness associated with primary function designs such as those that may satisfy flying qualities or minimum wing bending moment requirements. Often a minimum sensitivity design can be selected with little or no increase in complexity. If a control system design can be kept simple, there is little justification for not doing it.

F.1 DEFINITION AND BASIC RELATIONSHIPS

Consider the basic regulator, defined by the fundamental linear matrix differential equation

$$\dot{x}(t) = \left[F(p) - G(p)K\right]x(t) + G(p)u_c \quad x(0) = x_0 \qquad \text{(F-1)}$$

where $F(p)$ is an nxn plant matrix, $G(p)$ is an nxm control effectiveness matrix, K is an mxn matrix of feedback gains, x is an n dimensional state vector and p is a vector of varying parameters. $F(p)$ and $G(p)$ are functions of the varying parameter vector p.

The functional notation of Equation (F-1) is appropriate for aircraft because it defines the dependence of the dimensional stability

derivatives on the ever-changing environment of flight. For instance,

$$M_{\delta_e} = \frac{1}{2}\frac{\rho V^2 S\bar{c}}{I_{yy}} C_{m_{\delta_e}}(\alpha) = M_{\delta_e}(\rho, V, \alpha)$$

or, since air density is a function of altitude and temperature, it is appropriate to express M_{δ_e} as a function of altitude, temperature, velocity, and angle of attack,

To examine the behavior of the regulator subject to a parameter variation, define the sensitivity vector or influence function differential equation

$$\frac{d}{dt}\left(\frac{\partial x}{\partial p}\right) = (F - GK)\left(\frac{\partial x}{\partial p}\right) + \left(\frac{\partial F}{\partial p} - \frac{\partial G}{\partial p} K\right) x \qquad \text{(F-2)}$$

Equation (F-2) represents a forced or non-homogeneous matrix of differential equations. These equations can be investigated to determine how $\frac{\partial x}{\partial p}(t)$ can be made to be minimum in some sense. In particular, the solution of feedback systems to minimize $\frac{\partial x}{\partial p}(t)$ can be investigated.

Two observations are immediately apparent.

1. The amplitude of "motion" of the sensitivity vector elements $\frac{\partial x}{\partial p}(t)$ depend directly on the feedback gains. Large feedback gain magnitudes will tighten the regulation, suppressing not only regulator motion $x(t)$ linearly, but also suppressing sensitivity vector motions in a quadratic sense. To show this, take the Laplace transform of Equation (F-1) and solve for $x(s)$

$$x(s) = (Is - F + GK)^{-1} G u_c(s) \qquad \text{(F-3)}$$

Substituting this result into a solution for $\frac{\partial x}{\partial p}(s)$ from Equation (F-2) yields

$$\frac{\partial x}{\partial p}(s) = (Is - F + GK)^{-1}\left(\frac{\partial F}{\partial p} - \frac{\partial G}{\partial p}K\right)(Is - F + GK)^{-1} G u_c(s) \qquad \text{(F-4)}$$

A tight regulator, therefore, defines an insensitive system.

2. From Equation (F-2) it can be seen that the term $\frac{\partial F}{\partial p} - \frac{\partial G}{\partial p}K$ defines the extent to which the sensitivity vector "motions" are excited by regulator motions. A matrix of feedback gains that satisfies the equations

$$\frac{\partial F}{\partial p} - \frac{\partial G}{\partial p}K = 0, \quad \text{i.e.,} \quad K = \left[\frac{\partial G}{\partial p}\right]^{-1}\frac{\partial F}{\partial p} \qquad \text{(F-5)}$$

would completely remove all excitation from the sensitivity vector equation, forcing

$$\frac{\partial x}{\partial p}(t) = 0$$

and resulting in a zero sensitivity system with finite feedback gains, but this matrix of feedback gains of course does not guarantee stability, nor is it guaranteed that approximation to the inverse indicated by Equation (F-5) will be accurate.

In Section IV of the report it was shown that a maneuver load control system could be mechanized either as a feedback or command augmentation system, and this command augmentation could be modified to incorporate any matrix of feedback gains used to control the actual aircraft. The feedback system described in Section VI was designed for structural mode control, but any functional use, presumably sensitivity minimization, could be employed in the feedback system. The feedback gains could then be as defined by Equation (F-5) or any approximation employing least squares or linear optimal control.

If the feedback gains have been designed for structural mode control or some other purpose, an increment to the feedback gains can be added to consider the sensitivity minimization requirements in a way that guarantees stability. The incremental gains that address the sensitivity minimization problem can be obtained from the solution to the linear optimal control problem

$$V = \min_{x} \int_{o}^{\infty} \left[\left(\frac{\partial x}{\partial p} \right)^{T} Q \left(\frac{\partial x}{\partial p} \right) + x^{T} R x \right] dt \qquad \text{(F-6)}$$

$$\frac{d}{dt}\left(\frac{\partial x}{\partial p} \right) = (F - GK)\left(\frac{\partial x}{\partial p} \right) + \left(\frac{\partial F}{\partial p} - \frac{\partial G}{\partial p} K \right) x \qquad \text{(F-7)}$$

where K has been previously designed for other or primary control system purposes.

The solution to the problem presented by Equations (F-6) and (F-7) is a straightforward one and has been discussed elsewhere in this report. The optimal, minimum sensitivity vector regulator will have the form

$$\frac{d}{dt}\left(\frac{\partial x}{\partial p} \right) = \left[F - GK - \left(\frac{\partial F}{\partial p} - \frac{\partial G}{\partial p} K \right) R^{-1} \left(\frac{\partial F}{\partial p} - \frac{\partial G}{\partial p} K \right)^{T} P \right] \frac{\partial x}{\partial p} \qquad \text{(F-8)}$$

From Equations (F-1) and (F-2), it can be seen that the optimal regulator motions and the sensitivity vector "motions" are defined by the same system matrix. Therefore, the desensitized regulator of Equation (F-8) should result in the same form for the primary feedback structure, i.e.,

$$\dot{x} = \left[F - GK - \left(\frac{\partial F}{\partial p} - \frac{\partial G}{\partial p} K \right) R^{-1} \left(\frac{\partial F}{\partial p} - \frac{\partial G}{\partial p} K \right)^{T} P \right] x + G u_{c} \qquad \text{(F-9)}$$

Using these techniques, it would seem possible to define a feedback control system to satisfy not only a primary purpose, but also a secondary purpose of minimizing sensitivity while still guaranteeing stability.

1. Report No.	2. Government Accession No.	3. Recipient's Catalog No.
NASA CR-3118		

4. Title and Subtitle	5. Report Date
Active Control for the Total-In-Flight Simulator (ACTIFS)	April 1979
	6. Performing Organization Code

7. Author(s)	8. Performing Organization Report No.
E. G. Rynaski, D. Andrisani II, and N. Weingarten	AK-5280-F-11
	10. Work Unit No.

9. Performing Organization Name and Address	11. Contract or Grant No.
Calspan Corporation P. O. Box 235 Buffalo, New York 14221	F33615-73-C-3051
	13. Type of Report and Period Covered Contractor Report Final-Task 15
12. Sponsoring Agency Name and Address	14. Sponsoring Agency Code
National Aeronautics and Space Administration Washington, DC 20546	

15. Supplementary Notes

Study Managed By: Air Force Flight Dynamics Laboratory, Air Force Systems Command, Wright-Patterson Air Force Base, Ohio 45433

Langley Technical Monitor: David B. Middleton

16. Abstract

This report addresses the problem of identification of the aeroelastic equations of motion of an airplane and definitions of criteria and design principles for gust alleviation, maneuver load control and structural mode suppression of a large elastic airplane.

An identification procedure has been developed that is used to systematically improve or update the mathematical model of the aeroelastic behavior of an airplane. A mathematical model that was originally obtained by analytical or theoretical methods is made amenable to piecemeal acceptance of parameters estimated from the data taken during flight tests. By separately identifying selectable parts of the system, and then combining them, one largely avoids the problem of huge computation loads associated with trying to simultaneously identify several hundred parameters.

Linear optimal control theory was used to evolve a performance index specifying closed loop system dynamics. Control laws for the proper pole placement of seven modes of motion of the TIFS airplane, two rigid body and five elastic modes, were specified according to criteria developed. The phase variable canonical transformation was used to help specify a minimum complexity observer network that required no interconnections of the sensor outputs and no measurements of the control input. A conceptual design example of a simplified observer feedback control law for structural mode control of the TIFS airplane is presented.

Gust alleviation techniques involving direct gust measurements and maneuver load control techniques were also developed, resulting in a command augmentation system that simultaneously commands multiple surface deflections to a pilot command input.

17. Key Words (Suggested by Author(s))	18. Distribution Statement
Active Controls, Flight Control, Optimal Control, Structural Mode Control, Maneuver Load Control Gust Alleviation, System Identification, Flying Qualities, Observers Design	Unclassified - Unlimited Subject Category 08

19. Security Classif. (of this report)	20. Security Classif. (of this page)	21. No. of Pages	22. Price*
Unclassified	Unclassified	306	$11.75

* For sale by the National Technical Information Service, Springfield, Virginia 22161